

The tectonometamorphic development of the Ardencaple Fjord area, North East Greenland Caledonides



**Tor Even Aas
Cand. Scient. thesis
Department of Geosciences
University of Oslo**

CONTENTS

1. Introduction	4
1.1. Purpose of study	4
1.2. Geological setting	4
1.3. Field area	5
1.4. Logistics and equipment	6
1.5. Methods of work	6
1.6. Geothermobarometry	7
2. Tectonic setting	8
2.1. Regional Geology of North East Greenland	8
2.2. Geology of North East Greenland	11
2.3. The autochthonous basement and cover	14
2.4. The thrust sheets	14
2.4.1. Allochthonous basement	14
2.4.2. Krummedal/Smallefjord Sequence	15
2.4.3. Neoproterozoic and Lower Paleozoic sediments	16
2.4.3.1. Eleonore Bay Supergroup	16
2.5. Caledonian granite intrusions	18
2.6. Geology of the Ardencaple Fjord	19
2.6.1. Allochthonous basement: Early- to Mid Proterozoic gneisses	19
2.6.2. The Smallefjord Sequence	21
2.6.3. The Eleonore Bay Supergroup	21
2.6.4. Caledonian intrusives in the Ardencaple Fjord area	22
2.6.5. Structural trends	23
2.7. Purpose of investigation at Ardecaple Fjord	25
3. Geology of the study area	26
3.1. Introduction	26
3.2. Allochthonous basement	28
3.2.1. Tonalitic Gneisses	28
3.3. The Smallefjord Sequence	30
3.3.1. Biotite Gneiss Unit	31
3.3.1.1. Garnet-biotite schist layers	32
3.3.2. The Gneiss Unit	32
3.3.2.2. Calc-Silicate Layers	33
3.3.2.3. Augen- and Banded Gneisses	34
3.3.2.4. Meta-arenitic Sub Unit	35
3.3.3. The Migmatite Unit	37
3.4. The Eleonore Bay Supergroup	38
3.4.1. Schists of the Eleonore Bay Supergroup	39
3.5. Granites	40
3.5.1. Granitic veins	42
4. Metamorphic petrology	45
4.1. Introduction	45
4.2. Methodology	46
4.3. Geothermobarometry	47

CONTENTS

4.3.1. Geothermometry	47
4.3.1.1. The Fe-Mg garnet-biotite exchange thermometer	47
4.3.1.2. History of the garnet-biotite thermometer	48
4.3.2. Geobarometry	49
4.3.2.3. The GASP geobarometer	50
4.3.2.4. History of the GASP geobarometer	50
4.3.2.5. The GBPQ geobarometer	50
4.3.3. Thermodynamic Modeling using Whole-Rock Systems	52
4.4. Pitfalls of thermobarometry	53
4.4.1. Diffusion and net-transfer reactions	53
4.4.2. Garnet	56
4.4.3. Plagioclase	57
4.4.4. Biotite	57
4.5. Rock samples and reaction history	59
4.5.1. The high- to medium-grade Smallefjord Sequence	59
4.5.2. The Eleonore Bay Supergroup	65
4.6. Electron Microprobe analyses	67
4.7. Mineral selection criteria for thermobarometry	69
4.8. Calibrations	70
4.8.1. Presentation of applied geothermobarometers and their P-T plots	70
4.8.2. DOMINO P-T plots	71
4.8.3. GBPQ	74
4.8.4. GASP	75
4.9. Conclusion	76
5. Structural geology of the study area	80
5.1. Introduction	80
5.1.1. Previous work in the Ardencaple Fjord area	80
5.1.2. Terminology	83
5.2. The Lower Plate; Allochthonous basement	83
5.2.1. The DL1 event	85
5.2.2. The DL2 event	88
5.2.3. Summary of the Lower Plate	88
5.3. The Middle Plate; The Smallefjord Sequence	88
5.3.1. SM0 - primary sedimentary bedding	89
5.3.2. The DM1 event	89
5.3.3. The DM2 event	90
5.3.4. The DM3 event	92
5.3.5. The DM4 event	93
5.3.6. The DM5 event	95
5.3.7. Summary of the Middle Plate	96
5.4. The Upper Plate; The Eleonore Bay Supergroup	99
5.4.1. Previous work	99
5.4.2. The DU1 event	100
5.4.3. The DU2 event	100
5.4.4. The DU3 event	101

CONTENTS

5.4.5. The DU4 event	101
5.4.6. Summary of the Upper Plate	103
5.5. Summary	103
6. Discussion and conclusion	105
6.1. Introduction	105
6.2. Constraints on tectonometamorphic model	105
6.2.1. Structural field observations	105
6.2.2. Petrological constraints	107
6.2.3. Geothermobarometry	110
6.2.4. Thermodynamic modeling - DOMINO	111
6.2.5. Summary	112
6.3. Other models from the Ardencaple Fjord area	114
6.3.1. A proposed model based on geochronology	114
6.3.2. An alternative tectonic model of the Ardencaple Fjord area	117
6.4. Thought on the exhumation process	118
6.5. An alternative tectonometamorphic model	119
6.6. Thoughts on granites at Kildedalen	123
6.7. Some regional considerations	124
6.8. Conclusions	124

Acknowledgements

Professor Arild Andresen supervised this thesis. I appreciate the fact that he handed me this task and brought me up to North East Greenland twice; first as a field assistant in 2001, before field-work for this thesis was done the year after. Stimulating talks have been had throughout my time on this project. Arild's laid back style of leadership has been widely appreciated, and significant for my own development. Thus, there is quite a bit to thank Arild for.

I am quite grateful for the efforts of Dr. Callum Hetherington at the University of Oslo, who volunteered to help me out by sharing his knowledge of geology in general, and metamorphic petrology in particular. It has been a shear pleasure to learn and discuss geology both directly related, and incredibly remote, to this thesis.

Muriel Erambert is credited for her helpfulness concerning analysis obtained from the electron micro probe. I also appreciated her advices towards methodology.

Atle Rotevatn was my equal at Greenland the summer of 2002. Apart from the scope being geochronology, he wrote a thesis similar to mine. I have had a blast getting to know Atle, and I hope there is more to come.

Ivar Midtkandal and Mona Holte enrolled as field assistants for the summer of 2002, and did an excellent job carrying rocks around the Kildedalen area. They are both thanked for their effort, although Mona was merely returning the favour after I was her field assistant the preceding year.

1. Introduction

1.1. Purpose of study

This thesis focuses on the tectonometamorphic evolution and exhumation of high-grade rocks in Ardencaple Fjord, North East Greenland, and is a part of a research project at the University of Oslo investigating processes within the East Greenland Caledonides. The project, led by professor Arild Andresen, has endured more than a decade. The main objective of this project is to map and constrain the evolution of the Caledonian orogen in North East Greenland. Professor Andresen also hopes to be able to relate the evolution of the North East Greenland Caledonides to the Caledonides in the rest of the North Atlantic region.

The main emphasis of this thesis will be on the metamorphic evolution of different lithotectonic units of the North East Greenland Caledonides, that is the quantification of pressure and temperature evolution. Field observations and thermobarometric data forms the base from which a tectonic model for the study area is presented.

The execution of this thesis was done in cooperation with Atle Røtevatn, who wrote his Cand. Scient. thesis based on the same study area. The main emphasis in Røtevatn's thesis is Ar/Ar dating of the different lithotectonic units in order to present an exhumation model for the rocks in the study area. Røtevatn's results will be commented on briefly in this thesis.

1.2. Geological setting

Fragments of the Caledonian-Appalachian orogen is present in Scandinavia, Svalbard, the British Isles, NW Africa, North America and Greenland. The Caledonian fold belt outcrops for 1300 km in north-south direction along the coast in North East Greenland. The East Greenland Caledonides comprise an Archean to Paleoproterozoic autochthonous basement, with a Neoproterozoic (?) sedimentary cover sequence, underlying Caledonian nappes comprising allochthonous basement, Mesoproterozoic metasediments and Neoproterozoic metasediments. The lithologies present in the field area are nappes comprising allochthonous basement, the Mesoproterozoic Smallefjord Sequence and the Neoproterozoic Eleonore Bay Supergroup. These units are proposed to be separated by high-strain zones (Friderichsen et al., 1994).

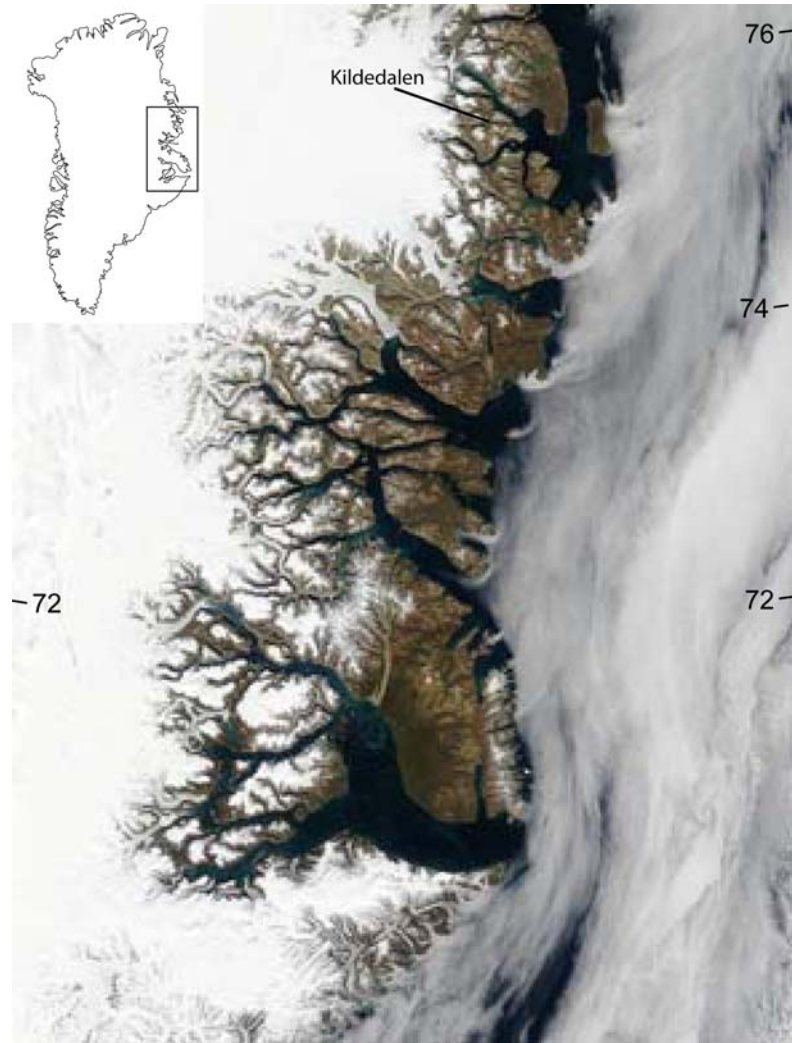


Figure 1.1. Satellite image of North East Greenland. The study area, Kildedalen is labelled at the top of the image. Courtesy of NASA.

1.3. Field area

The field area is located on both sides of a valley called Kildedalen (Figure 1.2.) located on the west side of Ardecaple Fjord in C. H. Ostenfelds Land, 76.15°N. Kildedalen stretches c. 40 km westwards from Ardecaple Fjord before it turns and stretches c. 35 km northwards, where it terminates near the inland ice cap. Field work was done from the Ardecaple Fjord and c. 20 km westwards (Figure 1.1.).



Figure 1.2. This image is a combination of three aerial photos taken over Kildedalen. Kildedalen stretches from Ardencaple Fjord in the east end of the photo, and westwards, before it turns northwest close to the ice seen in the west end of the photo. The study area extends, along Kildedalen, from the right side of the photo to the middle of Slamsø. Slamsø is the lake that can be seen in the middle of the image. The photo is roughly 50 km across.

1.4. Logistics and equipment

Field work was conducted in late July and August of 2002. The entire trip from Oslo and back endured from the 13th of July to the 24th of August. A total of 31 days were spent in the field. The Danish Polar Center arranged Twin Otter flights for the Mestersvig-Kildedalen roundtrip. Our group transported about 1000 kg of cargo both ways. We communicated with Danish Polar Center by radio and satellite phone on a regular basis. An expedition permit from the Danish Polar Center is required before field activities can be undertaken.

The maps used for the field work were blown up copies of the only available map at a scale 1:250 000. The copies were scaled 1:250 000, 1: 125 000 and 1:50 000. The two latter where merely enlarged copies of the 1:250 000 map. To record strike and dip of planar structures and trend and plunge of linear structures I used a 360° Silva compass. All bearing measurements are corrected for a magnetic declination of 27°W. GPS was used for practical navigation in the field and to record the coordinates and altitudes of geological localities.

1.5. Methods of work

The field work was done using traditional methods. Atle Rotevatn and myself covered as much ground as possible, taking both large scale and small scale photos for documentation. Samples were collected from key lithological units and brought to the University of Oslo for petrographic

descriptions and as potential samples for geochronological and thermobarometrical determinations. Thin sections of selected samples were made at the University of Oslo.

1.6. Geothermobarometry

Geothermobarometry was applied to quantify the metamorphic evolution of the rocks in the field area. Rock samples were analysed using the electron microprobe at the University of Oslo. Pressure conditions were estimated using the garnet-biotite-plagioclase-quartz barometer and temperatures were estimated using the garnet-biotite thermometer. Thermodynamic modeling based on whole-rock chemistry is applied in addition to thermobarometry. Domino-Theriak, a technique that calculates stable mineral assemblages at certain pressure and temperature conditions is used for this purpose.

2. Tectonic setting

2.1. Regional Geology of North East Greenland

The Caledonides in the North Atlantic region originated after closure of the Iapetus Ocean and collision of the Laurentian and Baltic plates in the Late Silurian/Early Devonian (Bryhni and Sturt, 1985). The remnants of the orogen are exposed in East Greenland, western Norway and Svalbard (Figure 2.1). In Norway large volumes of rock were thrust on top of the Baltic shield with its sedimentary cover resulting from the collision. These units are seen today as thin continuous nappes (Bryhni and Sturt, 1985). The nappes are divided into four main tectonostratigraphic units. From bottom to top these are: 1) Lowermost Allochthon, 2) Middle Allochthon, 3) Upper Allochthon and 4) Uppermost Allochthon. The Uppermost and the upper parts of the Upper Allochthon are interpreted as exotic terranes, believed to have originated within the Iapetus Ocean, or to be part of the Laurentian plate (Bryhni and Sturt, 1985).

The Caledonian fold belt of NE Greenland extends from latitude 70° N to 82° N, occupying most of the area between the coast and the Inland Ice (Higgins, 1988) (Figure 2.2). Higgins and Leslie (2000) divided the East Greenland Caledonides into three main lithological units (Figure 2.2):

- 1) An autochthonous Early- to Mid-Proterozoic basement complex.
- 2) An autochthonous to parautochthonous Late Proterozoic to Early Paleozoic cover sequence.
- 3) A regionally extensive thrust sheets composed of:
 - a) An Early- to Mid-Proterozoic allochthonous basement complex composed of orthogneisses and paragneisses.
 - b) A Mesoproterozoic supracrustal sequence (Krummedal and Smallefjord Sequences)
 - c) A Neoproterozoic (Eleonore Bay Supergroup) to early Paleozoic succession.

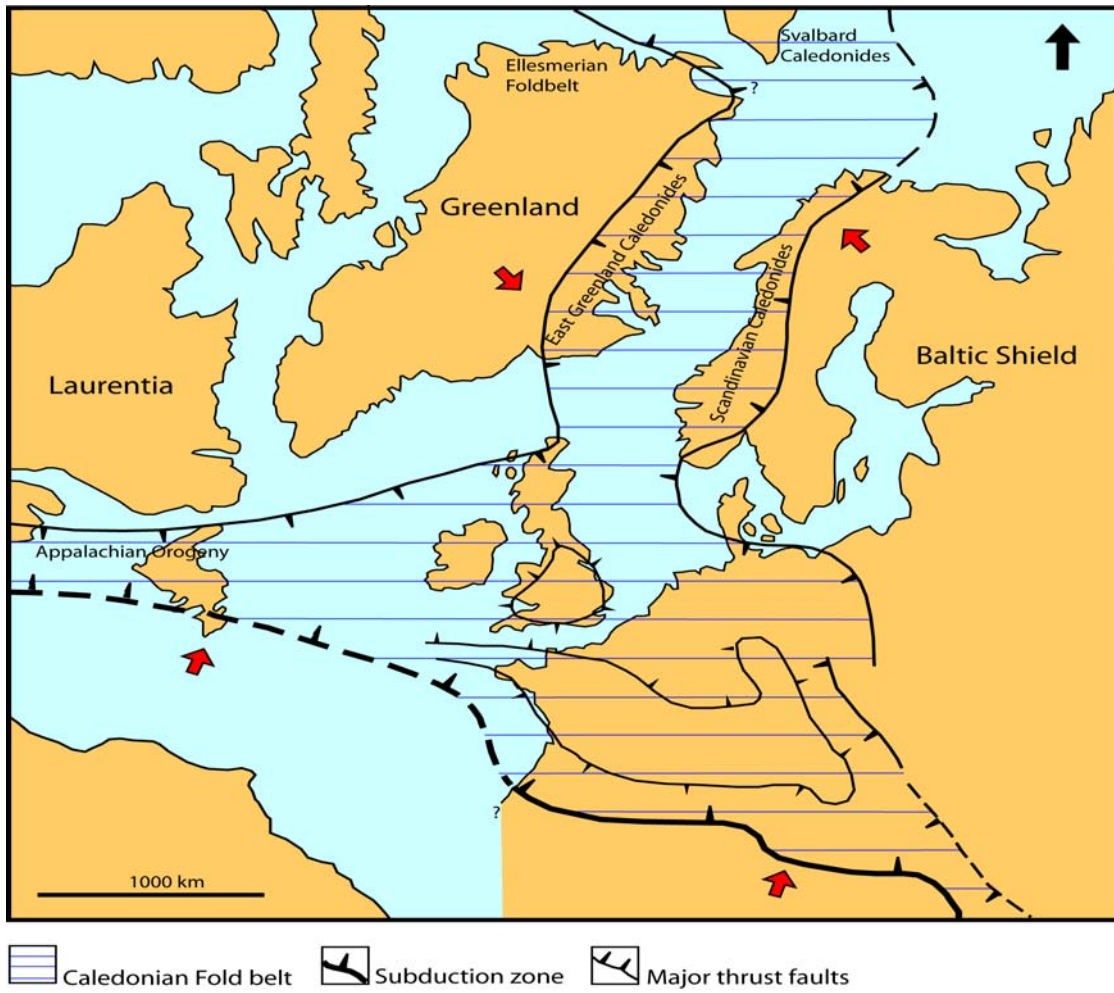


Figure 2.1 Simplified reconstruction of the Caledonian -Appalachian orogen prior to the opening of the North Atlantic ocean. Based on Gee and Sturt (1985) and Cocks and Torsvik (2002)

Several N-S striking shear zones, once thought to be thrust faults (Higgins, 1988) have recently shown to be long-lived extensional faults where the low grade Eleonore Bay Supergroup has been downfaulted and placed against the high grade Mesoproterozoic Krummedal and Smallefjord Sequences (Hartz and Andresen, 1995). The two major shear zones in the south-central part of the NE Greenland Caledonides are named the Fjord Region Detachment Zone (Andresen et al., 1996) and the Bastionen Fault (Higgins and Leslie, 2000) respectively (Figure 2.3). The Fjord Region Detachment Zone has been correlated to the Kildedalen Shear Zone of the Ardecaple Fjord area (Andresen et al., 1996) (Figure 2.2).

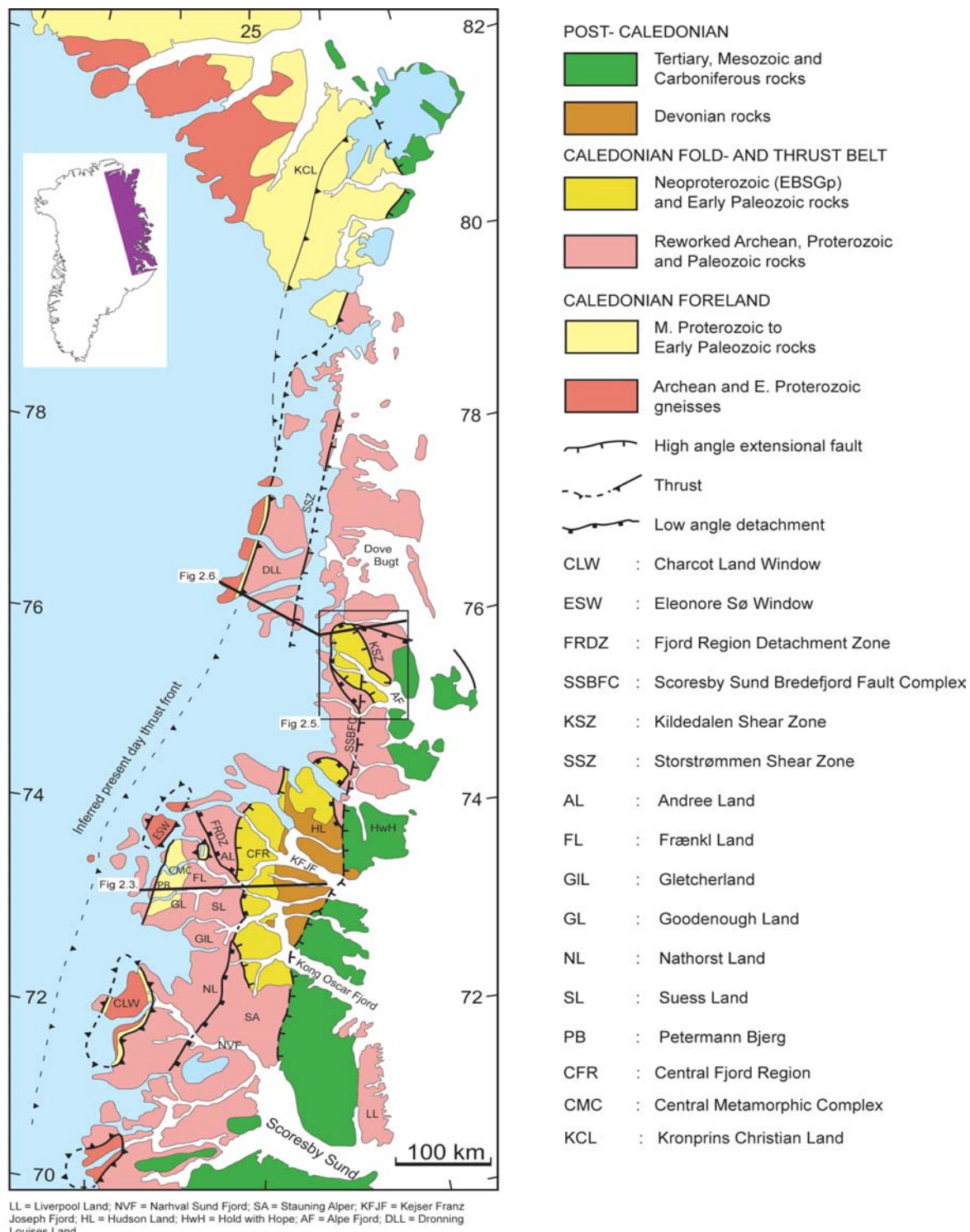


Figure 2.2 The East Greenland fold belt (Eriksen, 2003). The box indicates the Ardecaple Fjord area.

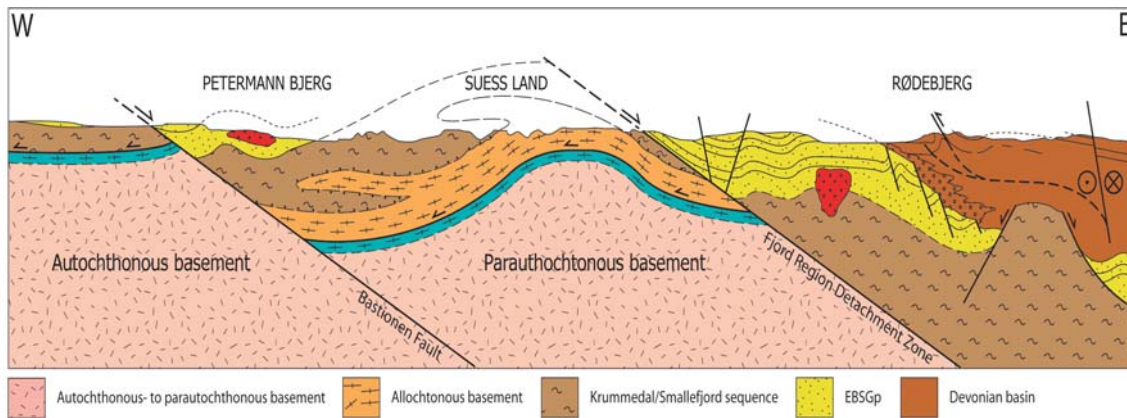


Figure 2.3 Simplified profile across the East Greenland Caledonides from west to east in the Central Fjord Region: 1) autochthonous basement; 2) autochthonous to paraautochthonous late Proterozoic to early Paleozoic cover sequence; 3) regionally overriding thrust sheet. The two fault zones (Bastionen Fault Zone and Fjord Region Detachment Zone) are approximately north-south striking and east dipping with a top-to-the-east displacement.

2.2. Geology of North East Greenland

The earliest expeditions to East Greenland took place in the 1820s, and several nations contributed to the exploration of Greenland throughout the 19th century (Haller, 1971), but these expeditions were few and sporadic. Geological exploration of Greenland was not done thoroughly until the danish geologist Lauge Koch set out on his first expedition in 1926 (Haller, 1971). Annual expeditions under his leadership systematically covered vast areas of Greenland until the activity ceased in 1958. Among the numerous scientists that Koch brought with him was the swiss geologist John Haller. Haller joined Koch's expeditions in 1949 and took part in them for the nine remaining years. By 1958, the expeditions had mapped large parts of NE Greenland in some detail (Haller, 1971).

Haller (1971) proposed “Stockwerk tectonics” (Figure 2.4) as a model to explain the formation of the East Greenland Caledonides. The model infers that a Caledonian migmatitic front moved up through the basement and into the overlying sediments. This process transformed the basement (infrastructure) and parts of the above lying sediments (superstructure) into migmatites, generating the “Central Metamorphic Complex”. The Central Metamorphic Complex comprises three domains - the Gletscherland complex, the Hagar sheet and the Niggli Spids dome (Higgins et al., 1981). These are outdated terms, but they are quite common in the older literature, and will be commented on briefly. The three migmatitic complexes are situated in the footwall of the Fjord

Region Detachment Fault from Frænkl Land in the north to Nathorst Land in the south (Higgins et al., 1981). The metamorphic complexes comprise a variety of gneisses and granites.

Stockwerk is a German word meaning floor or story, and one can see three storys in Haller's classic model (Figure 2.4) The migmatic centres (1) well up into bulges and take part in peculiar flow movements. 3) is the superstructure comprising low-grade or unmetamorposed sediments. 2) is the zone of disharmonic detachment. As the migmatic front rises, differences in plasticity between units 1) and 3) led to disharmonic folding on a large scale. The superstructure, unlike the infrastructure (1), is coherent and presumes open folds. The zone of detachment (2) is a direct consequence of the difference in plasticity between 1) and 3) (Haller, 1971). The detachment zone with disharmonic detachment folding is linked to pelitic strata. According to Haller (1971), this zone varies in thickness from 150 to 1500 m, depending on the lithology of metasedimentay rocks on the outer edge of the infrastructure. One important consequence of this model is that the infrastructure should postdate the superstructure (Haller, 1971).

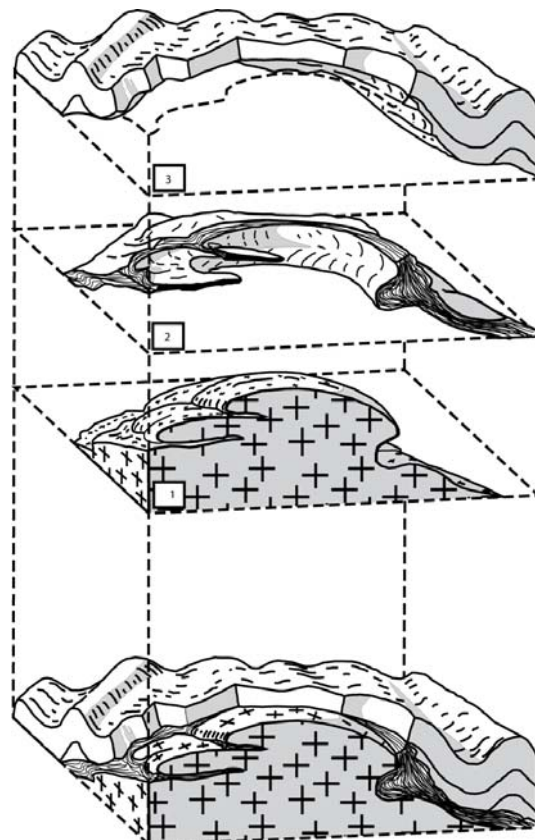


Figure 2.4 Haller's classic Stockwerk model. (1) is the infrastructure. (2) is the detachment zone, and (3) is the superstructure. The bottom part of the figure shows (1), (2) and (3) combined, as seen on Greenland (Haller, 1971)

The “Stockwerk” model was challenged in the late 1970’s when new field observations were collected and isotope studies were made (Henriksen and Higgins, 1976; Higgins, 1976; Higgins and Phillips, 1979). Rb-Sr whole rock and zircon analyses yielded ages of 2935-2300 Ma in a southward continuation of the Central Metamorphic Complex. Clear evidence of the infrastructure being older than the superstructure invalidated Haller’s model. Higgins et al. (1981) concluded that the area was part of a thrust belt with some insignificant late extensional faults.

Higgins et al. (1981) divided the rocks of NE Greenland into four main units:

- 1) Archean - Early Proterozoic basement gneiss complexes.
- 2) Middle Proterozoic metasediments, migmatites and granites.
- 3) Late Proterozoic and Lower Paleozoic sediments.
- 4) Caledonian orthogneisses.

Hartz and Andresen (1995) presented an alternative interpretation of the tectonic relationship between high grade and low grade rocks in East Greenland. Field observations from the Central Fjord Region (Figure 2.2) indicated that the shear zone between basement gneisses and overlying sediments is a late Caledonian extensional detachement zone with top-to-the-east displacement, and not a thrust fault as previously assumed (Higgins et al., 1981). This shear zone was named the Fjord Region Detachment Zone and supporting evidence was found in Forsblad Fjord, Kempes Fjord and Kejser Franz Joseph Fjord (Figure 2.2) (Andresen et al., 1996). The Fjord Region Detachment Zone is a north-south striking ductile to brittle shear zone separating high grade gneisses in the footwall from overlying low grade Eleonore Bay Supergroup. Several east and west dipping extensional faults occur in the hanging wall of the Fjord Region Detachment Zone. Some of these crustal scale extensional faults controlled the formation of the Old Red Extensional Basins (Hartz and Andresen, 1995).

Higgins and Leslie (2000) promoted a new model for the orogen, with an autochthonous basement complex overlain by a parautochthonous Late Proterozoic to Early Paleozoic cover sequence. These units were overridden by allochthonous thrust sheets comprised of Early Proterozoic to Early Paleozoic deposits. The orogen was then affected by late-stage orogen extension along several faults, including the Fjord Region Detachment Zone (Higgins and Leslie, 2000).

2.3. The autochthonous basement and cover

The Caledonian sole thrust is generally concealed by the ice sheet on Greenland. It appears striking N-NE in Dronning Louise Land and on the NE corner of Greenland (Figure 2.2).

The autochthonous basement is exposed in the north and northeastern areas of Greenland, in tectonic windows in the Central Fjord Region, and west of the thrust front in Dronning Louise Land (Figure 2.2). It comprises Archean to Paleoproterozoic ortho- and paragneisses. Pre Caledonian orogenic events have been suggested for the autochthonous basement (Kalsbeek et al., 2000). Iso-topic dating has constrained crystallization ages and tectonometamorphic events in Achean and Paleoproterozoic time. An upper age constraint for the formation of autochthonous basement gneisses in the Scoresby Sund region is 2520 Ma (Steiger et al., 1979). This age is constrained by zircon crystallization ages in granites and a K-Ar hornblende age of an amphibolitic dike cross-cutting the basement gneisses. A Paleoproterozoic metamorphic event (1.7-2.0 Ga) in the Charcot Land window is interpreted from a prograde transition from greenschist to amphibolite facies (Hansen et al., 1981). No evidence for Caledonian deformation has been observed in the autochthonous basement.

The autochthonous basement is overlain by a thin veneer of autochthonous to paraautochthonous Late Neoproterozoic low-grade sediments. The Vendian Tillite Group, a 1.3 km thick clastic sequence, is a constituent of the veneer. The autochthonous to paraautochthonous sediments are exposed west of the thrust front in Dronning Louise Land and in eastern North Greenland, and in the Eleonore Sø, Maridalen, Charcot Land and NN windows (Figure 2.2).

2.4. The thrust sheets

The thrust sheets of the East Greenland Caledonides comprise allochthonous basement, the Meso-proterozoic Krummedal/Smallefjord Sequence, the Neoproterozoic Eleonore Bay Supergroup, the Tillite Group and a succession of Cambrian to early Ordovician sediments..

2.4.1. Allochthonous basement

The allochthonous basement is the structurally lowest tectonic unit in the thrust sheets. It comprises Early- to Mid Proterozoic ortho- and paragneisses (Friderichsen et al., 1994). Allochthonous basement is sliced off from autochthonous basement, and is lithologically similar. As opposed to

autochthonous basement, the allochthonous basement is reworked during the Caledonian Orogeny. Pre-Caledonian structures are, however, preserved locally (Friderichsen et al., 1994). Allochthonous basement generally outcrops along the entire length of the East Greenland fold belt (Figure 2.2).

The ages recorded from the allochthonous basement are Archean to Neoproterozoic (Kalsbeek et al., 2000). Archean ages are not as widespread as early Neoproterozoic ages, that have been recorded from several localities within the NE Greenland Caledonides (Table 1). Rex and Gledhill (1981) conclude, based on isotopic evidence, that most of the gneisses could not have had a long crustal history before ~2000 Ma.

Table 1 Allochthonous basement ages

Rock Type and locality	Technique	Age (Ma)	References
Banded Gneiss, Danmarkshavn	U-Pb, zircon Rb-Sr, whole rock	~3000	Steiger et al., 1976
Granites, 72°N – 74°N	Rb-Sr, whole rock	c. 1950	Rex and Gledhill, 1981
Orthogneisses, 74°N – 76°N	Sm-Nd, Rb-Sr, whole rock	2110-2330	Kalsbeek et al., 1993
Gneiss, 76°N – 77°N	U-Pb, zircon	1974-1739	Kalsbeek et al., 1993
Orthogneisses, Dronningen av Louises Land	U-Pb, zircon	1909	Friderichsen et al., 1994

2.4.2. Krummedal/Smallefjord Sequence

A supracrustal-dominated lithotectonic unit overlying the allochthonous basement gneisses is called the Krummedal Sequence south of 74°N and the Smallefjord Sequence north of 74°N (Figure 2.2). The Krummedal Sequence of the Central Fjord Zone is correlated to the Smallefjord Sequence of the Ardencaple Fjord area (Friderichsen et al., 1994), and it crops out over most of the East Greenland fold belt along strike.

The Krummedal/Smallefjord Sequence comprises psammites, semi-pelites, pelites and mica schists. Quartzites, marbles and amphibolites are less common regionally, but occur locally in

Vestfjord in the Scoresby Sund area (Figure 2.2). Garnet and aluminium silicates (kyanite and sillimanite) are common. A total thickness of 8000 m for the metasediments is proposed (Higgins, 1988).

The Mesoproterozoic metasediments of the Smallefjord/Krummedal Sequence overlie, but in many places isoclinally folded together with the infracrustal gneisses. Hansen et al. (1978) reported Rb-Sr whole rock age and U-Pb monazite ages of about 1100 Ma. Later work concluded that the sequence was deposited between 1100 - 930 Ma (Kalsbeek et al., 2000).

U-Pb zircon and monazite data from the Krummedal Sequence by Leslie and Nutman (2003) in Renland, west of Scoresby Sund (Figure 2.2), indicated early Neoproterozoic metamorphism. This inferred Grenvillian deformational event (Leslie and Nutman, 2003) is possibly associated with the Paleoproterozoic gneiss and Mesoproterozoic metasediment interfolding in the area (Higgins, 1988).

Strachan et al. (1995) presented SHRIMP U-Pb zircon ages from the Smallefjord Sequence of 445 ± 10 Ma, which were interpreted as the age of Caledonian deformation and metamorphism. Marginally younger ages for Caledonian deformation in the Krummedal Sequence have also been recorded (Kalsbeek et al., 2000). Evidence of Pre-Caledonian tectonic events are scarce because of Caledonian overprinting, but 955 ± 13 Ma SHRIMP U-Pb ages on zircons from the Smallefjord Sequence have been recorded (Strachan et al., 1995). These zircons were interpreted to have grown during a high-grade tectonothermal event.

2.4.3. Neoproterozoic and Lower Paleozoic sediments

Neoproterozoic sediments comprise the Eleonore Bay Supergroup and the Peterman Bjerg Group. The Peterman Bjerg Group, located on the west side of the Central Metamorphic Complex (Figure 2.2), is correlated to the Eleonore Bay Supergroup. The Peterman Bjerg Group is not significant to this paper, and will not be commented on.

2.4.3.1. Eleonore Bay Supergroup

Eleonore Bay Supergroup crops out in NE Greenland between latitudes $71^{\circ}30'N$ and $76^{\circ}N$. The main outcrop area is in the Central Fjord Zone (Figure 2.2) (Sønderholm and Tirsgaard, 1993). The northernmost appearance of Eleonore Bay Supergroup is around Ardencaple

Fjord (Figure 2.2) where it appears in a NW-SE trending synform (Soper and Higgins, 1993). (Figure 2.2)

The Eleonore Bay Supergroup is divided into three main units (Sønderholm and Tirsgaard, 1993):

- 1) A 1300 meter lower siliciclastic unit.
- 2) A 1200 meter mixed carbonate and siliciclastic unit.
- 3) A 1500 meter upper unit comprising carbonate.

The Eleonore Bay Supergroup is overlain by the Tillite Group interpreted to be Vendian (Sønderholm and Tirsgaard, 1993).

The Eleonore Bay Supergroup, the Vendian tillites and the Cambrian to Middle Ordovician sequence were deposited in shallow marine to fluviodeltaic environments on a subsiding shelf along the eastern margin of Laurentia (Hambrey and Spencer, 1987).

The lower age limit of the Eleonore Bay Supergroup is poorly constrained. The lower part of the Eleonore Bay Supergroup contains detrital zircon with a lower intercept U-Pb discordia age of 1162 ± 36 Ma and detrital muscovite with K-Ar age of 1030 ± 22 Ma (Peucat et al., 1985). This implies that rock from the source area of the Eleonore Bay Supergroup were metamorphosed during the Grenvillian Orogeny. The deposition of the Eleonore Bay Supergroup must have started sometime after the end of this orogeny, e.g. 950 Ma in East Greenland (Sønderholm and Tirsgaard, 1993). The upper age limit of the Eleonore Bay Supergroup is constrained by the depositional age of the over lying Tillite Group, at about 610 Ma (Sønderholm and Tirsgaard, 1993). It is thus believed that the Eleonore Bay Supergroup was deposited in the interval 610-950 Ma (Figure 2.5) (Sønderholm and Tirsgaard, 1993).

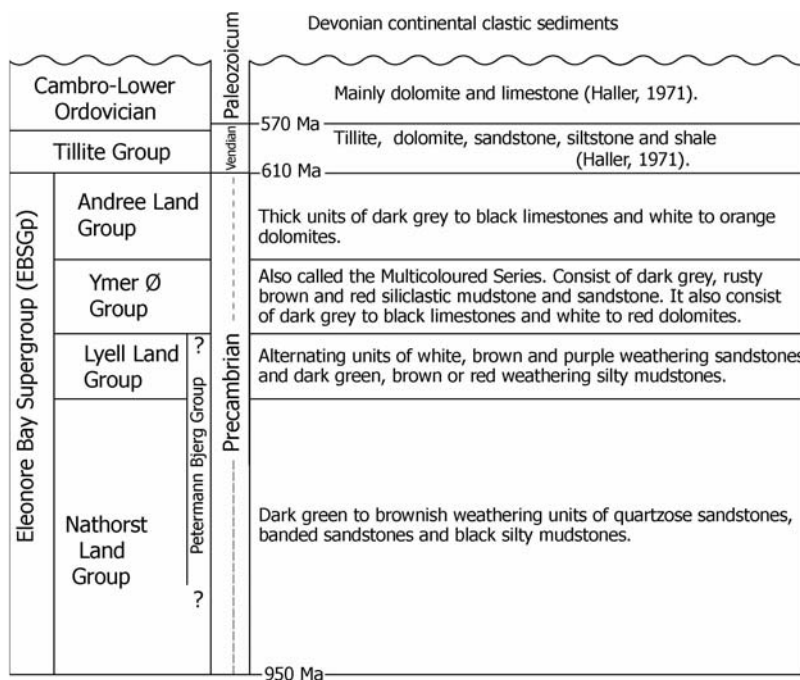


Figure 2.5 Stratigrafic column showing the different units of the Eleonore Bay Supergroup. Modified from Sønderholm and Tirsgaard (1993).

2.5. Caledonian granite intrusions.

Most intrusions in the East Greenland fold belt are Late- to post Caledonian granites. They are emplaced in the Krummedal/Smallefjord Sequence - Eleonore Bay Supergroup contact, and within the Eleonore Bay Supergroup between $72^{\circ} - 74^{\circ}\text{N}$ and $75^{\circ} - 76^{\circ}\text{N}$. Most dated samples record ages c. 420 Ma (Dallmeyer et al., 1994; Hartz et al., 2000; Hansen et al., 1994; Holte, 2003).

Caledonian granitic rocks occur as networks of sheets and veins in migmatite complexes, dipping sheeted complexes in the Smallefjord/Krummedal Sequence and as steep-sided, discordant plutons in the Eleonore Bay Supergroup (Strachan et al., 2001). Strachan et al. (2001) provides geochemical and isotopic evidence indicating that the granitic rocks are derived from crustal anatexis of the Smallefjord Sequence that was initiated during crustal thickening and continued during decompression. Hartz et al. (2000) reached the same conclusion for the granites in the Krummedal Sequence in the Central Fjord Region. There is no evidence indicating that granites

also formed from anatexis of the deeper allochthonous basement rocks (Jepsen and Kalsbeek, 1998).

Strachan et al. (2001) also dated zircons and monazites from granites in the Smallefjord Sequence and the Eleonore Bay Supergroup using U-Pb techniques. The recorded ages of ~431 - 428 Ma respectively, were indistinguishable within error and confirm that emplacement of the granites was contemporaneous at different structural levels. U-Pb monazite ages of 425 - 432 Ma are recorded from granites emplaced in the Krummedal Sequence and the Eleonore Bay Supergroup (Holte, 2003). These granites are interpreted to be syn-extensional in the Eleonore Bay Supergroup, and syn-contractional in the Krummedal Sequence, inferring syn-contractional extension at the time of granite emplacement (White et al., 2002; Holte, 2003).

Granitic sheets and dikes in the lower Krummedal/Smallefjord Sequence have been interpreted as pathways where granitic material has migrated to form plutons in the upper Krummedal/Smallefjord Sequence and the lower Eleonore Bay Supergroup (Strachan et al., 2001).

2.6. Geology of the Ardencaple Fjord

The Ardencaple Fjord area (Figure 2.2), including both Nørlund Land and C. H. Ostenfeld Land, is the area between Bessel Fjord (76° N) and Grandjean Fjord (75° N) (Figure 2.6). The Ardencaple Fjord trends NW and branches into two smaller fjordarms; Bredefjord and Smallefjord.

The Ardencaple Fjord area and the Central Fjord Region are geologically similar (Figure 2.2). The overriding thrust sheets comprising allochthonous basement, the Smallefjord Sequence and the Eleonore Bay Supergroup crop out in the Ardecaple Fjord area. As previously mentioned, the Smallefjord Sequence in the Ardecaple Fjord area is correlated to the Krummedal Sequence in the Central Fjord Region (Friderichsen et al., 1994).

2.6.1. Allochthonous basement: Early- to Mid Proterozoic gneisses

In the Ardecaple Fjord area allochthonous basement comprising Early- to Mid Proterozoic ortho- and paragneisses, crop out as a N-S striking belt next to the inland ice (Figure 2.6). Between Grandjean Fjord and Ejnar Mikkelsen Glacier lie orthogneisses composed of grey, banded hornblende-biotite, or tonalite-quartz dioritic gneisses, cut by up to 1 m wide sheets of granitic-grano-dioritic gneisses (Friderichsen et al., 1994). Mappable sheets of granitic gneisses up to 100 m wide are present. At Mågenes on the north shore of Grandjean Fjord quartz-monzonitic augen

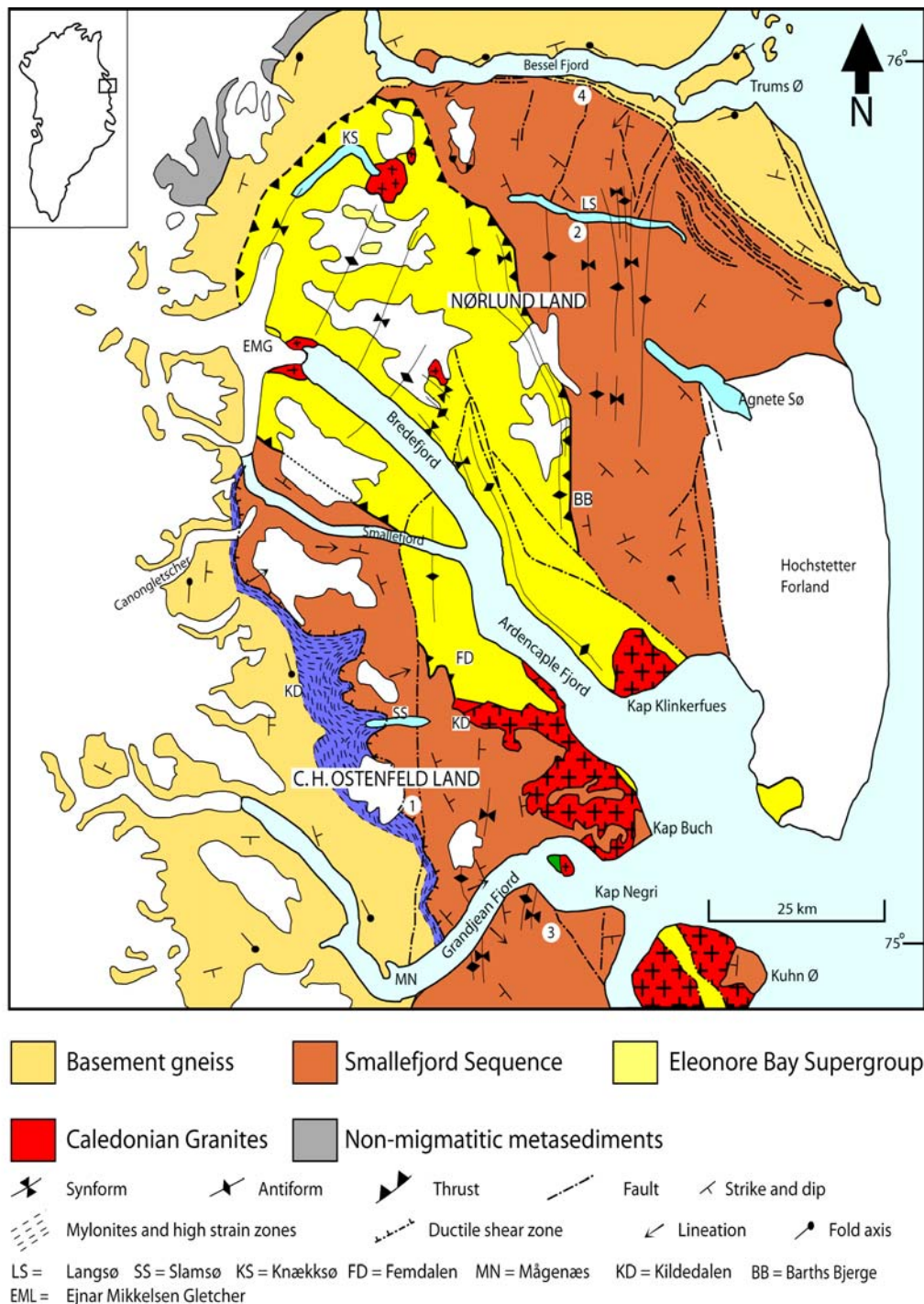


Figure 2.6 Simplified geological map of the Ardencaple Fjord area. Numbers 1-4 marks sample locations for pelites collected by Jones and Strachan (2000)

gneiss dominates. A 1.5 km wide granodioritic to monzo-granitic gneiss sheet has been traced west of Kildedalen (Friderichsen et al., 1994).

Paragneisses are migmatized supracrustal rocks interbanded with orthogneisses, including rusty brown mica schists, gneisses and amphibolites. These units are up to several hundred meters thick and mappable on a km scale. Impure marbles and quartzites are common, but not widely distributed (Friderichsen et al., 1994).

2.6.2. The Smallefjord Sequence

The Mesoproterozoic Smallefjord Sequence comprises medium- to coarse grained semi-pelitic schists and gneisses, which are interlayered with bands of psammite. The psammite bands may be several hundred metres thick. Calc-silicate lenses and orthoquartzite bands are present in areas around Slamsø and Langsø (Figure 2.6) (Friderichsen et al., 1994).

Due to migmatisation, semi-pelites and psammites are characterized by concordant and discontinuous layers and augen of quartzo-feldspathic material, up to 30 cm wide (Friderichsen et al., 1994). Migmatisation is most intense near Langsø and Barth Bjerge (Figure 2.6), where numerous concordant sheets of leucocratic granitoid material up to 150 m wide are present (Friderichsen et al., 1994).

Both deformed and undeformed metabasic intrusions are present, suggesting two distinct Precambrian intrusive events (Friderichsen et al., 1994).

Sheets of deformed granitic gneiss and augen granite are present in the areas of Agnete Sø, Langsø and Slamsø. Their contacts with host gneisses are sharp and discordant (Friderichsen et al., 1994).

A clockwise pressure/temperature evolution was inferred for the Smallefjord Sequence based on textural information, compositional data and constraints from a petrogenic grid (Jones and Strachan, 2000). These authors recorded peak temperatures in the range of 760-850°C and peak pressures of c. 9-10 kbar.

2.6.3. The Eleonore Bay Supergroup

The Neoproterozoic Eleonore Bay Supergroup in the Ardencaple Fjord area is exposed in a NNW - SSE trending depression on both sides of Ardencaple Fjord and Bredefjord (Soper and Higgins, 1993) (Figure 2.6).

It was discovered during reconnaissance flights and sled trips in the 1930s. The only detailed fieldwork recorded prior to 1988, was done in 1955 by Max Sommer. Studies in the late 1980s

and early 1990s (Higgins and Soper, 1994; Soper and Higgins, 1993; Sønderholm et al., 1989; Friderischen et al., 1994) showed that the Eleonore Bay Supergroup appears as a syncline, surrounded by underlying semipelites and psammites of the Smallefjord Sequence (Figure 2.5. and 2.6.). Soper and Higgins (1993) inferred the Eleonore Bay Supergroup - Smallefjord Sequence contact to be a Vendian extensional shear zone, related to the opening of the Iapetus ocean. The Vendian extensional shear zone was subsequently reactivated as a Caledonian thrust (Higgins and Soper, 1994). This view was challenged by Hartz and Andresen (1995), who interpreted the Eleonore Bay Supergroup - Krummedal Sequence contact in the Central Fjord Region to be Devonian extensional detachments, as did Strachan et al. (1995).

The dominant lithologies within the Eleonore Bay Supergroup present in the Ardencaple Fjord tract are: Nathorst Land Group; Lyell Land Group; and Ymer Ø Group (Soper and Higgins, 1993)(Figure 2.1). A minimum of 2 km of Nathorst Land Group is present north of Bredefjord. Up to 2 km of Lyell Land Group is present on both sides of Ardencaple Fjord. Ymer Ø Group can be found on Hochstetter Foreland (Soper and Higgins, 1993).

2.6.4. Caledonian intrusives in the Ardencaple Fjord area

The majority of Caledonian intrusives in the Ardencaple Fjord area are medium grained leucocratic granites. These intrusions appear throughout the Smallefjord Sequence and are especially dominant in the sequence's uppermost parts, particularly along the boundary to the over lying Eleonore Bay Supergroup. Large plutons are present west of Kap Buch, at Kap Klinkerfues, at the head of Bredefjord and on the east side of Knæksø, while numerous smaller bodies occur on Nørlund Land (Figure 2.6). The intrusion west of Kap Buch is, with its estimated 25 km diameter, by far the largest pluton in the area. It is thought to be emplaced in a series of phases due to its profound textural diversity (Hansen et al., 1994).

Hansen et al. (1994) interpreted the unfoliated granites to be syn-Caledonian as opposed to generally foliated pre-Caledonian granites. The foliated granites, obscuring the Smallefjord Sequence - Eleonore Bay Supergroup contact, were interpreted to be Caledonian (Hansen et al., 1994). However, age determinations by Hansen et al. (1994) are not well constrained. U-Pb zircon or monazite dating by Strachan et al. (2001) on granites from both the Smallefjord Sequence and the Eleonore Bay Supergroup yielded exclusively Caledonian ages: ~431-428 Ma. Several phases of

granitic dikes (deformed and undeformed) are present in the allochthonous basement and in the Smallefjord Sequence (Friderichsen et al., 1994; Strachan et al., 2001).

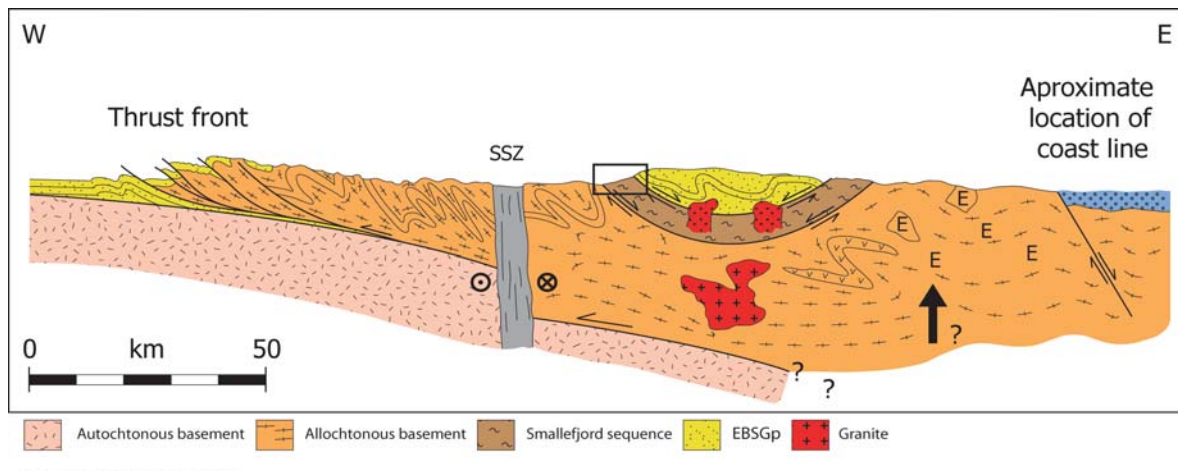


Figure 2.7 Simplified cross section of the Caledonides in the Ardencaple Fjord area. The western termination of the Smallefjord Sequence is mapped as the Kildedalen Shear Zone south of Ejnar Mikkelsen Gletcher, and a thrust fault north of Ejnar Mikkelsen Gletcher by Friderichsen et al. (1994). The N-S trending Storstrømmen Shear Zone is concealed by the inland ice west of the Ardencaple Fjord.

2.6.5. Structural trends

Folds and ductile shear zones are dominant structures in the Ardencaple Fjord area. The location of folds and shear zones described below can be found in figure 2.8.

The allochthonous basement is folded into large-scale polyphase folds with fold axes trending northwards from Grandjean Fjord towards Bessel Fjord, where they turn eastwards (Hansen et al., 1994).

In the Smallefjord Sequence folds are medium-scale and generally strike NE-SW to E-W. U-Pb zircon dating of deformed granitoid rocks have yielded Caledonian age for folding of the Smallefjord Sequence (Hansen et al., 1994).

The Eleonore Bay Supergroup is the most extensively folded unit in the area. Its main fold structures are the Brædal fold pair and Smallefjord anticline, the Troldedalen fold pair and the Knæksø syncline (Figure 2.8) (Higgins and Soper, 1994).

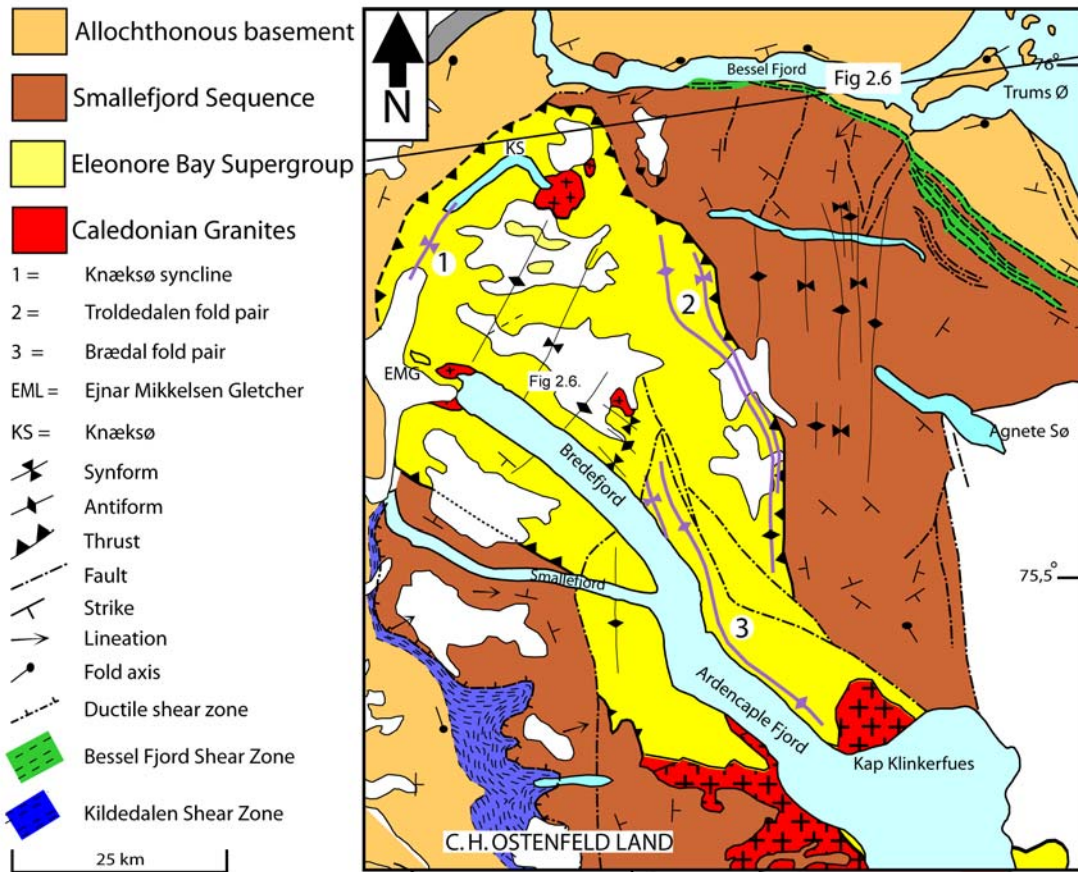


Figure 2.8This figure exposes a simplified geological map of the Ardecaple Fjord area. Shear zones and folds are emphasized in this figure. Modified from Higgins and Soper (1994)

Ductile shear zones separating the Smallefjord Sequence from allochthonous basement gneisses and the Eleonore Bay Supergroup are important structures in the Ardencaple Fjord area (Chapter 3 and 5). Two major shear zones separate the Smallefjord Sequence from underlying allochthonous basement;

- 1) the Bessel Fjord Shear Zone comprises mylonitic gneisses and schists and is interpreted to be extensional. SW of Trums Ø (Figure 2.8) the Bessel Fjord Shear Zone branches into two high strain zones (Friderichsen et al., 1994).
- 2) the Kildedalen Shear Zone comprises reworked allochthonous basement gneisses and is interpreted to be extensional. Although kinematic indicators are scarce, top-to-the-NE extensional displacement has been proposed by Friderichsen et al. (1994).

Ductile shear zones generally separate the Smallefjord Sequence from the overlying Eleonore Bay Supergroup, although some brittle fault boundaries are observed (Friderichsen et al., 1994). The shear zones are often intruded by intense granite sheeting (Higgins and Soper, 1994). Within the shear zones mylonitic gneisses and schists derived from the Smallefjord Sequence pass transitionally into foliated and lineated metasedimentary rocks of the Eleonore Bay Supergroup. Friderichsen et al. (1994) interpreted top-to-the-NE extensional displacement for the shear zones separating the Smallefjord Sequence and the Eleonore Bay Supergroup.

2.7. Purpose of investigation at Ardecaple Fjord

Kildedalen contains Caledonian extensional shear zones, and is thus suitable for a study of the extensional evolution within the Caledonian orogen. By studying the metamorphic relations within rocks and tectonic boundaries, a quantified P-T-t (pressure-temperature-time) path is estimated. This P-T-t path yields information on the kinetic development across tectonic boundaries, and has information about the peak metamorphic conditions for rocks in the Ardencaple Fjord area. This data, along with geochronological data obtained (Rotevatn, 2004), is at the base of a presented tectonic model from the area. With the geological situation in the Ardencaple Fjord area being typical for the East Greenland Caledonides, this model should be valid for the East Greenland Caledonides as a whole.

3. Geology of the study area

3.1. Introduction

The study area in Kildedalen (Figure 3.1) represents a transect from the allochthonous basement gneisses, across the Smallefjord Sequence into the lower part of the Eleonore Bay Supergroup. The rock units in the Kildedalen area (Figure 3.1) can be divided into three lithotectonic units (Friderichsen et al., 1994);

- 1) Neoproterozoic metasediments named the Eleonore Bay Supergroup.
- 2) Mesoproterozoic metasediments denoted the Smallefjord Sequence.
- 3) Early Proterozoic allochthonous basement gneisses.

The Smallefjord Sequence is further sub-divided into sub units based on variation in lithology (Figure 3.2):

- a) Migmatite Unit
- b) Gneiss Unit
 - Calc-silicate Layer Sub Unit
 - Augen- and banded gneiss Sub Unit
 - Meta-arenitic Sub-Unit
- c) Biotite-Gneiss Unit

The Kildedalen Shear Zone defines the upper part of allochthonous basement (Dallmeyer et al., 1994; Friderichsen et al., 1994), and the Slamsø Shear Zone defines the lower part of the Smallefjord Sequence (Figure 3.2).

The banded tonalitic to granodioritic gneisses of the Kildedalen Shear Zone, with its post-kinematic granitoid dikes, are truncated by the overlying Slamsø Shear Zone. The Slamsø Shear Zone is a north-south striking ductile to brittle east dipping extensional shear zone, where the shear strain is taken up in numerous garnet-biotite schist layers. It separates the tonalitic to granodioritic gneisses of the allochthonous basement from the mica rich gneisses of the Smallefjord Sequence. The younger age of the Slamsø Shear Zone relative to the Kildedalen Shear Zone is demonstrated by the post-kinematic granitoid dikes that post-dates formation of the Kildedalen Shear Zone, but are themselves cut by the Slamsø Shear Zone.

A north-south striking top-to-the-east extensional fault, interpreted to represent a northward continuation of the Post-Devonian Main Fault (Haller, 1971), appear to separate the Biotite-Gneiss Unit and the Gneiss Unit of the Smallefjord Sequence. The main strand of the fault is not exposed in the study area, but is most likely responsible for the north-south striking valley located northward of the last exposure of the fault plane. Its presence in the area is indicated by several minor late brittle north-south striking faults in the area (Figures 3.1; 3.2).

The nature of the contact between the Smallefjord Sequence and the Eleonore Bay Supergroup is unclear in the study area, due to several granitic bodies along the contact. Friderichsen et al. (1994) have interpreted the contact elsewhere in the Ardencaple Fjord area to be a high strain zone. Strachan (1994) argued that the high strain zone represents an extensional shear zone. Friderichsen et al. (1994, Figure 1) mark the high strain zone with a thrust symbol.

Although the presence of a high strain zone appears to exist between the Eleonore Bay Supergroup and the Smallefjord Sequence elsewhere in the Smallefjord area (Friderichsen et al., 1994), it has not been observed to cross the study area (Kildedalen).

Granitic and pegmatitic dikes cross-cut the allochthonous basement, the middle- and upper part of the Smallefjord Sequence and the Eleonore Bay Supergroup, but appear to be absent, or limited in number, in the lower part of the Smallefjord Sequence. The granite intrusions present in the Kildedalen area will be reviewed separately in this chapter, as opposed to the rest of the lithotectonic succession, that is described from bottom to top.

The main emphasis in this thesis will be on the Smallefjord Sequence, that was extensively investigated in the field. Only the very top of allochthonous basement and the very bottom of the Eleonore Bay Supergroup were investigated in the field.

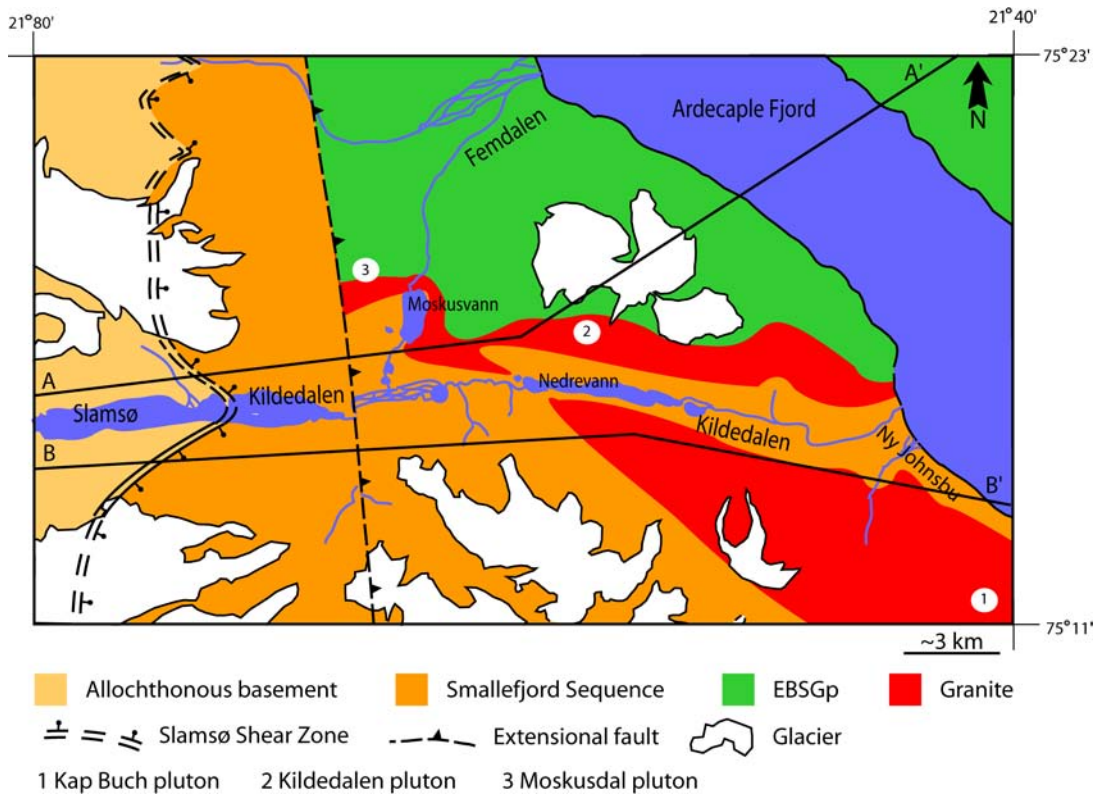


Figure 3.1 Simplified map of Kildedalen and surrounding areas showing the extent of the allochthonous basement gneisses, the Smallefjord Sequence and the Eleonore Bay Supergroup. Areas dominated by granitic intrusions are also included.

3.2. Allochthonous basement

The allochthonous basement comprises Early Proterozoic gneisses and some late Caledonian granite veins (Dallmeyer et al., 1994). The allochthonous basement in Kildedalen consists of highly sheared tonalitic gneisses (associated with the Kildedalen Shear Zone) with bands and layers of amphibole, that are cut by post-kinematic leuco-granitic veins. The top of the basement unit appears at the middle of Slamsø, where it is separated from the overlying Biotite-gneiss Unit of the Smallefjord Sequence by the Slamsø Shear Zone (Figure 3.1).

3.2.1. Tonalitic Gneisses

The valley slopes on both sides of Slamsø are dominated by banded tonalitic gneisses with variable proportions of amphibole, quartz, plagioclase and biotite (Figure 3.3). Layers of amphibolite (mafic dikes?) and less deformed bodies of granodiorite appear locally.

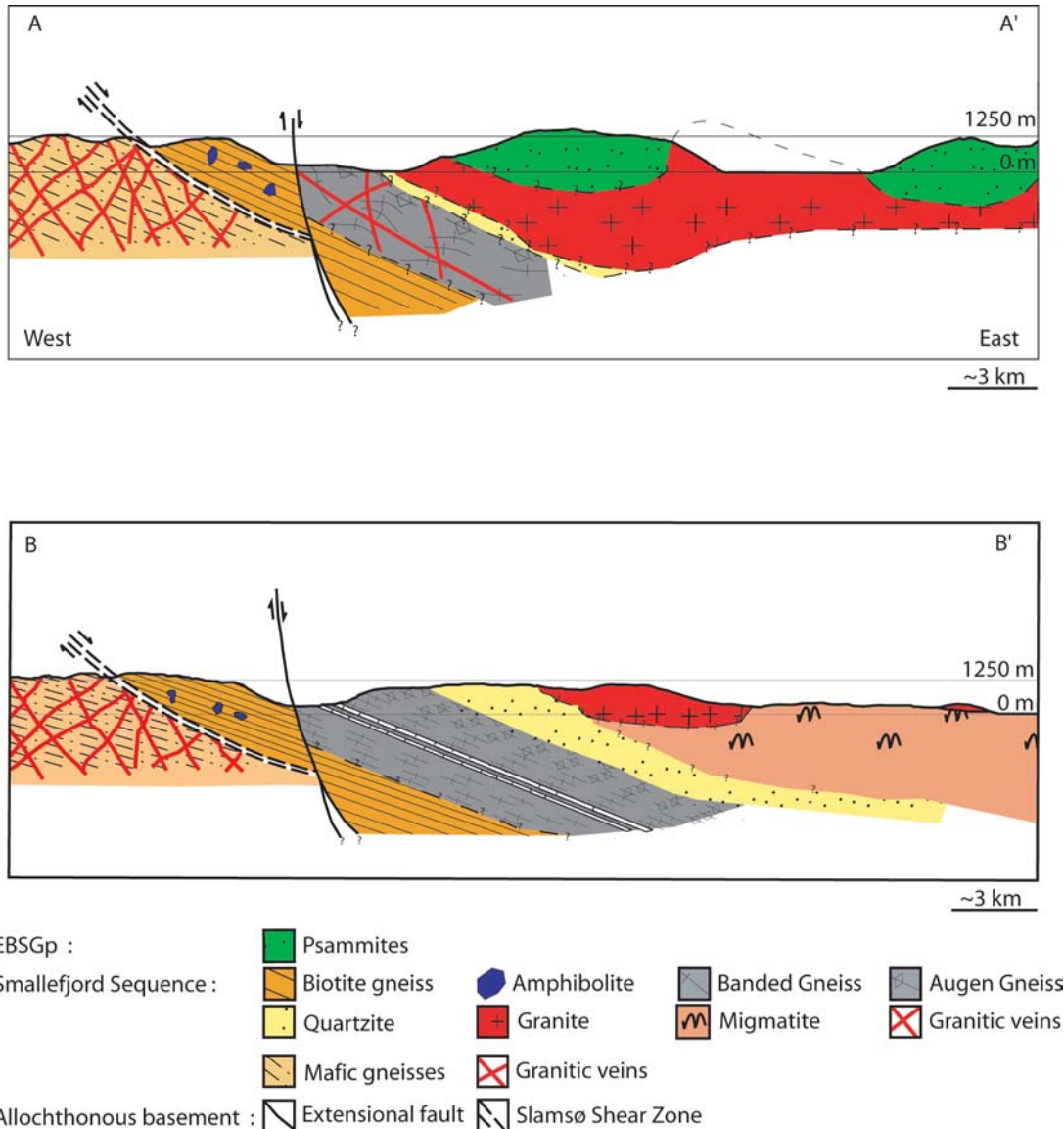


Figure 3.2 Simplified cross section showing inferred appearance of the rock units in the Ardencaple Fjord area. The cross section trends west-east along the north and south sides of Kildedalen, as indicated on the map (figure 3.1).

Parallel oriented amphibole and biotite define a well developed foliation, interpreted to be associated with the development of the Kildedalen Shear Zone, for which a consistent shear sense direction could not be defined. Lenses of unfoliated amphibolite are present within the core of the mafic gneisses. Unfoliated post-kinematic granitic dikes of grain size less than 1 m thick cross-cut the Gneiss Unit (Figure 3.3).



Figure 3.3 Allochthonous basement south of Slamsø. Dikes cut the host rock comprising tonalitic gneisses. The picture is c. 10 m across.

3.3. The Smallefjord Sequence

The Mesoproterozoic Smallefjord Sequence is variably migmatized prior to, or synchronous with an early phase of deformation with relatively large granitic sheets and bodies in its upper part. There is a gradual transition from the neosome poor Gneiss Unit in the lower part of the Smallefjord Sequence to the granite dominated upper part. It is therefore difficult to subdivide and map out separate lithological units. Based on several traverses across the Smallefjord Sequence we have, however, been able to distinguish the following lithotectonic units from top to bottom:

- 1) Migmatite Unit (>40% neosome)
- 2) Gneiss Unit
 - Meta-arenitic Sub Unit
 - Calc-silicate Layer Sub Unit
 - Augen- and banded gneisses Sub Unit
- 3) Biotite-Gneiss Unit

The appearance of the various units within the Smallefjord Sequence is shown in figure 3.1 (map) and figure 3.2 (cross-section).

3.3.1. Biotite Gneiss Unit

The Biotite Gneiss Unit (Figure 3.4) dominates the area between the lowermost part of the Slamsø Shear Zone and the inferred northern continuation of the Post-Devonian Main Fault. The Biotite Gneiss Unit borders tectonically to the overlying Gneiss Unit (3.3.2.), where a late brittle fault separates the two units, and to the underlying tonalitic gneisses of the allochthonous basement, where the two units are separated by the Slamsø Shear Zone (Figure 3.1).

The Biotite Gneiss Unit is fractured along east-west striking sub-parallel fractures. The Gneiss Unit is dominated by a medium to fine grained biotite gneiss without garnet over most of its outcrop area. Amphibolite lenses and layers of amphibolite, garnet-amphibolite and ultramafites were observed within the Biotite Gneiss Unit, but their primary contact relationship with the country rock remains unclear due to the overall high strain in the area. There are few signs of anatexis, in contrast to what is evident in the overlying Gneiss and Migmatite units of the Smallefjord Sequence.

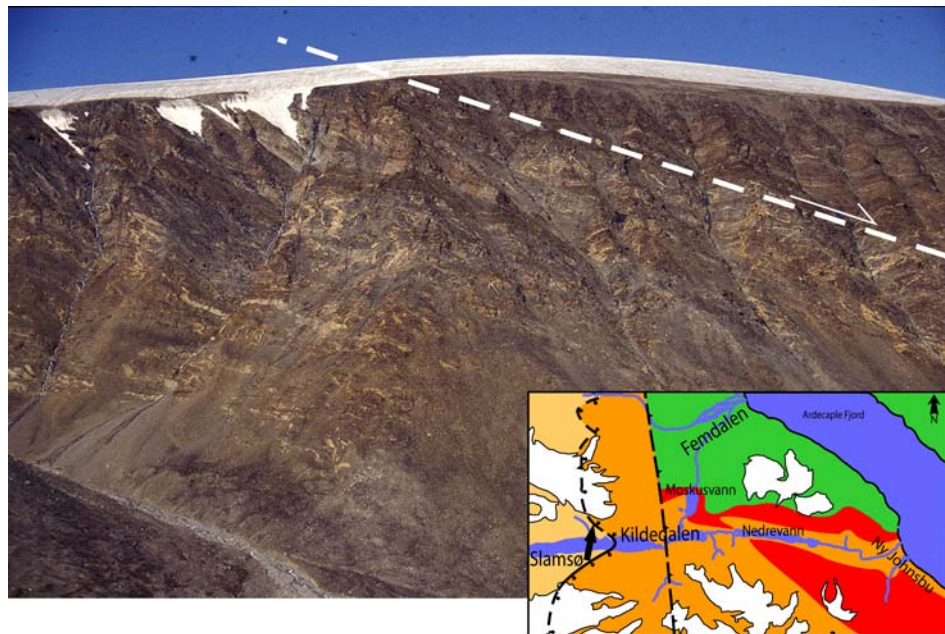


Figure 3.4 The mountain walls by Slamsø comprising both allochthonous basement and the Smallefjord Sequence. The dashed line represents the base of the Slamsø Shear Zone, and thus the contact separating the Smallefjord Sequence and the allochthonous basement. This part of allochthonous basement comprises the Kildedalen Shear Zone. The half-arrow indicates sense of shear. The Biotite gneisses are seen in the upper right hand corner of the picture. The arrow on the index map indicates location and bearing of photo. Mountain wall is c. 1200 m high.

3.3.1.1. Garnet-biotite schist layers

During a traverse along the north side of Slamsø two 30-50 m thick coarse-grained garnet-biotite schist layers were identified within the Biotite Gneiss Unit. Sharp possibly primary lithological contacts separate the garnet-biotite schists from the Biotite Gneiss Unit country rock. The main mineral assemblage comprises quartz + garnet +/- muscovite + biotite + plagioclase + sillimanite/kyanite. Compositional bands of mica and sillimanite make up the foliation while garnet, K-feldspar and plagioclase appear as combined porphyroblasts/porphyroclasts (Detailed petrography in Chapter 4.5). Sharp possibly primary lithological contacts separate the garnet-biotite schists from the Biotite Gneiss Unit country rock

3.3.2. The Gneiss Unit

A heterogeneous gneiss complex dominates the area on the south side of Kildedalen and east of the Post-Devonian Main Fault (Figure 3.5). The same gneiss complex was also observed at the SW corner of Moskusdal (Figure 3.1).

The presence of meta-arenites and calc-silicates interbedded with ordinary feldspathic gneisses, banded gneisses and zones of augengneisses suggest that one is dealing with a supracrustal sequence possibly intruded by a pre-to-syn tectonic coarse-grained granite. Lenses of quartz and feldspar were observed locally, which may represent highly deformed neosomes, generated during an early phase of the tectonothermal evolution.

The Gneiss Unit has a sharp contact to the structurally overlying Kildedalen pluton in the area south of Nedrevann (Figure 3.1). Its relations to the underlying Biotite Gneiss Unit could not be seen in Kildedalen due to glacial till in the area around Moskusvann. When traversing structurally downwards in the Gneiss Unit, the last exposure is by a small river in the middle of this valley. The underlying Biotite Gneiss Unit is exposed low on the western side of this north-south trending valley. An extensional fault (Figure 3.1) is therefore inferred to strike somewhat parallel to this north-south trending valley, and to have controlled post-Caledonian erosion.

With the exception of calc-silicate layers which have sharp contacts to the host rock banded gneiss, the contact relationships within the Gneiss Unit are transitional.

There are several generations of felsic dikes in the Gneiss Unit, but they all cut across the dominant gneiss foliation (Figure 3.5).

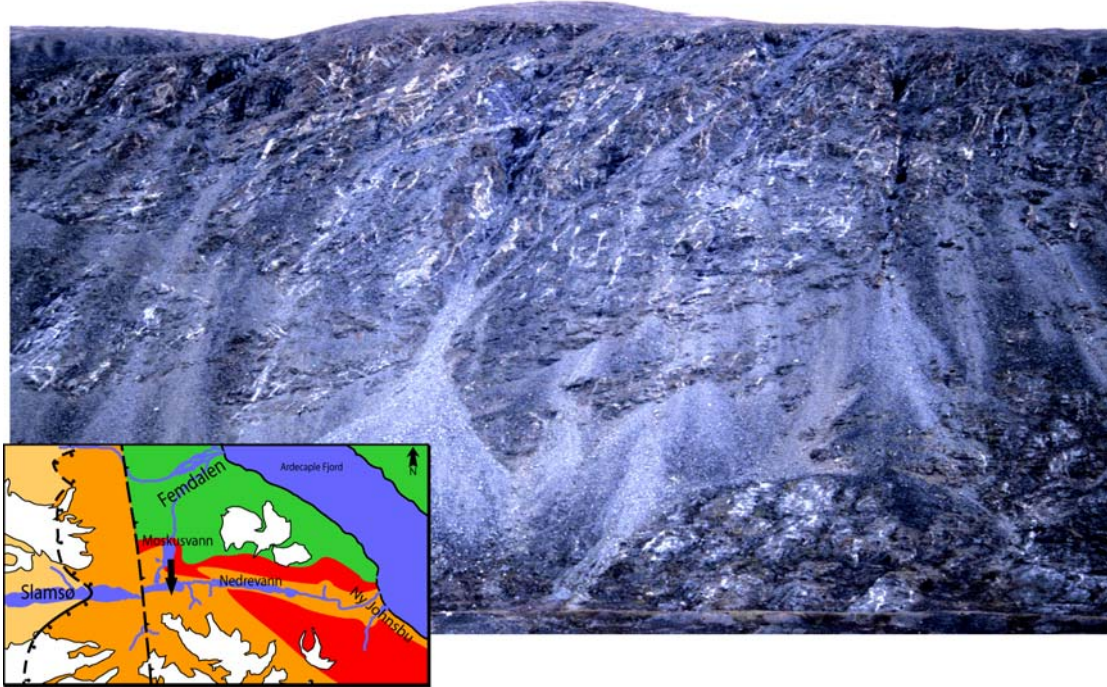


Figure 3.5 South facing picture of The Gneiss Unit where dominated by eye- and banded gneisses. Discordant quartz veins pierce the entire unit. The arrow indicates location and bearing of photo. The mountain wall is c. 1100 m high.

3.3.2.1. Calc-Silicate Layers

At least four layers of calc-silicate appear in a 150 m wide zone within the Gneiss Unit. The calc-silicate layers have an internal compositional banding, interpreted to be a primary sedimentary feature (Figure 3.6). Their contacts with the gneisses are sharp and conform, and the calc-silicate layers are folded together with the country rock gneisses. The calc-silicate layers pinch out occasionally and have a maximum thickness of about 2-3 m.

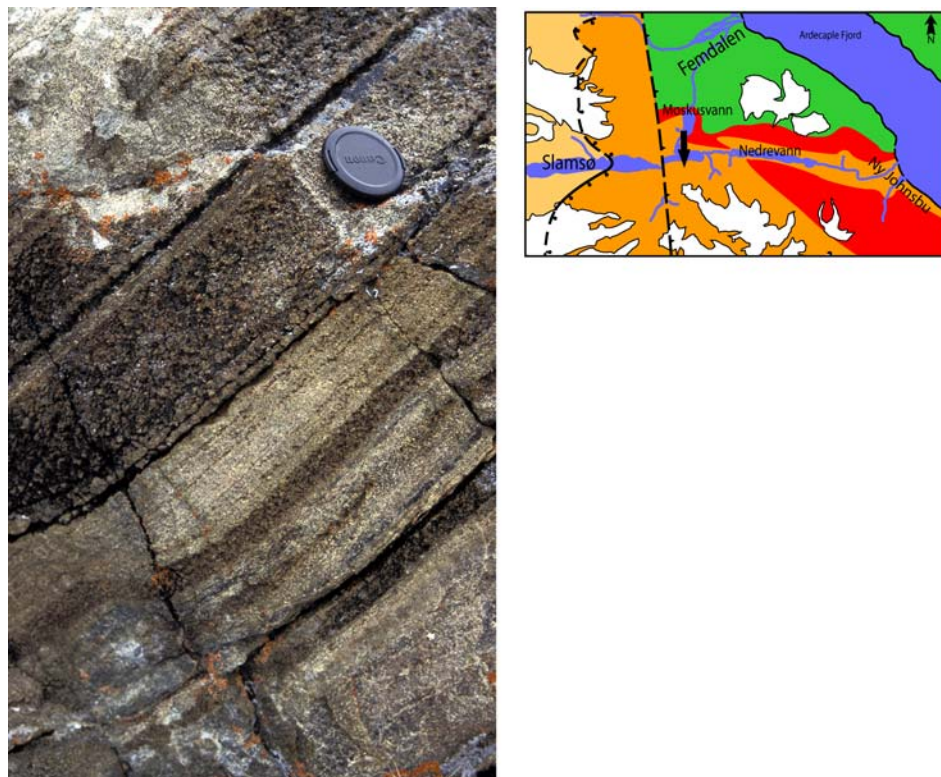


Figure 3.6 Calc-Silicate Layers conformly interfingering the Banded Gneisses. The arrow on the index map indicates location and bearing of photo.

3.3.2.2. Augen- and Banded Gneisses

Augen gneisses and banded feldspathic gneisses with a combined structural thickness of c. 1000 m occupy the area between Slamsø and Nedrevann (Figure 3.5). The rock forming minerals in the feldspathic gneisses are quartz, biotite and plagioclase besides K-feldspar. A compositional foliation is defined by aligned mica, quartz and feldspar (either as bands or augens).

The lower part comprises augen gneiss (Figure 3.7). The augens represent K-feldspar and they generally increase in size and become more stretched out, and eventually banded together going stratigraphically upwards. Thus banded gneisses overlie, and are transitionally separated from the augen gneisses. Thin layers of calc-silicate interbed the banded gneisses.

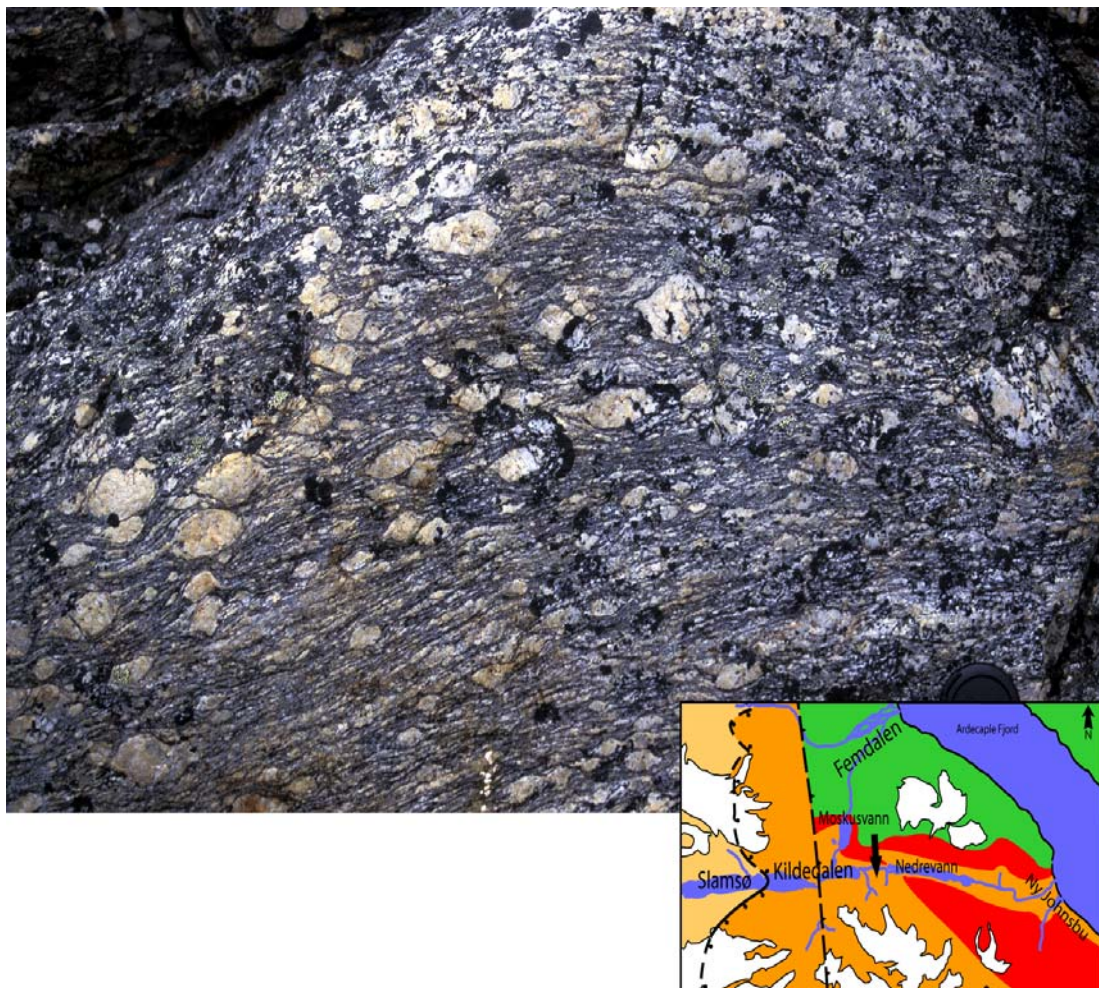


Figure 3.7 Well developed augen gneiss from The Gneiss Unit. The arrow indicates location and bearing of photo. The photo is c. 1 m wide.

3.3.2.3. Meta-arenitic Sub Unit

The meta-arenitic sub unit overlies the augen- and banded gneisses. The lower part of the meta-arenitic sub-unit is dominated by impure feldspathic quartzites and arkoses. and feldspar rich, but also comprises biotite, white mica and amphibole. Weak compositional banding of quartz and mica define the foliation. Biotite becomes increasingly more abundant moving stratigraphically upwards, and defines a strong foliation in the middle parts of the sub unit. The original bedding is seen as a weakly developed compositional banding controlled by variable proportions of white mica, biotite and amphibolite, all with a preferred orientation. This primary sedimentary bedding is not widespread (Figure 3.8).

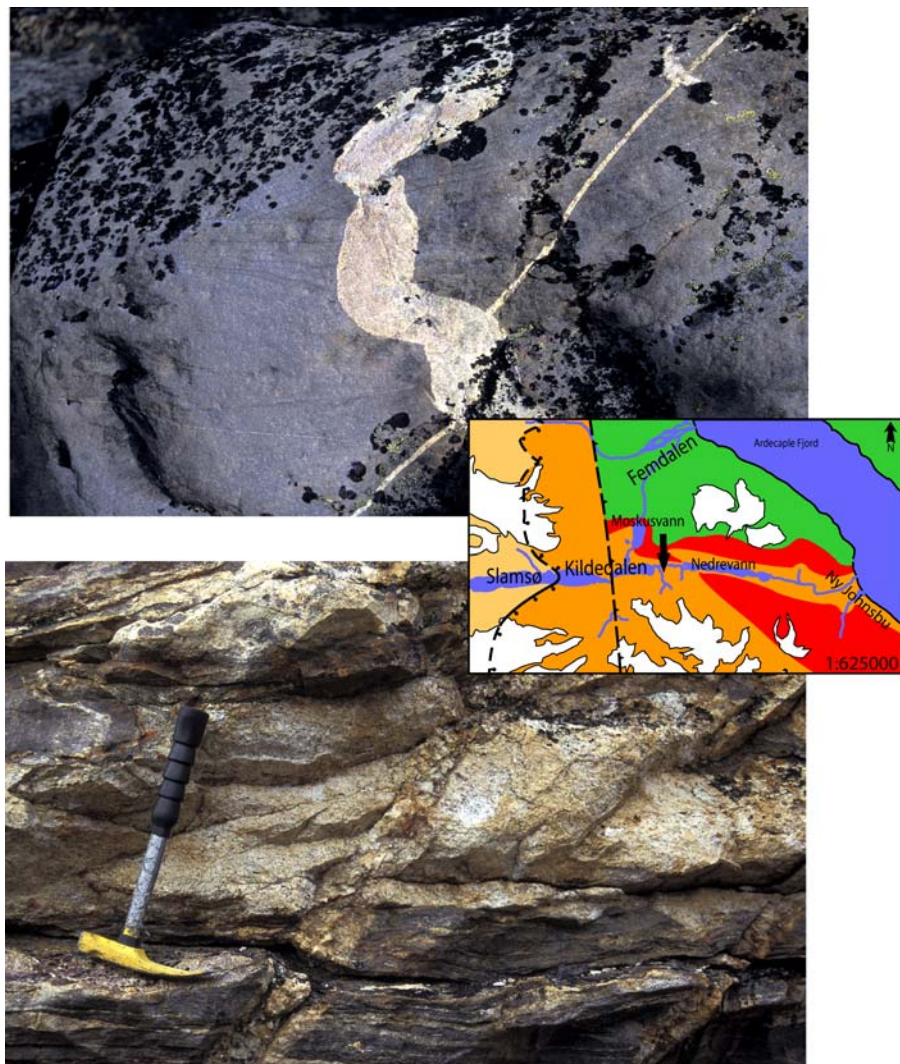


Figure 3.8 Top picture: Shows a granite dike intruding a quartz arenite with relict sedimentary structures. Picture is c. 1 m across. Bottom picture: Shows how the mineral content varies internally in the meta-arenite. The top third of the picture is feldspar-rich, the middle part quartz-rich and the bottom part is feldspar and biotite rich. A late undeformed leuco-granitic dike cuts the lithology. The arrow indicates location and bearing of photo.

Rather pure quartzites (orthoquartzites)(Figure 3.9) are common in the upper part of this sub unit. They appear finegrained and massive, with no evident compositional banding or foliation. The underlying feldspar and biotite rich foliated arenites are commonly observed as lenses situated within the meta-arenitic quartzites (Figure 3.8). Quartz-feldspar “sweat out” is seen locally within the metasediments.

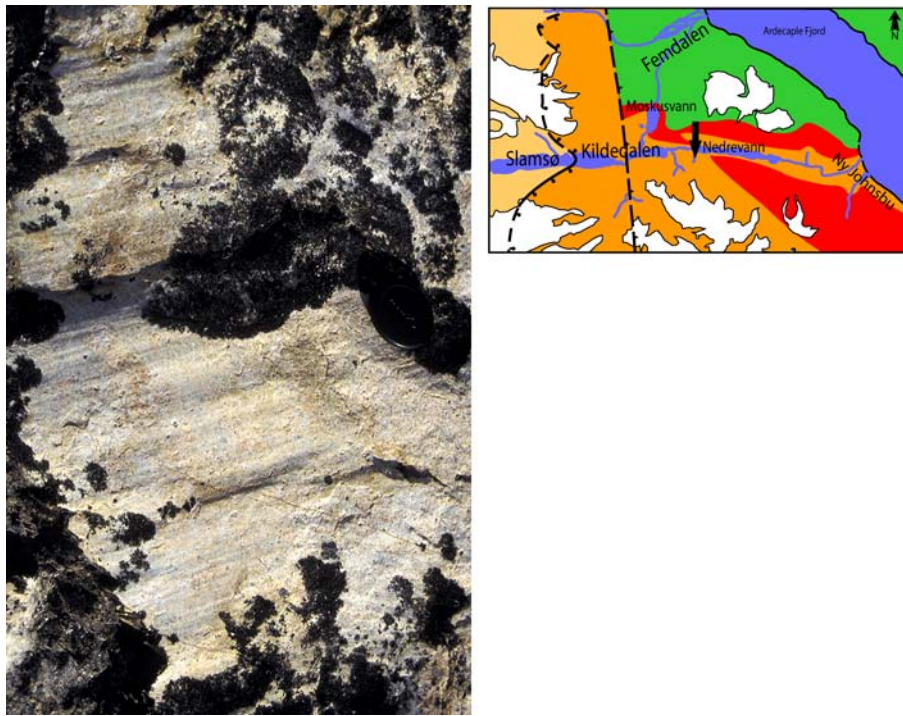


Figure 3.9 Quartzites from the lower part of the Gneiss Unit. The arrow on the index map indicates location and bearing of photo. Photo is c. 1 m wide.

3.3.3. The Migmatite Unit

The migmatites in the upper part of the Smallefjord Sequence outcrop continuously along the western shores of Ardencaple Fjord, and discontinuously within Kildedalen.

How the Migmatite Unit terminates towards east cannot be determined from the western shores of Ardencaple Fjord, because it either terminates within the fjord or somewhere on the east side of it. The migmatites dominate Kildedalen between the Ardencaple Fjord and the eastern bank of Nedrevann, where there is a gradual transition from migmatites to granites (Figure 3.1).

There is a gradual upwards increase in granite melts from the meta-arenite through the migmatite zone into the more massive granites along the contact between the Smallefjord Sequence and the Eleonore Bay Supergroup.

The migmatites around Ny Johnsbu (Figure 3.1) are characterized by isolated blocks or trains of the original supracrustals floating in the granitic neosome (Figure 3.10).

The migmatites comprise a fine grained leucosome composed of quartz, plagioclase and K-feldspar. A weak discontinuous mica foliation exists in the leucosome. Melanozome xenoliths, occati-

onally greater than 1 m across, but usually around 40-50 cm, occur frequently and are haphazardly oriented. Amphibolite xenoliths are by far the most common, but quartzite- and mica schist xenoliths are also regularly present. These xenoliths display a relict compositional banding, oriented randomly compared to the foliation in leucocratic neosome. The leucosome appears to have been flowing around the melanocratic xenoliths (Figure 3.10).

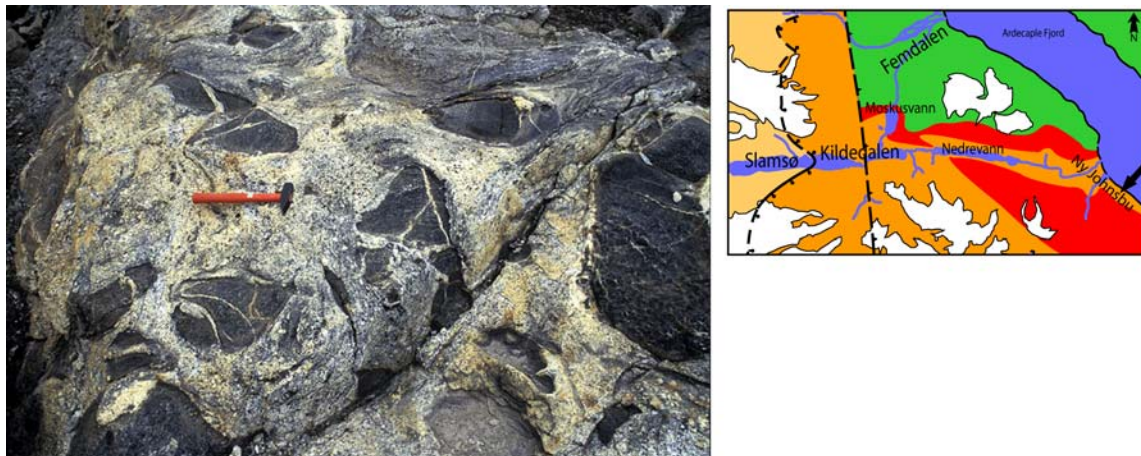


Figure 3.10 Typical appearance of the migmatites along the shores of Ardencaple Fjord. The arrow on the index map indicates location and bearing of the photo.

3.4. The Eleonore Bay Supergroup

The metasediments of the Eleonore Bay Supergroup in the Ardecaple Fjord - Bredefjord are subdivided into two groups; The Nathorst Land Group (lower) and the Lyell Land Group (upper) (Sønderholm and Tirsgaard, 1993). Only the lower part of the Nathorst Land Group, which is the only group present in Kildedalen (Higgins and Soper, 1994), was examined in this study. The metasediments of the Nathorst Land Group, striking northwesterly and dipping, moderately towards NE, have been intensively folded prior to the emplacement of two-mica granites. An excellent example of this is seen at Kap Klinkerfues (Figure 3.11).

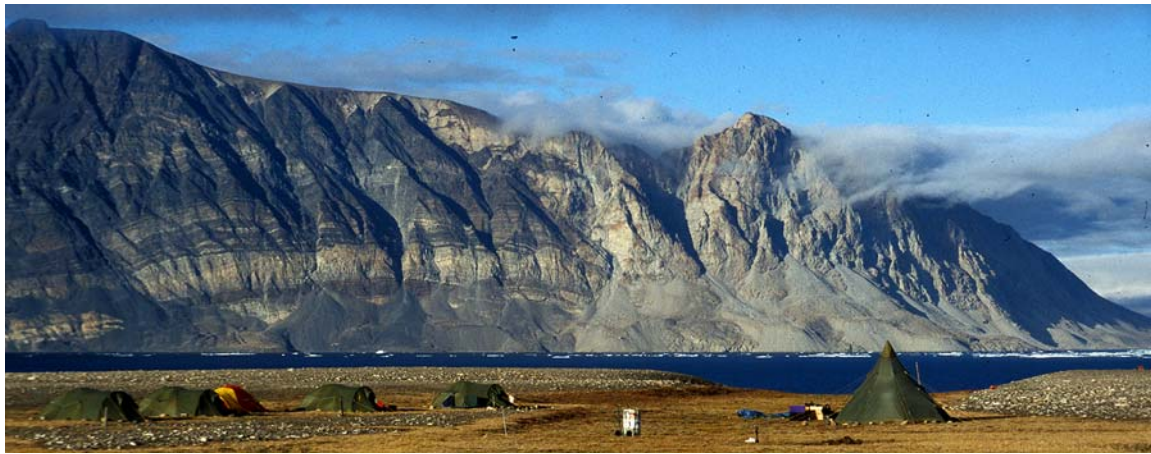


Figure 3.11 The Eleonore Bay Supergroup isfolded at Kap Klinkerfues. The Kap Klinkerfues pluton is the lightly coloured body in the picture. The hight of the mountain wall is c. 1300 m. The picture is taken towards east

3.4.1. Schists of the Eleonore Bay Supergroup

The Eleonore Bay Supergroup is exposed in the peaks on the north side of Kildedalen and in the hillside in the western part of Moskusdal (Figure 3.12).

Friderichsen et al. (1994) interpreted the Eleonore Bay Supergroup and the Smallefjord Sequence to be separated by an extensional shear zone north of Smallefjord. Field evidence for the inferred tectonic boundary was not found in Kildedalen. The contact between the Eleonore Bay Supergroup and the underlying Smallefjord Sequence is instead obscured by a granite intrusion in both areas where it is decently exposed (north of Nedrevann in Kildedalen and the western side of Moskusdal) (Figure 3.2). It is therefore not possible to state the nature of the contact based on the exposures in the Kildedalen area. If a tectonic contact exists between the two units, as postulated by Friderichsen et al. (1994), it either has to pre-date granite emplacement, or it must be a late brittle fault positioned north of our transect.

Around Kildedalen the Eleonore Bay Supergroup does not exhibit the large open folds that are commonly observed in this unit other places in The Ardencaple Fjord area (Higgins and Soper, 1994).

The Eleonore Bay Supergroup exposed on the west side of Moskusdal display a compositional foliation made up of aligned bands of mica and layers of quartz (Chapter 4.5) Granitic dikes, up to 1.5 m thick cut across the compositional foliation, but is weakly deformed itself. No distinct

contact metamorphic fabric was observed either towards the dikes nor towards the granitic intrusion.

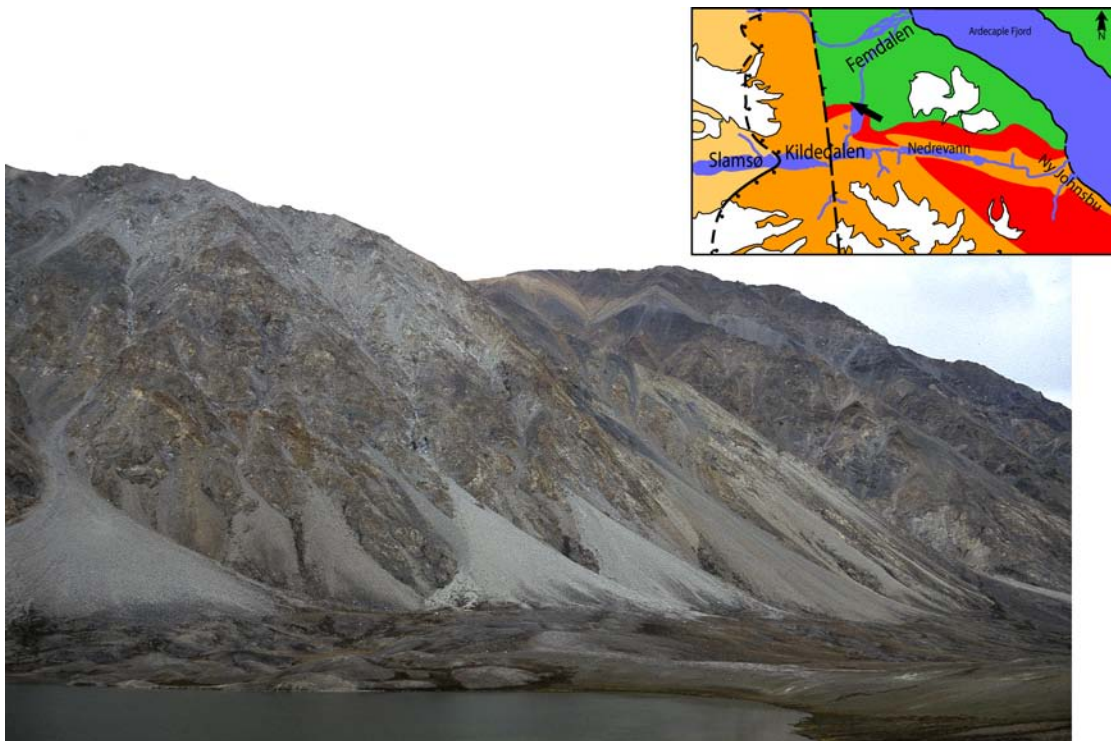


Figure 3.12 This picture shows the Eleonore Bay Supergroup on the western side of Moskusdal. Mountain wall is c. 1000 m high.

3.5. Granites

Large Caledonian granitic bodies (Strachan et al., 2001) are present in the upper part of the Smallefjord Sequence and the lower part of the Eleonore Bay Supergroup in Kildedalen, a phenomenon seen elsewhere in North East Greenland where the Smallefjord/Krummedal Sequence and Eleonore Bay Supergroup are exposed (Kalsbeek et al., 2001). The Kap Klinkerfues pluton is emplaced in the Eleonore Bay Supergroup on the east side of the Ardecaple Fjord (Hansen et al., 1994), and can easily be spotted from Kildedalen. The Kap Buch pluton (Figure 3.1) is interpreted by Hansen et al. (1994) to be emplaced in the transition between the Smallefjord Sequence and the Eleonore Bay Supergroup. They also indicate that the Kap Buch pluton extends from Kap Buch, through the Ny Johnsbu area and further along the north side of Kildedalen all the way to the west side of Moskusdal (Figure 3.1). Due to the Quarternary deposits on the valley floor in both Kildedalen and Moskusdal, this correlation of outcropping intrusive bodies across the valley

floor, cannot be made with certainty. I will therefor deal with the Moskusdal pluton, The Kildedalen pluton and the Kap Buch pluton (Figure 3.1).

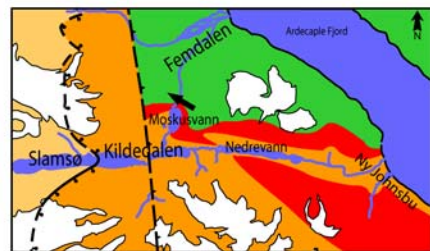


Figure 3.13 The Eleonore Bay Supergroup of western Moskusdal. Granitic dikes descending from the nearby granitic body cut this part of the Eleonore Bay Supergroup. The dike is c. 1 m across.

Both the Moskusdal pluton and the Kildedalen pluton obscure the contact between Smallefjord Sequence and Eleonore Bay Supergroup. The contact with the schists of The Eleonore Bay Supergroup is sharp. For the Moskusdal pluton, a cm-scale chilled margin is present in the granite. The granite content decreases going structurally downwards from the lower part of the plutons and into the migmatites of the Smallefjord Sequence. The contact between the lower part of the plutons and host rock can thus be said to be transitional.

No xenoliths were found in the Moskusdal pluton, as opposed to the other two plutons. The Kap Buch- and the Kildedalen-plutons contain mica-schist xenoliths that are similar to xenoliths in the Migmatite Unit of the Smallefjord Sequence. The Kildedalen plutons also have quartzite xenoliths that could be derived from the Quartzite Sub-unit of the Smallefjord Sequence.

A weak foliation defined by aligned biotite grains is common in the Kildedalen pluton. Quartz veins within the granite are stretched out and boundinaged parallel to the matrix foliation, indicating shortening perpendicular to the foliaiton.

The Kap Buch pluton comprises a strong compositional biotite foliation that is concordantly interbedded with less than 2 m thick quartzite layers.

3.5.1. Granitic veins

Granitic dikes and veins are ubiquitous throughout the allochthonous basement and Smallefjord Sequence, with the exception of the Biotite-gneiss Unit (lowest unit in the Smallefjord Sequence).

Antithetic dikes cut the allochthonous basement. Whether or not these were intruded in separated phases remain unclear, however, two texturally different types of dikes were observed. One type is coarse grained almost pegmatitic and up to several meters thick.

The other type is fine grained and usually less than 30 cm thick.

With the exception of the Biotite-Gneiss Unit, the Smalleford Sequence is cut by leuco-granitic dikes and sills. These veins were emplaced in several phases. Pre- or syn-kinematic veins, less than 0.5 m thick, are common in the Gneiss Unit, whereas post-kinematic dikes, less than 1.5 m thick, are commonly observed in the Migmatite Unit. A compositional foliation defined by biotite was observed in some of the fine to medium grained pre- to syn-kinematic veins, whereas the post-kinematic dikes are unfoliated. Some of the post-kinematic dikes are pegmatitic (Figure 3.16).

Medium to fine grained leuco-granitic dikes cut the Eleonore Bay Supergroup. They are less than 1 m thick and are pre- to syn-kinematic (Figure 3.13).

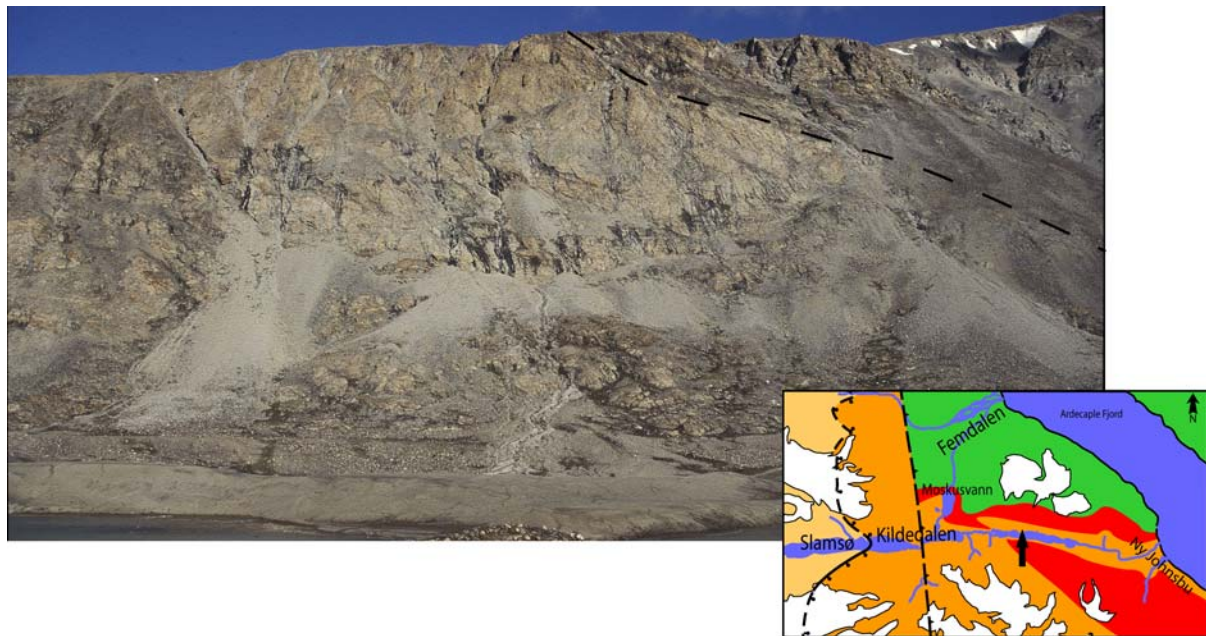


Figure 3.14 North facing photo of the Kildedalen pluton, outcropping between Nedrevann and Moskusdal. The arrow on the index map indicates location and bearing of photo. The dotted line indicates the border between Eleonore Bay Supergroup and the Kildedalen pluton. The mountain wall is c. 1200 m high.

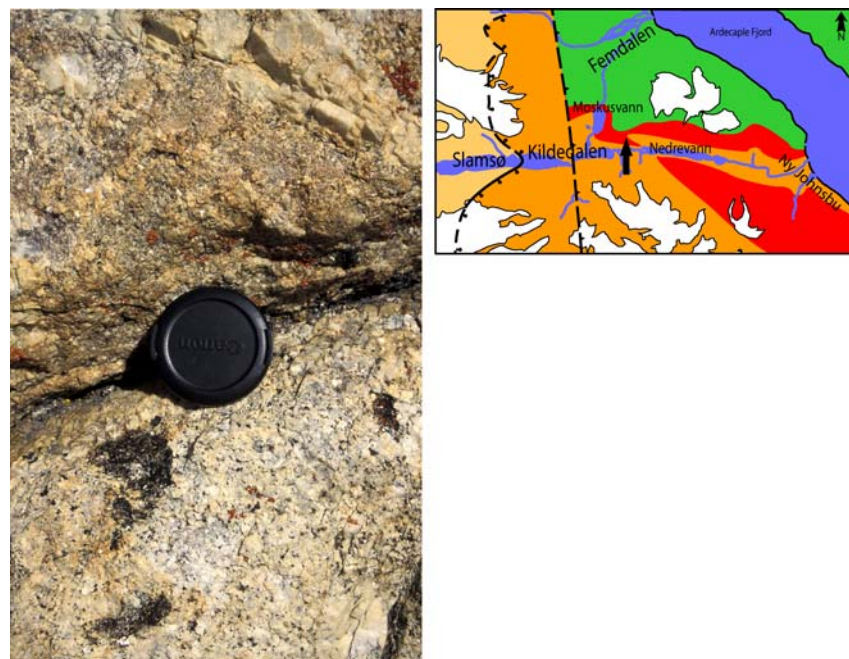


Figure 3.15 Typical appearance of the Kildedalen pluton. Here the more pegmatitic part. The arrow indicates location and bearing of photo.

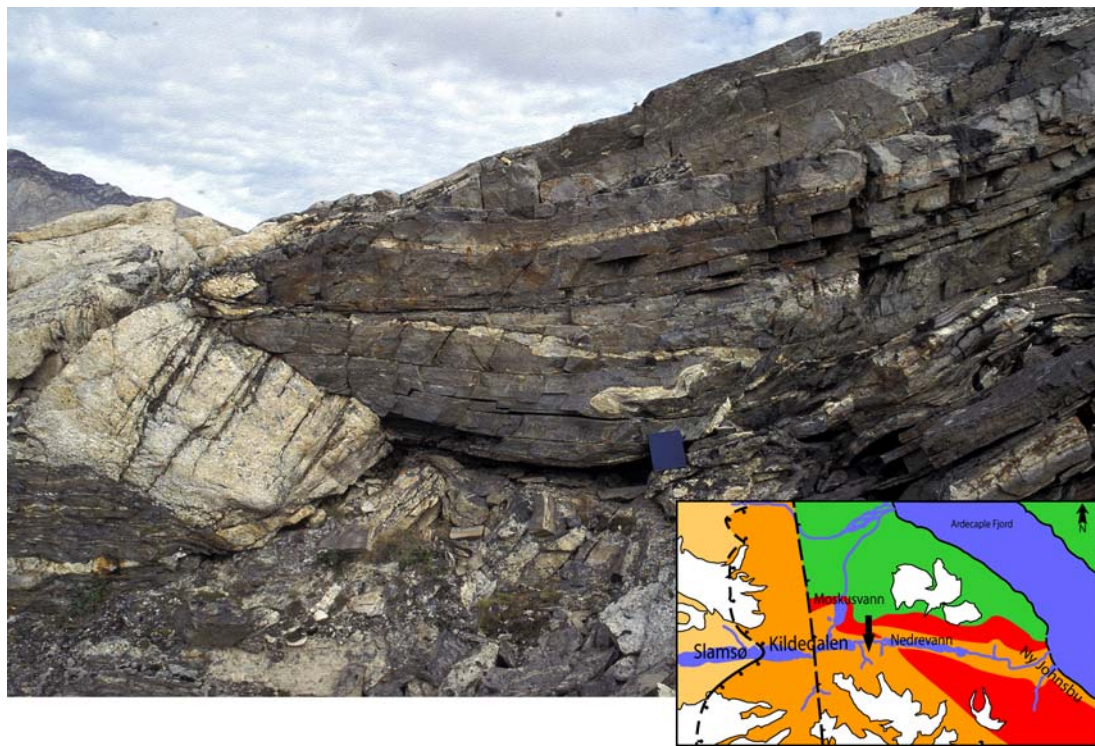


Figure 3.16 This picture shows two different generations of granitic veins, both marked by fine-dotted lines. The old one is severely folded, while the younger one goes straight through the Smallefjord Sequence. The coarsely dotted line marks the foliation. Notebook for scale. The arrow indicates location and bearing of photo.

4. Metamorphic petrology

4.1. Introduction

Three main lithotectonic units are exposed at Kildedalen; allochthonous basement, the Smallefjord Sequence and the Eleonore Bay Supergroup. Allochthonous basement comprises tonalitic gneisses, the Smallefjord Sequence comprises various gneisses, meta-arenites and migmatites, and the Eleonore Bay Supergroup comprises metapsammites.

These units are proposed by others to be tectonically separated (Friderichsen et al., 1994). An extensional shear zone (Kildedalen Shear Zone) is interpreted to separate allochthonous basement from the Smallefjord Sequence, and an extensional fault is interpreted to separate the Smallefjord Sequence from the Eleonore Bay Supergroup (Friderichsen et al., 1994; Strachan et al., 1995; Strachan et al., 2001). In Kildedalen we observed an additional extensional shear zone; the Slamsø Shear Zone overlying the Kildedalen Shear Zone. No evidence for the proposed tectonic boundary separating the Smallefjord Sequence and the Eleonore Bay Supergroup was observed (Figure 3.2). The presence or absence of this extensional feature is of importance for the kinematic evolution of the area, and in particular the exhumation history of the allochthonous basement and the Smallefjord Sequence.

To reveal information about the kinematic evolution of the area three rock samples were collected from rocks of useful composition for P-T studies (Figure 4.1). Samples were collected from either side of proposed tectonic boundaries:

- T6 is a garnet-biotite micaschist from the base of the Slamsø Shear Zone
- AA02-15 is a garnet-biotite micaschist from the upper part of the Slamsø Shear Zone
- AA02-23 is a garnet-biotite metapsammite from the Eleonore Bay Supergroup.

Metamorphic petrology, combined with geothermobarometry, is applied to these samples to elucidate the tectonometamorphic evolution of the Kildedalen area.

Petrographic studies are important, because they provide information on chemical and mineral equilibrium and reaction history (both prograde and retrograde). After petrographic examinations, techniques in geothermometry and geobarometry are applied to chart the P-T evolution of a rock.

Geothermobarometry is a tool for estimating the pressure and temperature of formation of a documented equilibrium mineral assemblage.

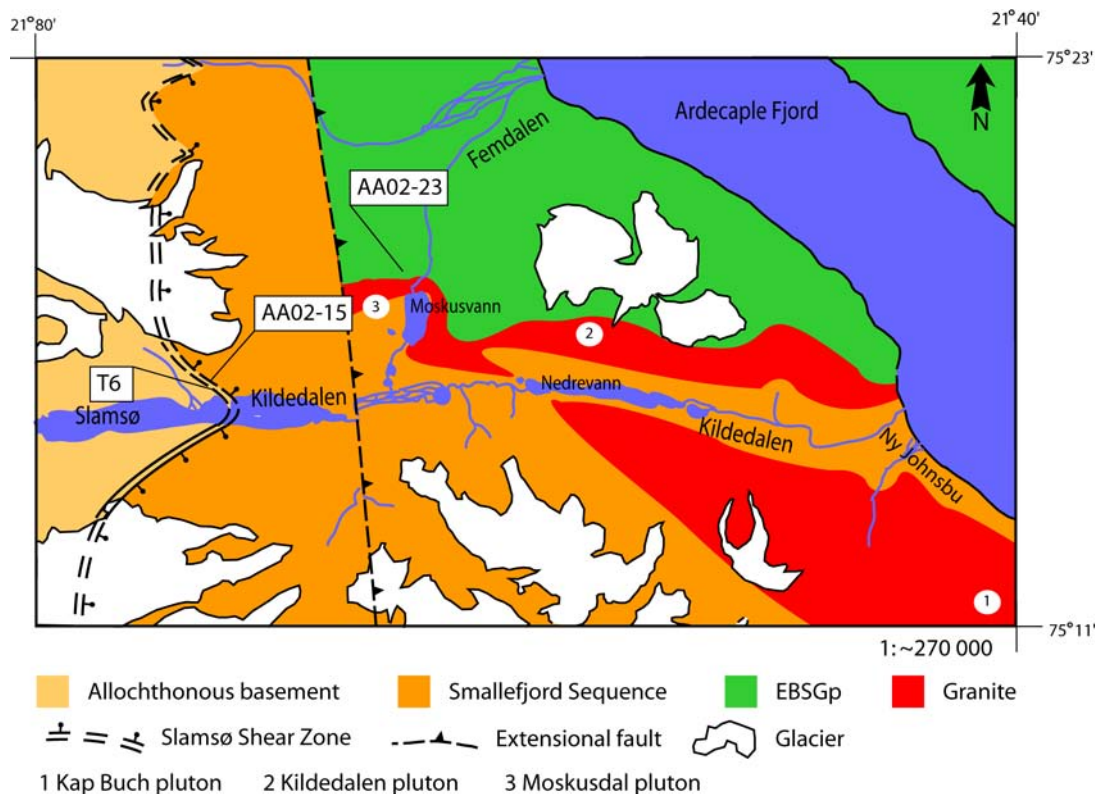


Figure 4.1 Simplified map that shows where the samples (T6; AA02-15; AA02-23) for P-T estimates were collected.

4.2. Methodology

Geothermobarometry and whole rock modeling (DOMINO) was applied to the rock samples collected at Kildedalen. These two methods of estimating pressure and temperature conditions in a rock are based on different types of chemical data: (1) element distribution in different minerals; (2) whole rock chemistry, respectively.

Chemical data of the key minerals were obtained by electron probe micro-analysis (EPMA) using the Cameca SX-100 at University of Oslo. The microprobe is equipped with 5 crystal spectrometers and software by Cameca. The microprobe was calibrated using a range of well characterized natural and synthetic standards. The microprobe was operated with an accelerating voltage of 15 kV, beam current of 10 nA with a focussed spot-size of 2-3 μm . Data reduction was carried out

with a PAP-type correction and all iron was assumed to be ferric iron. X-ray fluorescence analyses using classic fused glass bead techniques provided major-element whole rock chemistry. This work was done at the University of Oslo

4.3. Geothermobarometry

Geothermobarometry is the calculation of metamorphic pressures and temperatures of equilibration using the temperature- and pressure dependence of the equilibrium constant as a benchmark (Spear, 1993). Stable minerals and mineral assemblages are dynamic and will change in response to variations in pressure and temperature by reactions and/or chemical diffusion. Some mineral reactions are pressure sensitive (barometer) whereas others are temperature sensitive (thermometer). Different calibrations exist for different geothermobarometers. Some of the calibrations are based on empirical models, whereas others are based on naturally occurring rocks (Spear, 1993). There are two types of reactions; net-transfer reactions and exchange reactions.

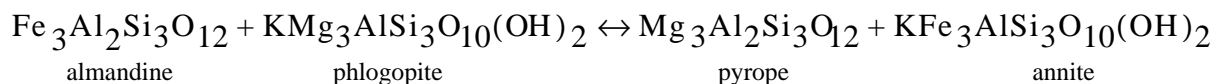
4.3.1. Geothermometry

Exchange reactions control a large number of the geothermometers. This kind of reaction involves the exchange of cations between silicates. Exchange reactions make good geothermometers because they are temperature sensitive and involve small volume changes ($\Delta V_{reaction}$).

A large number of exchange geothermometers have been studied over the last 30 years, and several slightly different calibrations exist for the most important ones (Spear, 1993). One of the most widely used well and calibrated geothermometer is the garnet-biotite exchange geothermometer (Holdaway, 2000), which will be applied in this work.

4.3.1.1. The Fe-Mg garnet-biotite exchange thermometer

The equilibrium equation between garnet and biotite can be written as follows (Spear, 1993):



This can be written as a cation exchange reaction between garnet and biotite:



Perchuk and Lavrent'eva (1983) presented and equation to calculate temperature:

$$T(C) = \frac{7843.7 + \Delta V(P - 6000)}{1.987 \ln K_D + 5.699} - 273 \quad (\text{Eq 1})$$

where V = a volume constant, P = pressure in bars, T = temperature in degrees celcius and K_D is the equilibrium constant.

Holdaway's (2000) more recent equation for calculating temperature is:

$$T(K) = \frac{40198 + 0.295P + G + B}{7.802 - 3R \ln K_D} \quad (\text{Eq 2})$$

where R (gas constant) = 8.3144 and P is in bar, $T(K)$ is temperature in Kelvin and G and B are evaluated in terms of Margules Parameters for garnet and biotite, respectively. K_D is the equilibrium constant (Holdaway, 2000).

4.3.1.2. History of the garnet-biotite thermometer

The first garnet-biotite calibrations were based on plots of K_D (distribution constant) vs. estimated values of T (Thompson, 1976; Holdaway and Lee, 1977). Ferry and Spear (1978) introduced the first experimental calibration, involving a KFMASH system with a low Al biotite. Hodges and Spear (1982) then mixed an assumed ideal biotite in the Ferry and Spear (1978) calibration with the Ganguly and Kennedy (1974) solution model for garnet and the Newton et al. (1977) CaMg garnet Margules parameters. Perchuk and Lavrent'eva (1983) made an experimental calibration using pelites with garnet, biotite (with high Al content) and cordierite. Ca and Mn in garnet and Ti in biotite were not analyzed in most run products but were assumed to be the same as in starting material. Ganguly and Saxena (1984) improved the non ideality in garnet, and Indares and Martignole (1985) highlighted the importance of correcting for non-ideality in biotite due to Ti and Al substitution. Berman (1990) and McMullin et al. (1991) used linear programming methods to develop a garnet-biotite geothermometer that includes the effects of Ti and Al in biotite. Gessmann et al. (1997) calibrated the garnet-biotite geothermometer in the pure KFMASH system, in addition to addressing the behaviour of aluminium in biotite, and formulated a geothermometer based on their data combined with data from Ferry and Spear (1978). Mukhopadhyay et al. (1997) estimated entropy, enthalpy and volume Margules parameters for the FeMgCa garnets using a

regression method. The advantage of this method is its ability to provide error values. Berman and Aranovich (1996) did similar work, but with mathematical programming methods.

Ganguly et al. (1996) estimated enthalpy and entropy Margules parameters for FeMgCaMn garnets based on new and previous experimental data. Their model is the only one available for the MnMg binary.

Holdaway et al. (1997) devised an optimization approach to compensate for the average dilution of Mn and Ca in garnet and Ti in biotite of the Perchuk and Lavrent'eva (1983) experiments. This method also includes corrections for estimated Fe^{3+} in biotite and garnet.

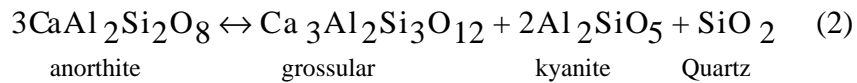
Holdaway (2000) presents a recent calibration where a comparison of various experimental data-sets and garnet Margules parameters are undertaken (Berman and Aranovich, 1996; Ganguly et al., 1996; Mukhopadhyay et al., 1997). Based on this an average garnet model was proposed, and this average garnet model was found to yield excellent results. Holdaway (2000) stresses the importance of not applying the exchange constants and Margules parameters from this work to other systems than garnet-biotite. The reason for this is that the parameters work well in combination for garnet-biotite because a systematic error in one parameter is compensated for by a systematic error in another, and in this way enhancing the accuracy of the results obtained.

4.3.2. Geobarometry

Many geobarometers are based on net transfer reactions that, by definition, produce and consume phases. Net-transfer reactions often result in a significant change in volume ($\Delta V_{reaction}$), and hence are suitable geobarometers. The equilibrium constant is thus said to be pressure sensitive (Spear, 1993). Various geobarometers have been proposed and used over the last three decades (Spear, 1993). One geobarometer that is thoroughly studied and widely used is the GASP geobarometer (garnet - aluminium silicate - plagioclase - quartz). GBPQ (garnet - biotite - plagioclase - quartz) is another barometer that is based on GASP, but is valid for samples depleted in aluminium silicates (Wu et al., 2004). Both GASP and GBPQ were applied to the samples collected at Kildedalen.

4.3.2.1. The GASP geobarometer

The GASP geobarometer is based on the reaction (Spear, 1993):



The ratio of the mol fraction of grossular in garnet to the mol fraction of anorthite in plagioclase defines the equilibrium constant; $K_{eq} = (X_{grs}/X_{an})^3$, so a decrease in K_{eq} indicates an increase in the anorthite content in plagioclase or a decrease in the grossular content of garnet, or both (Spear, 1993). Geobarometry is mainly applied on solid-solid reactions, which means that the partial pressures of fluid species can be neglected (Spear, 1993). Pressure was calculated using the equation (Winter, 2001):

$$0 = -48357 + 15066T(\text{K}) - 0.6608P(\text{MPa}) + RT\ln K \quad (\text{Eq 3})$$

which is the one applied by Ferry and Spear (1978), with modified thermodynamic constants. $R = 8.3144$ (gas constant), T is temperature, P is pressure and K is the equilibrium constant for non-ideal garnets (Ghent, 1976).

4.3.2.2. History of the GASP geobarometer

Two of the most cited calibrations of GASP are those of Hodges and Spear (1982) and Berman (1988, 1990). The Hodges and Spear calibration predates later end-member calibrations and recent garnet and plagioclase activity models. It uses a local charge balance plagioclase activity model with an activity coefficient of 2.0.

The Berman calibration includes the Koziol and Newton (1988) endmember calibration. It is based on Berman's own database and uses the garnet activity model of Berman (1990), the garnet-biotite geothermometer of McMullin et al. (1991) and the plagioclase model of Furhman and Lindsley (1988)

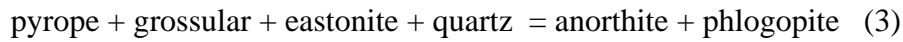
4.3.2.3. The GBPQ geobarometer

A recent calibration of the GBPQ geobarometer, (Wu et al., 2004) that is based on the GASP geobarometer, is applicable to rocks without aluminium silicates, muscovite, or both. The recently

calibrated garnet-biotite geothermometer (Holdaway, 2000) and the GASP geobarometer (Holdaway, 2001) yield P-T estimates for both experimental charges and natural rock assemblages that are much more precise than those obtained using alternative calibrations, and are thus used for the calibration of the GBPQ geobarometer (Wu et al., 2004).

The GBPQ geobarometer was calibrated and tested through three steps. First 224 aluminium-silicate bearing metapelites from the literature were collected to calibrate the GBPQ geobarometer. Second, an additional 89 aluminium-silicate bearing metapelites excluded from the original calibration, were used to test the validity of the GBPQ. Finally, the GBPQ geobarometer was applied to aluminium-silicate bearing and/or aluminium-silicate absent metapelites from different geological settings, to test the applicability of the GBPQ geobarometer. The results show that the GBPQ geobarometer may be applied to either aluminiumsilicate-bearing or aluminiumsilicate-absent, medium to high-grade metapelites.

GBPQ is based on the Mg- and Fe-model equilibria by Hoisch (1990;1991):



$\text{Pyrope} = \text{Mg}_3\text{Al}_2\text{Si}_3\text{O}_{12}$	$\text{Grossular} = \text{Ca}_3\text{Al}_2\text{Si}_3\text{O}_{12}$	$\text{Eastonite} = \text{K}(\text{Mg}_2\text{Al})(\text{Si}_2\text{Al}_2)\text{O}_{10}(\text{OH})_2$
$\text{Quartz} = \text{SiO}_2$	$\text{Anorthite} = \text{CaAl}_2\text{Si}_2\text{O}_8$	$\text{Phlogopite} = \text{KMg}_3(\text{AlSi}_3)\text{O}_{10}(\text{OH})_2$
$\text{Almandine} = \text{Fe}_3\text{Al}_2\text{Si}_3\text{O}_{12}$	$\text{Siderophyllite} = \text{K}(\text{Fe}_2\text{Al})(\text{Si}_2\text{Al}_2)\text{O}_{10}(\text{OH})_2$	$\text{Annite} = \text{KFe}_3(\text{AlSi}_3)\text{O}_{10}(\text{OH})_2$

Tabell 4.1 Mineral compositions for minerals involved in the reactions.

Activity models used by Wu et al. (2004) are the average garnet model of Holdaway (2000), the Al-avoidance model for plagioclase after Fuhrman and Lindsley (1988) and the biotite model from Holdaway (2000). The GBPQ formulas for pressure calculations are (Wu et al., 2004):

$$\text{P(1)(bars)} (1 - 0.081(-6\text{Fb} + \text{Mgb} + 2\text{Cab})) = -24450.7 + 40.238\text{T(K)} + 59256.2\text{X}_{\text{Fe(bio)}} + 5173.9(\text{X}_{\text{Mg(bio)}} - \text{X}_{\text{Al(bio)}}) + 6393.4\text{X}_{\text{Ti(bio)}} + 0.081\text{T(K)} (-\text{R ln}K_{(1)} - 6\text{Fa} + \text{Mga} + 2\text{Caa} - 788.7\text{X}_{\text{Fe(bio)}}) - 6\text{Fc} + \text{Mgc} + 2\text{Cac} \quad (\text{Eq 4})$$

$$\begin{aligned}
 P(2)(\text{bars}) (1 - 0.081(-6Fb + Feb + 2Cab)) = & -19871.0 + 30.75T(\text{K}) + 66622.5(X_{\text{Fe(bio)}} - X_{\text{Al(bio)}}) \\
 & + 1363.1X_{\text{Mg(bio)}} - 74704.2X_{\text{Ti(bio)}} + 0.081(T(\text{K})(-\text{Rln}K_{(2)} - 6Fa + Fea + 2Caa - 840.9X_{\text{Fe(bio)}} + \\
 & 52.2X_{\text{Mg(bio)}} + 840.9X_{\text{Al(bio)}} + 1111.2X_{\text{Ti(bio)}} - 6Fc + Fec + 2Cac))
 \end{aligned} \quad (\text{Eq } 5)$$

Calculated P(1) and P(2) are fairly equal, and an average value is used (Wu et al., 2004). Fa, Fb and Fc are polynominal expressions for the end-members of plagioclase, and Caa, Cab, Cac, Fea, Feb, Fec, Mga, Mgb and Mgc are polynominal expressions for the end-members of garnet (Appendix, Wu et al., 2004). $K_{(1)}$ and $K_{(2)}$ are equilibrium constants. The theromdynamic constants are intergrated into the equations (Wu et al., 2004).

4.3.3. Thermodynamic Modeling using Whole-Rock Systems

The samples (T6, AA02-15 and AA02-23) were analysed using x-ray flourecence to produce whole rock chemistry (weight % of oxides) for each sample. The DOMINO software (De Capitani and Brown, 1987) used in this study calculates stable equilibrium mineral assemblages for a given P-T range by Gibb's energy minimization. Based on whole rock chemistry analyses, the theriak algorithm calculates the Gibbs free energy for any mineral assemblage possible at designated point in P-T space. The assemblage with the lowest Gibbs free energy is assumed to be stable. DOMINO repeats the process across a range in P-T space and identifies points of identical stability and constructs stability fields in P-T space (De Capitani and Brown, 1987).

The assumptions made by theriak-DOMINO

The chemical systems analysed are considered to be closed, meaning the bulk composition is fixed. The number of independent variables are fixed at two, based on the assumption that there are only two types of energy, namely heat and energy related to pressure-volume work. The second law of thermodynamics states that the equilibrium state is the state in which the total entropy of the closed system and its surroundings is at a maximum. With independent variables being temperature and pressure, this state is also characterized by a minimum in the Gibbs free energy of the closed system (De Capitani and Brown, 1987).

The algorithm used to establish stable assemblages in P-T space can be summarized as follows (De Capitani and Brown, 1987) :

- 1 -Search each solution phase for the composition with the smallest Δ_fG . This will provide a list of considered phases.
- 2 -Find from all considered phases an assemblage with minimum Δ_fG .
- 3 -The new assemblage from step 2 is considered the new reference state. Δ_fG of all phases are computed relative to this assemblage. This change of foundation leaves us in the same situation as prior to step 1. Continuation goes again from step 1.

Thus theriak calculates stability at a point in P-T space and DOMINO creates stability fields in P-T space by connecting the theriak estimates.

Temperature, pressure and bulk composition is given. The list of considered phases contains initially the names, the compositions and Δ_fG for all possible phases of fixed composition. Δ_fG of each solution is a known function of the composition.

4.4. Pitfalls of thermobarometry

The estimation of peak metamorphic pressures and temperatures of a high grade rock will often be obscured by disequilibrium in the post-peak assemblage brought on by retrogression. The processes that are most important are phase reactions and intracrystalline diffusion (Spear and Florence, 1992). In order for geothermobarometry to be successfull, mineral compositions characteristic of the peak equilibrium conditions must be indentified and the effects of reaction history during cooling and the cooling rate considered. Ideally this includes knowledge about retrograde net-transfer reactions and exchange reactions (Spear and Florence, 1992). Identification of either exchange reactions and/or net-transfer reactions operating in a mineral assemblage is very important for thermobarometry (Spear and Florence, 1992). Failure to discuss these questions lead to errorous estimations of the metamorphic conditions prevelent in the rock.

4.4.1. Diffusion and net-transfer reactions

Volume, or Fickian, diffusion is an important concept in metamorphic petrology and is primarily controlled by the diffusion porosity of a mineral, the size of the diffusing species, the thermodynamic stability of the species in the crystalline lattice and the temperature. Due to the wide range of controlling factors it must be appreciated that individual elements and minerals are all influenced to a different degree by diffusion.

To show the importance of diffusion, and the effects it may have on the geothermometer used in this study, the results of an experiment regarding the (Fe/Fe+Mg) ratio in coexisting garnet and biotite when cooling from peak metamorphic conditions is shown in figure 4.2 (a)-(b). During cooling the Fe/(Fe+Mg) ratio in the garnet rim will increase as opposed to the Fe/Mg content in the biotite rim. Due to the higher efficiency of intracrystalline diffusion in biotite, its composition is homogeneous. In contrast garnet develops a heterogeneous chemistry and displays chemical zonations. This is because intracrystalline diffusion in garnet is inefficient at temperatures lower than 675 °C (Spear and Florence, 1992).

Numerical modeling by Spear (1991) shows that diffusion rates are great enough to homogenize a garnet at temperatures 650 - 700 °C. At lower temperatures garnet will develop zonations because the velocity of diffusion is not great enough to reach the core of the crystal. The extent of the chemical zonation, or degree of homogenization is also partially controlled by garnet radius (Figure 4.3).

Intracrystalline diffusion in biotite will be significant enough to homogenize biotite above ~500 °C irrespective of crystal size and cooling rate (Spear, 1991; Spear and Florence, 1992). It is also important to note that biotite will exhibit no decrease in the Fe/Mg content if infinitely abundant (Spear and Florence, 1992).

If a net-transfer reaction occurs concomitant with Fe-Mg exchange during cooling, the Fe/Mg ratio in both garnet and biotite will increase (Figure 4.2 (c)). In figure 4.2(d) garnet is the product and biotite the reactant, with an increasing Fe/(Fe+Mg) content in both minerals. Note that the garnet becomes physically smaller in figure 4.2(b)-(d)

Problems may thus appear in the aftermath of the biotite producing reaction (8). Biotite integrates the Fe released by garnet leading to a situation where retrograde biotite records a higher Fe content than peak metamorphism biotite. The Fe/(Fe+Mg) content will also increase during cooling (Figure 4.2(d)). If such biotite is used in a calibration along with core garnet, the calculated temperature will be too high (Spear and Florence, 1992).

Diffusion processes also influence the results of geobarometers dependent on net-transfer reactions.

The GASP geobarometer, based on the Ca content in garnet and plagioclase, depends on ratio of grossular to anorthite in the presence of quartz and aluminium silicate (Spear, 1993). For the

GASP geobarometer to be applicable, the rock must have produced or consumed plagioclase and garnet (Spear and Florence, 1992). The penetration distance for Ca in garnet is much less than for other elements (Fe, Mg, Mn) due to the slower diffusivity for Ca, and hence Ca content of the garnet core is likely to have been in equilibrium with plagioclase at peak metamorphic conditions (Spear and Florence, 1992).

Plagioclase does not re-equilibrate by diffusion. The intracrystalline diffusion of NaSi-CaAl in plagioclase, at temperatures below 900°C is too slow. Hence the only way plagioclase can re-equilibrate with coexisting garnet is to recrystallize to a new composition. It is common for

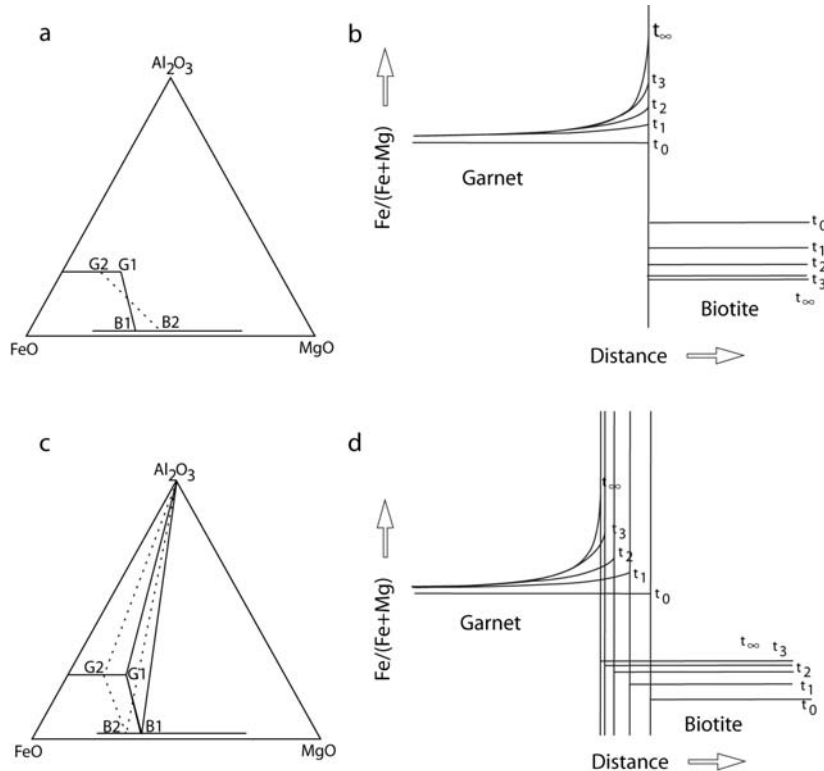


Figure 4.2 (a) and (c) are AFM diagrams while (b) and (d) show composition versus distance. (a) and (b) show the results of Fe-Mg exchange between biotite and garnet at different timesteps. (c) and (d) show development of the same exchange reaction as (a)(b), plus the net-transfer reaction garnet + K-feldspar + H₂O = sillimanite + biotite + quartz. From Spear and Florence (1992)

plagioclase to recrystallize, but the amount of recrystallized plagioclase and its location cannot be determined by thermodynamic arguments alone (Spear and Florence, 1992).

During retrogression the X_{Grs} content in garnet rims decreases, and X_{An} increases in plagioclase. The recrystallizing plagioclase will only be in equilibrium with the garnet rims. Thus if the

recrystallized plagioclase is used together with garnet cores for the determination of peak metamorphism the results will be erroneous.

4.4.2. Garnet

Chemical zonation in garnet and mineral inclusions provide information about a rock's evolution on the prograde- and retrograde paths. A classic paper on diffusion in garnets suggests two typical zoning patterns in almandine-rich garnets (Yardley, 1977). Low-grade terrane garnets commonly have Mn and Ca enriched in the core relative to the rim, and Fe and Mg content highest at the rim. This type of zonation is attributed to chemical fractionation between the garnet and the matrix during prograde growth (Yardley, 1977). The elements in high-grade terrane garnets are generally evenly distributed across the crystals, However, Mn can be enriched at the rims (Yardley, 1977). Later work (Spear, 1993; Carlson, 2002) has suggested that the latter zoning pattern is the result of diffusion.

The behaviour of garnet during cooling, shown in figure 4.3, visualizes the results of an experiment on the development of chemical zonation in different garnet crystal sizes when cooled from 750 °C to 400 °C at 10 °C/Ma. The results for a 1000 μm garnet are shown; The dotted lines are thermobars and the solid lines are final zonation profiles. The zonation is presented with respect to the Fe/Mg ratio within garnet. Zonation of the garnets' core (radius = 0 μm) does not halt until the temperature is approximately 650 °C. Although the garnet composition changes continuously during cooling, the difference in Fe/Mg ratio between core (radius=0 μm) and rim (radius=1000 μm) develops exponentially, and is pronounced at temperatures < 650 °C (Figure 4.3(a)). Two other zonation profiles (100 μm and 500 μm) indicate that the effects on the chemical composition of the core is strongly influenced by garnet radius (Spear 1991).

Figure 4.3(b) shows the calculated core temperature plotted against normalized radius at a cooling rate of 10 °C/Ma. The garnets surveyed have a radius of 100 μm, 500 μm, 1000 μm and 5000 μm. This plot indicates that the highest possible calculated core temperature is 700 °C for a garnet with a radius = 1000 μm, if the cooling rate is set at 10 °C/Ma. The dotted 5000 μm lines also show that increased cooling rate will yield higher values for calculated core temperatures (Spear 1991).

Carlson (2002) addresses the differences in intergranular diffusion-rates between elements. The work suggests that even in the absence of textural evidence of incomplete reaction, common pro-grade metamorphic reactions may not achieve equilibrium for many elements. The rates of intergranular diffusion of Fe and Mg are sufficient to produce centimeter-scale equilibration over metamorphic time scales, even at the lowest temperatures of metamorphism. The diffusion of Mn is believed to increase from sluggish to relatively rapid intergranular diffusion rates between lower and upper greenschist facies, while Ca has a relatively slow intergranular diffusion-rate and is likely not to equilibrate at temperatures lower than upper amphibolite facies (Figure 4.4) (Carlson, 2002).

4.4.3. Plagioclase

Rather than re-equilibrate, plagioclase recrystallizes if conditions permit. A consequence of this is that plagioclase composition is commonly heterogeneous in a rock at both amphibolite- and granulite facies (Spear and Florence, 1992). This means that plagioclase grains for GASP barometry must be carefully selected. For calculations of peak metamorphic conditions one would be advised to avoid aggregates of plagioclase (Spear and Florence, 1992).

4.4.4. Biotite

Biotite is involved in retrograde exchange reactions. Although diffusion is relatively efficient in biotite (Spear, 1991), it does not guarantee the homogeneity of biotite. Fe and Mg are commonly replaced by Ti and Al in naturally occurring biotite (Indares and Martignole, 1985). A positive correlation exists between Ti in biotite and metamorphic grade (Figure 4.12) (Dymek, 1983) whereas the Al content is more a function of rock chemistry (Indares and Martignole, 1985)

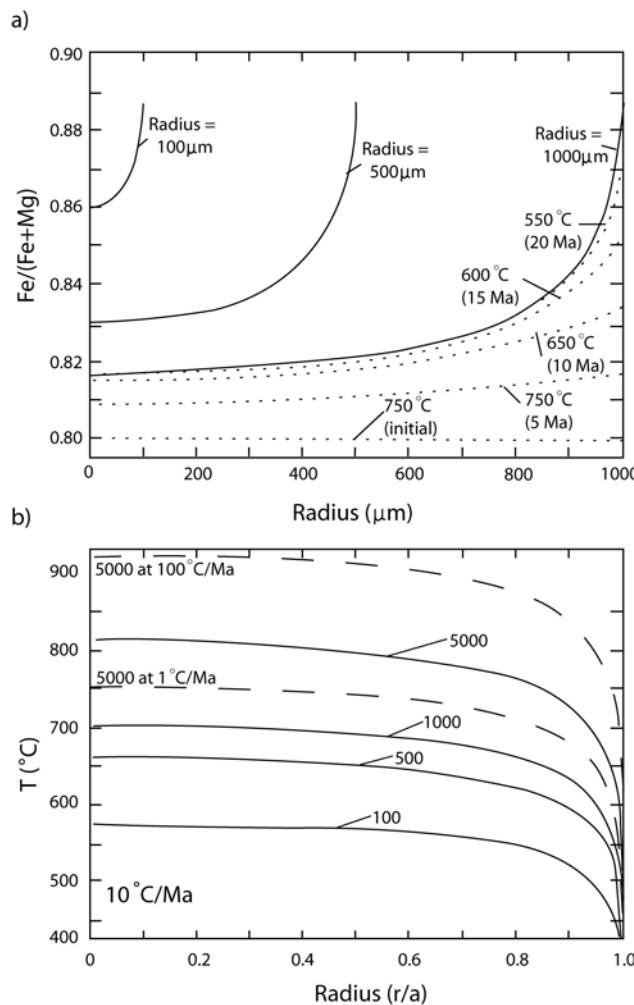


Figure 4.3 (a) Plots modified from Spear (1991). $\text{Fe}/(\text{Fe}+\text{Mg})$ versus radius for garnets cooled from 750 $^{\circ}\text{C}$ to 400 $^{\circ}\text{C}$. The cooling rate is set to 10 $^{\circ}\text{C}/\text{Ma}$. The solid lines show final zonation profiles. The dashed lines show the evolution of diffusion zoning for garnets of radius 1mm. (b) Shows calculated temperatures versus normalized radius for garnets of different size when the cooling rate is set at 10 $^{\circ}\text{C}/\text{Ma}$. The 5000 μm garnet is also plotted for cooling rates 1 $^{\circ}\text{C}/\text{Ma}$ and 100 $^{\circ}\text{C}/\text{Ma}$ (dashed lines).

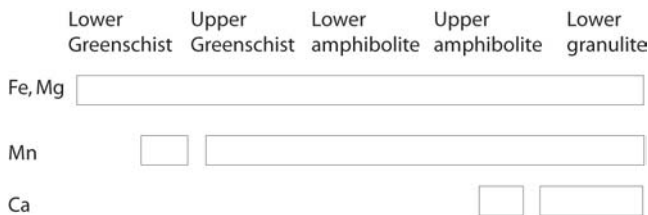


Figure 4.4 The blocks indicate at which metamorphic facies different elements are likely to equilibrate through diffusion. Ca equilibrates only from upper amphibolite facies. Modified from Carlson (2002).

4.5. Rock samples and reaction history

Large garnet, plagioclase and K-feldspar crystals are consequently labelled “blasts” (porphyroblasts) in the following petrological descriptions of the rock samples T6, AA02-15 and AA02-23. The (porphyroblasts) blasts are recrystallized through deformation, and could also be labelled “clasts” (porphyroclasts). The abbreviations used in the following mineral reactions are based on Kretz (1983). The abbreviation for feldspar is equal to the one used in DOMINO (De Capitani and Brown, 1987).

Grt	Garnet	Ilm	Ilmenite	Bt	Biotite
Phg	Phengite	Fst	Feldspar	Mt	Magnetite
Qtz	Quartz	Sil	Sillimanite	Rt	Rutile
St	Staurolite	Chl	Chlorite	Ky	Kyanite
Crd	Cordierite	Opx	Orthopyroxene	Pl	Plagioclase

Table 4.2 Overview of mineral abbreviations (De Capitani and Brown, 1987).

4.5.1. The high- to medium-grade Smallefjord Sequence

The extensional Slamsø Shear Zone separates the Smallefjord Sequence from the underlying allochthonous basement (Chapter 5.2). Several sheared garnet-biotite schists layers of the Smallefjord Sequence make up the shear zone. Samples of two 20 m thick layers of garnet-mica schist were selected for P-T calculations. The structurally lowermost sample (T6) is a garnet-mica schist from the bottom of Slamsø Shear Zone. Sample AA02-15 was obtained from the middle part of Slamsø Shear Zone, 200 m above the contact.

T6

T6 is a mylonitic pelite with distinct S, C and C' bands. The S and C bands are sub-parallel and comprise ribbon quartz and biotite. The C' bands (shear bands) cut the S and C bands at c. 30° and consist of biotite.

The matrix comprises quartz, plagioclase, K-feldspar, biotite, ilmenite and chalcopyrite (Figure 4.5), and exhibits a mylonitic texture.

Bands of syn-kinematic biotite and quartz that have flowed around porphyroblasts of garnet and plagioclase (Figure 4.6). Quartz bands comprise quartz sub-grains.

The sieve textured, subhedral and generally fractured garnet porphyroblasts are less than 3000 µm in diameter. Inclusions in the porphyroblasts are predominantly quartz, but also include ilmenite, biotite, plagioclase and amphibole (Figure 4.5). Plagioclase porphyroblasts are the same size as the garnets. Some plagioclase porphyroblasts display carlsbader twinning.

Mineral reactions in T6

The stability field of the mineral assemblage garnet + quartz + plagioclase + K-feldspar + biotite + ilmenite + chalcopyrite in this sample can be constrained to less than 900°C by not crossing the reaction:



Textural arguments for not crossing reaction (5) are the stability of quartz and biotite and absence of orthopyroxene.

The absence of rutile sets an upper pressure limit at c. 12 kbar after:



AA02-15

This rock is a mylonitic pelite (Figure 4.7, 5.12) with a matrix comprising quartz, plagioclase, K-feldspar, sillimanite, muscovite and biotite. Continuous bands of mica and discontinuous bands of quartz, developed through metamorphic differentiation, dominate the matrix. Blasts of garnet and plagioclase are present along with large aggregates of K-feldspar. The S and the C bands depict the penetrative foliation and are cut by the younger C' shear bands (Figure 5.11). The S and C bands are sub-parallel and comprise ribbon quartz and aligned biotite and muscovite. The C' bands are continuous and made up of biotite and muscovite.

Muscovite and biotite are both common, with biotite being more abundant and fine grained than muscovite. Muscovite and biotite are present in bands that flow around garnets. The quartz bands

are syn-kinematic and contain inclusions of biotite. The serrated grain boundaries within the ribbon quartz domains suggest that quartz is unrecovered.

Sillimanite occurs as slender crystals within the mica bands, but can also be observed as clusters that are bent during deformation, suggesting sillimanite is both pre- and syn kinematic. Truncated pre-kinematic kyanite is present at the center of sillimanite clusters (Figure 4.8).

Garnet and plagioclase appear as subhedral porphyroblasts while K-feldspar appears as anhedral porphyroblasts, and aggregates of blasts. Plagioclase blasts and K-feldspar blasts are both less than 1500 µm across. Plagioclase blasts are pinitized internally and elongated with rounded smooth rims. K-feldspar blasts are elongated with smooth rims.

Fine grained K-feldspar is also present in the matrix, and as inclusions in garnets. Some K-feldspar inclusions display both albite and carlsbader twinning in a perthite texture. This is evidence of feldspar evolution during cooling.

Garnet crystals appear as elongate porphyroblasts that are 1500-3000 µm in length. Inclusions in garnet include biotite, quartz, plagioclase and zircon. Some garnet rims are retrogressed and the embayment is filled with fine grained biotite, plagioclase, sillimanite and muscovite. The garnets are fractured

Mineral reactions in sample AA02-15

The observed mineral assemblage consists of garnet + quartz + plagioclase + K-feldspar + biotite + muscovite + sillimanite +/- kyanite.

Leucosome lenses in the metasediments of the Smallefjord Sequence indicate partial melting, the presence of aluminium silicate + K-feldspar, and garnet enclosing plagioclase, biotite and quartz indicates that the reactions:



took place. These prograde reactions define minimum P-T conditions of c. 750-800 °C and 6.5 kbar. The peak metamorphic conditions can be constrained at < 900 °C by not crossing reaction (5), and less than c. 12 kbars by not crossing reaction (6)

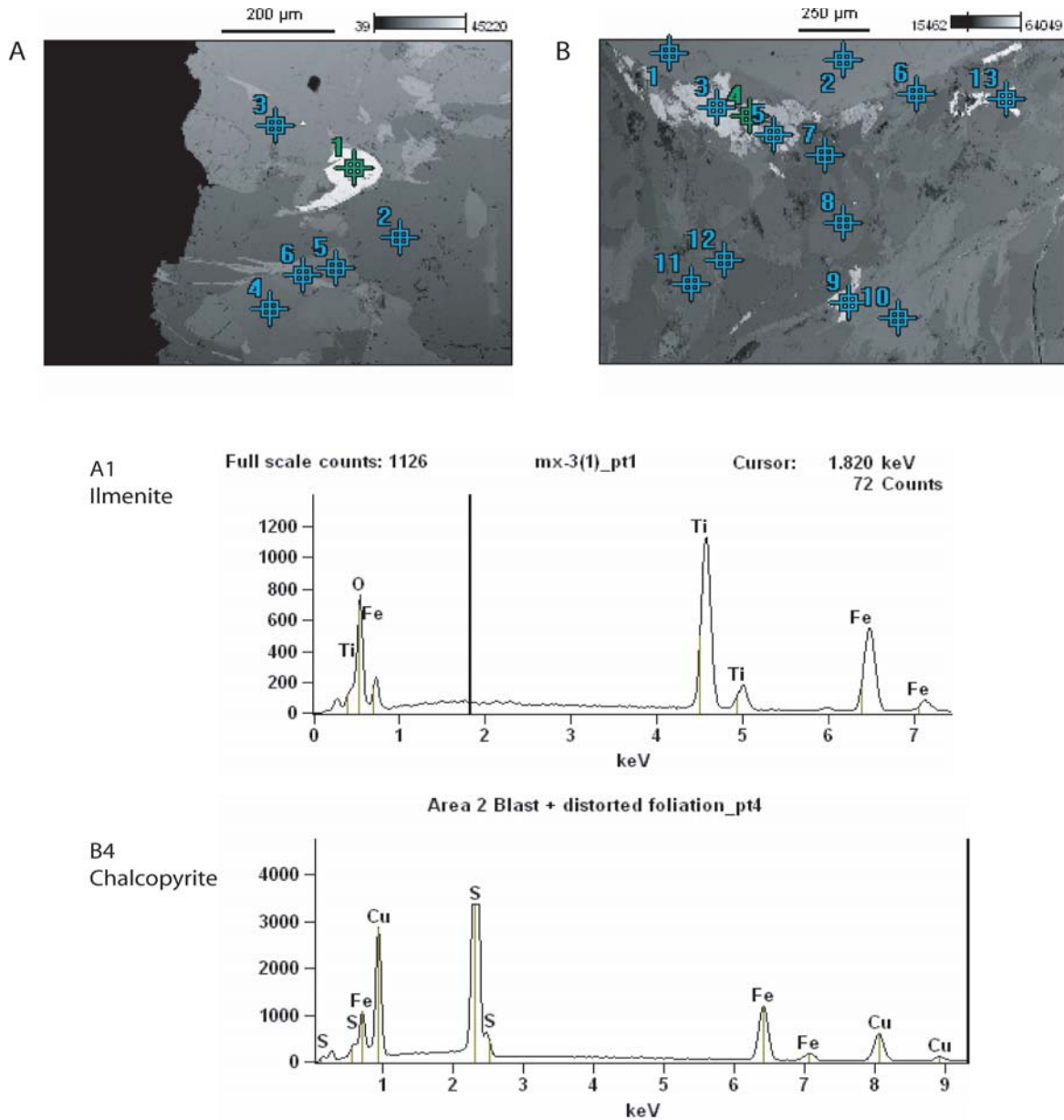


Figure 4.5 Back scattered electron images showing the appearance of ilmenite and chalcopyrite in sample T6.

Textural arguments for not crossing reaction (5) are that quartz and biotite are stable phases and the absence of orthopyroxene.

Retrograde cooling is represented through reaction:



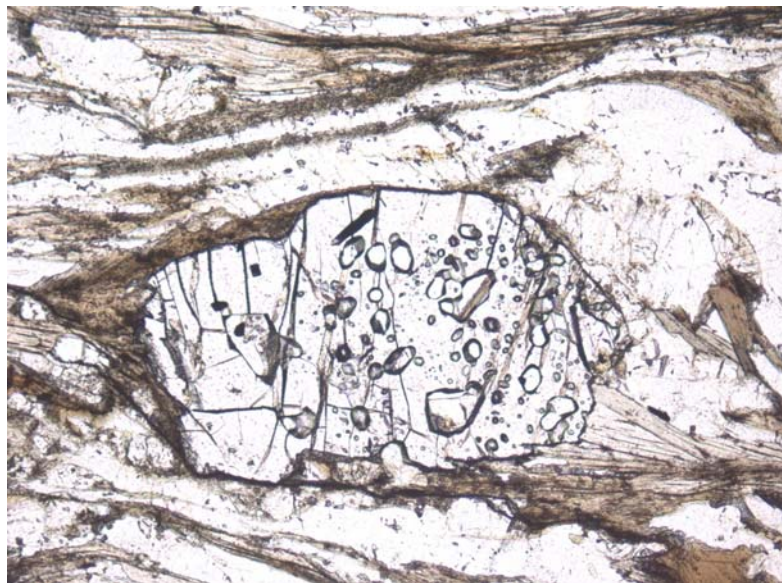
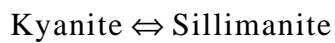


Figure 4.6 Thin section photo from sample T6. The large centered crystal is a garnet that contains inclusions. Bands of quartz (light) and biotite (dark) were formed syn-kinematically and flow around the garnet porphyroblast. The picture is 5 mm across.

Garnet is resorbed and replaced by plagioclase, biotite, quartz and aluminium silicates along the grain boundaries.

The relict kyanite predating the syn-kinematic assemblage shows that this sample has been in the kyanite stability field. Sillimanite is formed from the breakdown of kyanite:



Muscovite is also commonly produced, along with sillimanite, from the breakdown of kyanite in the presence of K- feldspar and H₂O:



Sillimanite coexisting with biotite and muscovite can be seen in bands parallel to foliation.

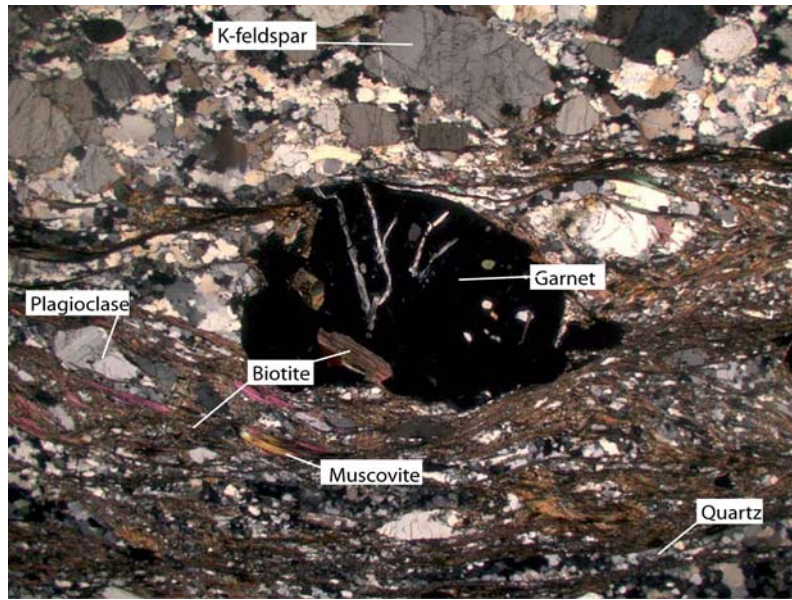


Figure 4.7 Thin section picture (4 mm across) of the main mineral assemblage in sample AA02-15.

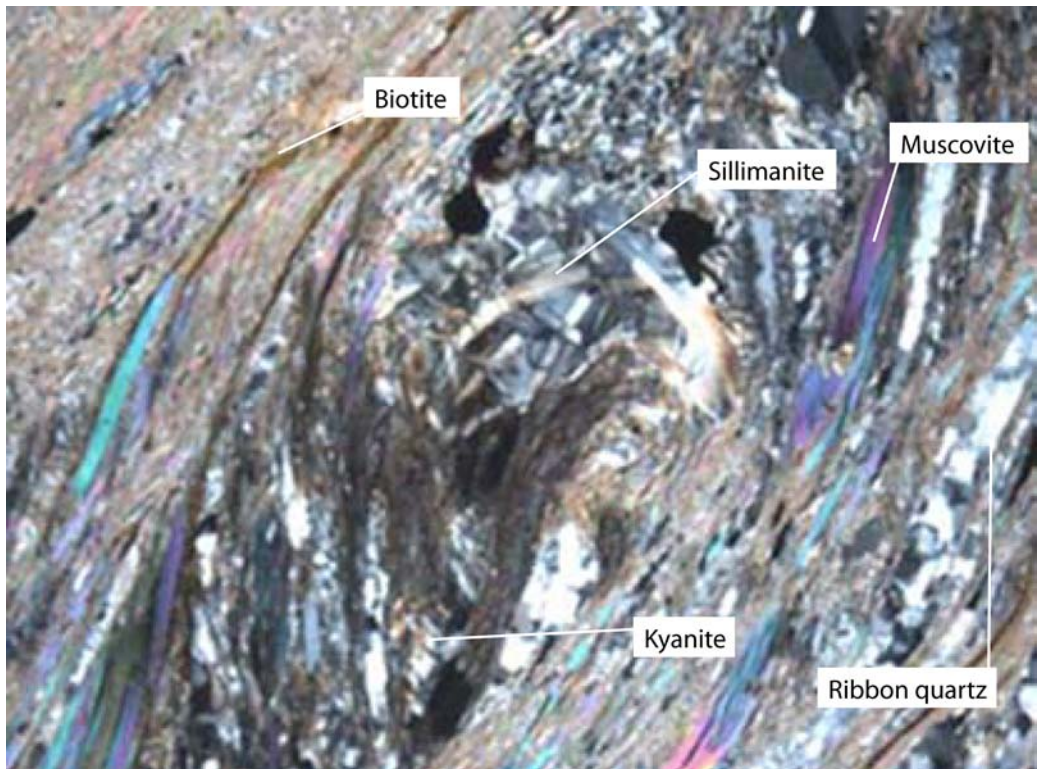


Figure 4.8 Thin section photo micrograph that shows how bands of mica and ribbon quartz flow ductilely while kyanite and sillimanite have been truncated. Picture is 3 mm across.

4.5.2. The Eleonore Bay Supergroup

AA02-23

The EBSGp sample is a metapsammite located close to a granitic pluton that obscures the proposed tectonic boundary between the Smallefjord Sequence and the EBSGp (Figure 4.1).

The matrix comprises quartz + K-feldspar + sillimanite + biotite + muscovite + ilmenite. Continuous bands of quartz and K-feldspar, and discontinuous bands of mica depict the foliation. Although this rock is deformed, quartz is completely recovered. Quartz dominates the matrix. The garnet crystals are elongate and the foliation bends around them. No shear related textures are seen in this rock.

Muscovite is the most abundant mica and is concentrated in the mica bands, where the elongated crystals are oriented parallel to each other and define a foliation. Biotite is distributed in discontinuous bands parallel to foliation, or as constituents of the dominant muscovite bands. Biotite is also observed situated perpendicular to the main foliation, thus biotite is both syn- and post kinematic.

The garnet crystals are anherdial, 500-2000 µm in length, homogeneously distributed and display a range of textures, depending on the amount of retrogression.

The less reworked garnet crystals are idioblasts that display poikiloblastic- to sieve texture, with inclusions of quartz, plagioclase, ilmenite and sillimanite. Weak corona textures border some of the garnets from surrounding crystals. Inclusion trails record relict foliation (Figure 4.9).

In the more strongly retrogressed crystals the garnet has been partly of fully replaced by aggregates of fibrolitic sillimanite and feldspar. The fibrolite is commonly present as clusters and is post-kinematic with respect to the penetrative foliation (Figure 4.10).

Porphyroblasts of plagioclase, less than 500 µm in length, can also be found, but they are not as abundant as the garnet porphyroblasts.

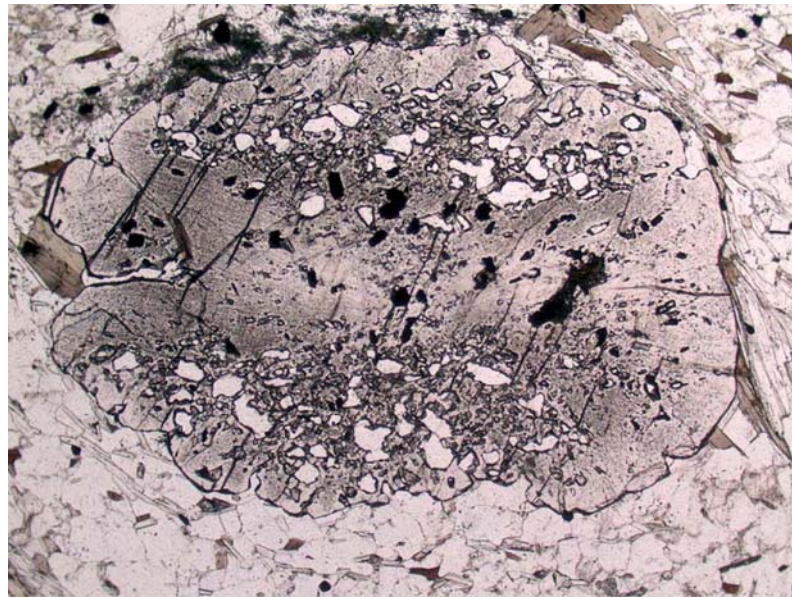


Figure 4.9 The picture shows inclusion trails in garnet crystals. This inclusion trail represents a relict foliation different from the composition matrix foliation. Image is c. 3 mm across.



Figure 4.10 The picture shows a fibrolite (Sillimanite) complex surrounding a garnet prophyroblast.

Mineral reactions in sample AA02-23

The observed mineral assemblage consists of garnet, plagioclase, quartz, biotite, muscovite, K-feldspar and ilmenite. The absence of staurolite indicates that the staurolite-out reaction after Bickle and Archibald (1984) was passed, which sets a minimum temperature of c. 650 – 675°C. The presence of sillimanite and absence of kyanite suggests prograde metamorphism was either within the sillimanite field, or in the kyanite field close to the sillimanite field. If kyanite was present on the prograde path, it is reacted out of the assemblage on the retrograde path. This assumption set an upper pressure to c. 8.5 kbar. No indications of melting was observed in the Eleonore Bay Supergroup. This indicates that reaction (7) did not occur, which sets an upper temperature to c. 720°C.

4.6. Electron Microprobe analyses

T6

The garnets, which are 1500-3000 μm across, display compositional zoning (Figure 4.11). The garnets show increasing almandine ($X_{\text{Alm}} = 0.58-0.71$), and decreasing pyrope ($X_{\text{Py}} = 0.13-0.24$) and grossular ($X_{\text{Grs}} = 0.10-0.23$) from core to rim (Figure 4.11). Minor constituents are spessartine ($X_{\text{Sps}} = 0.01-0.03$) and andradite ($X_{\text{Adr}} = 0.01-0.05$).

A garnet zonation profile (Figure 4.11) displays a drop in grossular along with increasing Fe/(Fe+Mg) both at the rim. The core and outer core is homogeneous. The sudden drops in Ca in the core is due to numerous inclusions in the core of these garnets.

Plagioclase has a range of composition: $X_{\text{An}} = 0.45-0.76$; $X_{\text{Al}} = 0.24-0.54$.

Figure 4.12 documents a trend for the Ti content in biotite. Biotite which is isolated in quartz bands, and thus unable to react with the matrix, has a higher Ti content than biotite associated with the matrix. The isolated biotite is thought to be equilibrated at a higher metamorphic grade than matrix biotite (Dymek, 1983).

AA02-15

The garnet shows increasing almandine ($X_{\text{Alm}} = 0.64-0.79$) from core to rim, and decreasing pyrope ($X_{\text{Py}} = 0.11-0.20$) and grossular ($X_{\text{Grs}} = 0.02-0.16$) from core to rim. Minor components are spessartine ($X_{\text{Sps}} = 0.01-0.07$) and andradite ($X_{\text{Adr}} = 0.01-0.07$). The garnets are 1500-3000

μm across and display compositional zoning within crystals (Figure 4.11). The plagioclase has a range of composition: $X_{\text{An}} = 0.27\text{-}0.31$; $X_{\text{Al}} = 0.69\text{-}0.73$.

Due to diffusion, the interior of the crystal is unzoned, as is common for the garnets of a high metamorphic grade (Spear, 1992). Possible pro-grade zonation patterns are considered to be

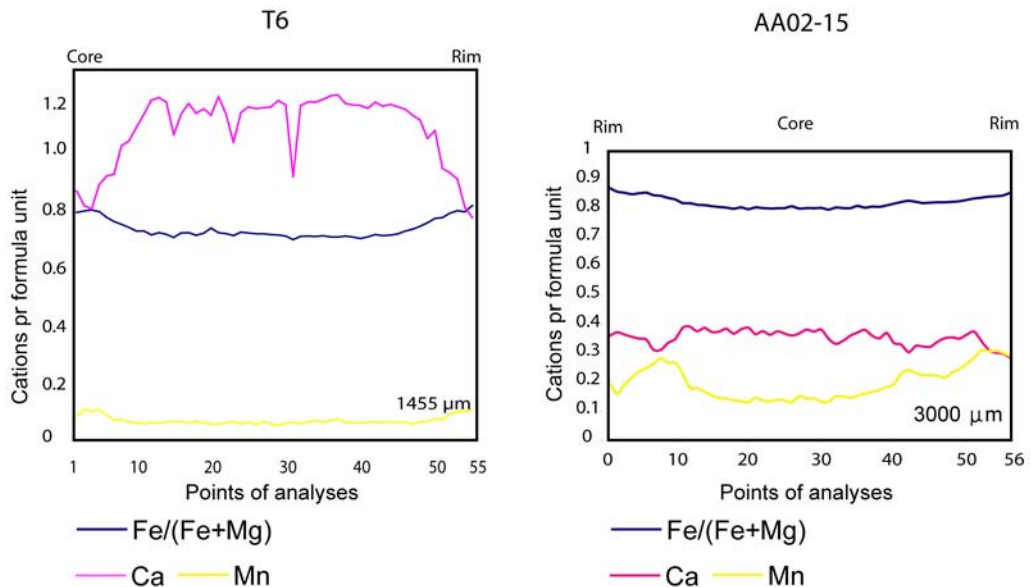


Figure 4.11 zonation profiles in garnet from T6 and AA02-15.

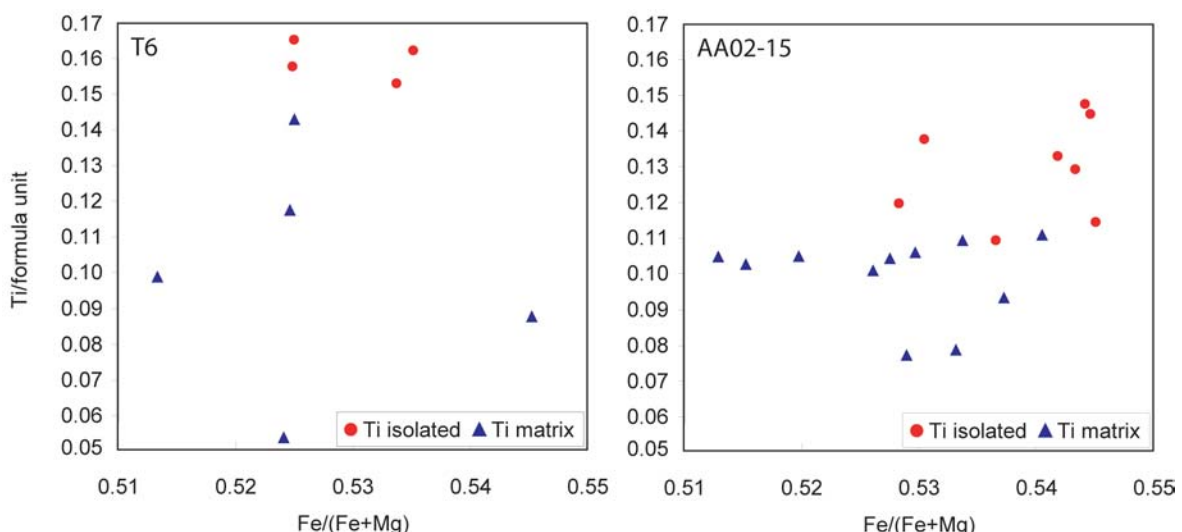


Figure 4.12 Electron microprobe data document a trend for Ti in biotite: The Ti content is higher in biotites enclosed in quartz than it is for biotite in contact with matrix. This is typical for both T6 and AA02-15.

erased by diffusion at peak metamorphism. The interior of these garnets are thus thought to represent the equilibrated peak composition. The retrograde net transfer reaction that produced anorthite lowers the Ca content at the garnet rim.

$\text{Fe}/(\text{Fe}+\text{Mg})$ increases from core to rim and Mn decreases at the rim.

The Ti content in biotite isolated in quartz bands is higher than the Ti content in matrix biotite (Figure 4.12).

AA02-23

The garnets show increasing almandine ($X_{\text{Alm}} = 0.70 - 0.84$) and pyrope ($X_{\text{Py}} = 0.09 - 0.06$) from core to rim, and decreasing spessartine ($X_{\text{SpS}} = 0.16 - 0.05$) and grossular ($X_{\text{Grs}} = 0.09 - 0.01$) from core to rim. The garnet crystals are 800-2500 μm across. The plagioclase has a range of composition: $X_{\text{An}} = 0.08-0.10$; $X_{\text{Al}} = 0.90-0.92$. No isolated biotite was observed in this sample.

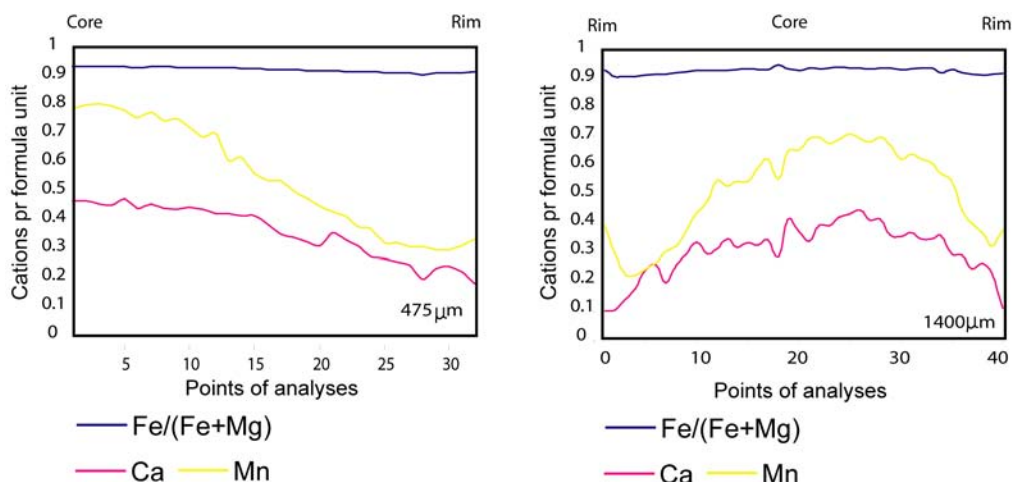


Figure 4.13 Zonation profiles from two garnet porphyroblasts from sample AA02-23 of the EBSGp. The profiles show the patterns of $\text{Fe}/(\text{Fe}+\text{Mg})$, Ca and Mn across the garnet crystals.

The zonation profiles (Figure 4.13) record a flat slope for $\text{Fe}/(\text{Fe}+\text{Mg})$. Ca and Mn show a steady decrease from core to rim. This indicates that the garnets grew during prograde metamorphism and were not subjected to strong intracrystalline diffusion.

4.7. Mineral selection criteria for thermobarometry

It is of great importance that the mineral assemblage used in geothermobarometric calculation is equilibrated. If the selected assemblage is in dis-equilibrium, the estimated temperatures and pres-

sures will be erroneous. The textural position of different grains of garnet, biotite and plagioclase must be considered in order to decide on an assemblage that is equilibrated.

Crystals assumed to be in equilibrium during peak metamorphic conditions;

- Cores from large garnets. Due to slow intracrystal diffusion in garnet the cores are least probable of being affected on the retrograde path.
- Relatively large plagioclase porphyroblasts that grew prograde and are not recrystallized.
- Biotite crystals isolated in ribbon quartz should be equilibrated at peak metamorphism due to their incapability to react with the matrix along the retrograde path.

Crystals assumed to be in equilibrium during post-peak metamorphic conditions;

- Garnet rims and adjacent plagioclase and biotite crystals. Garnet and adjacent biotite will re-equilibrate along the retrograde path through exchange reactions.
- Plagioclase recrystallizes adjacent to garnet on the retrograde path through net-transfer reactions.

4.8. Calibrations

4.8.1. Presentation of applied geothermobarometers and their P-T plots

Two calibrations of the garnet-biotite geothermometer (Perchuk and Lavrent'eva (1983) and Holdaway (2000), the GASP geobarometer (Figure 4.15)(Ferry and Spear, 1978) and the GBPQ geobarometer (Figure 4.14)(Wu et al., 2004) were applied to estimate the P-T conditions. Representative electron microprobe analyses used for geothermobarometry are shown in Table 4.3 (Complete data-set can be viewed in Appendix 1).

GASP is widely used and numerous calibrations exists, and a review is presented by Holdaway (2001). Ferry and Spear (1978) use a simple non-ideal garnet model for the net-transfer of Ca. Later work included effects of other elements into more complicated garnet activity models (Hodges and Spear, 1982; Berman, 1988; Koziol and Newton, 1988; Holdaway, 2001), but the less complex Ferry and Spear (1978) geobarometer yield good pressure calculations.

The GBPQ geobarometer (Wu et al., 2004) is calibrated using the mineral assemblage garnet - biotite - plagioclase - quartz. It is developed specifically for samples depleted in aluminium silicates, as is the situation for sample T6 from allochthonous basement.

Special activity models are used for plagioclase (Fuhrman and Lindsley, 1988), biotite (Holdaway, 2000) and garnet (Holdaway, 2000;2001)

The samples Wu et al. (2004) used for calibration fall in the mineral composition range: $X_{Grs} = 3\text{-}23\%$ (mostly 5-10%); $X_{An} = 17\text{-}93\%$ (mostly 20-40%); aluminium content in biotite = 3-23% (mostly 10-20%). Although Todd (1998) points to great uncertainties in calculated pressures in rocks where $X_{Grs} < 10\%$ and $X_{An} < 30$, Holdaway (2001) and Wu et al. (2004), respectively, claim that GASP and GBPQ are usable if $X_{Grs} > 3\%$ and $X_{An} > 17\%$.

The mineral compositions in the rock samples from Kildedalen generally fall within the limits of safe compositions as laid out by Holdaway (2001) and Wu et al. (2004).

The GBPQ geobarometer of Wu et al. (2004) (Eq 4 and 5) combined with the garnet-biotite geothermometer of Holdaway (2000) (Eq 2) will be selected to represent the samples that are analysed. For this reason the GBPQ is the most suitable barometer that is calibrated for each of the samples (T6, AA02-15 and AA02-23). The aluminium-silicate and muscovite absent mineral assemblage of sample T6 is not valid for any other existing barometer at present. The GBPQ is calibrated towards the garnet-biotite geothermometer of Holdaway (2000), which will be applied to determine temperature.

4.8.2. DOMINO P-T plots

The results from DOMINO, calculated from whole rock chemistry (Table 4.4) are presented as P-T plots below. The lines on the diagrams represent reactions where specific minerals become stable or unstable. Mineral reactions of importance to the samples surveyed are coloured. Mineral stability is indicated by arrows pointing in the direction of an “in reaction” (All reactions are listed in Appendix 2-4). Stability fields for the mineral assemblage of each sample are colored. Mineral abbreviations are after Kretz (1983): garnet = Grt; Biotite = Bt; Cordierite = Ctd; Kyanite = Ky; Sillimanite = Sil; Quartz = Qtz; Feldspar = Fst; Magnetite = Mg; Phengite = Phg; Rutile = Rt; Staurolite = St; Ilmenite = Ilm; Orthopyroxene = Opx; Chlorite = Chl (Kretz, 1983). The feldspar abbreviation is from De Capitani and Brown (1987).

garnet					
Sample	T6	T6	AA02-15	AA02-15	AA02-23
	Core	Rim	Core	Rim	Rim
SiO ₂	38,520	37,564	36,473	37,343	36,766
FeO	26,090	32,382	33,647	35,472	36,594
CaO	8,010	4,703	2,512	2,506	1,665
Cr ₂ O ₃	0,010	0,029	0,029	0,051	0,000
MgO	6,100	3,891	4,613	3,114	2,013
Al ₂ O ₃	21,710	21,398	21,727	21,228	20,659
K ₂ O	0,010	0,000	0,013	0,010	0,002
TiO ₂	0,000	0,000	0,002	0,000	0,043
MnO	0,360	0,882	1,067	1,703	2,088
Total	100,830	100,852	100,085	101,427	99,868
Cations based on 12 oxygen atoms					
Si	2,998	2,984	2,924	2,979	3,000
Fe ²⁺	1,680	2,110	2,096	2,298	2,485
Fe ³⁺	0,018	0,038	0,146	0,062	0,011
Ca	0,585	0,350	0,189	0,187	0,127
Mg	0,708	0,461	0,551	0,370	0,245
Al	1,992	2,004	2,053	1,996	1,987
K	0,001	0,000	0,001	0,001	0,000
Ti	0,000	0,000	0,000	0,000	0,003
Mn	0,024	0,059	0,072	0,115	0,144
Cr	0,001	0,003	0,003	0,005	0,000
Total	8,006	8,013	8,049	8,021	8,004
Biotite					
Sample	T6	T6	AA02-15	AA02-15	AA02-23
	Rim	Matrix	Matrix	Rim	Rim
SiO ₂	36,963	36,646	35,576	35,198	33,871
FeO	18,595	18,516	19,832	19,431	23,913
CaO	0,066	0,029	0,001	0,000	0,008
Na ₂ O	0,124	0,271	0,344	0,249	0,239
MgO	12,242	11,441	9,343	9,700	6,828
Al ₂ O ₃	17,832	17,583	18,993	20,068	18,832
K ₂ O	8,732	9,303	9,045	9,003	8,428
TiO ₂	1,391	2,332	1,808	1,084	2,590
MnO	0,005	0,076	0,026	0,080	0,112
Total	96,002	96,242	94,973	94,817	94,826
Cations based on 11 oxygen atoms					
Si	2,753	2,730	2,703	2,676	2,628
Fe	1,158	1,154	1,260	1,236	1,551
Ca	0,005	0,002	0,000	0,000	0,001
Na	0,018	0,039	0,051	0,037	0,036
Mg	1,359	1,271	1,058	1,099	0,790
Al	1,566	1,544	1,701	1,798	1,722
K	0,830	0,884	0,877	0,873	0,834
Ti	0,097	0,163	0,129	0,078	0,189
Mn	0,000	0,003	0,002	0,005	0,007
Total	7,789	7,795	7,781	7,802	7,758
Plagioclase					
Sample	T6	T6	AA02-15	AA02-15	AA02-23
	Rim	Blast	Blast	Rim	Rim
SiO ₂	50,549	48,277	60,369	59,626	65,625
FeO	0,063	0,000	0,000	0,023	0,041
CaO	14,161	16,296	6,386	7,092	2,020
Na ₂ O	3,644	2,531	8,101	7,717	10,852
MgO	0,000	0,000	0,000	0,000	0,023
Al ₂ O ₃	30,871	32,755	24,648	25,284	21,228
K ₂ O	0,028	0,006	0,160	0,072	0,123
TiO ₂	0,000	0,000	0,000	0,000	0,005
MnO	0,008	0,017	0,000	0,000	0,000
Total	99,327	99,899	99,668	99,818	99,921
Cations based on 8 oxygen atoms					
Si	2,343	2,242	2,709	2,678	2,895
Fe	0,002	0,000	0,000	0,001	0,002
Ca	0,616	0,710	0,269	0,299	0,084
Na	0,328	0,228	0,705	0,672	0,928
Mg	0,000	0,000	0,000	0,000	0,002
Al	1,687	1,793	1,304	1,338	1,104
K	0,002	0,000	0,009	0,004	0,007
Ti	0,000	0,000	0,000	0,000	0,000
Mn	0,000	0,001	0,000	0,000	0,000
Total	4,978	4,975	4,996	4,991	5,021

Table 4.3 Representative electron microprobe analyses from garnet, plagioclase and biotite from T6, AA02-15 and AA02-23. Biotite labelled “matrix” are obtained from within bands of quartz.

Sample	SiO ₂	Al ₂ O ₃	Fe ₂ O ₃	MnO	MgO	CaO	Na ₂ O	K ₂ O	TiO ₂	SUM
	(%)	(%)	(%)	(%)	(%)	(%)	(%)	(%)	(%)	(%)
AA02-15 2	58,94	17,92	9,44	0,1	3,12	1,02	1,27	4,02	0,85	98,16
AA02-15 1	58,93	17,91	9,39	0,1	3,14	1,01	1,28	4,05	0,85	98,03
T6 2	65,04	12,96	10,41	0,09	3,27	3,35	0,77	1,76	0,45	99,34
T6 1	65,22	13,01	10,38	0,09	3,28	3,33	0,77	1,75	0,44	99,52
AA02-23 2	64,01	16,52	6,69	0,07	1,31	0,28	1,6	3,32	1,03	96,46
AA02-23 1	65,83	16,81	6,76	0,07	1,32	0,29	1,61	3,31	1,04	98,68
NIM-G 98	76,09	12,03	2,03	0,02	0,03	0,73	3,3	5,03	0,09	100,04

Table 4.4 XRF whole-rock data for T6, AA2-15 and AA02-23. Two batches were prepared and analysed for each sample, hence (1) and (2) in the table. NIM-G 98 is a calibrated standard.

Smallefjord Sequence (T6)

T6 contains the mineral assemblage garnet, quartz, plagioclase, K-feldspar, biotite, ilmenite, chalcopyrite. The DOMINO stability field for this assemblage is at 800-1000°C and 3.5-12.5 kbar. The stability field is constrained by rutile-out, sillimanite-out, cordierite-out and orthopyroxene-out reactions (Figure 4.16):

- Rutile out (A): Grt Ilm Bt Fst Mt Qtz Rt = Grt Ilm Bt Fst Mt Qtz
- Sillimanite out (B): Grt Ilm Bt Fst Mt Qtz = Grt Ilm Bt Fst Mt Qtz
- Cordierite out (C): Grt Ilm Bt Fst Crd Mt Qtz = Grt Ilm Bt Fst Mt Qtz
- Orthopyroxene in (D): Grt Ilm Bt Fst Mt Qtz = Grt Ilm Bt Opx Fst Mt Qtz

Smallefjord Sequence (AA02-15)

The mineral assemblage for AA02-15 is quartz, biotite, muscovite, plagioclase, garnet, sillimanite, kyanite, K-feldspar and ilmenite. The DOMINO stability fields for this assemblage overlap and plot at 575-750°C and 3.5-10 kbar (Figure 4.17). The stability fields are defined by the aluminium silicate polymorph, one field is stable within the kyanite field and the other within the sillimanite field. The stability fields are constrained by various reactions:

4.8.3. GBPQ

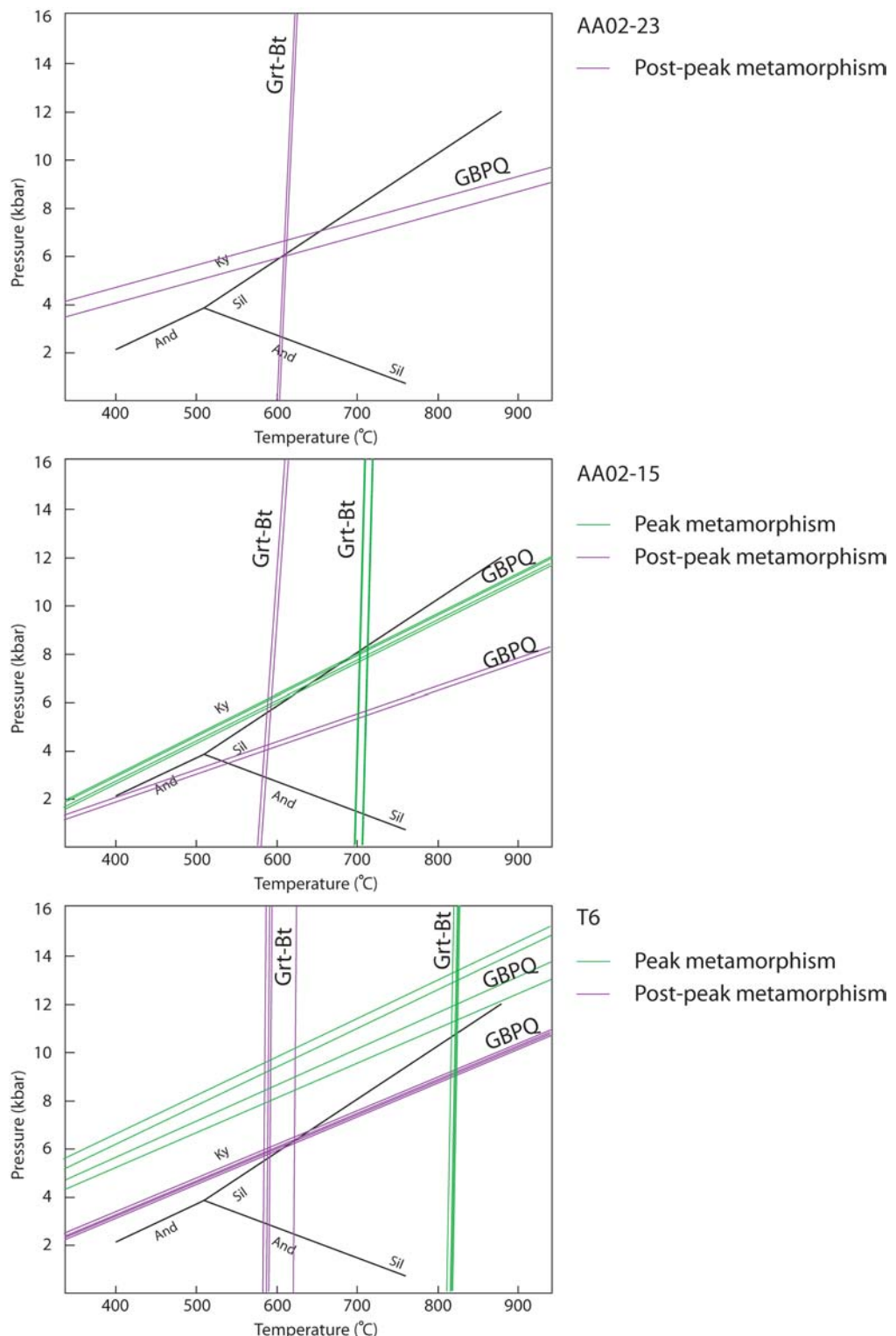


Figure 4.14 P-T plots based on the GBPQ barometer (Wu et al., 2004) and the garnet-biotite thermometer calibration by Holdaway (2000). The diagrams show peak- and post peak metamorphic condindition for T6 and AA02-15. Only post peak conditions are calculated for AA02-23. Each line represents a P or T calculation for a garnet-biotite pair or a garnet-plagioclase pair.

4.8.4. GASP

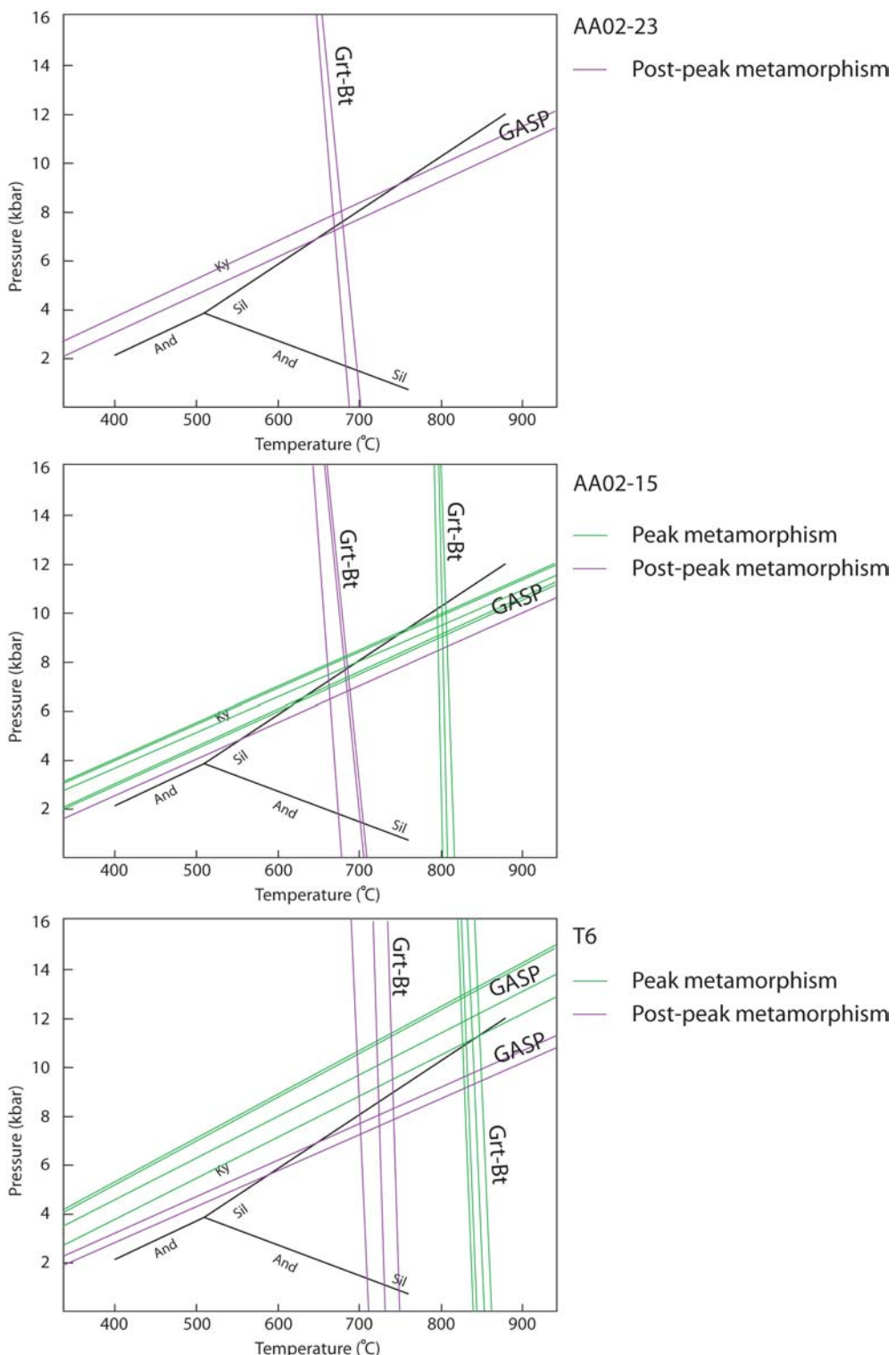


Figure 4.15 P-T plots based on the GASP calibration by Ferry and Spear (1978) and the garnet-biotite thermometer calibration by Perchuk and Lavrent'eva (1983). The diagrams show peak- and post peak metamorphic condindition for T6 and AA02-15. Only post peak conditions are calculated for AA02-23. Each line represents a P or T calculation for a garnet-biotite pair or a garnet-plagioclase pair.

- Garnet in (A): Grt Ilm Bt Phg Fst Mt Qtz Sil = Ilm Bt Phg Fst Mt Qtz Sil
 Phengite out (B): Grt Ilm Bt Phg Fst Mt Qtz Sil = Grt Ilm Bt Fst Mt Qtz Sil
 Sillimanite in (C): Grt Bt Phg Fst Mt Qtz Rt = Grt Bt Phg Fst Mt Qtz Rt Sil
 Staurolite out (D): Grt Ilm Bt Phg Fst Mt Qtz Sil St = Grt Ilm Bt Phg Fst Mt Qtz Sil
 Kyanite in (E): Grt Bt Phg Chl Fst Mt Qtz Rt = Grt Bt Phg Chl Fst Mt Qtz Rt Ky
 Kyanite out (F): Grt Bt Phg Fst Ky Mt Qtz Rt = Grt Bt Phg Fst Mt Qtz Rt Sil
 Kyanite out (G): Grt Bt Phg Fst Ky Mt Qtz Rt = Grt Bt Phg Fst Mt Qtz Rt

EBSGp (AA02-23)

The mineral assemblage for AA02-23 is quartz, K-feldspar, fibrolitic sillimanite, biotite, muscovite, ilmenite and garnet. The stability field for this assemblage is at 600–750°C and 3–10 kbar (Figure 4.18). The stability field is constrained by these reactions:

- Sillimanite in (A): Grt Ilm Bt Phg Fst Qtz St = Grt Ilm Bt Phg Fst Qtz Sil
 Sillimanite in (B): Grt Ilm Bt Phg Fst Ky Qtz = Grt Ilm Bt Phg Fst Sil Qtz
 Ilmenite in (C): Grt Bt Phg Fst Qtz Rt Sil = Grt Ilm Bt Phg Fst Qtz Rt Sil
 Phengite out (D): Grt Ilm Bt Phg Fst Qtz Sil = Grt Ilm Bt Fst Qtz Sil

4.9. Conclusion

Calculated pressures and temperatures were obtained using GBPQ geobarometry (Wu et al., 2004) and garnet-biotite geothermometry (Holdaway, 2000) (Figure 4.14).

Estimated peak metamorphic conditions for T6 cover the range 820 – 830°C and c. 11.3–13.0 kbar. Post-peak metamorphic conditions cover the range 580 – 620°C and c. 5.6–6.3 kbar (Figure 4.16). Estimated peak metamorphic conditions for AA02-15 cover the range 690 – 715°C and c. 7–8 kbar. Post-peak metamorphic conditions cover the range 585 – 600°C and c. 4 kbar (Figure 4.17). Estimated post-peak metamorphic conditions for AA02-23 cover the range 610 – 615°C and c. 6.0–6.5 kbar (Figure 4.18).

There is a correlation between the results from geothermobarometry and whole rock modeling for AA02-15 and AA02-23. For T6, the DOMINO stability field plots with lower pressure than the pressure calculated through geobarometry. The geothermobarometric results are considered to be representative for this sample. This issue is further discussed later in this thesis.

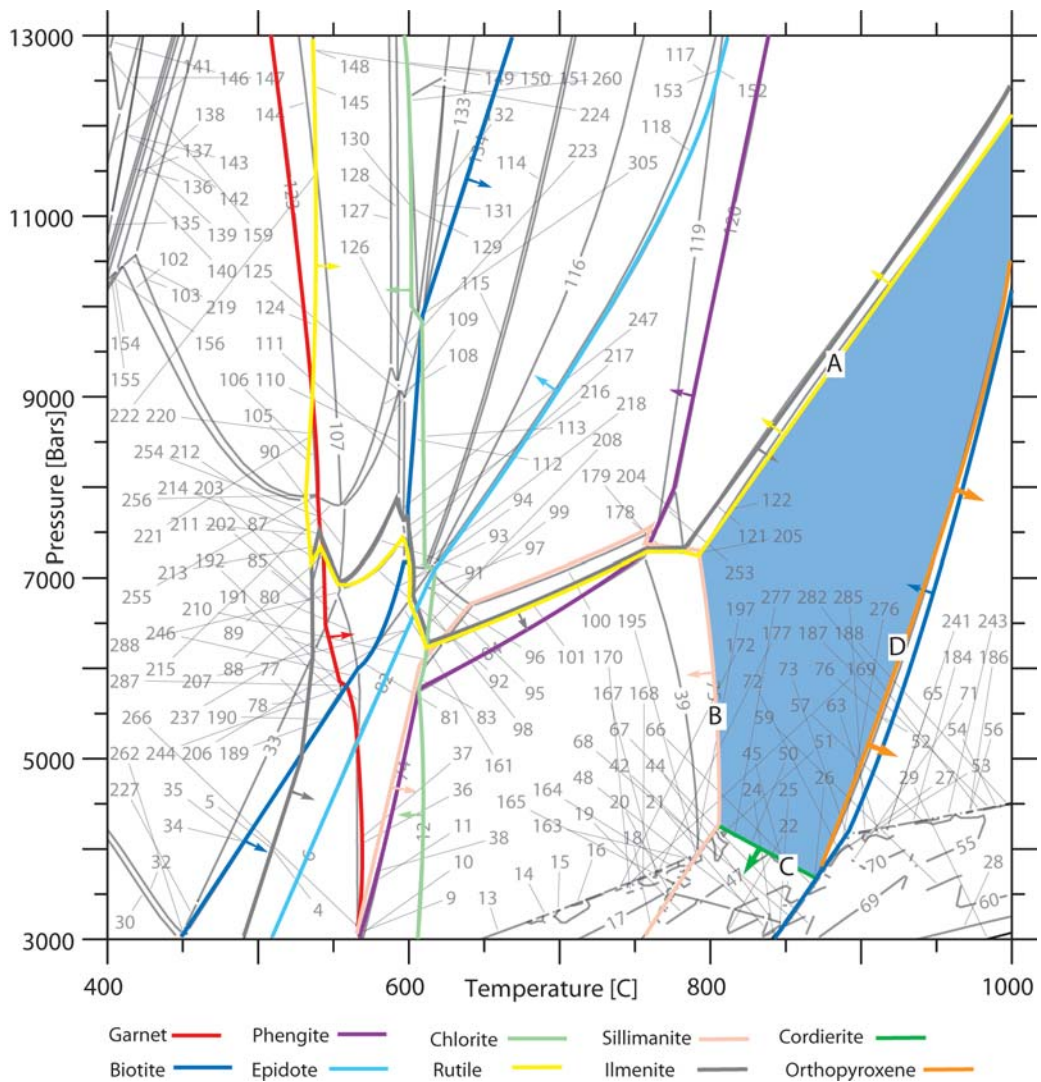


Figure 4.16 DOMINO plot for sample T6. The shaded area represents the stability field for the mineral assemblage in this sample. The arrows shooting off reaction lines indicate where the respective mineral is stable

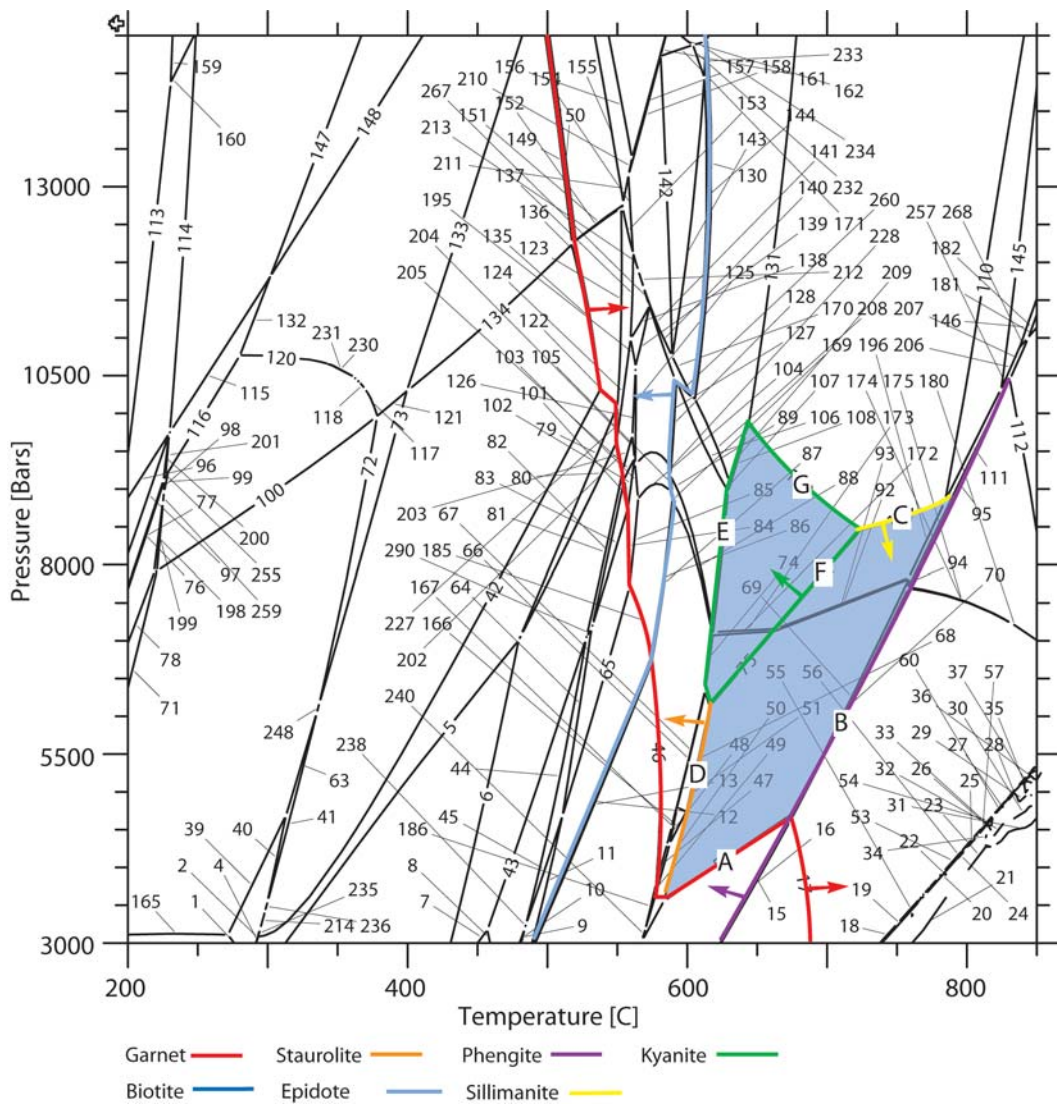


Figure 4.17 DOMINO plot of AA02-15 from the Smallefjord Sequence. The stability fields are shaded blue. Kyanite is stable in the upper field and sillimanite is stable in the lower field. The arrows shooting off reaction lines indicate where the respective mineral is stable.

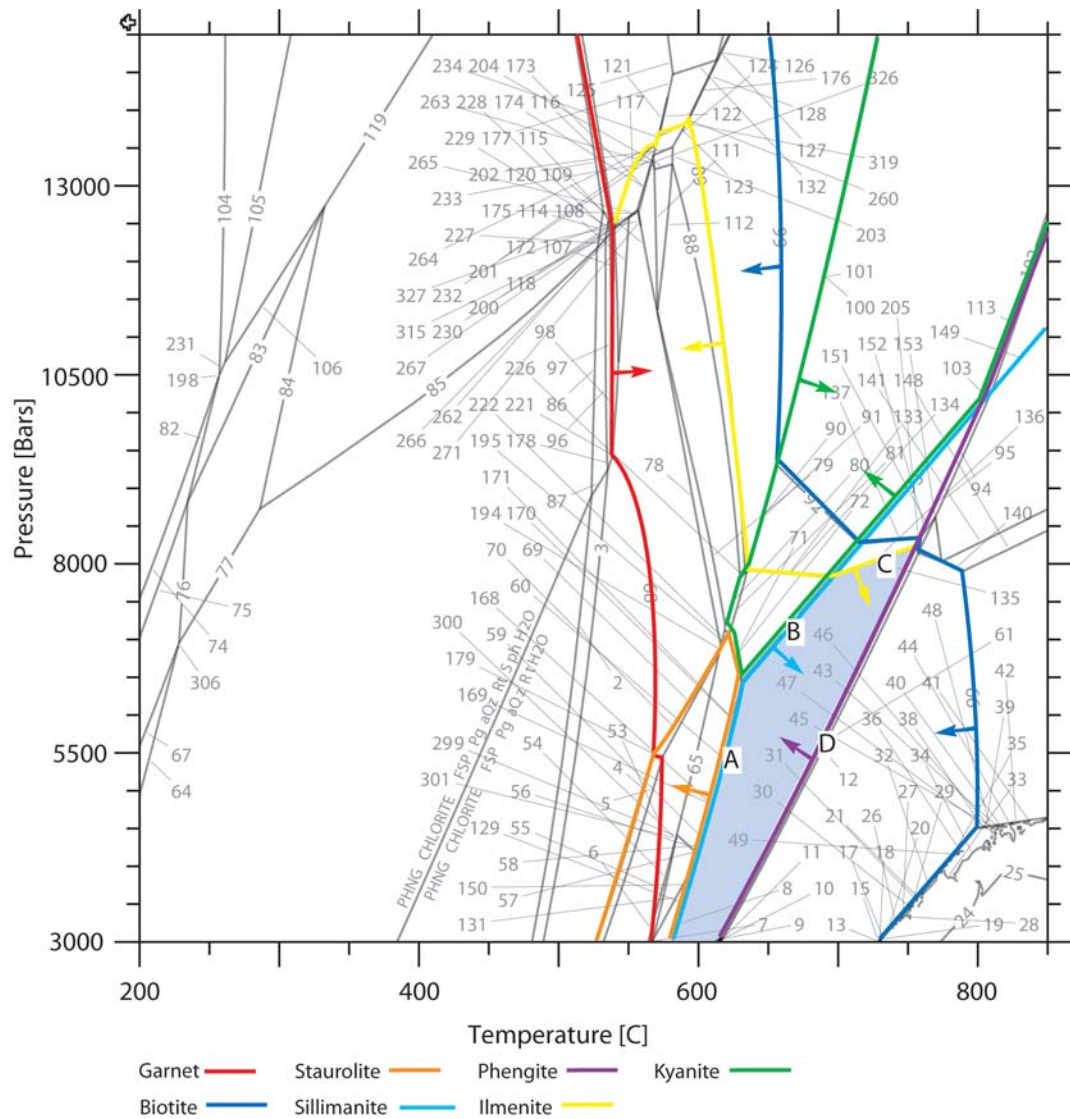


Figure 4.18 DOMINO plot of AA02-23. The stability field is shaded grey. The arrows shooting off reaction lines indicate where the respective mineral is stable

5. Structural geology of the study area

5.1. Introduction

Previous studies have divided the study area into three main lithotectonic units (Friderichsen et al., 1994). These are the high grade rocks in the allochthonous basement (Lower Plate), the Smallefjord Sequence (Middle Plate) and the low grade Eleonore Bay Supergroup (Upper Plate). The structural relationship between the main units in the Ardencaple Fjord area has been extensively debated (see next section). The main structures in Kildedalen are the ductile Kildedalen Shear Zone in the upper part of the Lower Plate, the ductile-brittle Slamsø Shear Zone (Slamsø Shear Zone) comprising both Lower Plate and the Middle Plate, and a steep late brittle extensional fault offsetting all three lithotectonic units. These major tectonic features all strike approximately north-south and have a variable dip towards east.

Granitic bodies are emplaced in the upper part of the Middle Plate and the lower part of the Upper Plate. The contact between the Middle and Upper Plate in the study area is, as already mentioned, obscured by a granite intrusion. The upper level of the Middle Plate is migmatized. Both granitic dikes and sills cut the Middle Plate and are observed in the upper part of the Lower Plate. Brittle extensional faults are quite common throughout the Middle Plate

Identification of the Kildedalen and the Slamsø Shear Zones and the postulated high strain zone between the Middle and Upper Plate indicate that structures and mineral assemblages observed in the three units developed at highly different crustal levels. Hence the Lower, Middle and Upper Plate should have different tectonothermal histories.

5.1.1. Previous work in the Ardencaple Fjord area

The structural relationship between allochthonous basement, the Smallefjord Sequence and the Eleonore Bay Supergroup in the Ardencaple Fjord area has been discussed and interpreted by several people (Soper and Higgins, 1993; Friderichsen et al., 1994; Higgins and Soper, 1994; Strachan, 1994; Strachan et al., 2001).

Strachan (1994) documented recumbent folds in the allochthonous basement gneisses underlying the Kildedalen Shear Zone. The foldhinges are curvilinear about a regional, orogen parallel, north

to NE trending mineral extension lineation. Comparable structures in North East Greenland deform the Eleonore Bay Supergroup and are thus interpreted to be Caledonian in age (Strachan, 1994).

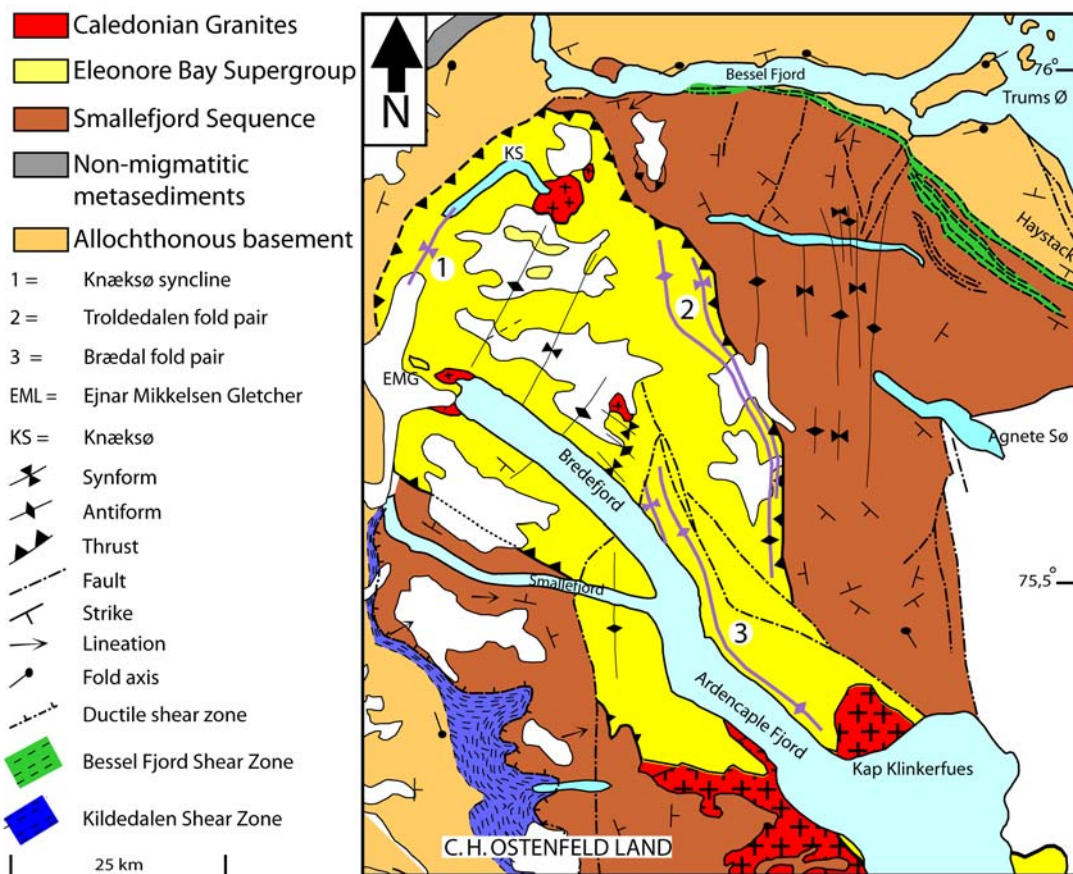


Figure 5.1 Simplified map showing the distribution of the main lithotectonic units and dominant structures in the Ardecaple Fjord area. Modified from Strachan et al. (2001).

West of Slamsø, the orogen-parallel structures are truncated by mylonitic gneisses. The mylonites are interpreted to have been formed during east-west extension that reworked the upper part of allochthonous basement, and deformed the Smalllefjord Sequence and the lower part of the Eleonore Bay Supergroup (Strachan, 1994). The Kildedalen Shear Zone appears as a major north-south striking extensional shear zone (~200-1000 m thick) comprising blastomylonitic gneiss derived from the allochthonous basement. An extensional shear zone south of Bessel Fjord (Bessel Fjord Shear Zone) (Figure 5.1), affecting both the allochthonous basement and the Smalllefjord Sequence, is interpreted to represent a northward continuation of the Kildedalen Shear Zone

(Strachan, 1994). The Bessel Fjord Shear Zone is ~200 m thick and SE striking (Strachan, 1994). In the Haystack area (Figure 5.1), shear deformation is recorded as three high strain zones within the Smallefjord Sequence, in addition to the main shear zone along the allochthonous basement-Smallefjord Sequence contact. The contact separating the Eleonore Bay Supergroup and the Smallefjord Sequence at Kildedalen has been interpreted, but not documented, as a high strain zone (Friderichsen et al., 1994) with an extensional component (Strachan, 1994).

Ductile extensional shear zones located along the boundaries of all three lithotectonic units (Allochthonous basement, the Smallefjord Sequence and the Eleonore Bay Supergroup) represent an intensification of the regional fabrics. An amphibolite facies L-S fabric seen in the upper part of allochthonous basement, in the Smallefjord Sequence and the Eleonore Bay Supergroup results from the transposition of lithological banding (Friderichsen et al., 1994). The associated folds are tight to isoclinal, commonly reclined folds of banding. Fold axes are generally parallel to an east/northeast to east trending mineral lineation (Friderichsen et al., 1994).

Soper and Higgins (1993) interpreted these shear zones to have experienced extensional displacement during the formation of the Vendian Eleonore Bay Supergroup basin, then reactivated subsequently as Caledonian thrusts with limited displacement. This interpretation was, however, shortlived (Hartz and Andresen, 1995).

An alternative interpretation was put forward by Strachan (1994) and Strachan et al. (2001) who concluded that the Smallefjord Sequence and the Eleonore Bay Supergroup are separated by Caledonian extensional shear zones SW and NE of the Eleonore Bay Supergroup outcrops in the Ardencaple Fjord area (Figure 5.1). The mylonites in the shear zones are derived from both the Smallefjord Sequence and the Eleonore Bay Supergroup. The extensional displacement parallel to the mylonitic lineation is indicated by sense of shear and folding of deformed granite veins, extensional shear bands and mesoscopic shear zones (Strachan, 1994). Sedimentary structures are found in metasediments which have undergone greenschist facies metamorphism (Strachan et al., 2001).

NW to north striking, tight-to-open, upright folds within the NE margin of the Smallefjord Sequence are interpreted as late Caledonian structures post-dating the regional extension. The NE boundary of the Eleonore Bay Supergroup is characterized by the inversion of strata associated with a

fold pair and thrust displacements (Strachan, 1994; Friderichsen et al., 1994) (Figure 5.1). Soper and Higgins (1993) report folds in the Eleonore Bay Supergroup that are truncated by Caledonian granites. These are thus interpreted to predate regional extension. This indicates a complex polyphase Caledonian deformational history for the Ardencaple Fjord area with successive extensional and contractional events.

5.1.2. Terminology

The structural history of the three tectonic units in the Kildedalen area (Figure 5.2) will be described separately. The abbreviations used in the following structural assessment are as follows; The capital letters indicate either deformational event (D), fold generated by deformational events (F) or planar structures (S). The capital superscript refers to the tectonic unit in which it is observed. ^L = allochthonous basement (Lower Plate), ^M = Smallefjord Sequence (Middle Plate) and ^U = Eleonore Bay Supergroup (Upper Plate). The subscript number indicates the relative order of the observation, with increasing numbers meaning younger ages. The oldest deformational event in the basement will for example be denoted D^L₁. Folds and foliations have their own internal subscript numbering, that is not controlled by deformational event subscripts. For example, the oldest observed folds in the Lower Plate is labelled F^L₁, independent of which deformational event that formed the folds. A Schmidt equal-area stereonet has been used to plot structural observations throughout this chapter.

5.2. The Lower Plate; Allochthonous basement

Only the upper part of the allochthonous basement was investigated in the field. The upper termination of the allochthonous basement is marked by the north-south striking and east dipping Kildedalen Shear Zone. This ductile shear zone reworked the tonalitic gneisses of the allochthonous basement in the western part of Kildedalen, and is more than 1 km thick (Friderichsen et al., 1994). It is cut by two sets of post-kinematic leuco-granitic veins. These are themselves truncated by the overlying Slamsø Shear Zone.

A simplified cartoon illustrating the age relationship between the interpreted shear-zones is presented in figure 5.3.

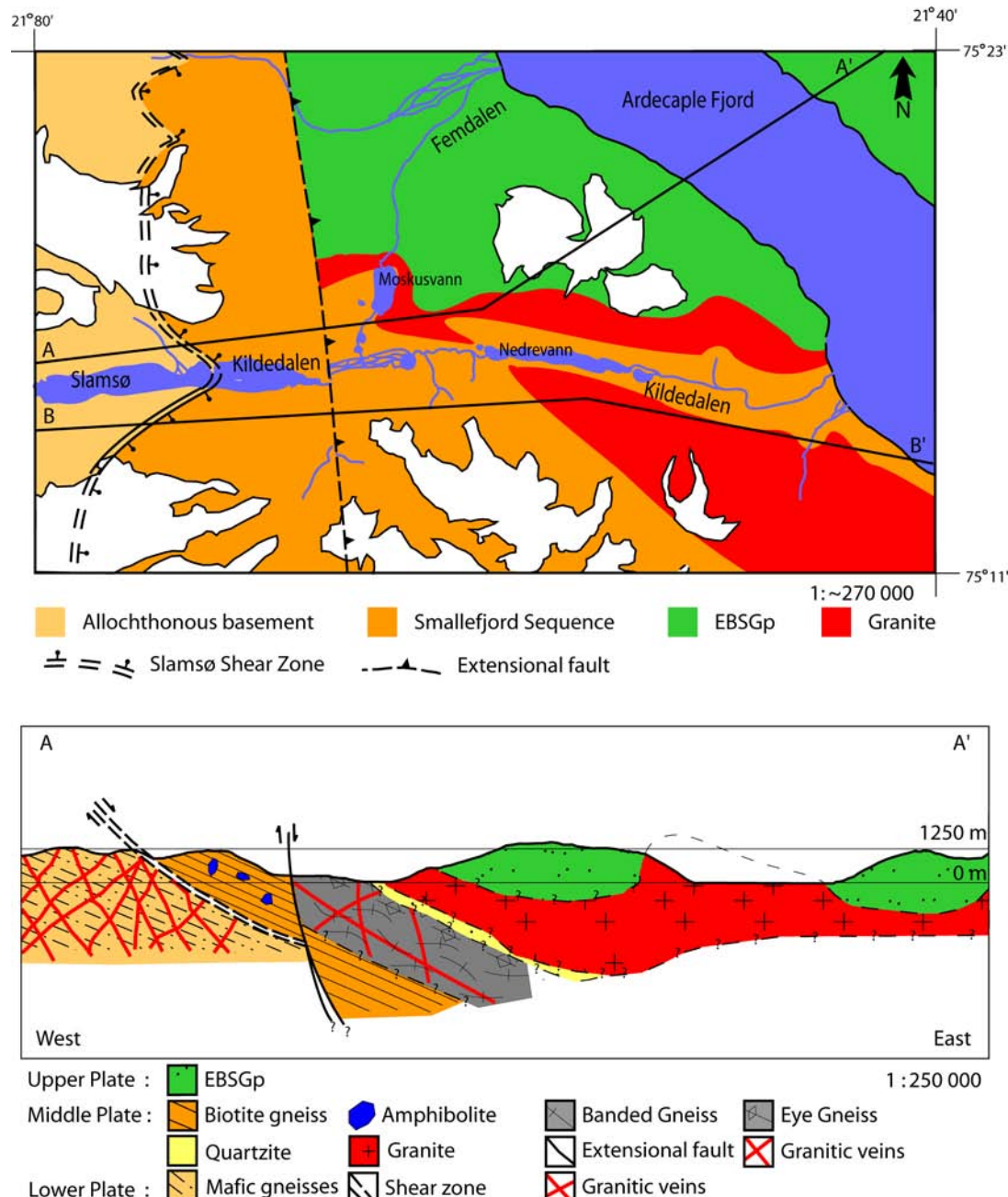


Figure 5.2 Simplified map and cross section showing the Lower-, Middle- and Upper Plate, and their tectonostratigraphic relationships.

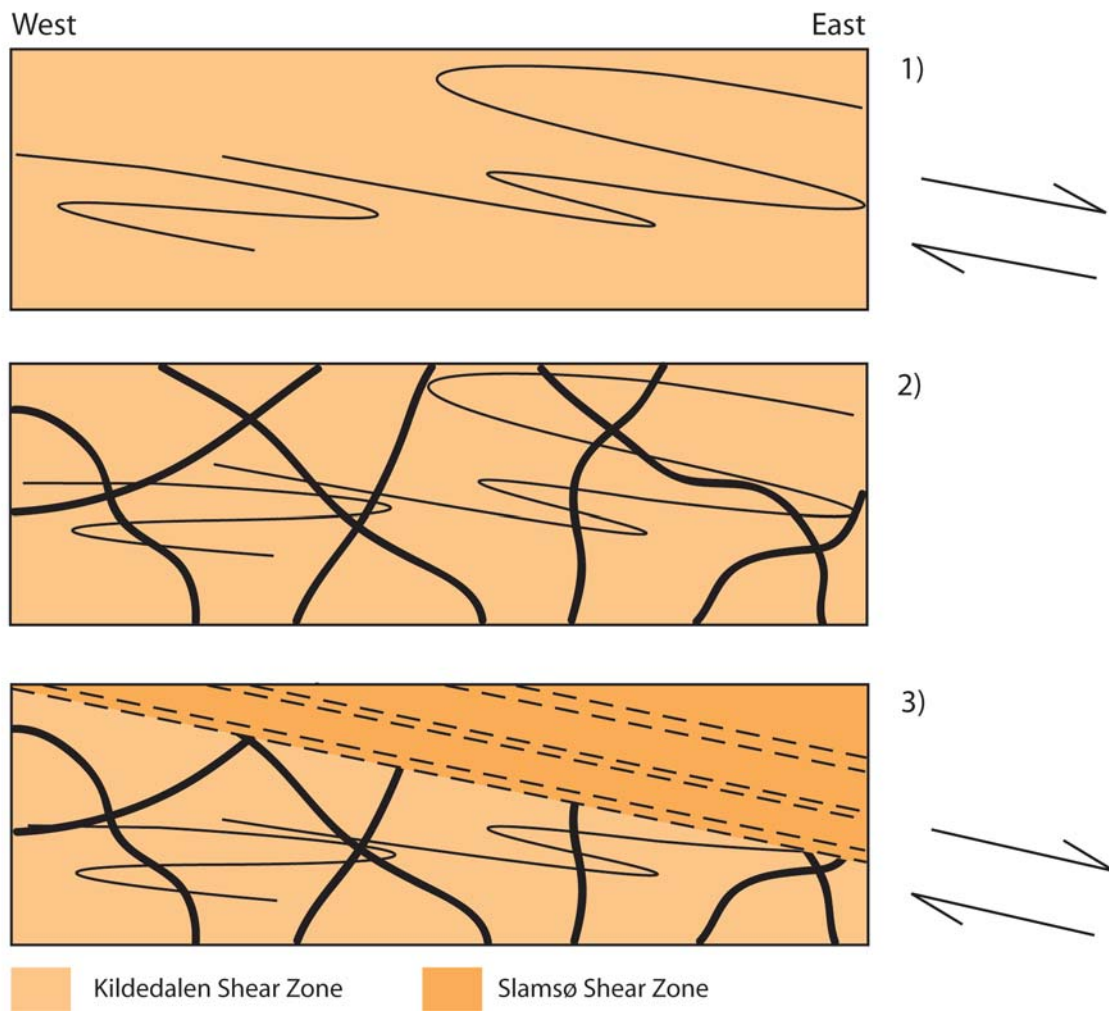


Figure 5.3 This three stage evolutionary model illustrates the interpretation of the development of the Kildedalen Shear Zone and the Slamsø Shear Zone. The Kildedalen Shear Zone develops at stage (1) and is dissected by leuco-granitic veins in stage (2). The Slamsø Shear Zone cut through the upper part of the Kildedalen Shear Zone in stage (3).

5.2.1. The D^L₁ event

The Kildedalen Shear Zone formed during D^L₁, which is the oldest observed deformational event in the allochthonous basement. D^L₁ is characterized by ductile deformation during which the compositional banding in the allochthonous basement is folded into approximately north-south trending isoclinal folds, F^L₁, on a m to cm scale. D^L₁ is interpreted to have formed in the dominant foliation S^L₁, seen in the rock. It developed as an axial planar foliation (Figure 5.4) comprising alternating bands of recrystallized feldspar and aligned amphibole/biotite. The measured

axial surfaces of F^L_1 is subparallel to S^L_1 (Figure 5.4). Strachan (1994) report east-west mineral lineations parallel to the fold axes. The few lineations that were observed at Kildedalen had similar orientations.

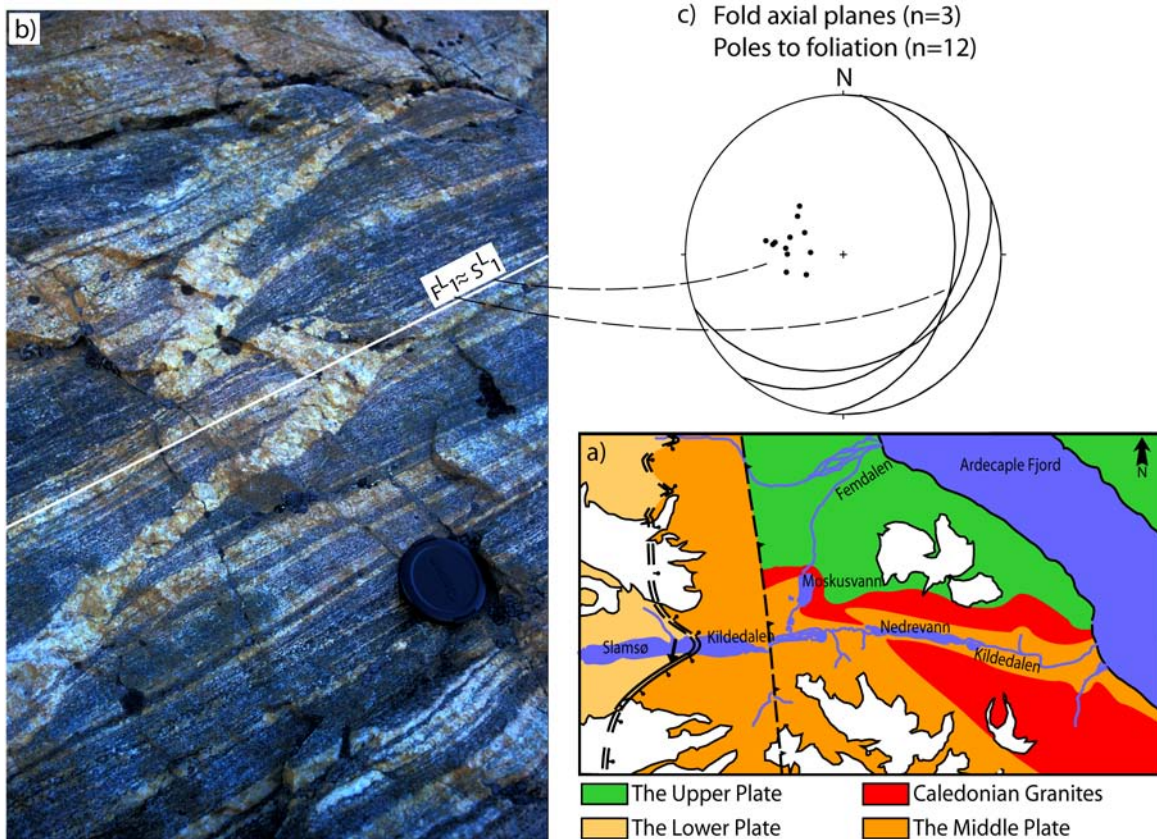


Figure 5.4 Typical appearance of the tonalitic gneisses in the Lower Plate in Kildedalen. The arrow in (a) marks where picture (b) is taken. (b) F^L_1 folds with S^L_1 axial plane foliation from D^L_1 . (c) Stereographic projection of axial planes of folds and of poles to the dominant foliation. Note the coherence between (c) and d) measurements. (b) illustrates (c) well, but it is not the only location that the measurements were obtained.

Ductile shear bands that indicate a top-to-the-east movement are commonly present within the Kildedalen Shear Zone (Figure 5.5). The shear bands are believed to have developed along with the isoclinal folds during the D^L_1 event, or at a later stage under similar P-T conditions.

The banded gneisses of the Kildedalen Shear Zone are cross-cut by numerous post D^L_1 granitic dikes. From a distance (Figure 5.6) these dikes appear to belong to two dikes sets, one almost sub-parallel to the Slamsø Shear Zone and one perpendicular to the shear zone.

The dikes vary in thickness from a few desimeters to several meters. It is evident that the dikes cut the isoclinal folds (F^L_1), and must therefore post-date D^L_1 . The dikes are truncated by the Slamsø Shear Zone (Figure 5.3), hence they pre-date this shear zone.

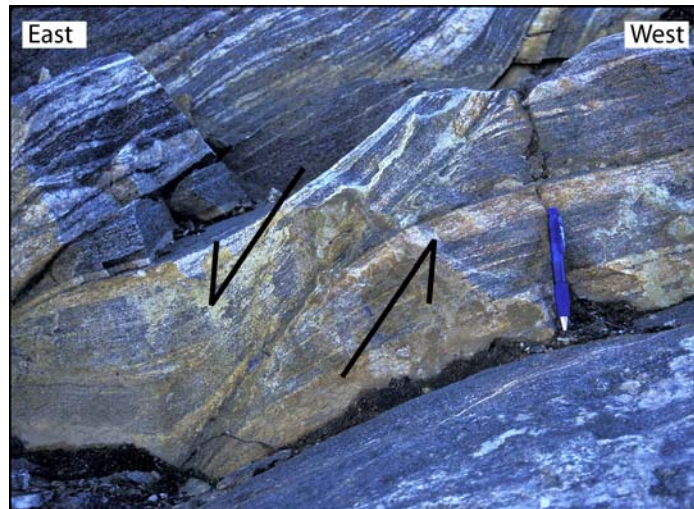


Figure 5.5 This picture shows a shear band related to D_1^L . The arrows indicate top-to-the-east displacement. (The location of this picture is metres away from Figure 5.4)

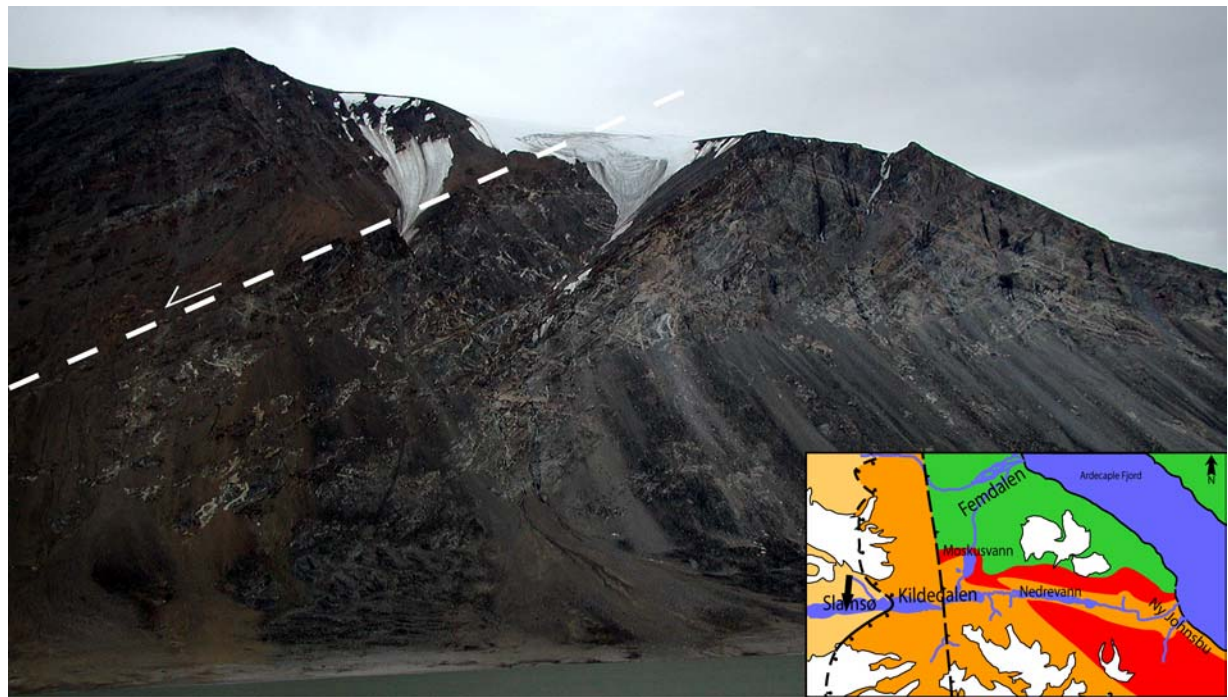


Figure 5.6 Picture showing allochthonous basement and the Smallefjord Sequence on the south side of Slamsø. The dashed line represents the contact separating the Slamsø Shear Zone (Smallefjord Sequence) and the underlying Kildedalen Shear Zone (allochthonous basement). Dikes commonly seen in allochthonous basement terminate abruptly at the base of the Smallefjord Sequence. Displacement along the Slamsø Shear Zone is top-to-the-east (half-arrow). The mountain wall is c. 1000 m high. The picture is taken towards shouth, as indicated by the arrow on the map.

5.2.2. The D^L_2 event

Brittle faults are representative of D^L_2 . They were only observed on a cm scale, and exhibit both extensional displacement.

5.2.3. Summary of the Lower Plate

The evolution of the Lower Plate based on structural observations is shown in figure 5.7, where the evolution is expressed as a three stage cartoon, with two deformational events.

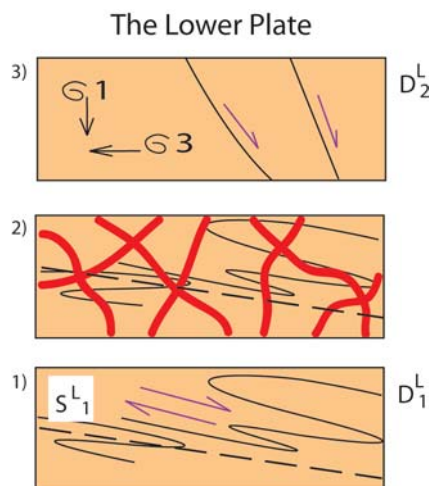


Figure 5.7 Simplified cartoon showing the structural evolution of the Lower Plate. (1) is the first stage associated with the formation of the Kildedalen Shear Zone; (2) represents the intrusion of dikes, and (3) is associated with formation of folds. The dashed lines represent foliation. Solid lines are folds at stages (1) and (2), and faults during stage (3). The thick red lines represent granitic dikes.

5.3. The Middle Plate; The Smallefjord Sequence

The Smallefjord Sequence (3.3.) comprises biotite gneiss, augen gneiss, banded gneiss, quartzites, migmatites and several relatively large granitic bodies. The Slamsø Shear Zone defines the base of the Smallefjord Sequence in the study area.

Strachan et al. (2001) postulate that dikes emplaced in the Smallefjord Sequence controlled segregation and transport of crustally derived granitic melts to higher structural levels. A network of dikes was proposed to have developed during non-coaxial extensional shear in the lower part of the Smallefjord Sequence (Figure 5.8). On the basis of this, a study of the dike orientation in a selected area within the Smallefjord Sequence was undertaken (Figure 5.12), in addition to metamorphic petrology studies (Chapter 4).

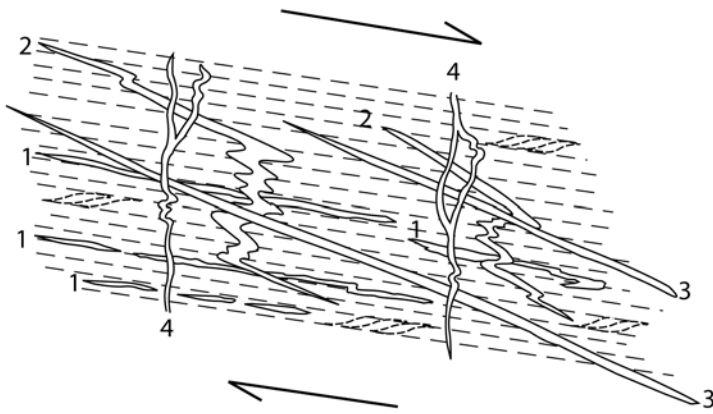


Figure 5.8 Diagrammatic model indicating the relationship between the strain field and the emplacement direction of dikes within the Smallefjord Sequence (Strachan et al., 2001). Four different sheets of dikes occur. The sheets emplaced first are denoted 1 and the ones to be emplaced at last are denoted 4. 1-3 is formed during progressive simple shear, whereas 4 is interpreted to be formed by subvertical flattening. The dashed lines are the main foliation of the host rock. The arrows indicate top-to-the-east extensional shear.

5.3.1. S^M_0 - primary sedimentary bedding

Metasediments with preserved primary sedimentary structures (S^M_0) such as cross-bedding, is preserved locally in the Smallefjord Sequence (Figure 5.9).

5.3.2. The D^M_1 event

The early stages in the tectonometamorphic evolution of the Smallefjord Sequence is poorly known. Data from the garnet bearing high strain zones in the lower part of the Smallefjord Sequence indicates an important event prior to development of the Slamsø Shear Zone and the dominant foliation (S^M_2) in the area. Textrural observations reveal that porphyroblasts of garnet and feldspar are deformed (Figure 5.11) by the D^M_2 event that created the Slamsø Shear Zone (5.3.3.). This indicates the presence of a pre- D^M_2 deformational event. The S^M_1 foliation must have developed during D^M_1 , although this foliation is overprinted.

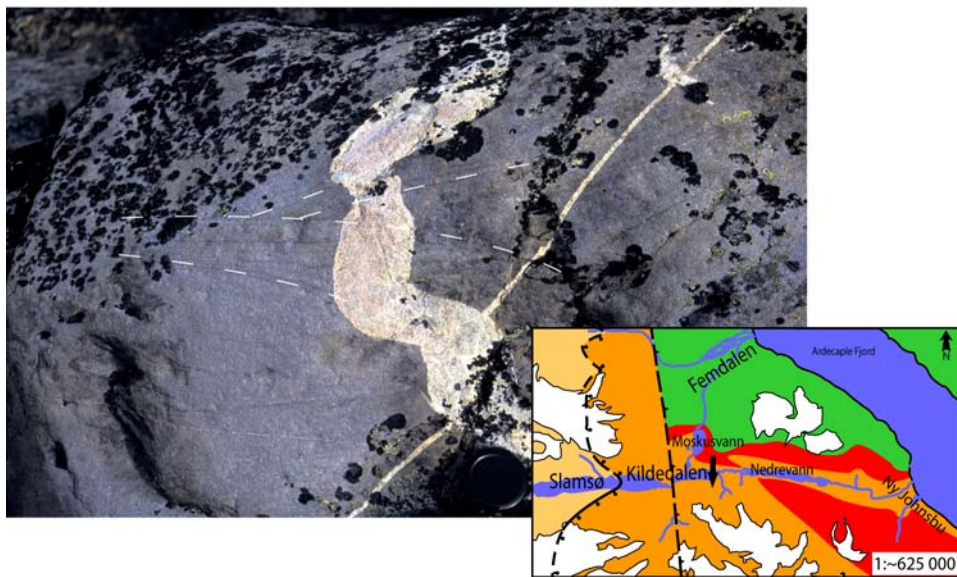


Figure 5.9 Primary sedimentary structures (S^M_0) as seen in metapsammites of the Smallefjord Sequence. The dashed lines represent cross-lamination and show that the psammite at this locality is inverted. Post S^M_0 dikes cut S^M_0 . The arrow on the map shows location and bearing of the picture

5.3.3. The D^M_2 event

D^M_2 produced the Slamsø Shear Zone, which is a ductile north-south striking extensional top-to-the-east shear zone at the base of the Middle Plate (Figure 5.3). The Slamsø Shear Zone affect several lithologies, the main ones being biotite gneisses and mylonitic garnet-mica schists. The garnet-mica schists appear as continuous horizons throughout the shear zone. The biotite gneisses are volumetrically superior to the garnet-mica schists (Figure 5.11). The dominant compositional foliation in the area, S^M_2 , is interpreted to have originated during D^M_2 . In the garnet-mica schists S^M_2 consists of bands of alternating ribbon quartz and bands of mica (Figure 5.11). The orientation of S^M_2 is similar for the garnet-mica gneisses and the biotite gneisses. Millimetre scale bands of feldspar or biotite/amphibole define S^M_2 in the gneiss layers, whereas bands of ribbon quartz or biotite/muscovite define the foliation in the garnet-mica schists. Thickness of the shear zone in this area is c. 250 m. The shear sense indicators are particularly common in the garnet-mica horizons (Figure 5.11). Shear bands, rotated porphyroclasts (Figure 5.10) and sheath folds are observed. Indicators of shear was generally hard find in the Gneiss Unit or the Migmatite Unit, which both

overlie the biotite gneisses in the Smallefjord Sequence (3.3.). Dikes or sills were not observed in the Slamsø Shear Zone.



Figure 5.10 This figure shows a feldspar porphyroblast that is rotated as a result of noncoaxial deformation during D^M_2 . The host rock is a biotite gneiss within the Slamsø Shear Zone. The arrows indicate a top-to-the-east shear.

The mylonitic textures and sense of shear are profound in garnet-mica schists (Figure 5.11).

The C and S bands made up of ribbon quartz or aligned mica are parallel to sub-parallel to each other. The C' bands are extensional shear bands comprising biotite. C' truncates S and C (Figure 5.11).

Post (?) D^M_2 leuco-granitic dikes and sills that cut S^M_0 are recorded in the middle part of the Middle Plate (Figure 5.12), where they are emplaced in augen and banded gneisses. The granitic veins are fine to medium grained and normally less than 50 cm thick. These veins exhibit no systematic pattern, and their orientations are scattered on a stereonet (Figure 5.12). This indicates that the model where veins are thought to be formed during non-coaxial shear (Strachan et al., 2001), is not viable for the Smallefjord Sequence at Kildedalen.

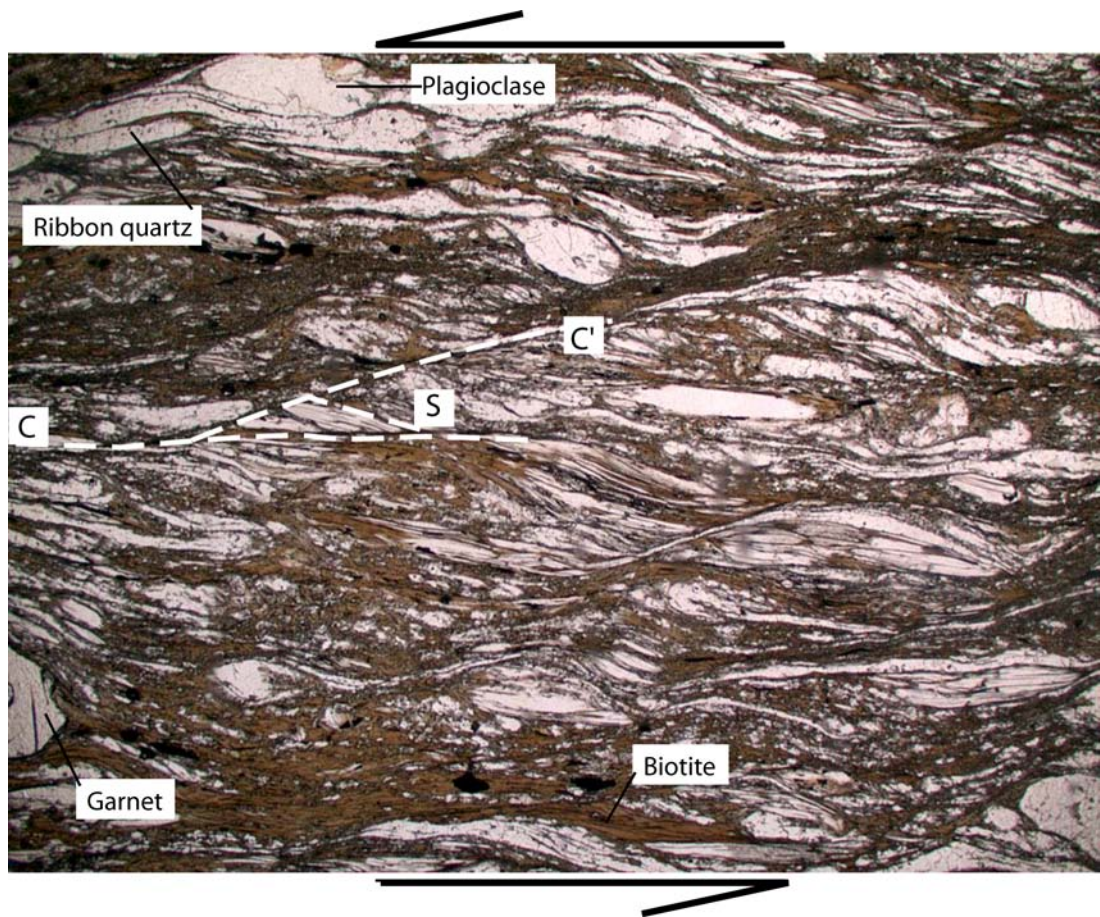


Figure 5.11 Thin section picture showing the extensional shear bands (C') within the garnet-mica schist. The C bands are aligned micas and sillimanites. The arrows indicate the sense of shear that created this texture. Dashed lines represent one example of each of the C, S and C' bands. Image is c. 5 mm across.

5.3.4. The D^M_3 event

The D^M_3 event folded the Smallefjord Sequence. The post D^M_2 leuco-granitic dikes and sills are also folded, and the fold axis trend to the east (Figure 5.13). An axial plane foliation denoted S^M_3 developed as a result of this flattening. This is the dominant foliation in the Smallefjord Sequence (Figure 5.15). Whether or not S^M_3 is parallel or sub-parallel to S^M_0 is unclear. S^M_3 is a compositional foliation comprising bands of quartz, mica, feldspar or amphibole, depending on a sample's position in the Middle Plate.

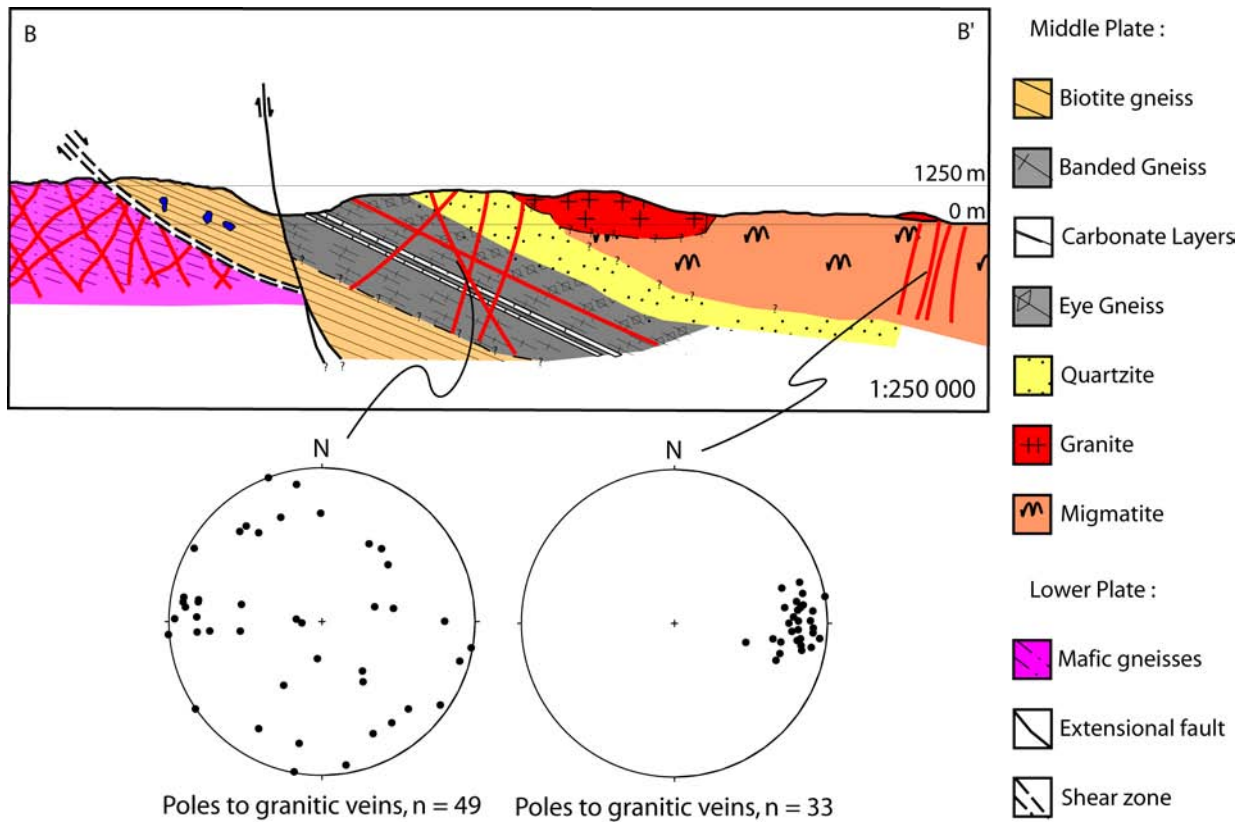


Figure 5.12 The lower left stereonet shows the orientation of the post D^M_2 leuco-granitic veins, that were observed in the Gneiss Unit. The lower right stereonet shows the orientation of the post D^M_3 leuco-granitic veins, that were observed in the Migmatite Unit. The location of the cross-section B-B' is shown on figure 5.1

F^M_1 folds are generally symmetrical, recumbent and isoclinal (Figure 5.14). The folds document significant flattening and the plane of maximum finite stretch is parallel the axial plane foliation S^M_3 (Figure 5.14).

5.3.5. The D^M_4 event

D^M_4 includes folding of the dominant foliation (S^M_3) and the post D^M_2 leuco-granitic veins. This deformational event is not seen throughout Kildedalen, but it is particularly common in the middle part of the Smallefjord Sequence. The folds are gentle- to open, and D^M_4 (Figure 5.16) did not generate a new foliation (Figure 5.15). The strain regimes for D^M_3 and D^M_4 are distinctly different. Relative to the present configuration, the Middle Plate experienced vertical shortening during D^M_3 and horizontal shortening during D^M_4 . The amount of relative shortening of rocks

during D^M_4 is far less than it was for D^M_3 , as can be seen by studying the difference in fold geometries for F^M_1 (Figure 5.14) and F^M_2 (Figure 5.16).

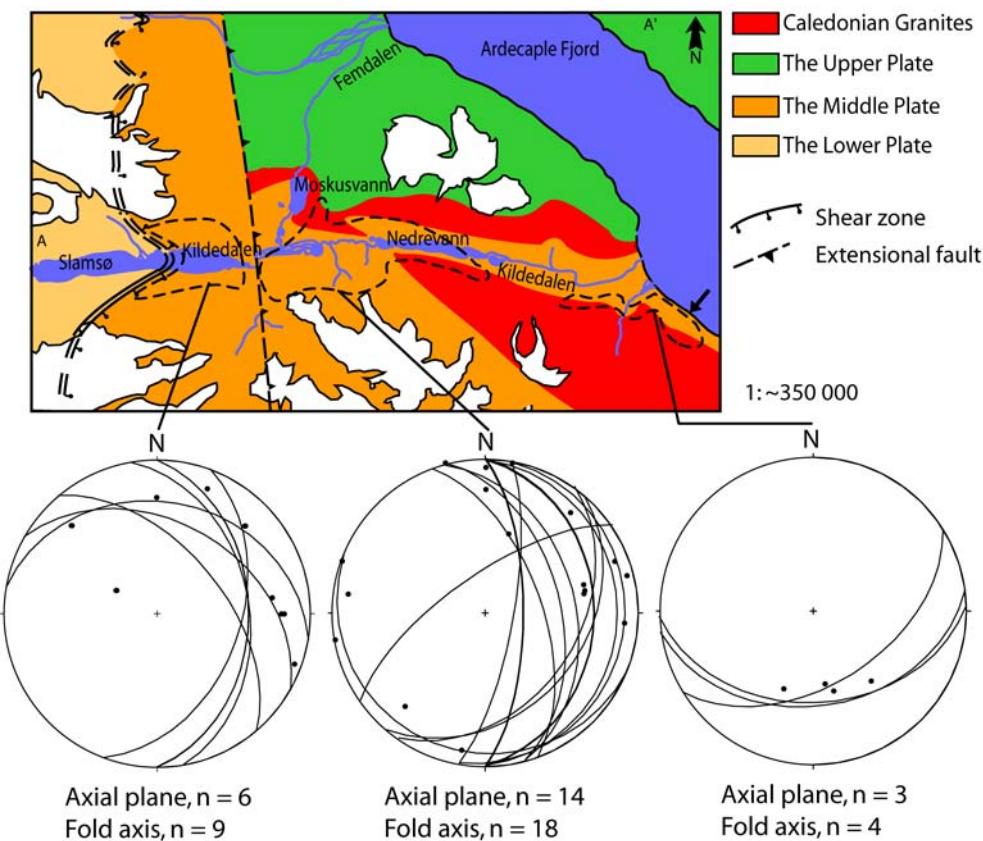


Figure 5.13 The D^M_3 event causes the folding of granitic veins and the creation of F^M_1 . The three stereonets on the figure show the appearance of the folds in main areas of the Smallefjord Sequence. The dashed lines defines the areas where the data was obtained.

Post D^M_4 medium grained to pegmatitic leuco-granitic dikes cut the Smallefjord Sequence (Figure 5.16). They cut straight through the middle and upper part of the Smallefjord Sequence, but were not observed in the biotite gneisses from the lower part of the Smallefjord Sequence. Whether or not the post D^M_4 veins from the middle part of the Smallefjord Sequence have a systematic orientation is unclear. Post D^M_4 veins emplaced in migmatites in the upper part of the Smallefjord Sequence do have a systematic orientation. They strike N-S and dip steeply to the west (Figure 5.12). This implies that the dikes in the migmatite domain formed as a result of E-W extension at this crustal level.

As opposed to pre D^M_4 veins, the post D^M_4 veins are undeformed. Some, but not all of the post D^M_4 veins have a pegmatitic texture. Thus a vein with pegmatitic texture is post D^M_4 , because pre D^M_4 veins do not display a pegmatitic texture.

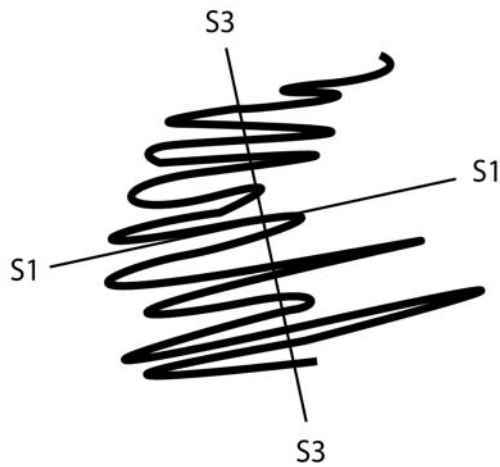
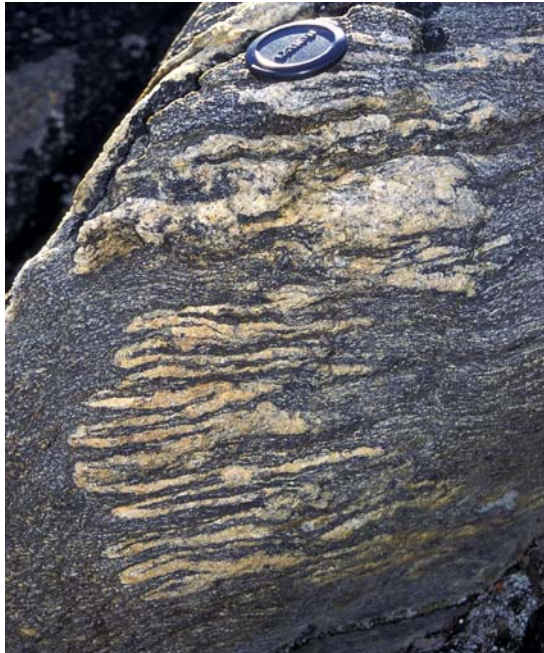


Figure 5.14 The figure shows ptygmatic folds (neosome) (F^M_1) in the Smallefjord Sequence created by D^M_3 . The picture is taken in the upper part of the Middle Plate. S1 is the plane of maximum finite stretch and S3 is the plane of minimum finite stretch.

5.3.6. The D^M_5 event

The brittle extensional faults (D^M_5) show great variation in strike and dip (Figure 5.17). Faults with a significant displacement are scarce in the Smallefjord Sequence at Kildedalen. There is one fault that has a significant displacement, but the fault zone proper cannot be seen due to glacial and fluvioglacial deposits (Figure 5.2). This fault strikes N-S and runs along the middle of a N-S trending valley situated east of Slamsø. This fault displaces the biotite gneisses relative to the overlying eye gneisses. The presence of this fault is undisputable, and it is adequately documented in other areas (Strachan et al., 2001). Other brittle extensional faults were observed in the same area (Figure 5.18).

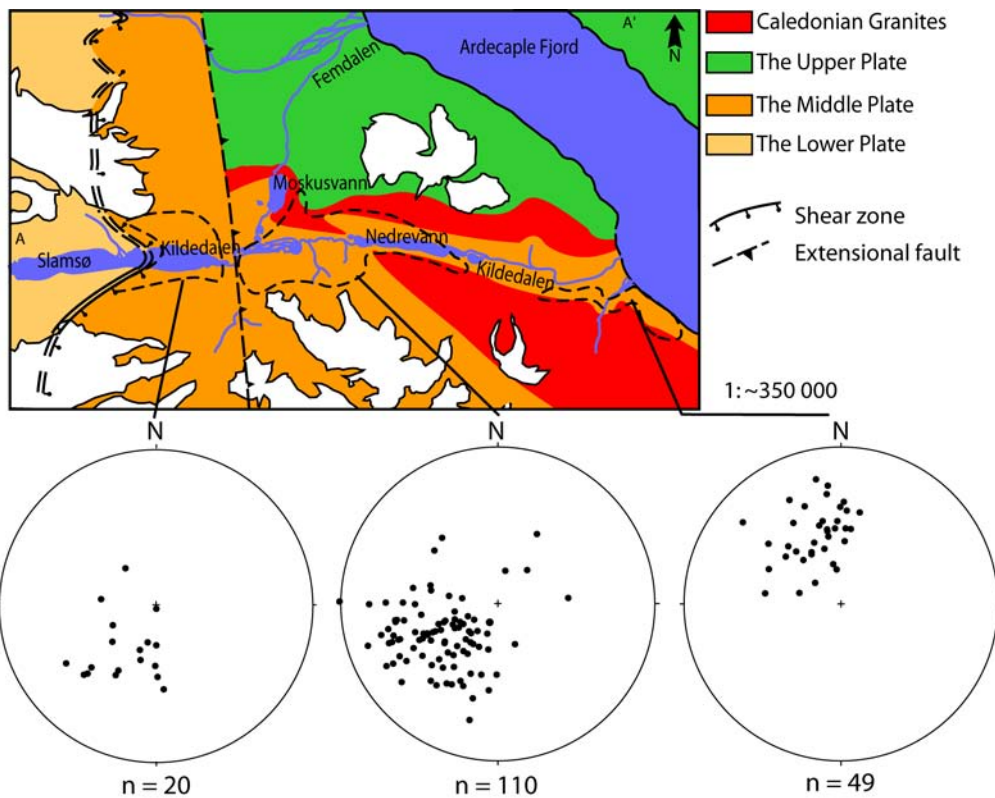


Figure 5.15 The poles to the dominant compositional banding/foliation in the Smallefjord Sequence is plotted in stereonets (Schmidt equal area net), and the dashed lines on the simplified map constrains the sample areas. This foliation represents the dominant compositional foliation (S^M_3).

5.3.7. Summary of the Middle Plate

The structural evolution of the Middle Plate based on my structural observations is summarized in figure 5.19. This cartoon simply visualizes and summarizes the already discussed structural evolution of the Middle Plate. The evolutionary model si composed of 8 stages and 5 deformational events.

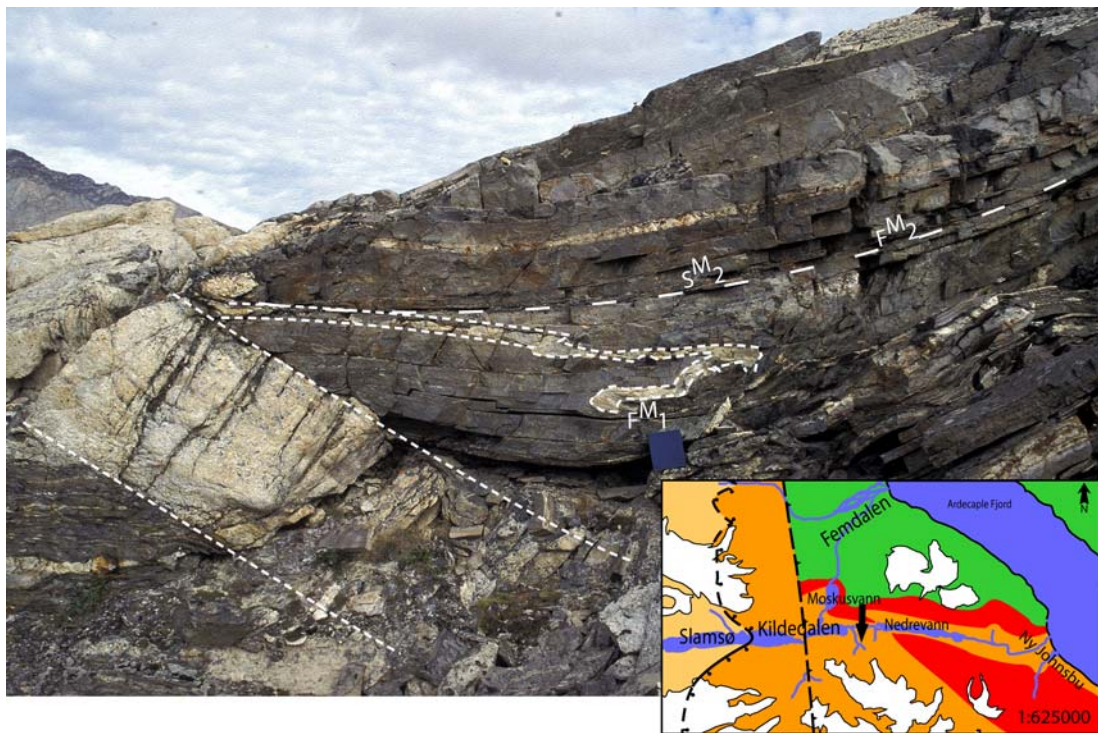


Figure 5.16 Both $D_{M_3}^M$ and $D_{M_4}^M$ have affected the older (relatively thin) veins whereas the youngest veins (relatively thick) cut through the host rock unaffected. Field book for scale. The bearing of the picture is indicated by the arrow on the map.

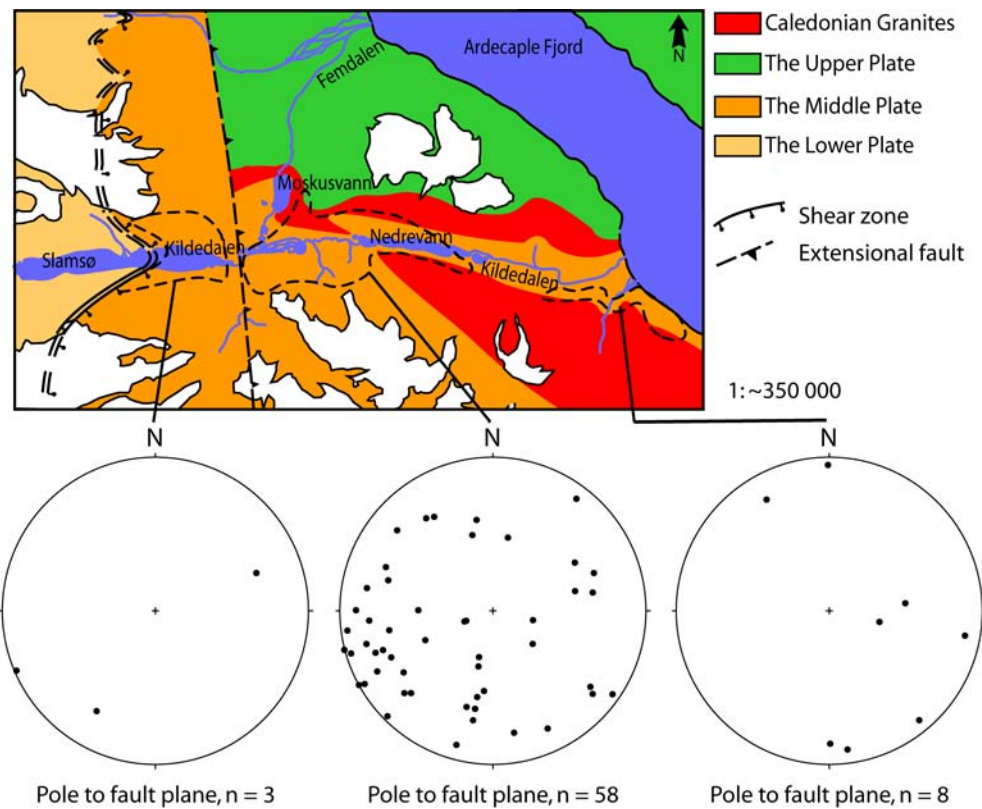


Figure 5.17 Poles to the brittle fault planes generated in the D_5^M event is plotted in the stereonet (Schmidt equal area net) in the figure. The three main areas from which the data was obtained are outlined on the simplified map.



Figure 5.18 Northward picture of extensional faults in the Smallefjord Sequence. Arrows and dashed lines indicate the location of fault planes and the direction of displacement. This locality is located just east of Slamsø and the exposure is about 8 m high.

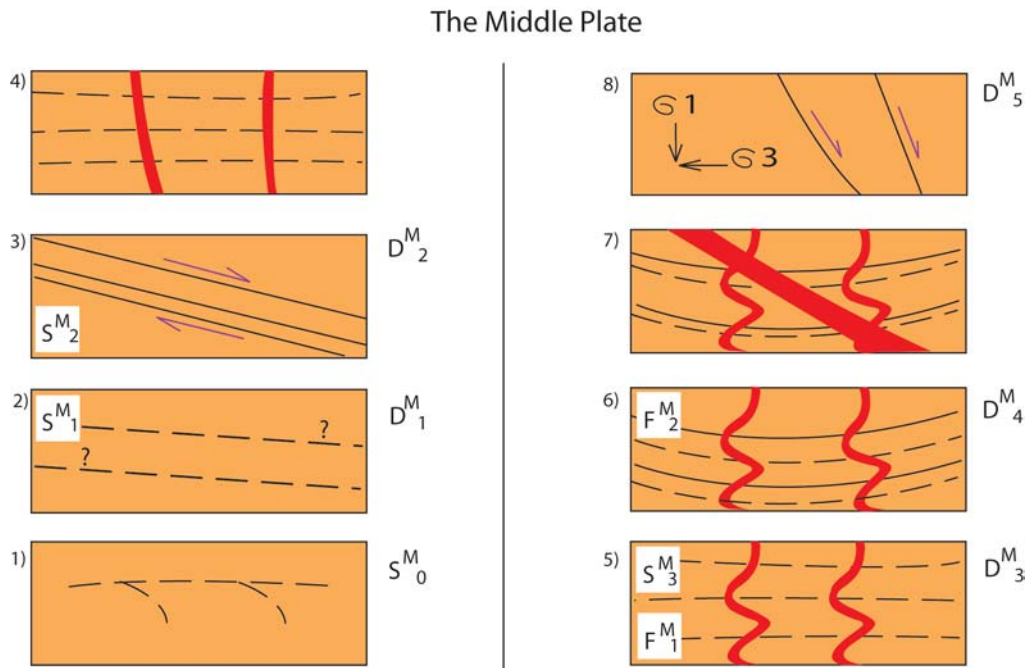


Figure 5.19 Simplified cartoon that summarizes the structural development of the Middle Plate. The numbers (1) through (8) represent evolutionary stages, including pulses of magma emplacement. For example, stage (7) represent intrusion of dikes, but there is deformational event occurring at stage (7). (1) is oldest, (8) is youngest. In (1) there are questionmarks around the foliation planes. This simply means that there is no information on the characteristics of S^M_1 . The dashed lines represent the dominant foliation. The solid lines at stage (3) represent the development of the Slamsø Shear Zone, and the solid lines at stage (8) represent late brittle extensional faults. The solid lines at stage (6) and (7) represent folding of the dominant foliation. Granitic dikes are represented by red, thick lines.

5.4. The Upper Plate; The Eleonore Bay Supergroup

5.4.1. Previous work

The regional orientation of the Eleonore Bay Supergroup in the Ardencaple Fjord area is generally subhorizontal and/or gently warped into broad open folds. Locally, there are however, areas of large scale tight folds (Higgins and Soper, 1994). These include the two anticline/syncline fold pairs; the Troldedal -and the Brædal fold pair and one large syncline called the Ejnar Mikkelsen gletcher syncline (Figure 5.1). The Brædal fold pair strikes NNW-SSE along the east side of, and into Bredefjord. The Brædal fold pair can be observed at Kap Klinkerfues (Higgins and Soper, 1994). The trend of the fold pairs and the syncline is subparallel to the contact between the Eleonore Bay Supergroup and the underlying Smallefjord Sequence or allochthonous basement (Higgins and Soper, 1994).

5.4.2. The D^U_1 event

The sediments of the Eleonore Bay Supergroup were deposited on a submarine, subsiding shelf in Vendian time (Higgins and Soper, 1994). D^U_1 represented by the oldest observed foliation (S^U_1) in the Eleonore Bay Supergroup, appear as a relict metamorphic foliation recorded in the form of inclusion trails in garnet porphyroblasts (Figure 4.9). This fabric appears to be unrelated to the fabrics associated with the younger D^U_1 event.

5.4.3. The D^U_2 event

Large scale regional folds (F^U_1) originated during D^U_2 . This event is widespread in North East Greenland and evidence can be seen in the Kap Klinkerfues outcrop on the east side of Ardencale Fjord (Figure 5.20), and high up in the mountain wall on the NW corner of Femalen (Figure 5.21).



Figure 5.20 The Kap Klinkerfues pluton cuts F^U_1 folds of the D^U_1 event in the Eleonore Bay Supergroup at Kap Klinkerfues, on the east side of Ardencale Fjord. Folds can easily be observed within the box. The picture is taken towards east. The mountain walls are c. 1300 m high.

Syn D^U_2 leuco-granitic veins intruded the Eleonore Bay Supergroup at Kildedalen, and are folded along with the already existing axial plane cleavage to already formed folds. The observed veins cut the dominant foliation, and they have a thickness of less than 1 m (Figure 5.22) but are not abundant.

The outcrop of the F^U_1 folded granitic dikes indicates that they formed during sub-vertical coaxial compression, relative to the present configuration. D^U_2 formed an axial planar foliation, S^U_2 , that is the dominant foliation. This is a compositional foliation comprising alternating layers of quartz and aligned biotite.



Figure 5.21 D^U_2 folds (F^U_1) observed in the lightly-colored layer (where it terminates towards left in the picture) along with D^U_4 extensional faults in the Eleonore Bay Supergroup. Although it looks like contractional faults, due to the oblique view, they are extensional faults. The picture is taken towards north.

5.4.4. The D^U_3 event

D^U_3 generated sinistral kink folds and kink bands at a small scale (Figure 5.23). These post-date D^U_2 , because they affect S^U_2 . The orientation of the kink bands in Moskusdal indicates that they were formed in an approximately east-west compressional regime, relative to the present configuration.

5.4.5. The D^U_4 event

The D^U_4 event is associated with brittle extensional faults. Due to insufficient data no definite structural patterns for the faults can be presumed. The few faults observed suggest they are north striking and top-to-the-east dipping. Brittle extensional faults were observed high up in the mountain wall on the north side of Femdalen (Figure 5.21).

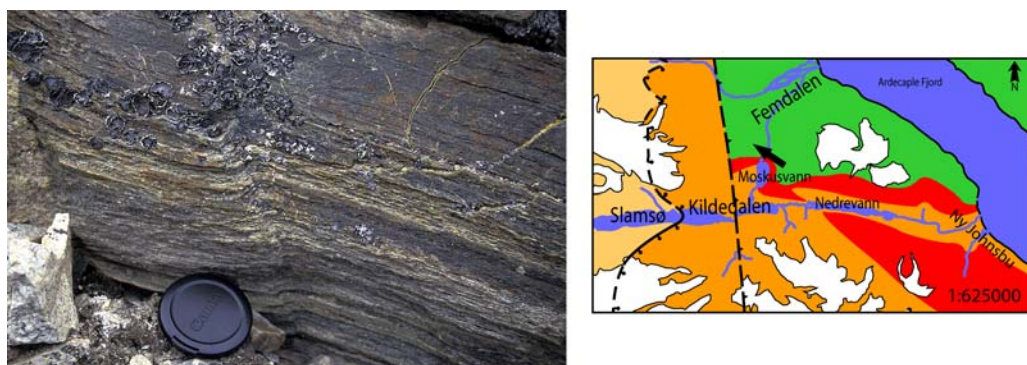
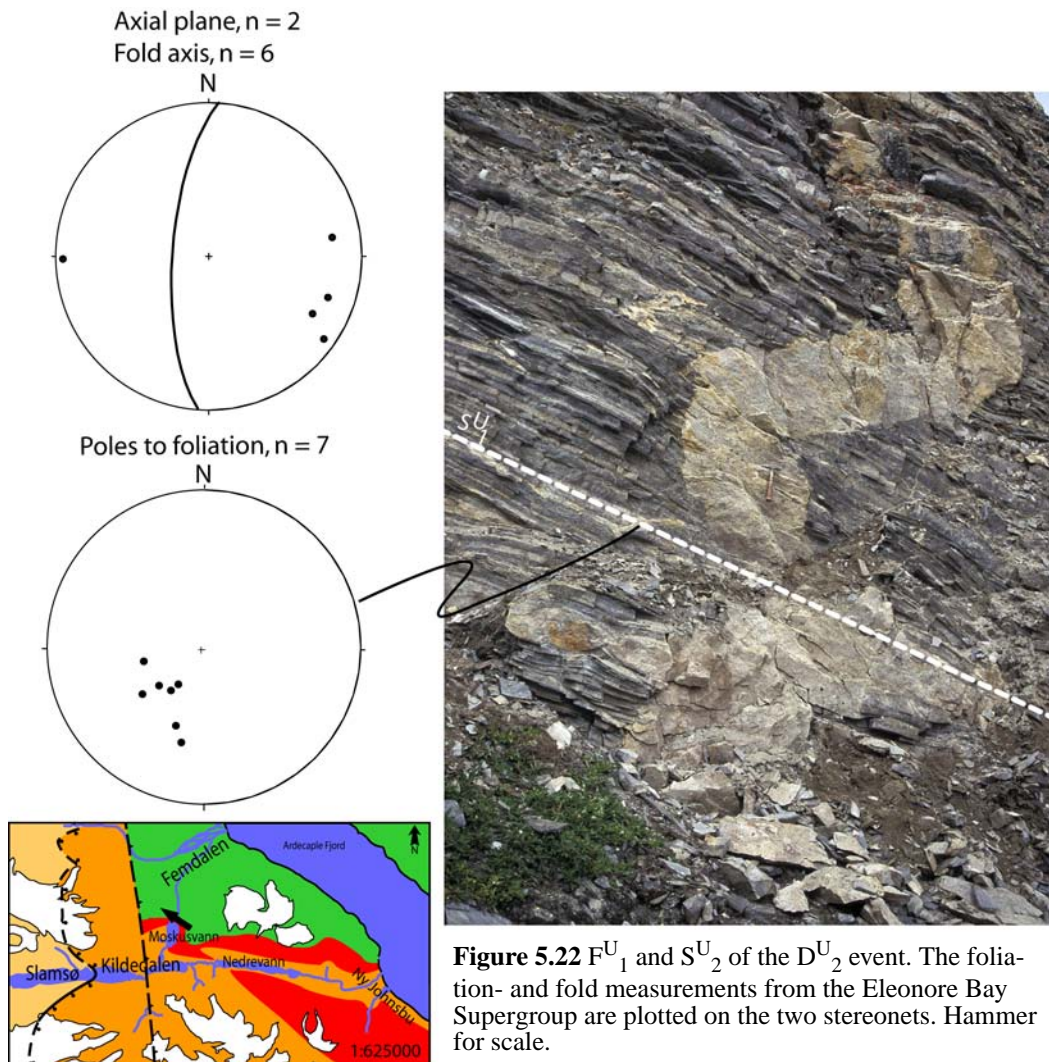


Figure 5.23 Kink fold with kink band from the lower part of the Eleonore Bay Supergroup. The arrow reveals location and bearing on the picture.

5.4.6. Summary of the Upper Plate

The evolution of the Upper Plate, based on structural observations, is presented in figure 5.24. The figure comprises 6 stages of evolution and 4 deformational events.

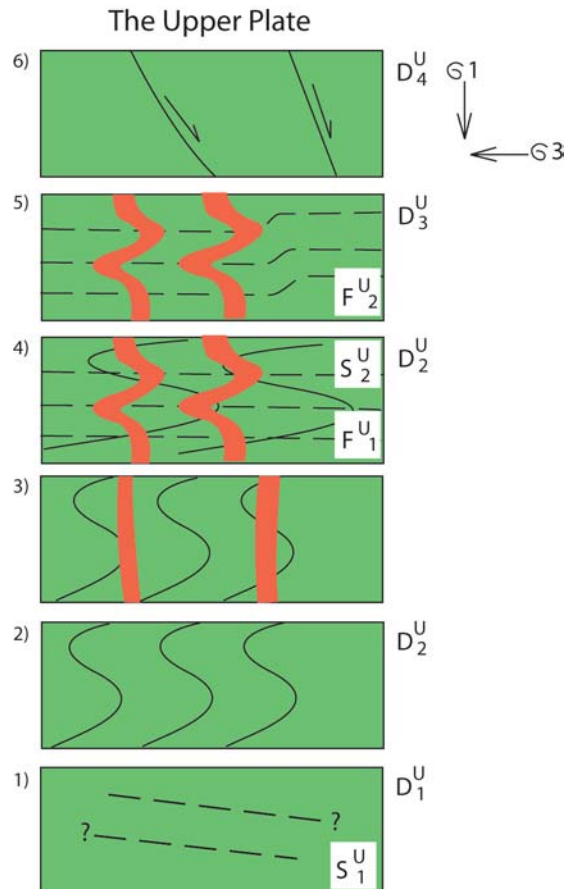


Figure 5.24 Simplified cartoon that summarizes the structural evolution of the Upper Plate. The number (1) through (6) represent evolutionary stages (do not necessarily follow deformational events). For example, (3) is intrusion of dikes, which is not a deformational event. The questionmarks around the foliation in (1), indicate that there is no information about this foliation. The dashed lines represent the dominant foliation, whereas the solid black lines at stages (2) - (4) represent the large scale folds (Figure 5.20). The solid lines at stage (6) represent brittle extensional faults. The thick red lines are granitic dikes.

5.5. Summary

Deformational events have been described separately for Lower Plate, Middle Plate and Upper Plate. Although some of the described events are similar, they can not be safely correlated to each other across plate borders based on field observations.

Primary sedimentary depositional structures are recorded at Middle Plate level. All the other observed foliations are of metamorphic character.

The Lower Plate is intensely sheared, but with the exception of a mylonitic schist layer at the bottom of the Middle Plate, there is no evidence for shearing at structurally higher levels.

Granitic veins cut all plates, and were emplaced in several phases. Veins at different plate levels cannot be safely correlated with each other across plate boundaries. The veins in the Lower Plate are antithetic. With the exception of the post D^M_4 veins in the Middle Plate, all veins at this level display variable dips and strikes.

The Middle and Upper Plate record phases of shortening. One where the shortening is horizontal and one where the shortening is vertical, relative to the present configuration. All plate levels have late, extensional and compressional brittle faults.

6. Discussion and conclusion

6.1. Introduction

In this chapter the structural and metamorphic observations will be discussed. A model for the tectonometamorphic evolution of the Ardencaple Fjord area, based on these observations, will be presented.

6.2. Constraints on tectonometamorphic model

6.2.1. Structural field observations

Structures and deformational events mapped out in the Lower-, Middle- and Upper Plates at Kildedalen cannot be easily correlated from one tectonic level to another. It is probable, however, that some deformational events and their related structures are represented in all 3 plates. D^L_2 , D^M_5 and D^U_5 are late brittle faults that seem to be present in all 3 units (Figure 6.1). D^M_3 and D^U_2 , and D^M_4 and D^U_3 responsible for the macroscopic folds in the area, can possibly also be correlated across tectonic contacts.

Field observations indicate significant extensional displacement across the Kildedalen Shear Zone in the upper part of the allochthonous basement, and across the Slamsø Shear Zone at the base of the Smallefjord Sequence. The Slamsø Shear Zone comprises several zones of mylonitic biotite-garnet pelites, where most of the shear strain is interpreted to have been localized. This interpretation implies that the shear, or displacement across this shear zone, is heterogeneous and can be divided into zones (individual zones of high shear strain). Thus the accumulated displacement across the Slamsø Shear Zone equals the sum of displacement across all the high strain zones. Samples T6 from the base, and AA02-15 from the upper part of the Slamsø Shear Zone, are both taken from such sheared layers. If this interpretation of the structural geology is correct, the difference in P-T conditions between T6 and AA02-15 should be substantially greater than indicated by their present position. Hence, it is concluded that T6 has undergone more exhumation by the Slamsø Shear Zone than AA02-15. Geothermobarometry should reveal whether this is a valid assumption or not.

If geothermobarometry record a clockwise P-T path for both samples (T6 and AA02-15), the field interpretation of extensional displacement across the Slamsø Shear Zone is supported. If it is

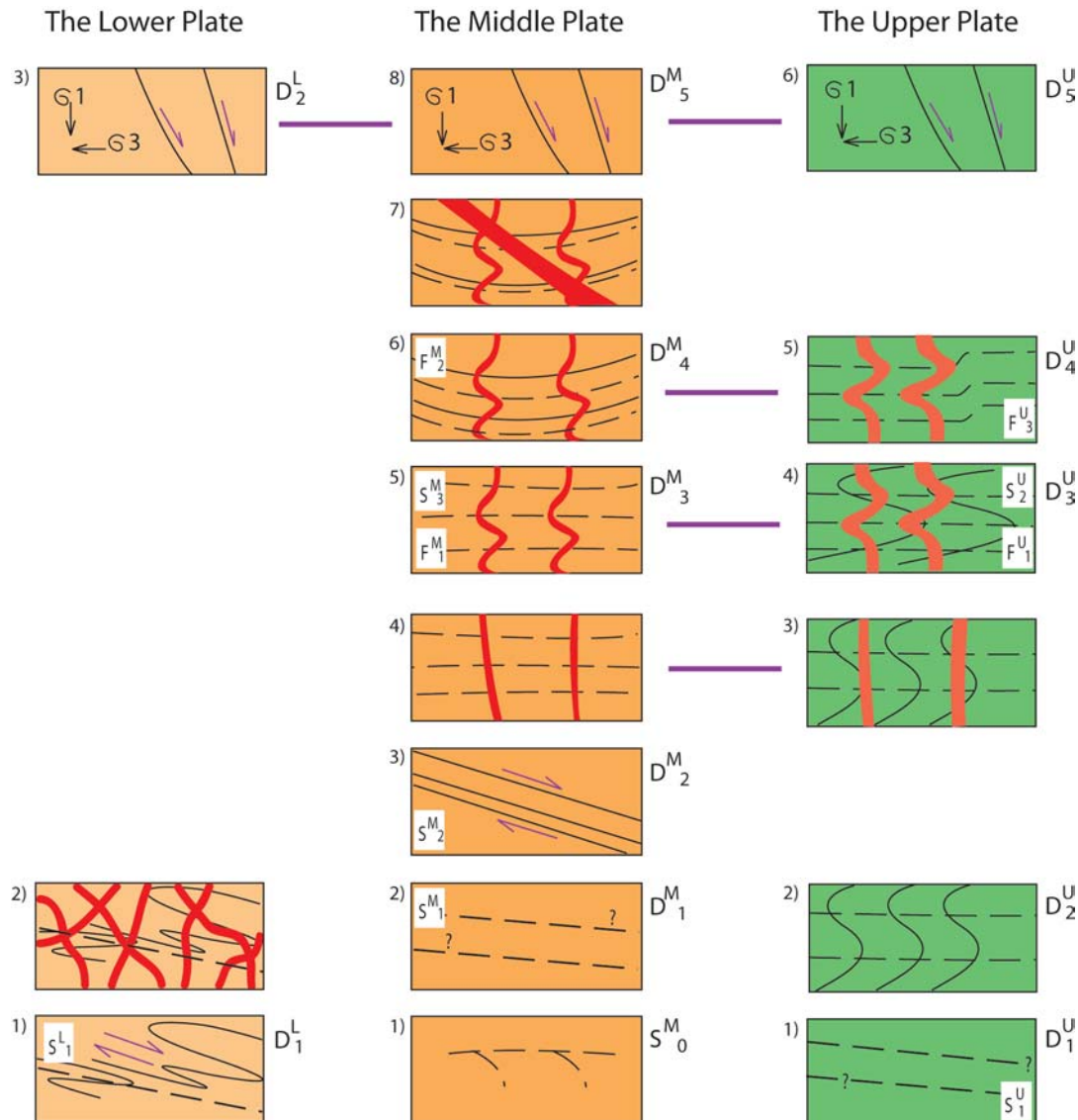


Figure 6.1 Simplified cartoon aiming to relate deformational events and their related structures across plate boundaries. Possible correlations between plate levels are indicated by purple lines. The purple arrows indicate direction of displacement, and the black arrows indicate directions of most and least stress. Question-marks indicate that the properties of foliation are not known.

assumed that shear is localized within numerous high-strain zones, the difference between P-T conditions for T6 and AA02-15 should be greater at peak than post-peak metamorphism. If these inferred high-strain shear zones do not exist, the difference between peak P-T conditions for T6 and AA02-15 should equal the difference between post-peak P-T for the two samples, respectively.

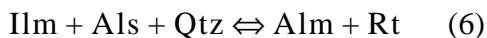
The late brittle fault at the base of the Slamsø Shear Zone, and also below T6 and AA02-15, will have little or no influence on the tectonic exhumation history of the two samples.

Apart from a late brittle fault, no tectonic boundaries were found between AA02-15 of the Smallefjord Sequence and AA02-23, situated in the lower part of the Eleonore Bay Supergroup. A high strain zone separating the Eleonore Bay Supergroup and the Smallefjord Sequence has been proposed by others (Friderichsen et al., 1994), but this tectonic feature was not observed around Kildedalen. If this tectonic contact is present, it is concealed by an undeformed granite pluton emplaced along the Eleonore Bay Supergroup-Smallefjord Sequence contact. Thus a tectonic contact, if it exists, must predate emplacement of the pluton. This tectonic contact, if present, will have influenced the tectonic exhumation of T6 and AA02-15, but not AA02-23. We have no evidence for an extensional fault above AA02-23, which may have influenced the exhumation of AA02-23. However, this does not rule out the possibility of tectonic boundaries at higher structural levels within the EBSGp.

One late, steep brittle extensional fault cut through the Smallefjord Sequence structurally above AA02-15. The magnitude of displacement on this fault is unknown. This fault has not significantly influenced exhumation of T6 and AA02-15.

6.2.2. Petrological constraints

As described in chapter 4.5, maximum temperature and pressure for peak metamorphic conditions in samples T6 and AA02-15 are constrained by two reactions:



T6 garnets have ilmenite inclusions indicating that prograde growth took place on the ilmenite side (lower P side) of reaction (6). Maximum peak metamorphic conditions for T6 and AA02-15 is thus constrained by reactions to be less than 830°C and 13 kbars

AA02-15 contains pre-kinematic kyanite and syn-kinematic sillimanite. The phase reaction:



implies that the pressure decreased sometime after kyanite formation, favouring sillimanite stability. Furthermore, retrograde biotite, plagioclase, quartz and aluminium silicate formed by the breakdown of garnet, implying that the rock passed reaction (7) on the retrograde path. This indicates that AA02-15 has undergone a retrograde development from high-grade conditions to medium-grade conditions (Figure 6.2).

The field relationships indicate that T6 has been at greater depth than AA02-15. The interpretation that extensional displacement along one or more of the high strain zones within the Slamsø Shear Zone exhumed T6 relative to AA02-15, supports the assumption that T6 experienced higher P-T conditions than AA02-15. This assumption, along with observed kyanite in AA02-15, justifies the proposition that T6 experienced P-T conditions associated with kyanite stability, although no kyanite is present in the rock.

AA02-23 contains coexisting sillimanite and K-feldspar. The absence of kyanite and presence of sillimanite indicates that prograde metamorphism remained in the sillimanite stability field. Although kyanite is absent in this sample, it cannot be excluded that the sample contained kyanite on the prograde path, and that kyanite has been reacted out during retrogression. No evidence for anatexis was observed in the EBSGp, which implies that reaction (7) was never crossed. Thus reaction (7) constrains peak temperatures to less than c. 720°C, whereas the kyanite stability field constrains maximum pressure to c. 8 kbars (Figure 6.2).

Several metamorphic events?

The recorded metamorphism of the Smallefjord Sequence is interpreted to be related to Caledonian migmatitization and granite emplacement at c. 425-430 Ma (Strachan et al., 2001). Garnet zonation profiles may possibly yield information on older (e.g Grenvillian or an early Caledonian event), or younger metamorphic events inflicted with the Smallefjord Sequence.

At high grade metamorphism, the element distribution in garnet will homogenize at temperatures greater than c. 700°C (Chapter 4.4.2.), and possibly older metamorphic events will be overprinted. A low-grade metamorphic event, that is unable to overprint the preceding high-grade metamorphic event, is traceable within garnet zonation profiles. Garnet growth along the prograde path of a low grade metamorphic event should affect the zonation profile, and yield a decrease in the

Fe/(Fe+Mg) ratio due to increased temperatures in the system, and an increase in Ca due to increasing pressure in the system.

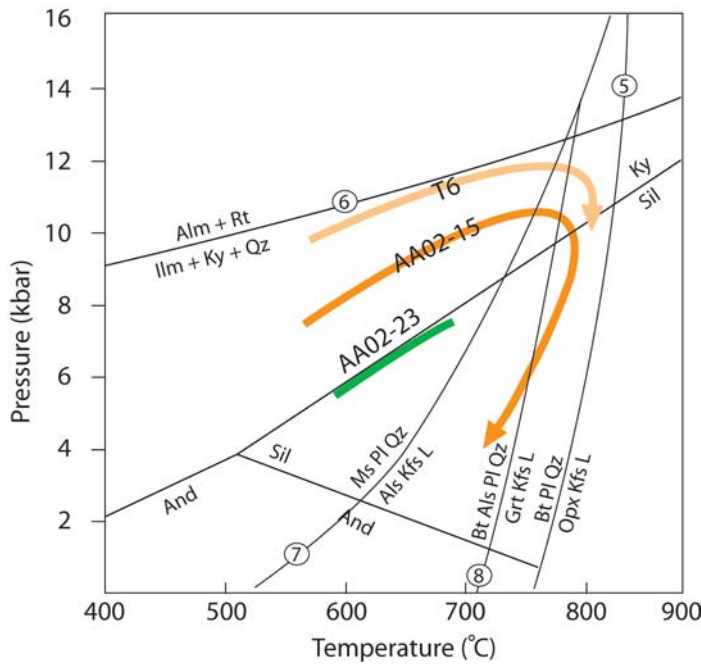


Figure 6.2 The interpreted P-T paths for T6, AA02-15 and AA02-23 in a petrogenetic grid in a PT diagram. The paths are constrained by known mineral reactions. Petrological examinations of each sample identified which reactions had been crossed or not. Reactions (7) and (8) are from Le Breton and Thomson (1988), (5) is from Spear and Parrish (1996) and (6) is from Bohlen et al. (1983). Aluminium silicate stability after Salje (1986). The trajectory of the P-T paths is poorly constrained and may be slightly different from the ones on the figure.

The zonation profiles for T6 and AA02-15 (Figure 4.11) both exhibit fairly flat compositional curves for the Fe/(Fe+Mg) ratio from core to rim, with a slight increase towards the rim. This indicates that peak temperature was high enough for garnet to homogenize, and erase patterns from the prograde path. This temperature estimate is supported by the co-existence of kyanite and K-feldspar (AA02-15). The increase in the Fe/(Fe+Mg) ratio towards the garnet rims is interpreted to represent retrogression from peak metamorphism (Spear and Florence, 1992).

The Ca content in garnet is controlled by reaction (2), and the Ca content in garnet will decrease with decreasing pressure (Spear, 1993). Both zonation profiles (Figure 4.11) record relatively flat element distribution curves for Ca from outer core to rim. There are areas with lower Ca concentration in the central parts of the garnets, but this is interpreted to be due to plagioclase inclusions. AA02-15 record a flat Ca curve in the inner core, whereas T6 records an increase from the very center of the garnet towards the outskirts of the inner core. This distinct increase is interpreted to

represent the prograde path of the high-grade peak metamorphism in T6. The diffusion rate for Ca is slow, and in this case too slow, for the inner parts of garnet to homogenise completely.

The Ca decrease towards the garnet rims is interpreted to be related to a decrease in pressure.

Mn is expected to increase at the rim in high grade garnets (Yardley, 1977), but exhibits a decrease in this sample. This indicates that the garnet is retrogressed.

The garnet zonation profiles for AA02-23 (Figure 4.13) record a trend where Mn and Ca is enriched in the core relative to the rims, whereas the Fe and Mg content is greatest at the rims. This is common for prograde growth in low-grade garnets (Yardley, 1977; Spear and Florence, 1992; Spear et al., 1999; White and Hodges, 2003; Tropper and Recheis, 2003).

The Ca decreases, whereas the Fe/(Fe+Mg) ratio increases slightly at the garnet rims. This is interpreted to represent the post-peak retrograde development, which both decreasing pressure and temperature.

The Mn content increases notably just where Ca starts to decrease dramatically, suggesting that the Mn content is somehow related to the Ca content. This is however, unclear. The heterogeneous zonation profiles for garnet indicate that temperatures at peak metamorphism for AA02-23 was less than 700°C.

The element distribution profiles for garnet in T6 and AA02-15 record a high-grade metamorphic event, where the element distribution is homogenized and possibly older metamorphic events are overprinted. Element distribution patterns indicating retrogression were observed at the rims. No low-grade metamorphic events were observed within the garnets.

Garnets in AA02-23 record a prograde growth that is typical for low-grade garnets. Thus, high-grade Caledonian metamorphism appear not recorded in this sample.

6.2.3. Geothermobarometry

The GBPQ geobarometer (Wu et al., 2004) and the garnet-biotite geothermometer (Holdaway, 2000) were applied to samples T6, AA02-15 and AA02-23.

Selection of metamorphic minerals for thermobarometry was done based on the criteras discussed in chapter 4.7. P-T estimates for both peak- and post-peak metamorphic conditions were obtained for T6 and AA02-15. Only post-peak metamorphic conditions were calculated for AA02-23, as

petrological circumstances in this rock conflict with the criterias formulated for estimation of peak metamorphic conditions (4.7).

Estimated peak metamorphic conditions for T6 is in the range 820 – 830°C and c. 11.3-13.0 kbar. Post-peak metamorphic conditions is in the range 580 – 620°C and c. 5.6-6.3 kbar.

Estimated peak metamorphic conditions for AA02-15 is in the range 690 – 715°C and c. 7-8 kbar. Post-peak metamorphic conditions is in the range 585 – 600°C and c. 4 kbar.

Estimated post-peak metamorphic conditions for AA02-23 is in the range 610 – 615°C and c. 6.0-6.5 kbar.

The garnet cores used for P-T calculations, might not reflect the absoulte peak metamorphic composition of garnet. Diffusion of elements is effective at temperatures greater than 700°C , and this might have changed the peak composition of garnets slightly. Field observations in Kildedalen suggest that T6 and AA02-15 have been significantly exhumed through displacement along the Slamsø Shear Zone. Tectonically controlled exhumation is commonly associated with isothermal decompression (Ring et al., 1999), which is likely to have occurred at Kildedalen. Isothermal decompression reduces pressure quickly, followed by subsequent decrease in temperature. If diffusion was effective during isothermal decompression, decreasing Ca content from core to rim should evolve. This is not the case for the garnets in T6 and AA02-15.

Thus, the garnet cores are thought to represent peak metamorphic conditions, or conditions close to peak metamorphic conditions.

6.2.4. Thermodynamic modeling - DOMINO

DOMINO produced stability fields for mineral assemblages in P-T space based on whole rock chemistry.

The stability field for the high-grade T6 metapelite are in a large area in P-T space, 3-12 kbar and 800 – 1000°C .

AA02-15 record two areas of stability. The stability field for the kyanite bearing assemblage, thought to represent peak pressure, is constrained between 7-10 kbar and temperature c. 600 – 700°C . The stability field for the sillimanite bearing assemblage, thought to represent peak temperature, record stability between 4-8.5 kbar and c. 600 – 800°C .

The AA02-23 stability field indicates metamorphism constrains less than 8 kbar and c. 575 – 750°C. However, from chapter 6.2.1. the temperature is inferred to have been less than 700C.

6.2.5. Summary

Structural field observations, petrological data, geothermobarometry and thermodynamic modeling are in fair agreement with each other. For AA02-15, the temperature calculated through geothermometry is probably 20 – 50°C too low due to garnet homogenization through diffusion. The thermometric calculation puts AA02-15 on the low-temperature side of reaction (8), suggesting it didn't cross this reaction on the prograde path. This reaction is clearly crossed, as is documented in plagioclase-, quartz- and biotite inclusions i garnet. Thus, the calculated temperature is slightly too low. This is probably due to intracrystalline diffusion in garnet at conditions close to peak conditions, changing the peak composition of garnet just enough to slightly reduce the calculated temperature.

The clockwise P-T paths for T6 and AA02-15 determined petrologically and supported through thermobarometry support the field assumption of extensional displacement within the Slamsø Shear Zone. Information about the P-T evolution of AA02-23 is more limited.

If the Slamsø Shear Zone was contractional, a counter-clockwise P-T path for samples T6 and AA02-15 would be recorded by geothermobarometry.

Geothermobarometry documents that T6 has been subjected to higher P-T conditions than AA02-15. The difference in calculated peak-pressure for T6 and AA02-15 is c. 4 kbar, whereas this difference is reduced to c. 1.5 kbar for post-peak conditions. This change supports a tectonic model with an extensional high strain zone between samples T6 and AA02-15.

Calculations for post-peak metamorphic conditions are fairly similar for T6 and AA02-23, c. 600°C and 6 kbar. AA02-15 record post-peak metamorphic conditions of c. 600°C and 4 kbar. The calculated post-peak pressures are in agreement with the structural position of the three localities.

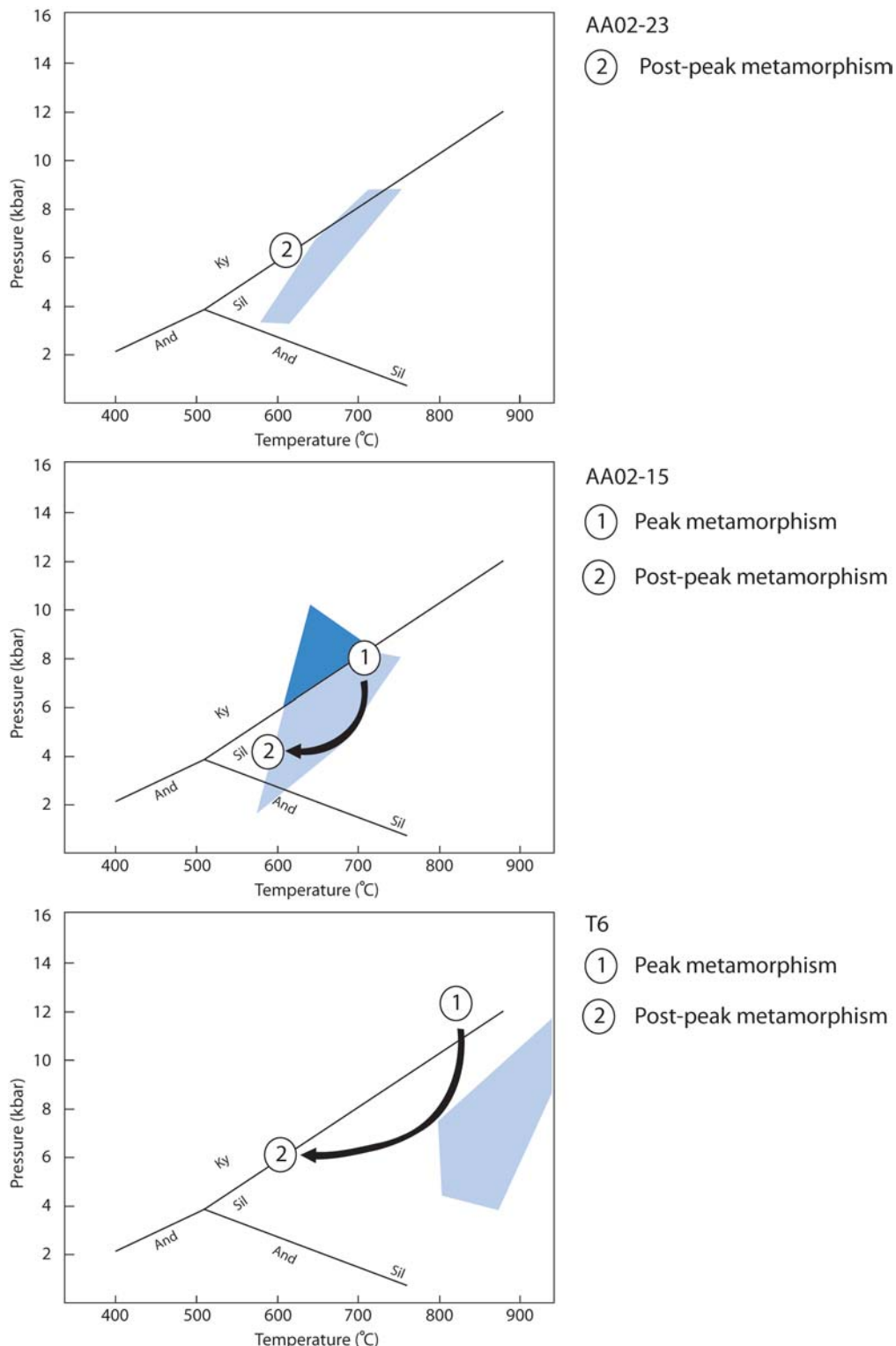


Figure 6.3 Diagrams showing the calculated peak- and post-peak metamorphic conditions (GBPQ geobarometer (Wu et al., 2004) and garnet-biotite geothermometer (Holdaway, 2000)) for T6, AA02-15 and AA02-23 respectively. DOMINO stability fields are shaded areas, and in AA02-15 the darker field is for kyanite stability and the lighter field represents sillimanite stability. The arrows from (1) to (2) display the inferred path in P-T space for the rocks during retrogression.

Estimated post-peak conditions for AA02-23 are considered similar to peak conditions for AA02-23, of which there is no information. The reason for this assumption is that the garnet element distribution profiles of AA02-23 exhibit a prograde zonation pattern, as it is typical seen in low grade rocks (Spear and Florence, 1992). An increase in temperature up to 650 – 700°C would homogenize these garnets. There is also no sign of kyanite, which constrains P to less than c. 6 kbar. These constraints are comparable to the calculated post-peak conditions.

The thermodynamic modeling data from DOMINO give good correlation with geothermobarometric data for AA02-15 and AA02-23. For T6, DOMINO give lower pressure estimates than geobarometry. The underestimation of pressure is related to the rutile - ilmenite transition (A) in the termodynamic calculations. At higher pressure rutile + magnetite is thermodynamically favourable, which is promoted by higher oxygen fugacities and/or water activity. Reducing either of these two parameters would promote the stability of ilmenite at higher pressures, resulting in a better correlation between DOMINO and geothermobarometric calculations. The GPBQ barometer applied to T6 is tailor made for these kind of rocks (aluminium silicate absent), suggests that the barometry results are more sensible than the DOMINO stability field for this sample.

6.3. Other models from the Ardencaple Fjord area

6.3.1. A proposed model based on geochronology

Røtevatn (2004) demonstrated a systematic younging of ages from higher towards lower lithotectonic units in Kildedalen:

- (1) Samples from the Lower Plate (allochthonous basement) record muscovite and biotite cooling ages of c. 379-383 Ma.
- (2) Samples from the Middle Plate (Smallefjord Sequence) record muscovite and biotite cooling ages of c. 410-415 Ma.
- (3) Samples from the Upper Plate (Eleonore Bay Supergroup) record muscovite and biotite cooling ages of c. 418-423 Ma.

The thermochronological data combined with field observations formed the basis for the following tectonic model for the Ardencaple Fjord area (Røtevatn, 2004). This model can be outlined in three steps:

- 1) Tecton-controlled uplift of the Eleonore Bay Supergroup that led to increased topography and erosion rates, possibly accompanied by tectonic denudation at higher crustal levels. The resulting exhumation eventually cooled the Eleonore Bay Supergroup below closure temperature for Ar diffusion in muscovite at c. 418-423 Ma.
- 2) The contractional event was followed by extension and the formation of an extensional shear zone below the Eleonore Bay Supergroup, resulting in uplift and cooling of the Smallefjord Sequence at c. 410-415 Ma. This is thought to closely date the formation of the inferred shear zone separating Eleonore Bay Supergroup and the Smallefjord Sequence.
- 3) Post-contractional extension and the formation of the Slamsø Shear Zone (subsequent to the formation of the Kildedalen Shear Zone). This cooled rock of the allochthonous basement at c. 379-383 Ma, which is thought to closely date the formation of the Slamsø Shear Zone.

Problems with this model

The Kap Klinkerfues pluton is dated at c. 425 Ma (Strachan et al., 2001), an age that is in accordance with age determinations for granites emplaced at the same structural level as the Kap Klinkerfues. It seems likely that the Kap Klinkerfues, Kap Buch and the Moskusdal granite represent parts of the same body, or at least from the same magmatic event. The formation age of the migmatite, that directly underlies the Kap Buch pluton, is c. 423 Ma (pers. com. E. Rehnstrøm). This constrains the upper age for the Kap Buch and the Moskusdal plutons to 423 Ma. The Moskusdal granite is undeformed, which implies that the proposed high strain zone separating the Eleonore Bay Supergroup and the Smallefjord Sequence must predate the granite emplacement. In Rotevatn's model, this high strain zone is interpreted to be present at 410-415 Ma, which is post granite emplacement. Displacement along this proposed shear zone later than c. 423 can be discarded.

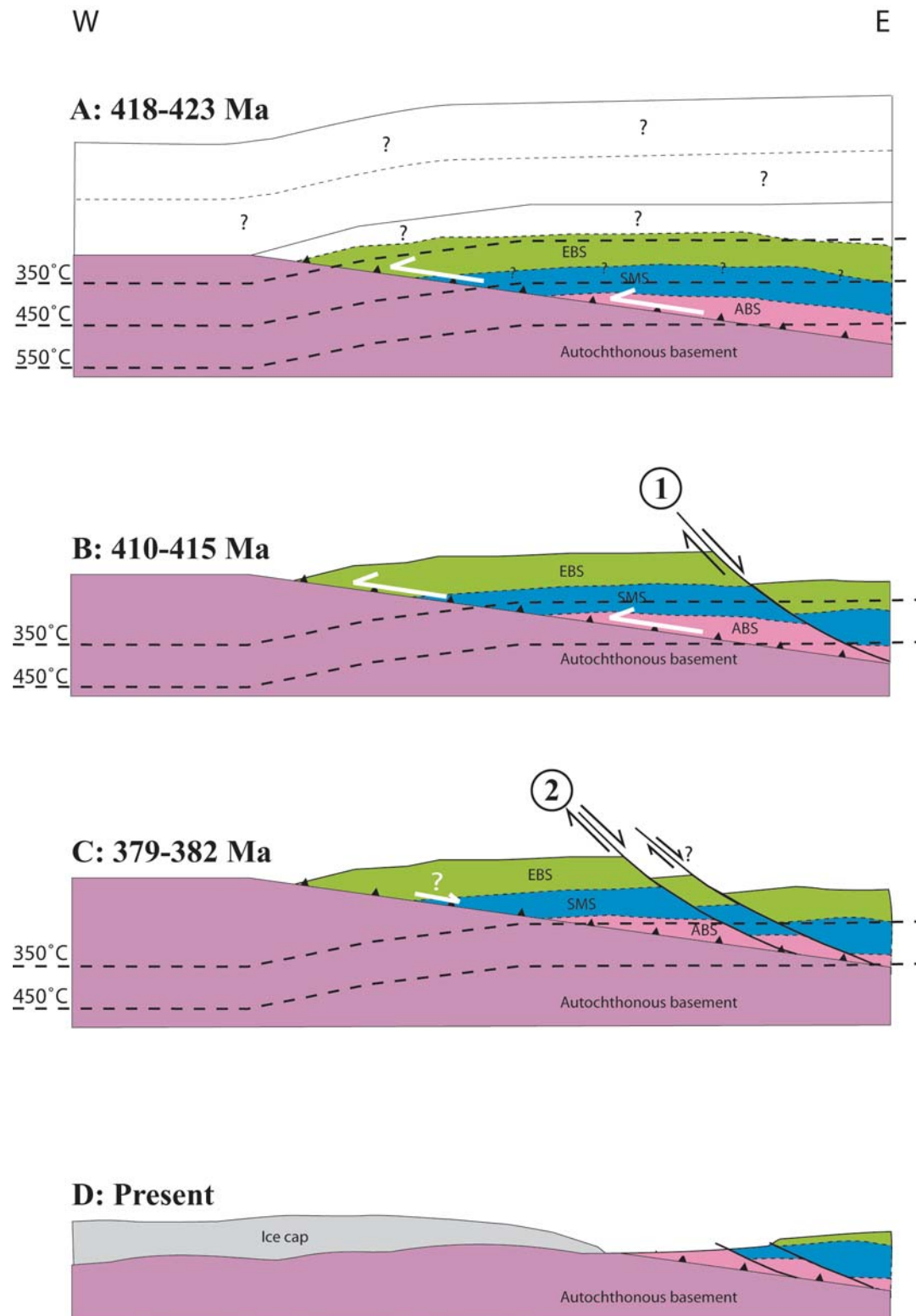


Figure 6.4 Tectonic model for the Ardencaple Fjord area based on Ar/Ar cooling ages Røtevatn (2004). (1) represents the inferred shear zone separating the Eleonore Bay Supergroup and the Smallefjord Sequence. (2) represents the Slamsø Shear Zone.

6.3.2. An alternative tectonic model of the Ardencaple Fjord area

Jones and Strachan (2000) proposed a P-T path (Figure 6.5) for the Smallefjord Sequence based on 4 metapelite samples collected from the Smallefjord Sequence in the Ardencaple Fjord area. Geothermobarometry and inferred mineral reactions constrain a clockwise P-T path in a petroge-
nic grid (Jones and Strachan, 2000). The GASP and garnet-biotite calibrations were used to obtain pressure and temperature, respectively. Information from the early stage of prograde metamorp-
hism and deformation was obtained from garnet cores and their inclusions. The prograde path is interpreted to be cease at the onset of synchronous cooling and extensional shear fabric develop-
ment (Jones and Strachan, 2000).

A four stage tectonometamorphic model was proposed for the Smallefjord Sequence, focusing on explaining the enhanced geotherm in these rocks:

- (1) - Crustal thickening as a result overthrusting of Laurentia by Baltica, which is precluded by the low metamorphic grade characteristics of the Eleonore Bay Supergroup. The age of peak metamorphism is estimated to be c. 445-440 Ma.
- (2) - On the prograde path the thickened Laurentian lithosphere is detached. Low angle, ductile top-to-the-north orogen-parallel shear then brought eclogites and granulites up to mid-crustal levels, which experienced an enhanced geotherm due to advection from the upwelling mantle.
- (3) - Continued convergence then resulted in further thickening and prograde metamorphism of the Smallefjord Sequence, with resulting anatexis and instigation of ductile thrusts along the Smallefjord Sequence borders.
- (4) - Retrograde metamorphism is associated with the onset of ductile extension and tectonic denudation, resulting in the juxtaposition of the high-grade Smallefjord Sequence and the low-grade Eleonore Bay Supergroup. This was accompanied by emplacement of syn-kinematic granites at contrasting crustal levels at c. 430 Ma (decompressional melting).

The final stages of the Caledonian orogeny in North East Greenland were controlled by oblique marginal thrusting, strike-slip displacement along steep, ductile shear zones and development of N-S-trending folds (Jones and Strachan, 2000).

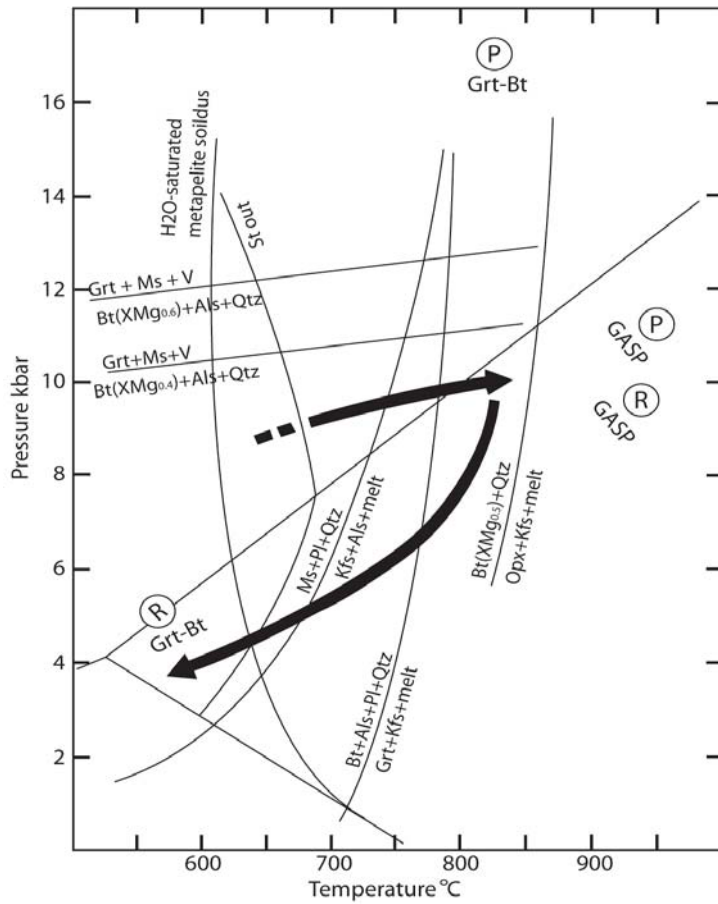


Figure 6.5 This diagram shows pressure plotted against temperature. The thick black arrows show the P-T evolution in the Smallefjord Sequence over time. The thin lines show reactions between mineral phases. The upper temperature limit of $Bt (XMg 0.5) + Qtz$ after Spear and Parrish (1996). K-equilibrium lines for GASP barometry and garnet-biotite thermometry indicated; P = peak a,d R = retrograde. Modified figure from Jones and Strachan (2000).

6.4. Thought on the exhumation process

Ring et al. (1999) define key terms regarding the movement of deep crustal rocks to levels of exposure. Exhumation is defined as the unroofing history of a rock as caused by tectonic and /or surficial processes. Erosion is defined as the surficial removal of mass at a spatial point in the landscape by both mechanical and chemical processes. Denudation is defined as the removal of rock by tectonic and /or surficial processes at a specified point at or under the Earth's surface. These definitions will be adopted here.

Three main processes are thought to be responsible for exhumation: (1) Erosion, (2) Normal faulting and (3) Ductile thinning in the lower crust. Ring et al. (1999) concludes that erosion is too important to be neglected when dealing with exhumation. The rate at which erosion happens varies, and is greatest in regions that are mountainous, tectonically active and wet.

It is evident that normal faults aid the exhumation of metamorphic rocks, as has been invoked in a number of orogens (Ring et al., 1999). The total offset and original dip of deep-seated normal faults are poorly resolved, leading to problems quantifying the relative contribution of normal faulting to exhumation.

Penetrative deformation fabrics present in most exhumed mountain belts indicate that ductile flow is an important process. Ductile flow can either cause vertical thinning as is associated with sub-horizontal foliation, or vertical thickening as is associated with sub-vertical foliation. Hence, ductile thinning can aid or hinder exhumation. General observations from orogens indicate that ductile thinning commonly aids exhumation (Ring et al., 1999). Ductile thinning by itself cannot fully exhume rocks and additional processes are required to bring rocks back to the earth's surface (Platt et al., 1998).

It seems probable that buried rocks of the NE Greenland Caledonides were exhumed through an interplay of erosion, extensional faulting and ductile thinning. Numerous extensional features are present (Fjord Region Detachment Zone, Storstrømmen Shear Zone, Slamsø Shear Zone (late phase), Kildedalen Shear Zone etc), juxtaposing assemblages of contrasting metamorphic grade. The general sub-horizontal foliation in the East Greenland Caledonides indicates that it is plausible that ductile thinning has aided exhumation there. Erosion must also be taken into account.

6.5. An alternative tectonometamorphic model

A tectonometamorphic model for the study area is based on the geothermobarometry analyses on samples from Kildedalen. The geothermal gradient used for calibrations is $30^{\circ}\text{C km}^{-1}$ and 1 kbar is thought to equal 3 km depth. Available geochronological data is also included (Rotevatn, 2004). The geochronological data used is not obtained from samples T6, AA02-15 and AA02-23, but from different samples collected at Kildedalen.

The presented model can be outlined in four main stages (Figure 6.6):

(A) - An initial stage, prior to the westward movement of nappes overriding the Laurentian platform.

(B) - Thrusting along the sole fault on North East Greenland. This process resulted in an increased topographical elevation, and most likely an increased erosion rate. Erosion rates will have inflicted directly with the upper Eleonore Bay Supergroup and whatever was on top of it. AA02-23 is interpreted to be on the retrograde path at this stage. At some point AA02-23 passed through the recorded post-peak conditions of c. 650°C and 6.0-6.5 kbar (18-20 km depth), which is interpreted to represent the lowest temperature at which chemical diffusion was still efficient in this sample. Data by Rotevatn (2004) indicate that the temperature in AA02-23 decreased to below 350 – 400°C at c. 418-423 Ma. This implies that AA02-23 was at c. 20 km depth prior to c. 418-423 Ma.

T6 and AA02-15 were probably still on the prograde path at this stage. All the crustal shortening did not only occur by displacement along the sole fault, but also along several other thrusts that branch off the sole thrust. It is thus proposed that the Slamsø Shear Zone originated as a contractional shear zone at this stage, reactivated as an extensional shear zone at a later stage. Extensional reactivation of thrusts is documented in North East Greenland (Hartz et al., 2001). However, no field evidence suggesting contractional displacement in the Slamsø Shear Zone was observed, but this is still a plausible suggestion.

During this inferred contractional stage, AA02-23 was exhumed simultaneous with T6 and AA02-15 being buried. At Grejsdal, located in the Central Fjord Zone (Figure 2.2), extension at shallow crustal level is simultaneous with contraction at a deeper crustal level (Andresen et al., 2004). Late during this stage, T6 and AA02-15 probably reached peak metamorphic conditions, respectively c. 820 C and 10.5-12 kbar (33-36 km depth) and c. 700 C and 8 kbar (24 km depth).

C) This stage is dominated by the onset of extensional displacement along the Kildedalen Shear Zone, and subsequently the Slamsø Shear Zone. The Slamsø Shear Zone truncates the Kildedalen Shear Zone, and is therefore interpreted to postdate the Kildedalen Shear Zone. Tectonic denudation controlled by the Slamsø Shear Zone is interpreted to be of significance during exhumation

of the lower part of the Smallefjord Sequence, where T6 and AA02-15 were located, and allochthonous basement. Extensional displacement along the Slamsø Shear Zone, interpreted to have taken place at c. 379-382 Ma (Røtevatn, 2004), is thought to have instigated the retrograde P-T path seen in samples T6 and AA02-15 (Figure 6.3). Post-peak T6 record 680-720 C and 5.6-6.3 kbar (17-20 km depth) and post-peak AA02-15 record 680-700 C and c. 4 kbar (12 km depth).

The difference in depth (vertical depth) between T6 and AA02-15 during peak metamorphism is 9-12 km, whereas this difference is reduced to 5-7 km during the post-peak conditions. Using the dip of the Slamsø Shear Zone (30°) and the difference in depth (vertical depth) between T6 and AA02-15, the minimum displacement along this shear zone is calculated to be c. 15-20 km.

Whether this extensional movement is accompanied by contraction or extension along the sole fault remains unclear.

D) A late phase of exhumation under brittle conditions of the Slamsø Shear Zone further juxtaposes allochthonous basement and the Smallefjord Sequence. The fact that this is a brittle fault, suggests that the temperature in the rocks was too low for chemical reequilibration to take place. Thus, this stage has no implications on the geobarometry analyses of the rock samples, but is still significant for the understanding of the complete exhumation history of the rocks that outcrop at surface level today. More or less significant late brittle faults, especially observed in the Smallefjord Sequence, and erosion then continued to exhume the rocks at Kildedalen. Due to brittle extension along the Slamsø Shear Zone, the difference in depth between T6 and AA02-15 at present is c. 500 m, which is significantly less than it was at post-peak conditions late in stage C.

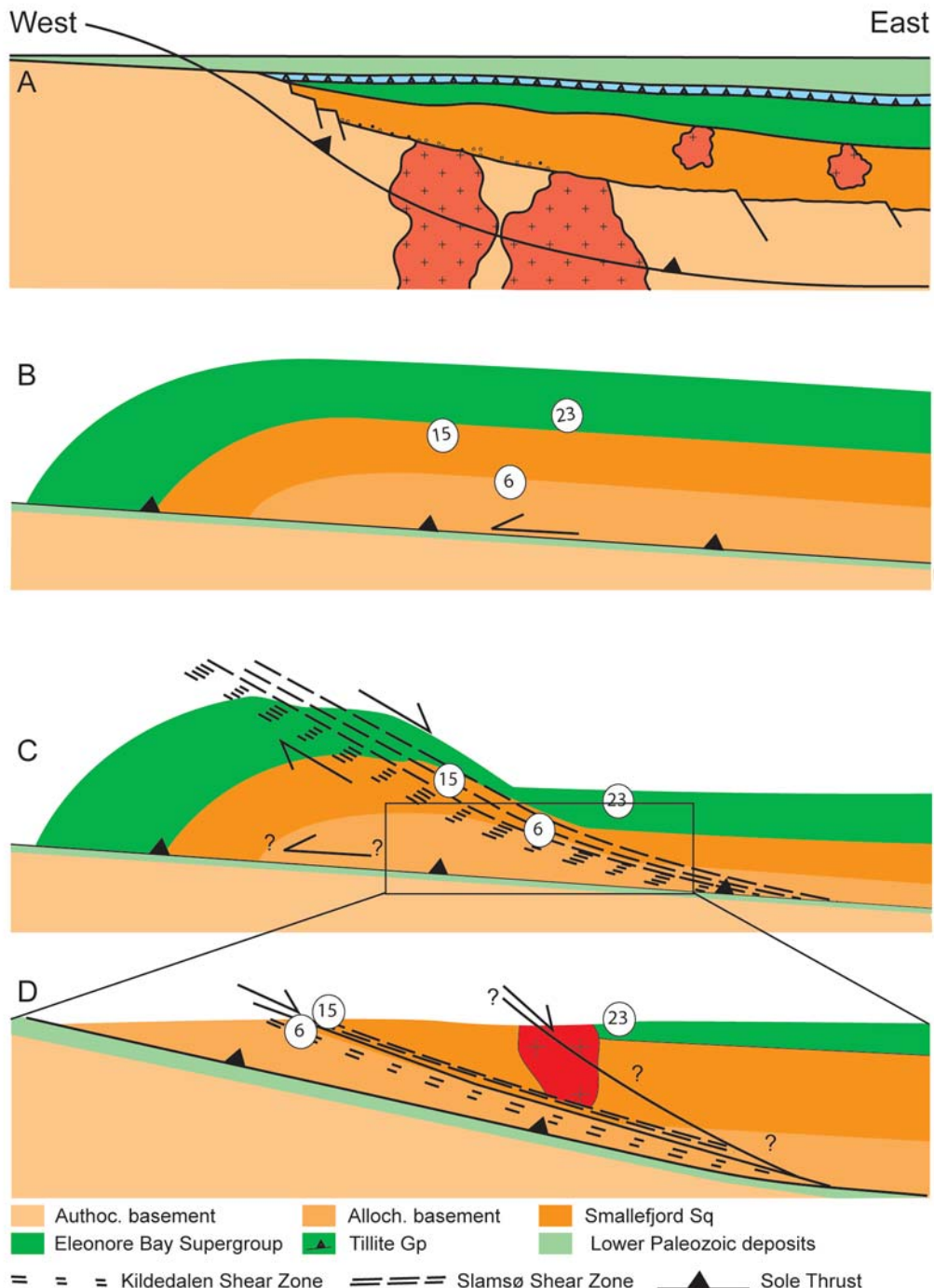


Figure 6.6 Simplified cartoon showing the tectonic development of the East Greenland Caledonides. A) Is the intial stage, before displacement along the sole thrust. B) Authochthonous basement is overridden by overlying rock units due to thrusting. C) Extensional movement along Kildedalen and Slamsø Shear Zones. Whether these occurred simultaneously, or if thrusting along the sole fault was still ongoing, remains unclear. D) A brittle extensional fault separates the two shear zones. The occurence of the postulated fault (Strachan et al., 2001) obscured by the granite separating the Eleonore Bay Supergroup and the Smallefjord Sequence remains unclear.

6.6. Thoughts on granites at Kildedalen

Strachan et al. (2001) postulated that (1) granitic melt emplacement were contemporaneous at contrasting structural levels and (2) that non-coaxial extensional shear controlled the segregation and transport of crustally derived granitic melts to higher structural levels at Kildedalen.

Field evidence from Kildedalen document that there are several generations of dikes. Some are syn-tectonic (foliated and folded migmatites and dikes at Middle Plate and folded and foliated dikes in the Lower Plate) and others are post tectonic (plutons in the Upper Plate and unaffected dikes that cut the migmatites of the Middle Plate).

Neither in our own observations, nor in the pictures shown by Strachan et al. (2001), are there convincing evidence of top-to-the-east simple shear. The observed folds may just as well be the result of vertical flattening. This idea postulated, but not documented, by Strachan et al. (2001), seems very unlikely based on field observations at Kildedalen.

The relationships between dikes at different plate levels present interesting problems. For example, the undeformed dikes that cut the meta-arenites of the middle and the migmatites of the upper part of the Smallefjord Sequence. They appear to be post- to syn-kinematic features. Are the ones cutting the meta-arenites associated with the same phase as the ones cutting the migmatites? They have similar textures and mineralogy. Furthermore, are these late undeformed dikes related to the undeformed plutons emplaced further up in the Eleonore Bay Supergroup? Geochronology suggests there is no relationship, as one dike cutting the migmatites yields Ar/Ar muscovite cooling age of c. 377 Ma (Rotevatn, 2004). Although more data is needed, this one sample indicates there may be no relationship between granite plutons in the Eleonore Bay Supergroup and the late, undeformed dikes of the Smallefjord Sequence.

Published geochemical and isotope data (Hansen et al., 1994; Jepsen and Kalsbeek, 1998; Kalsbeek et al., 2001) relate the formation of Caledonian granites to partial melting of metasediments in the Smallefjord Sequence, and migration of the resulting melts to structurally higher levels. This interpretation is also applicable at the Kildedalen area, where migmatites are present in the upper part of the Smallefjord Sequence and granite plutons in the overlying Eleonore Bay Supergroup.

6.7. Some regional considerations

Enormous areas that underwent eclogite facies deformation are present in the East Greenland and Scandinavian Caledonides. The profound eclogite province in East Greenland outcrop between ca 77°N and 81°N (Gilotti and Krogh, 2001; 2002). The eclogites are situated in allochthonous basement

that are a part of nappes that were thrust onto the Laurentian craton through westward movement. This compressional event is at least thought to be ongoing at Silurian time (Hurst et al., 1983). Nappe movement led to higher topographic relief east of Greenland, causing deposition of Silurian turbidites on top of a carbonate shelf in Kronprins Christian Land (Figure 2.2), which is located far up north-east on Greenland. This 2-4 km thick turbidite deposition is folded and cut by steep reverse faults and low angle thrusts, features related to relatively late westward movement of the nappes.

It is evident that eclogites and other high P-T assemblages situated in the nappes are transported to NE Greenland from somewhere east of their present position (Hurst et al., 1983). Thus the eclogites found on North East Greenland must have originated somewhere east of Greenland as well. Continental subduction is the favored mechanism for the formation of ultrahigh-P terranes (Andersen et al., 1991). However, the presence of eclogites on both sides of the Caledonian orogen requires a clarification as to the extent to which crustal thickening contributed to eclogite formation.

Eclogites are not the scope of this thesis, however, they do document significant exhumation within the East Greenland Caledonides.

6.8. Conclusions

The clockwise P-T paths for the rocks from the Smallefjord Sequence at Kildedalen presented in this thesis are consistent with similar work done on the Smallefjord/Krummedal Sequence in North East Greenland (Vold, 1997; Jones and Strachan, 2000; Gilotti and Elvevold, 2002; Jones and Escher, 2002; White and Hodges, 2003), where rapid tectonically-induced exhumation is the favoured mechanism to explain the obtained clockwise P-T paths. Reported peak conditions are in fair agreement with each other, covering the range 785-915°C and 9-12 kbar (Vold, 1997; Jones and Strachan, 2000; Gilotti and Elevevold, 2002; Jones and Escher, 2002; White and Hodges, 2003).

Ellevold et al. (2003) worked on eclogites emplaced in allochthonous basement that recorded a clockwise pressure/temperature evolution path with temperature 800-850°C and pressure 14-17 kbar.

The presence or absence of the proposed high-strain zone separating the Eleonore Bay Supergroup and the Smallefjord Sequence cannot be determined using the available thermobarometry analyses alone. The reason for this is that both sample T6 and AA02-15 are situated within the Slamsø Shear Zone, thus their P-T paths are influenced by movement along this shear zone, and not only movement along the proposed shear zone. If these samples are also influenced by an overlying high strain zone, it will be impossible to decide to what extent either of the two shear zones affected the rock samples. If this problem is to be solved with thermobarometric analyses alone, the P-T evolution of a rock-sample emplaced between the Slamsø Shear Zone and the proposed high strain zone is required.

This extensional shear zone has been proposed in the two tectonic models that exist from the Ardencaple Fjord area. In one model (Rotevatn, 2004), the high strain zone is proposed to have a significant extensional displacement at c. 415 Ma, being a direct cause for the denudation of the Smallefjord Sequence. The other model (Jones and Strachan, 2000) proposes that extensional displacement along this shear zone occurred at c. 430 Ma, simultaneously with emplacement of the very pluton, by which it is overprinted today. In either case, this pluton should be significantly deformed by shear strain. Field examinations of this pluton shows that it is undeformed. A weak discontinuous biotite foliation, that is not parallel to the strike of the proposed shear zone, is the only structure/textue that is present within this intrusive body. Thus, if this shear zone existed, it was only active prior to granite emplacement at c. 430 Ma.

Muscovite and biotite cooling ages at c. 410-415 Ma is recorded for the Smallefjord Sequence structurally underlying the granite (Rotevatn, 2004). If the extensional shear zone separating Eleonore Bay Supergroup and the Smallefjord Sequence does exist in this area, one would expect these cooling ages to be closer to 430 Ma, as a result of exhumation that is associated with this shear zone.

I conclude that this shear zone does not exist at Kildedalen, thus the P-T paths for T6 and AA02-15 are influenced exclusively by the Slamsø Shear Zone.

Extension along the Slamsø Shear Zone, documented by thermobarometry, at c. 380 Ma (Røtevatn, 2004) conflicts with the model of Jones and Strachan (2000), who have interpreted extension to occur at c 430 Ma.

An interesting question then arises: what happens southwards to the extensional shear zone separating the Eleonore Bay Supergroup documented at Smallefjord? It has been interpreted, but not documented, to continue along the Eleonore Bay Supergroup - Smallefjord Sequence border through the Kildedalen area (Strachan, 1994). It is probable that the shear zone instead can be correlated to the Slamsø Shear Zone, located at the base of the Smallefjord Sequence at Kildedalen. Geochronology work on the Smallefjord Sequence at Smallefjord would be quite helpful when investigating the possibility of correlating the Slamsø Shear Zone to the shear zone at Smallefjord.

The tectonometamorphic model presented in this thesis is in accordance with geothermobarometric calculations, field observations and geochronology from the Kildedalen area.

References:

- Andersen, T. B., Jamtveit, B., Dewey, D. F. & Swensson, E., 1991: Subduction and eduction of continental crust: Major mechanisms during continent-continent collision and orogenic extensional collapse, a model based on the South Norwegian Caledonides. *Terra Nova* 3. 303 - 310
- Andresen, A., Hartz, E. H. & Vold, J., 1996: A late orogenic extensional origin for the infracrustal gneiss domes of the East Greenland Caledonides 72 – 74°N. *Tectonophysics* 285. 353 - 369
- Andresen, A., Rehnstrøm, E.F. & Holte, M.K. (2004): Synchronous, but contrasting deformational regimes at different crustal depths: geochronology of syn-tectonic granites in the NE Greenland Caledonides. *GFF v. 126.* 77
- Berman, R. G., 1988: Internally-consistent thermodynamic data for stoichiometric minerals in the system Na₂O-K₂O-CaO-MgO-FeO-Fe₂O₃-Al₂O₃-SiO₂-TiO₂-H₂O-CO₂. *Journal of Petrology* 29. 633-645
- Berman, R. G., 1990: Mixing properties of Ca-Mg-Fe-Mn garnets. *American Mineralogist* 75. 328 - 344
- Berman, R. G. & Aranovich, L. Y., 1996: Optimized standard state and solution properties of minerals. I. Model calibration for olivine, orthopyroxene, cordierite, garnet and ilmenite in the system FeO-MgO-CaO-Al₂SiO₅-TiO₂-SiO₂. *Contributions to Mineralogy and Petrology* 126. 1 - 24
- Bickle, M. J. & Archibald, N. J., 1984: Chloitoid and staurolite stability: implications for metamorphism in the Archean Yilgarn Block; Western Australia. *Journal of Metamorphic Geology* 2. 179 - 203
- Bohlen, S. R., Wall, V. J. & Boettcher, A. L., 1983: Experimental investigations and geological applications of equilibria in the system FeO-TiO (sub 2) -Al (sub2) O (sub 3) -SiO (sub 2) -H (sub 2) O. *American Mineralogist* 68. 1049 - 1058
- Bryhni, I. & Sturt, B. A., 1985: Caledonides of Southwestern Norway. In Gee, D. G. & Sturt, B. A. (eds): *The Caledonide Orogen - Scandinavia and Related Areas*, 89-107. Wiley and Sons, Chichester
- Carlson, W. D., 2002: Presidential address - Scales of disequilibrium and rates of equilibration during metamorphism. *American Mineralogist* 87. 185 - 204
- Cocks, L. R. M. & Torsvik, T. H., 2002: Earth geography from 500 to 400 million years ago: a faunal and palaeomagnetic review. *Journal of the Geological Society, London* 159. 631 - 644

- Dallmeyer, R. D., Strachan, R. A. & Henriksen, N., 1994: $^{40}\text{Ar}/^{39}\text{Ar}$ mineral age record in NE Greenland: implications for tectonic evolution of the North Atlantic Caledonides. *Journal of the Geological Society, London* 151. 615 - 628
- De Capitani, C. & Brown, T. H., 1987: The computation of chemical equilibrium in complex systems containing non-ideal solutions. *Geochimica et Cosmochimica Acta - Journal of the Geochemical Society and the Meteoritical Society* 51. 2639 - 2652
- Dymek, F. R., 1983: Titanium, aluminium and interlayer cation substitution in biotite from high grade gneisses, West Greenland. *American Mineralogist* 68. 880 - 899
- Ellevold, S., Thrane, K. & Gilotti, J. A., 2003: Metamorphic history of hig-pressure granulites in Payer Land, Greenland Caledonides. *Journal of metamorphic geology* 21. 49 - 63
- Eriksen, B. H. 2003: Late Devonian Collapse?: basin sedimentation and basin inversion, NE Greenland. *Cand. Scient thesis, University of Oslo.* 113pp
- Ferry, J. M. & Spear, F. S., 1978: Experimental calibration of the partitioning of Fe and Mg between biotite and garnet. *Contributions to Mineralogy and Petrology* 66. 113 - 117
- Friderichsen, J. D., Henriksen, N. & Strachan, R. A., 1994: Basement- cover relationships and regional structure in the Grandjean Fjord -Bessel Fjord region (75°N - 76°N), Nort-East Greenland. *Rapport. Grønlands Geologiske Undersøkelse* 162. 17 - 33
- Fuhrman, M. L. & Lindsley, D. H., 1988: Ternary-feldspar modeling and thermometry. *American Mineralogist* 73. 201 - 215
- Ganguly, M. L. & Kennedy, G. C., 1974: The energetics of natural garnet-solid solution. 1. Mixing of the aluminosilicate end members. *Contributions to Mineralogy and Petrology* 48. 137 - 148
- Ganguly, J. & Saxena, S., 1984: Mixing properties of aluminosilicate garnets: constraints from natural and experimental data, and application to geothermobarometry. *American Mineralogist* 69. 88 - 97
- Ganguly, J., Cheng, W. & Tirone, M., 1996: Thermodynamics of aluminosilicate garnet solid solution: new experimental data, an optimized model, and thermometric applications. *Contributions to Mineralogy and Petrology* 126. 137 - 151
- Gee, D. G. & Sturt, B, 1985: The Caledonian Orogen - Scandinavia and Related Areas, Wiley & Sons; Chichester, 1266 pp
- Gessmann, C. K., Spiering, B. & Raith, M., 1997: Experimental study of the Fe-Mg exchange between garnet and biotite: Constraints on the mixing behavior and analyses of the cation-exchange mechanisms. *American Mineralogist* 82. 1225 - 1240

- Ghent, E. D., 1976: Plagioclase - garnet - Al₂SiO₅ - quartz: a potential geobarometer - geothermometer. *American Mineralogist* 61. 710 - 714
- Gillotti, J. A. & Elvevold, S., 2002: Extensional exhumation of a high-pressure granulite terrane in Payer Land, Greenland Caledonides; Structural, petrologic, and geochronologic evidence from metapelites. *Canadian Journal of Earth Sciences* 39. 1169 - 1187
- Gillotti, J. A. & Krogh, R. E. J., 2001: Ultrahigh pressure metamorphism in the Greenland Caledonides: microstructural and thermobarometric evidence. *Abstract with Programs - Geological Society of America* 33;6. 382-383
- Gillotti, J. A. & Krogh, R. E. J., 2002: First evidence for ultrahigh pressure metamorphism in the North-East Greenland Caledonides. *Geology. Geological Society of America* 30;6. 551-554
- Haller, J. 1971: In De Sitter, L. U. (eds): *Geology of the East Greenland Caledonides*. Interscience, London
- Hambrey, M. J. & Spencer, A. M., 1987: Late Precambrian glaciation of central East Greenland. *Meddelelser om Grønland. Geoscience* 19. 1 - 50
- Hansen, B. T., Steiger, R. H. & Higgins, A. K., 1981: Isotopic evidence for a Precambrian metamorphic event within the Charcot Land window, East Greenland Caledonian fold belt. *Bulletin of the Geological Society of Denmark* 29. 151 - 160
- Hansen, B. T., Henriksen, N. & Kalsbeek, F., 1994: Age and origin of Caledonian granites in the Grandjean Fjord - Bessel Fjord region (75° - 76° N), North-East Greenland. *Rapport. Grønlands Geologiske Undersøkelse* 162. 139 - 151
- Hansen, B. T., Higgins, A. K. & Bær, M. T., 1978: Rb-Sr and U-Pb age patterns in polymetamorphic sediments from the southern part of the East Greenland Caledonides. *Bulletin Geological Society of Denmark* 27. 55 - 62
- Hartz, E. H. & Andresen, A., 1995: Caledonian sole thrust of central East Greenland: A crustal-scale Devonian extensional detachment? *Geology* 23. 637 - 640
- Hartz, E. H., Andresen, A., Martin, M. W. & Hodges, K. V., 2000: U-Pb and $^{40}\text{Ar}/^{39}\text{Ar}$ constraints on the Fjord Region Detachment Zone: a long lived extensional fault in the central East Greenland Caledonides. *Journal of the Geological Society, London* 157. 795 - 809
- Henriksen, N. & Higgins, A. K., 1976: The East Greenland Caledonian fold belt. In Escher, A. & Watts, W. S. (eds): *Geology of Greenland*, 182 - 246. Geological Survey of Greenland

- Higgins, A. K., 1988: The Krummedal supracrustal sequence in East Greenland. In Winchester, J. A. (ed): *Later Proterozoic stratigraphy of the Northern Atlantic region*, 86 - 96. Blackie & son ltd, Glasgow & London
- Higgins, A. K., 1976: Pre-Caledonian metamorphic complexes within the southern part of the East Greenland Caledonides. *Journal of the Geological Society, London* 132. 289 - 305
- Higgins, A. K., Friderichsen, J. D. & Thyrsted, T., 1981: Precambrian metamorphic complexes in the East Greenland Caledonides (72° - 74° N) - their relationships to the Eleonore Bay Group, and Caledonian orogenesis. *Rapport. Grønlands geologiske undersøkelse* 104. 5 - 46
- Higgins, A. K. & Leslie, A. G., 2000: Restoring thrusting in the East Greenland Caledonides. *Geology* 28. 1019 - 1022
- Higgins, A. K. & Phillips, W. E. A., 1979: East Greenland Caledonides; an extension of the British Caledonides. In Harris, A. L., Holland, C. H. & Leake, B. E. (eds): *The Caledonides of the British Isles; reviewed*, 19 - 32. Geological Society of London
- Higgins, A. K. & Soper, N. J., 1994: Structure of the Eleonore Bay Supergroup at Ardencaple Fjord, North-East Greenland. *Rapport. Grønlands Geologiske Undersøkelse* 162. 91 - 101
- Hodges, K. V. & Spear, F. S., 1982: Geothermometry, geobarometry and the Al_2SiO_5 triple point at Mt. Moosilauke, New Hampshire. *American Mineralogist* 67. 1118 - 1134
- Holdaway, M. J., 2000: Application of new experimental and garnet Margules data to the garnet-biotite geothermometer. *American Mineralogist* 85. 881 - 892
- Holdaway, M. J., 2001: Recalibration of the GASP geobarometer in light of recent garnet and plagioclase activity models and versions of the garnet-biotite geothermometer. *American Mineralogist* 86. 1117 - 1129
- Holdaway, M. J., Mukhopadhyay, B., Dyar, M. D., Guidotti, C. V. & Dutrow, B. L., 1997: Garnet-biotite geothermometry revised: new Margules parameters and natural specimen data set from Maine. *American Mineralogist* 82. 582 - 595
- Holdaway, M. J. & Lee, S. M., 1977: Fe-Mg cordierite stability in high grade pelitic rocks based on experimental, theoretical and natural observations. *Contributions to Mineral Petrology* 63. 175 - 198
- Hoisch, T. D., 1990: Empirical calibration of six geobarometers for the mineral assemblage quartz + muscovite + biotite + plagioclase + garnet. *Contributions to Mineralogy and petrology* 104. 225 - 234

- Hoisch, T. D., 1991: Equilibria within the mineral assemblage quartz + muscovite + biotite + garnet + plagioclase, and implications for the mixing properties of octaherally-coordinated cations in muscovite and biotite. *Contributions to Mineralogy and Petrology* 108. 43 - 54
- Holte, M., 2003: Timing of contractional and extensional events in the NE Greenland Caledonides, a U-Pb isotopic study. *Cand. Scient. thesis, University of Oslo.* 122pp
- Hurst, J. M., McKerrow, W. S., Soper, N. J. & Surlyk, F., 1983: The relationship between Caledonian nappe tectonics and Silurian turbidite deposition in North Greenland. *Journal of the Geological Society, London* 140. 123 - 131
- Indares, A. & Martignole, J. 1985: Biotite-garnet geothermobarometry in the granulite facies: the influence of Ti and Al in biotite. *American Mineralogist* 70. 272 - 278
- Jepsen, H. F. & Kalsbeek, F., 1998: Granites in the Caledonian fold belt of East Greenland. *Danmarks og Grønlands Geologiske Undesøgelse Rapport.* 28. 73 - 82
- Jones, K. A. & Strachan, R. A., 2000: Crustal thickening and ductile extension in the NE Greenland Caledonides: a metamorphic record from anatetic pelites. *Journal of Metamorphic Geology* vol 18, no 6. 719 - 735
- Jones, K. A. & Escher, J. C., 2002: Near-isothermal decompression within a clockwise P-T evolution recorded in migmatitic mafic granulites from Clavering Ø, NE Greenland; implications for the evolution of the Caledonides. *Journal of Metamorphic Geology* 20. 365 - 378
- Kalsbeek, F., Nutman, A. P. & Taylor, P. N., 1993: Palaeoproterozoic basement province in the Caledonian fold belt of North-East Greenland. *Precambrian research* 63. 163 - 178
- Kalsbeek, F., Thrane, K., Nutman, A. P. & Jepsen, H. F., 2000: Late Mesoproterozoic to early Neoproterozoic history of the East Greenland Caledonides: evidence for Grenvillian orogenesis? *Journal of the Geological Society, London* 157. 1215 - 1225
- Koziol, A. M. & Newton, R. C., 1988: Redetermination of the anorthite breakdown reaction and improvement of the plagioclase-garnet-Al₂SiO₅-quartz geobarometer. *American Mineralogist* 73. 216 - 223
- Kretz, R., 1983: Symbols for rock-forming minerals. *American Mineralogist* 68. 277 - 279
- Le Breton, N. & Thomson, A. B., 1988: Fluid absent (dehydration) melting of biotite in metapelites in the early stages of crustal anatexis. *Contributions to Mineralogy and Petrology* 99. 226 - 237
- Leslie, A. G. & Nutman, A. P., 2003: Evidence for Neoproterozoic orogenesis and early high temperature Scandian deformation events in the southern East Greenland Caledonides. *American Mineralogist* 85. 881 - 892

- McMullin, D. W. A., Berman, R. G. & Greenwood, H. J., 1991: Calibration of the SGAM thermo-barometer for pelitic rocks using data from phase-equilibrium experiments and natural assemblages. *Canadian Mineralogist* 29. 889 - 908
- Mukhopadhyay, B., Holdaway, M. J. & Koziol, A. M., 1997: A statistical model of thermodynamic mixing properties of Ca-Mg-Fe²⁺ garnets. *American Mineralogist* 82. 165 - 181
- Newton, R. C., Charlu, T. V. & Kleppa, O. J., 1977: Thermochemistry of high pressure garnets and clinopyroxene in the system CaO-MgO-Al₂O₃-SiO₂. *Geochimica et Cosmochimica Acta* 41. 369 - 377
- Perchuk, L. L. & Lavrent'eva, I. V., 1983: Experimental investigation of exchange equilibria in the system cordierite-garnet-biotite. In: Saxena, S. K. (eds): *Kinetics and Equilibrium in Mineral Reactions, Advances in Physical Geochemistry* 3. 199 - 239. Springer-Verlag, New York
- Peucat, J. J., Tisserant, D., Caby, R. & Clauer, N., 1985: Resistance of zircons to resetting in a prograde metamorphic sequence of Caledonian age, East Greenland. *Canadian Journal of Earth Sciences* 22. 330 - 338
- Ring, U., Brandon, M. T., Willett, S. D. & Lister, G. S., 1999: Exhumation processes. In: Ring, U., Brandon, M. T., Willett, S. D. & Lister (eds) *Exhumation Processes: Normal Faulting, Ductile Flow and Erosion*. Geological Society, London, Special Publications, 154. 1 - 27
- Rex, D. C. & Gledhill, A. R., 1981: Isotopic studies in the East Greenland Caledonides (72° - 74° N) - Precambrian and Caledonian ages. *Report. Geological Survey of Greenland* 104. 47 - 74
- Rotevatn, A. 2004: Timing of thrusting and extension in the East Greenland Caledonides: ⁴⁰Ar/³⁹Ar thermochronology and kinematics from Ardencaple Fjord (75°N). *Cand. Scient. thesis, University of Oslo.* 130pp
- Salje, E., 1986: Heat capacities and entropies of andalusite and sillimanite: the influence of fibrolitisation on the phase diagram of the Al₂SiO₅ polymorphs. *American Mineralogist* 7. 366 - 371
- Soper, N. J. & Higgins, A. K., 1993: Basement-cover relationships in the East Greenland Caledonides: evidence from the Eleonore Bay Supergroup at Ardencaple Fjord. *Transactions of the Royal Society of Edinburgh: Earth Sciences* 82. 103 - 115
- Spear, F. S., 1991: On the interpretation of peak metamorphic temperatures in light of garnet diffusion during cooling. *Journal of Metamorphic Geology* 9. 379 - 388

- Spear, F. S., 1993: The calculation of metamorphic phase equilibria 1: Geothermometry and geo-barometry. In (eds): *Metamorphic Phase Equilibria and Pressure-Temperature-Time Paths*, 511 - 545. Mineralogical Society of America
- Spear, F. S. & Florence, F. P., 1992: Thermobarometry in granulites: pitfalls and new approaches. *Precambrian Research* 55. 209 - 241
- Spear, F. S., Kohn, M. J., Cheney, J. T., 1999: P-T paths from anatetic pelites. *Contributions to Mineral Petrology* 134. 17 - 32
- Spear, F. S. & Parrish, R., 1996: Petrology and cooling rates of the Valhalla complex, British Columbia, Canada. *Contributions to Mineralogy and Petrology* 34. 7-32
- Steiger, R. H., Hansen, B. T., Schuler, C. H., Bar, M. T. & Henriksen, N., 1979: Polyorogenic nature of the southern Caledonian fold belt in East Greenland: an isotopic age study. *Journal of Geology* 87. 475 - 495
- Strachan, R. A., Nutman, A. P. & Friderichen, J. D., 1995: SHRIMP U-Pb geochronology and metamorphic history of the Smallefjord Sequence, north-east Greenland Caledonides. *J. Geological Society of London* 152. 1995b
- Strachan, R. A., Martin, M. W. & Friderichsen, J. D., 2001: Evidence for contemporaneous yet contrasting styles of granite magmatism during extensional collapse of the northeast Greenland Caledonides. *Tectonics* 20. 458 - 473
- Sønderholm, M., Collinson, J. D. & Tirsgaard, H., 1989: Stratigraphic and sedimentological studies of the Eleonore Bay Group (Precambrian) between $73^{\circ} 30'$ and 76° N in East Greenland. Report. *Geological Survey of Greenland* 145. 97 - 102
- Sønderholm, M. & Tirsgaard, H., 1993: Lithostratigraphic framework of the Upper Proterozoic Eleonore Bay Supergroup of east and North-East Greenland. *Bulletin. Grønlands Geologiske Undersøkelse* 167. 38
- Todd, C. S., 1998: Limits on the precision of geothermometry at low grossular and anorthite content. *American Mineralogist* 83. 1161 - 1167
- Thompson, A. B., 1976: Mineral reactions in pelitic rocks: 1. Prediction of P-T-X (Fe-Mg) phase relations. *American Journal of Science* 276. 401 - 424
- Thompson, A. B., 1976: Mineral reactions in pelitic rocks: 2. Calculation of some P-T-X (Fe-Mg) phase relations. *American Journal of Science* 276. 425 - 454
- Vold, J., 1997: Et studie av den tectonometamorfe utviklingen av gneisene i liggblokkene til "the Fjord Region Detachment Zone" på Kap Hedlund, sentrale Øst Grønland. *Cand. Scient. thesis, University of Oslo.* 117pp

- White, A. P., Hodges, K. V., Martin, M. W. & Andresen, A., 2002: Geological constraints on middle-crustal behaviour during broadly synorogenic extension in the central East Greenland Caledonides. *International Journal of Earth Sciences* 91. 187 - 208
- White, A. P. & Hodges, K. V., 2003: Pressure-temperature-time evolution of the Central East Greenland Caledonides: quantitative contraints on crustal thickening and synorogenic extension. *Journal of metamorphic Geology* 21. 875 - 897
- Winter, J. D, 2001: Thermodynamics of Metamorphic Reactions. In Lynch, P. (eds): *An Introduction to Igneous and Metamorphic Petrology*, 535 - 561. Prentice Hall
- Wu, C. M., Zhang. J. & Ren, L. D.; 2004: Empirical Garnet-Biotite-Plagioclase-Quartz (GPBQ) Geobarometry in Medium- to High-Grade Metapelites. *Journal of Petrology* 45. 1907 - 1921
- Yardley, B. W. D., 1977: An empirical study of diffusion in garnet. *American Mineralogist*, 62. 793 - 800

Appendix 1 - Electron Micro Probe Analysis

Sample	garnet - T6 - Allochthonous basement						T6 - Rim					
	T6 Core	T6 Core	T6 Core	T6 Core	T6 Rim	T6 Rim	T6 Core	T6 Core	T6 Rim	T6 Rim	T6 Rim	T6 Rim
SiO ₂	38.520	38.600	38.590	38.370	38.730	37.544	37.564	38.230	38.430	38.210	38.460	37.950
FeO	26.090	26.000	26.340	26.080	25.860	31.873	32.382	29.590	29.280	29.590	29.690	31.700
CaO	8.010	7.960	8.050	8.190	8.120	5.022	4.703	5.300	5.550	5.480	5.450	4.830
Cr ₂ O ₃	0.010	0.020	0.020	0.030	0.080	0.022	0.029	0.070	0.000	0.020	0.000	0.010
MgO	6.100	5.860	5.820	5.760	6.050	4.081	3.891	5.580	5.590	5.490	5.450	3.590
Al ₂ O ₃	21.710	21.850	21.820	21.890	21.940	21.589	21.398	21.750	21.950	21.930	21.920	21.600
K ₂ O	0.010	0.000	0.010	0.000	0.000	0.011	0.000	0.010	0.010	0.000	0.010	0.030
TiO ₂	0.000	0.030	0.030	0.000	0.020	0.025	0.000	0.010	0.020	0.000	0.000	0.020
MnO	0.360	0.370	0.350	0.340	0.400	0.779	0.882	0.460	0.530	0.520	0.520	1.160
Total	100.830	100.690	101.040	100.680	101.200	100.936	100.852	101.000	101.380	101.250	101.500	100.900
Cations based on 12 oxygens												
Si	2.998	3.004	2.999	2.993	2.998	2.975	2.984	2.989	2.991	2.982	2.993	3.005
Fe ²⁺	1.680	1.692	1.712	1.701	1.685	2.063	2.110	1.914	1.898	1.903	1.926	1.676
Fe ³⁺	0.018	0.000	0.000	0.000	0.000	0.045	0.038	0.019	0.007	0.026	0.006	0.020
Ca	0.585	0.581	0.587	0.599	0.589	0.373	0.350	0.389	0.405	0.401	0.398	0.359
Mg	0.708	0.680	0.674	0.670	0.698	0.482	0.461	0.650	0.648	0.639	0.632	0.424
Al	1.992	2.004	1.999	2.012	2.002	2.016	2.004	2.004	2.013	2.017	2.011	2.016
K	0.001	0.000	0.001	0.001	0.000	0.001	0.000	0.001	0.001	0.001	0.001	0.000
Ti	0.000	0.002	0.001	0.001	0.001	0.002	0.000	0.001	0.001	0.001	0.001	0.000
Mn	0.024	0.024	0.023	0.022	0.026	0.052	0.059	0.030	0.030	0.030	0.030	0.078
Cr	0.001	0.002	0.002	0.007	0.002	0.003	0.007	0.000	0.000	0.000	0.000	0.000
Total	8.006	7.990	8.000	7.996	8.000	7.996	8.015	8.013	8.007	8.002	8.009	7.987
X Mg	0.235	0.228	0.225	0.224	0.233	0.160	0.153	0.217	0.217	0.213	0.211	0.166
X Fe	0.563	0.568	0.571	0.569	0.562	0.699	0.712	0.644	0.637	0.643	0.646	0.663
X Ca	0.194	0.195	0.196	0.200	0.197	0.124	0.116	0.129	0.135	0.134	0.133	0.140
X Mn	0.008	0.008	0.008	0.008	0.009	0.017	0.020	0.010	0.010	0.010	0.010	0.030

Appendix 1 - Electron Micro Probe Analysis

Biotite - T6 - Allochthonous basement							
Sample	T6 Rim	T6 Rim	T6 Rim	T6 Rim	T6 Trapped	T6 Trapped	T6 Trapped
SiO ₂	36.963	35.200	36.109	31.931	38.180	35.833	36.250
FeO	18.595	19.812	18.610	21.033	14.307	18.533	18.602
CaO	0.066	0.028	0.045	0.162	0.157	0.001	0.004
Na ₂ O	0.124	0.193	0.155	0.135	0.369	0.201	0.282
MgO	12.242	10.962	11.524	13.062	15.067	11.451	11.504
Al ₂ O ₃	17.832	17.929	17.275	18.295	17.560	17.349	17.320
K ₂ O	8.732	9.127	9.222	5.115	8.190	9.360	9.270
TiO ₂	1.391	1.196	1.621	0.709	0.922	1.977	2.207
MnO	0.005	0.026	0.050	0.087	0.034	0.061	0.089
Total	96.002	94.476	94.651	90.532	94.791	94.812	95.580
Cations based on 11 oxygen atoms							
Si	2.753	2.702	2.745	2.541	1.393	2.720	2.726
Fe	1.158	1.272	1.183	1.400	0.540	1.177	1.170
Ca	0.005	0.002	0.003	0.012	0.001	0.000	0.000
Na	0.018	0.029	0.023	0.021	0.024	0.030	0.041
Mg	1.359	1.254	1.306	1.550	0.698	1.296	1.289
Al	1.566	1.622	1.548	1.716	0.782	1.552	1.535
K	0.830	0.894	0.894	0.519	0.405	0.907	0.889
Ti	0.097	0.086	0.116	0.053	0.043	0.141	0.156
Mn	0.000	0.002	0.003	0.006	0.001	0.004	0.006
Total	7.789	7.862	7.823	7.818	3.887	7.829	7.815
X _{fe}	0.460	0.503	0.475	0.475	0.436	0.476	0.476
X _{Mg}	0.540	0.497	0.525	0.525	0.564	0.524	0.524

Appendix 1 - Electron Micro Probe Analysis

Sample	Plagioclase - T6 - Allochthonous basement						T6 - Rim					
	T6 Blasts	T6 Blasts	T6 Blasts	T6 Blasts	T6 Rim							
SiO ₂	48.684	47.103	47.822	47.753	48.277	50.549	55.476	52.887	48.684	52.723	60.816	60.563
FeO	0.089	0.050	0.000	0.166	0.000	0.063	0.000	0.005	0.089	0.023	0.012	0.003
CaO	15.888	16.362	16.257	16.249	16.296	14.161	10.042	11.984	15.888	12.605	6.561	6.883
Na ₂ O	2.700	2.101	2.389	2.420	2.531	3.644	5.880	4.983	2.700	4.629	7.844	7.805
MgO	0.000	0.000	0.000	0.000	0.000	0.000	0.000	0.000	0.000	0.000	0.000	0.000
Al ₂ O ₃	32.434	33.073	33.037	32.944	32.755	30.871	27.525	28.997	32.434	29.360	24.753	25.143
K ₂ O	0.017	0.027	0.017	0.030	0.006	0.028	0.065	0.017	0.017	0.017	0.072	0.118
TiO ₂	0.010	0.002	0.010	0.000	0.000	0.000	0.000	0.007	0.010	0.010	0.028	0.000
MnO	0.000	0.008	0.000	0.035	0.017	0.008	0.000	0.019	0.000	0.000	0.000	0.000
Total	99.824	98.749	99.571	99.600	99.899	99.327	98.991	98.924	99.824	99.404	100.061	100.517
Cations based on 8 oxygen atoms												
Si	2.260	2.215	2.228	2.227	2.242	2.343	2.539	2.443	2.260	2.427	2.715	2.696
Fe	0.003	0.002	0.000	0.006	0.000	0.002	0.000	0.000	0.003	0.003	0.000	0.000
Ca	0.692	0.721	0.710	0.711	0.710	0.616	0.431	0.519	0.692	0.544	0.275	0.287
Na	0.243	0.192	0.216	0.219	0.228	0.328	0.522	0.446	0.243	0.413	0.679	0.674
Mg	0.000	0.000	0.000	0.000	0.000	0.000	0.000	0.000	0.000	0.000	0.000	0.000
Al	1.775	1.833	1.814	1.811	1.793	1.687	1.485	1.579	1.775	1.593	1.302	1.320
K	0.001	0.002	0.002	0.002	0.000	0.002	0.004	0.001	0.001	0.001	0.004	0.007
Ti	0.000	0.002	0.002	0.002	0.000	0.000	0.000	0.000	0.001	0.001	0.000	0.000
Mn	0.000	0.002	0.002	0.002	0.001	0.000	0.000	0.001	0.001	0.001	0.000	0.000
Total	4.974	4.965	4.978	4.975	4.978	4.978	4.981	4.990	4.970	4.980	4.975	4.984
Xanorthite	0.740	0.790	0.767	0.757	0.653	0.452	0.538	0.740	0.568	0.288	0.299	0.701
Xalbite	0.260	0.210	0.233	0.235	0.243	0.347	0.548	0.462	0.538	0.260	0.432	0.299

Appendix 1 - Electron Micro Probe Analysis

Sample	garnet - AA02-15 - Smallefjord Sequence						AA02-15					
	AA02-15 Core	AA02-15 Core	AA02-15 Core	AA02-15 Rim								
SiO ₂	36.473	37.061	37.470	36.883	37.343	36.766	36.676	36.744	36.898	36.843		
FeO	33.647	34.236	33.626	34.074	35.472	36.594	37.599	37.213	37.425	35.521		
CaO	2.512	2.436	2.646	2.461	2.506	1.665	0.624	0.905	1.228	2.405		
Cr ₂ O ₃	0.029	0.013	0.006	0.004	0.051	0.000	0.006	0.019	0.000	0.039		
MgO	4.613	4.510	4.749	1.542	3.114	2.013	1.908	2.061	2.124	3.001		
Al ₂ O ₃	21.727	21.488	21.598	20.776	21.228	20.659	20.657	20.757	20.733	21.090		
K ₂ O	0.013	0.004	0.012	0.024	0.010	0.002	0.024	0.005	0.008	0.014		
TiO ₂	0.002	0.005	0.030	0.012	0.000	0.043	0.032	0.040	0.033	0.000		
MnO	1.067	0.974	1.112	4.736	1.703	2.088	2.784	2.479	2.226	1.577		
Total	100.085	100.729	101.249	100.516	101.427	99.868	100.312	100.227	100.679	100.490		
Cations based on 12 oxygens												
Si	2.924	2.953	2.962	2.997	2.979	3.000	2.990	2.991	2.991	2.991		
Fe ²⁺	2.096	2.159	2.123	2.291	2.298	2.485	2.511	2.499	2.484	2.310		
Fe ³⁺	0.146	0.112	0.091	0.023	0.062	0.011	0.048	0.030	0.048	0.078		
Ca	0.189	0.182	0.196	0.188	0.187	0.127	0.048	0.069	0.093	0.182		
Mg	0.551	0.536	0.560	0.187	0.370	0.245	0.232	0.250	0.257	0.361		
Al	2.053	2.018	2.012	1.990	1.996	1.987	1.985	1.991	1.981	2.004		
K	0.001	0.000	0.001	0.002	0.001	0.000	0.002	0.001	0.001	0.001		
Ti	0.000	0.000	0.002	0.001	0.000	0.003	0.002	0.003	0.003	0.000		
Mn	0.072	0.066	0.074	0.326	0.115	0.144	0.192	0.171	0.153	0.108		
Cr	0.003	0.001	0.001	0.000	0.005	0.000	0.001	0.002	0.000	0.004		
Total	8.049	8.037	8.030	8.008	8.021	8.004	8.016	8.010	8.016	8.026		
X Mg	0.180	0.175	0.184	0.062	0.122	0.081	0.077	0.083	0.085	0.119		
X Fe	0.734	0.743	0.727	0.768	0.778	0.829	0.844	0.838	0.834	0.786		
X Ca	0.062	0.060	0.064	0.062	0.062	0.042	0.016	0.023	0.031	0.060		
X Mn	0.024	0.022	0.024	0.108	0.038	0.048	0.063	0.057	0.050	0.035		

Appendix 1 - Electron Micro Probe Analysis

Sample	Biotite - AA02-15 - Smalleford Sequence						AA02-15 Rim
	AA02-15 Trapped	AA02-15 Trapped	AA02-15 Trapped	AA02-15 Rim	AA02-15 Rim	AA02-15 Rim	
SiO ₂	35.576	35.876	34.746	36.299	35.198	35.508	36.150
FeO	19.832	19.189	19.196	19.880	19.431	19.475	19.280
CaO	0.001	0.000	0.008	0.021	0.000	0.003	0.053
Na ₂ O	0.344	0.222	0.222	0.232	0.249	0.256	0.212
MgO	9.343	9.607	9.524	9.335	9.700	10.088	10.166
Al ₂ O ₃	18.993	19.416	18.875	19.297	20.068	19.367	19.680
K ₂ O	9.045	9.354	9.232	8.901	9.003	8.797	9.022
TiO ₂	1.808	1.688	1.890	2.087	1.084	1.471	1.458
MnO	0.026	0.063	0.045	0.059	0.080	0.022	0.050
Total	94.973	95.419	93.743	96.115	94.817	94.989	96.101
							95.545
Cations based on 11 oxygen atoms							
Si	2.703	2.706	2.676	2.713	2.676	2.689	2.702
Fe	1.260	1.210	1.236	1.243	1.236	1.234	1.205
Ca	0.000	0.000	0.001	0.001	0.000	0.000	0.001
Na	0.051	0.032	0.033	0.034	0.037	0.038	0.031
Mg	1.058	1.080	1.093	1.040	1.099	1.139	1.133
Al	1.701	1.726	1.714	1.700	1.798	1.729	1.734
K	0.877	0.900	0.907	0.849	0.873	0.850	0.860
Ti	0.129	0.120	0.137	0.147	0.078	0.105	0.102
Mn	0.002	0.004	0.003	0.004	0.005	0.001	0.005
Total	7.781	7.778	7.800	7.731	7.802	7.785	7.775
X _{Fe}	0.544	0.528	0.531	0.544	0.529	0.520	0.516
X _{Mg}	0.456	0.472	0.469	0.456	0.471	0.480	0.484

Appendix 1 - Electron Micro Probe Analysis

Sample	Plagioclase - AA02-15 - Smalllefjord Sequence											
	AA02-15 Blasts	AA02-15 Blasts	AA02-15 Blasts	AA02-15 Blasts	AA02-15 Rim							
SiO ₂	60.369	61.391	61.160	60.935	61.329	48.799	48.025	59.626	59.737			
FeO	0.000	0.089	0.058	0.080	0.055	0.028	0.000	0.023	0.073			
CaO	6.386	6.387	6.137	6.481	6.538	16.796	16.470	7.092	7.091			
Na ₂ O	8.101	8.162	7.975	8.007	8.062	2.437	2.089	7.717	7.799			
MgO	0.000	0.000	0.000	0.000	0.000	0.000	0.000	0.000	0.003			
Al ₂ O ₃	24.648	24.831	24.861	24.763	24.646	32.426	32.959	25.284	25.381			
K ₂ O	0.160	0.111	0.095	0.075	0.105	0.034	0.014	0.072	0.078			
TiO ₂	0.000	0.003	0.013	0.000	0.012	0.000	0.007	0.000	0.000			
MnO	0.000	0.013	0.015	0.000	0.019	0.000	0.005	0.000	0.001			
Total	99.668	100.990	100.317	100.344	100.770	100.524	99.573	99.818	100.167			
Cations based on 8 oxygen atoms												
Si	2.709	2.717	2.720	2.714	2.721	2.255	2.236	2.678	2.675			
Fe	0.000	0.003	0.002	0.003	0.002	0.001	0.000	0.001	0.003			
Ca	0.269	0.265	0.256	0.271	0.272	0.728	0.719	0.299	0.298			
Na	0.705	0.700	0.688	0.692	0.693	0.218	0.189	0.672	0.677			
Mg	0.000	0.000	0.000	0.000	0.000	0.000	0.000	0.000	0.000			
Al	1.304	1.295	1.303	1.300	1.289	1.767	1.809	1.338	1.339			
K	0.009	0.006	0.005	0.004	0.006	0.002	0.001	0.004	0.004			
Ti	0.000	0.000	0.001	0.000	0.001	0.000	0.000	0.000	0.000			
Mn	0.000	0.000	0.001	0.000	0.001	0.000	0.000	0.000	0.000			
Total	4.996	4.988	4.975	4.984	4.984	4.971	4.954	4.991	4.996			
Xanorthite	0.276	0.275	0.271	0.281	0.282	0.769	0.792	0.308	0.305			
Xalbite	0.724	0.725	0.729	0.719	0.718	0.231	0.208	0.692	0.695			

Appendix 1 - Electron Micro Probe Analysis

Sample	garnet - AA02-23 - Eleonore Bay Supergroup						AA02-23	
	AA02-23 Core	AA02-23 Core	AA02-23 Core	AA02-23 Rim	AA02-23 Rim	AA02-23 Rim	AA02-23 Rim	AA02-23
SiO ₂	36.744	37.241	37.129	36.783	37.200	36.520	36.766	36.676
FeO	32.731	34.101	33.183	33.587	37.900	36.905	36.594	37.599
CaO	3.154	2.740	2.853	2.935	0.711	1.357	1.665	0.624
Cr ₂ O ₃	0.000	0.000	0.000	0.060	0.000	0.000	0.000	0.006
MgO	1.350	1.411	1.341	1.341	2.262	1.970	2.013	1.908
Al ₂ O ₃	20.710	20.869	20.976	20.736	20.854	20.833	20.659	20.657
K ₂ O	0.006	0.008	0.000	0.010	0.000	0.029	0.002	0.024
TiO ₂	0.038	0.065	0.040	0.027	0.002	0.010	0.043	0.032
MnO	5.734	4.756	5.160	5.018	2.195	2.570	2.088	2.784
Total	100.503	101.228	100.686	100.543	101.125	100.196	99.868	100.312
Cations based on 12 oxygens								
Si	2.991	3.004	3.006	2.992	2.999	2.978	3.000	2.990
Fe ²⁺	2.179	2.294	2.280	2.243	2.520	2.445	2.485	2.511
Fe ³⁺	0.046	0.006	0.000	0.038	0.030	0.065	0.011	0.048
Ca	0.241	0.207	0.217	0.224	0.054	0.104	0.127	0.048
Mg	0.164	0.170	0.162	0.163	0.272	0.239	0.245	0.232
Al	1.987	1.984	2.002	1.988	1.981	2.002	1.987	1.985
K	0.001	0.001	0.000	0.001	0.000	0.003	0.000	0.002
Ti	0.003	0.005	0.003	0.002	0.000	0.001	0.003	0.002
Mn	0.395	0.325	0.354	0.346	0.150	0.178	0.144	0.192
Cr	0.000	0.000	0.000	0.006	0.000	0.000	0.001	0.001
Total	8.015	8.002	7.990	8.013	8.011	8.022	8.004	8.016
X Mg	0.054	0.057	0.054	0.054	0.090	0.079	0.081	0.077
X Fe	0.735	0.766	0.757	0.757	0.843	0.828	0.829	0.844
X Ca	0.080	0.069	0.072	0.074	0.018	0.034	0.042	0.016
X Mn	0.131	0.108	0.117	0.115	0.050	0.059	0.048	0.063

Appendix 1 - Electron Micro Probe Analysis

Biotite - AA02-23 - Eleonore Bay Supergroup						
Sample	AA02-23 Rim	AA02-23 Rim	AA02-23 Rim	AA02-23 Rim	AA02-23 Rim	AA02-23 Rim
SiO ₂	33.871	33.978	34.406	33.980	33.794	33.794
FeO	23.913	24.451	22.611	23.534	23.734	23.734
CaO	0.008	0.046	0.031	0.008	0.000	0.000
Na ₂ O	0.239	0.175	0.360	0.214	0.315	0.315
MgO	6.828	6.372	6.505	6.801	6.604	6.604
Al ₂ O ₃	18.832	19.491	19.395	18.936	18.928	18.928
K ₂ O	8.428	8.475	8.683	8.657	8.480	8.480
TiO ₂	2.590	2.420	2.564	2.494	2.412	2.412
MnO	0.112	0.077	0.075	0.070	0.048	0.048
Total	94.826	95.491	94.633	94.698	94.320	94.320
Cations based on 11 oxygen atoms						
Si	2.628	2.621	2.656	2.637	2.636	2.636
Fe	1.551	1.577	1.460	1.527	1.548	1.548
Ca	0.001	0.003	0.002	0.001	0.000	0.000
Na	0.036	0.026	0.054	0.032	0.048	0.048
Mg	0.790	0.733	0.748	0.787	0.768	0.768
Al	1.722	1.772	1.765	1.732	1.740	1.740
K	0.834	0.834	0.855	0.857	0.844	0.844
Ti	0.189	0.176	0.186	0.182	0.177	0.177
Mn	0.007	0.005	0.005	0.005	0.003	0.003
Total	7.758	7.747	7.730	7.760	7.763	7.763
X _{Fe}	0.663	0.683	0.661	0.660	0.668	0.668
X _{Mg}	0.337	0.317	0.339	0.340	0.332	0.332

Appendix 1 - Electron Micro Probe Analysis

Sample	Plagioclase - AA02-23 - Eleonore Bay Supergroup					
	AA02-23 Rim	AA02-23 Rim	AA02-23 Rim	AA02-23 Rim	AA02-23 Rim	AA02-23 Rim
SiO ₂	65.625	65.066	65.843	66.119	65.554	65.961
FeO	0.041	0.049	0.059	0.000	0.021	0.084
CaO	2.020	2.338	2.255	2.233	2.282	2.137
Na ₂ O	10.852	10.479	10.347	10.263	10.281	10.467
MgO	0.023	0.000	0.000	0.000	0.000	0.000
Al ₂ O ₃	21.228	21.419	21.689	21.301	21.273	21.335
K ₂ O	0.123	0.087	0.075	0.083	0.057	0.086
TiO ₂	0.005	0.022	0.002	0.000	0.000	0.015
MnO	0.000	0.056	0.012	0.027	0.000	0.000
Total	99.921	99.519	100.285	100.030	99.471	100.087
Cations based on 8 oxygen atoms						
Si	2.895	2.883	2.890	2.906	2.899	2.900
Fe	0.002	0.002	0.002	0.000	0.001	0.003
Ca	0.084	0.097	0.093	0.092	0.095	0.088
Na	0.928	0.900	0.880	0.875	0.882	0.892
Mg	0.002	0.000	0.000	0.000	0.000	0.000
Al	1.104	1.119	1.122	1.104	1.109	1.106
K	0.007	0.005	0.004	0.005	0.003	0.005
Ti	0.000	0.001	0.000	0.000	0.000	0.001
Mn	0.000	0.002	0.000	0.001	0.000	0.000
Total	5.021	5.009	4.992	4.982	4.989	4.995
Xanorthite	0.083	0.097	0.095	0.095	0.097	0.090
Xalbite	0.917	0.903	0.905	0.905	0.903	0.910

Appendix 2 – DOMINO reactions for T6

Appendix 2 – DOMINO reactions for T6

66): GRNT ILMENITE OPX (2)FSP aCd Mt aQz H2O = GRNT ILMENITE OPX (2)FSP Cd Mt aQz H2O
67): GRNT ILMENITE OPX (2)FSP aCd Mt aQz H2O = GRNT ILMENITE OPX (2)FSP Cd Mt aQz H2O
68): GRNT ILMENITE OPX (2)FSP Cd Mt aQz H2O = GRNT ILMENITE OPX (2)FSP aCd Mt aQz H2O
69): GRNT ILMENITE OPX (2)FSP Cd Mt aQz H2O = GRNT ILMENITE OPX (2)FSP aCd Mt aQz H2O
70): GRNT ILMENITE OPX (2)FSP aCd Mt aQz H2O = GRNT ILMENITE OPX (2)FSP Cd Mt aQz H2O
71): GRNT ILMENITE OPX (2)FSP aCd Mt aQz H2O = GRNT ILMENITE OPX (2)FSP Cd Mt aQz H2O
72): GRNT ILMENITE OPX (2)FSP aCd Mt aQz H2O = GRNT ILMENITE OPX (2)FSP Cd Mt aQz H2O
73): GRNT ILMENITE OPX (2)FSP Cd Mt aQz H2O = GRNT ILMENITE OPX (2)FSP aCd Mt aQz H2O
74): GRNT ILMENITE BIOTITE PHNG CHLORITE FSP Mt aQz H2O = GRNT ILMENITE BIOTITE CHLORITE FSP Mt aQz Si H2
75): GRNT ILMENITE BIOTITE (2)FSP Mt aQz Si H2O = GRNT ILMENITE BIOTITE (2)FSP Mt aQz H2O
76): GRNT ILMENITE BIOTITE OPX (2)FSP Mt aQz H2O = GRNT ILMENITE OPX (2)FSP Mt aQz H2O
77): AMPH PHNG EPI CHLORITE (2)FSP aQz Sph H2O = AMPH ILMENITE PHNG EPI CHLORITE (2)FSP aQz Sph H2O
78): AMPH ILMENITE PHNG EPI CHLORITE (2)FSP aQz Sph H2O = AMPH ILMENITE PHNG EPI CHLORITE (2)FSP aQz H2O
79): AMPH ILMENITE PHNG EPI CHLORITE (2)FSP aQz H2O = AMPH GRNT ILMENITE PHNG EPI CHLORITE (2)FSP aQz H2O
80): AMPH GRNT ILMENITE PHNG EPI CHLORITE (2)FSP aQz H2O = AMPH GRNT ILMENITE PHNG EPI CHLORITE FSP aQz H
81): AMPH GRNT ILMENITE PHNG EPI CHLORITE FSP aQz H2O = GRNT ILMENITE BIOTITE PHNG EPI CHLORITE FSP aQz H
82): GRNT ILMENITE BIOTITE PHNG EPI CHLORITE FSP aQz H2O = GRNT ILMENITE BIOTITE PHNG CHLORITE FSP Mt aQz
83): GRNT ILMENITE BIOTITE PHNG CHLORITE FSP Mt aQz H2O = GRNT ILMENITE BIOTITE PHNG FSP Mt aQz Si H2O
84): GRNT ILMENITE BIOTITE PHNG FSP Mt aQz Si H2O = GRNT ILMENITE BIOTITE FSP Mt aQz Si H2O
85): AMPH PHNG EPI CHLORITE FSP aQz Sph Zo H2O = AMPH ILMENITE PHNG EPI CHLORITE FSP aQz Sph Zo H2O
86): AMPH ILMENITE PHNG EPI CHLORITE FSP aQz Sph Zo H2O = AMPH ILMENITE PHNG EPI CHLORITE FSP aQz Rt Zo H
87): AMPH ILMENITE PHNG EPI CHLORITE FSP aQz Rt Zo H2O = AMPH ILMENITE PHNG EPI CHLORITE FSP aQz Zo H2O
88): AMPH ILMENITE PHNG EPI CHLORITE FSP aQz Zo H2O = AMPH GRNT ILMENITE PHNG EPI CHLORITE FSP aQz Zo H2O
89): AMPH GRNT ILMENITE PHNG EPI CHLORITE FSP aQz Zo H2O = AMPH GRNT PHNG EPI CHLORITE FSP aQz Rt Zo H2O
90): AMPH GRNT PHNG EPI CHLORITE FSP aQz Rt Zo H2O = AMPH GRNT PHNG EPI CHLORITE FSP aQz Rt H2O
91): AMPH GRNT PHNG EPI CHLORITE FSP aQz Rt H2O = AMPH GRNT ILMENITE PHNG EPI CHLORITE FSP aQz Rt H2O
92): AMPH GRNT ILMENITE PHNG EPI CHLORITE FSP aQz Rt H2O = AMPH GRNT ILMENITE PHNG EPI CHLORITE FSP aQz H
93): AMPH GRNT ILMENITE PHNG EPI CHLORITE FSP aQz H2O = AMPH GRNT ILMENITE BIOTITE PHNG EPI CHLORITE FSP
94): AMPH GRNT ILMENITE BIOTITE PHNG EPI CHLORITE FSP aQz H2O = AMPH GRNT BIOTITE PHNG EPI CHLORITE FSP a
95): AMPH GRNT BIOTITE PHNG EPI CHLORITE FSP aQz Rt H2O = GRNT BIOTITE PHNG EPI CHLORITE FSP aQz Rt H2O
96): GRNT BIOTITE PHNG EPI CHLORITE FSP aQz Rt H2O = GRNT BIOTITE PHNG EPI CHLORITE FSP Mt aQz Rt H2O
97): GRNT BIOTITE PHNG EPI CHLORITE FSP Mt aQz Rt H2O = GRNT BIOTITE PHNG CHLORITE FSP Mt aQz Rt H2O
98): GRNT BIOTITE PHNG CHLORITE FSP Mt aQz Rt H2O = GRNT BIOTITE PHNG FSP Ky Mt aQz Rt H2O
99): GRNT BIOTITE PHNG FSP Mt aQz Rt H2O = GRNT BIOTITE PHNG FSP Ky Mt aQz Rt H2O
0100): GRNT BIOTITE PHNG FSP Mt aQz Rt H2O = GRNT BIOTITE PHNG FSP Mt aQz Rt Si H2O
0101): GRNT BIOTITE PHNG FSP Mt aQz Rt Si H2O = GRNT ILMENITE BIOTITE PHNG FSP Mt aQz Si H2O
0102): AMPH PHNG EPI CHLORITE FSP Pg aQz Sph Zo H2O = AMPH PHNG EPI CHLORITE FSP aQz Sph Zo H2O
0103): AMPH PHNG EPI CHLORITE Pg aQz Sph Zo H2O = AMPH PHNG EPI CHLORITE FSP Pg aQz Sph Zo H2O
0104): AMPH PHNG EPI CHLORITE Pg aQz Sph Zo H2O = AMPH PHNG EPI CHLORITE Pg aQz Rt Zo H2O
0105): AMPH PHNG EPI CHLORITE Pg aQz Sph Zo H2O = AMPH PHNG EPI CHLORITE Pg aQz Rt Zo H2O
0106): AMPH PHNG EPI CHLORITE Pg aQz Rt Zo H2O = AMPH GRNT PHNG EPI CHLORITE Pg aQz Rt Zo H2O
0107): AMPH GRNT PHNG EPI CHLORITE Pg aQz Rt Zo H2O = AMPH GRNT PHNG EPI CHLORITE Pg aQz Rt H2O
0108): AMPH GRNT PHNG EPI CHLORITE Pg aQz Rt H2O = AMPH GRNT PHNG EPI CHLORITE FSP Pg aQz Rt H2O
0109): AMPH GRNT PHNG EPI CHLORITE FSP Pg aQz Rt H2O = AMPH GRNT PHNG EPI CHLORITE FSP aQz Rt H2O
0110): AMPH GRNT PHNG EPI CHLORITE FSP aQz Rt H2O = AMPH GRNT PHNG EPI CHLORITE FSP Mt aQz Rt H2O
0111): AMPH GRNT PHNG EPI CHLORITE FSP Mt aQz Rt H2O = AMPH GRNT PHNG CHLORITE FSP Mt aQz Rt H2O
0112): AMPH GRNT PHNG CHLORITE FSP Mt aQz Rt H2O = AMPH GRNT BIOTITE PHNG CHLORITE FSP Mt aQz Rt H2O
0113): AMPH GRNT BIOTITE PHNG CHLORITE FSP Mt aQz Rt H2O = AMPH GRNT BIOTITE PHNG FSP Mt aQz Rt H2O
0114): AMPH GRNT BIOTITE PHNG FSP Mt aQz Rt H2O = AMPH GRNT BIOTITE PHNG EPI FSP Mt aQz Rt H2O
0115): AMPH GRNT BIOTITE PHNG EPI FSP Mt aQz Rt H2O = AMPH GRNT BIOTITE PHNG EPI FSP aQz Rt H2O
0116): AMPH GRNT BIOTITE PHNG EPI FSP aQz Rt H2O = GRNT BIOTITE PHNG EPI FSP aQz Rt H2O
0117): GRNT BIOTITE PHNG EPI FSP aQz Rt H2O = GRNT BIOTITE PHNG EPI FSP Mt aQz Rt H2O
0118): GRNT BIOTITE PHNG EPI FSP Mt aQz Rt H2O = GRNT BIOTITE PHNG FSP Mt aQz Rt H2O
0119): GRNT BIOTITE PHNG FSP Mt aQz Rt H2O = GRNT BIOTITE PHNG (2)FSP Mt aQz Rt H2O
0120): GRNT BIOTITE PHNG (2)FSP Mt aQz Rt H2O = GRNT BIOTITE (2)FSP Mt aQz Rt H2O
0121): GRNT BIOTITE (2)FSP Mt aQz Rt H2O = GRNT ILMENITE BIOTITE (2)FSP Mt aQz Rt H2O
0122): GRNT ILMENITE BIOTITE (2)FSP Mt aQz Rt H2O = GRNT ILMENITE BIOTITE (2)FSP Mt aQz H2O
0123): AMPH PHNG EPI CHLORITE Pg aQz Sph Zo H2O = AMPH GRNT PHNG EPI CHLORITE Pg aQz Sph Zo H2O
0124): AMPH GRNT PHNG EPI CHLORITE Pg aQz Sph Zo H2O = AMPH GRNT PHNG EPI CHLORITE Pg aQz Rt Zo H2O
0125): AMPH GRNT PHNG EPI CHLORITE FSP Mt aQz Rt H2O = AMPH GRNT PHNG CHLORITE FSP Mt Pg aQz Rt H2O
0126): AMPH GRNT PHNG CHLORITE FSP Mt Pg aQz Rt H2O = AMPH GRNT PHNG CHLORITE FSP Mt aQz Rt H2O
0127): AMPH GRNT PHNG EPI CHLORITE Pg aQz Rt H2O = AMPH GRNT PHNG EPI CHLORITE Mt Pg aQz Rt H2O
0128): AMPH GRNT PHNG EPI CHLORITE Mt Pg aQz Rt H2O = AMPH GRNT PHNG CHLORITE Mt Pg aQz Rt H2O
0129): AMPH GRNT PHNG CHLORITE Mt Pg aQz Rt H2O = AMPH GRNT BIOTITE PHNG CHLORITE Mt Pg aQz Rt H2O
0130): AMPH GRNT BIOTITE PHNG CHLORITE Mt Pg aQz Rt H2O = AMPH GRNT BIOTITE PHNG Mt Pg aQz Rt H2O

Appendix 2 – DOMINO reactions for T6

0131): AMPH GRNT BIOTITE PHNG Mt Pg aQz Rt H2O = AMPH GRNT BIOTITE PHNG FSP Mt Pg aQz Rt H2O
 0132): AMPH GRNT BIOTITE PHNG FSP Mt Pg aQz Rt H2O = AMPH GRNT PHNG FSP Mt Pg aQz Rt H2O
 0133): AMPH GRNT PHNG FSP Mt Pg aQz Rt H2O = AMPH GRNT PHNG FSP Mt aQz Rt H2O
 0134): AMPH GRNT PHNG FSP Mt aQz Rt H2O = AMPH GRNT BIOTITE PHNG FSP Mt aQz Rt H2O
 0135): AMPH PHNG PUMPI CHLORITE GLAUC Lw aQz Sph H2O = AMPH PHNG EPI CHLORITE GLAUC Lw aQz Sph H2O
 0136): AMPH PHNG EPI CHLORITE GLAUC Lw aQz Sph H2O = AMPH PHNG EPI CHLORITE GLAUC Lw aQz Sph Zo H2O
 0137): AMPH PHNG EPI CHLORITE GLAUC Lw aQz Sph Zo H2O = PHNG EPI CHLORITE GLAUC Lw aQz Sph Zo H2O
 0138): PHNG EPI CHLORITE GLAUC Lw aQz Sph Zo H2O = PHNG EPI CHLORITE GLAUC Pg aQz Sph Zo H2O
 0139): PHNG EPI CHLORITE GLAUC Pg aQz Sph Zo H2O = AMPH PHNG EPI CHLORITE GLAUC Pg aQz Sph Zo H2O
 0140): AMPH PHNG EPI CHLORITE GLAUC Pg aQz Sph Zo H2O = AMPH PHNG EPI CHLORITE Pg aQz Sph Zo H2O
 0141): PHNG PUMPI CHLORITE GLAUC Di Lw aQz Sph H2O = AMPH PHNG PUMPI CHLORITE GLAUC Lw aQz Sph H2O
 0142): AMPH PHNG PUMPI CHLORITE GLAUC Lw aQz Sph H2O = AMPH PHNG EPI PUMPI CHLORITE GLAUC Lw aQz Sph H2O
 0143): AMPH PHNG EPI PUMPI CHLORITE GLAUC Lw aQz Sph H2O = AMPH PHNG EPI CHLORITE GLAUC Lw aQz Sph H2O
 0144): AMPH GRNT PHNG EPI CHLORITE Pg aQz Sph Zo H2O = AMPH GRNT PHNG EPI CHLORITE Pg aQz Sph H2O
 0145): AMPH GRNT PHNG EPI CHLORITE Pg aQz Sph H2O = AMPH GRNT PHNG EPI CHLORITE Pg aQz Rt H2O
 0146): PHNG PUMPI CHLORITE GLAUC Lw aQz Sph H2O = ACTINOLITE PHNG PUMPI CHLORITE GLAUC Lw aQz Sph H2O
 0147): ACTINOLITE PHNG PUMPI CHLORITE GLAUC Lw aQz Sph H2O = AMPH PHNG PUMPI CHLORITE GLAUC Lw aQz Sph H2O
 0148): AMPH GRNT PHNG EPI CHLORITE Pg aQz Sph H2O = AMPH GRNT PHNG EPI CHLORITE Pg aQz Rt Sph H2O
 0149): AMPH GRNT PHNG EPI CHLORITE Pg aQz Rt Sph H2O = AMPH GRNT PHNG EPI CHLORITE Pg aQz Rt H2O
 0150): AMPH GRNT PHNG CHLORITE Mt Pg aQz Rt H2O = AMPH GRNT PHNG Mt Pg aQz Rt H2O
 0151): AMPH GRNT PHNG Mt Pg aQz Rt H2O = AMPH GRNT PHNG FSP Mt Pg aQz Rt H2O
 0152): GRNT BIOTITE PHNG EPI FSP Mt aQz Rt H2O = GRNT BIOTITE PHNG EPI (2)FSP Mt aQz Rt H2O
 0153): GRNT BIOTITE PHNG EPI (2)FSP Mt aQz Rt H2O = GRNT BIOTITE PHNG (2)FSP Mt aQz Rt H2O
 0154): AMPH PHNG EPI CHLORITE GLAUC FSP aQz Sph Zo H2O = AMPH PHNG EPI CHLORITE FSP aQz Sph Zo H2O
 0155): PHNG EPI CHLORITE GLAUC FSP aQz Sph Zo H2O = AMPH PHNG EPI CHLORITE GLAUC FSP aQz Sph Zo H2O
 0156): PHNG EPI CHLORITE GLAUC Pg aQz Sph Zo H2O = PHNG EPI CHLORITE GLAUC FSP aQz Sph Zo H2O
 0157): AMPH PHNG EPI PUMPI CHLORITE GLAUC Lw aQz Sph H2O = AMPH PHNG EPI CHLORITE GLAUC Lw aQz Sph H2O
 0158): AMPH PHNG PUMPI CHLORITE GLAUC Lw aQz Sph H2O = AMPH PHNG EPI PUMPI CHLORITE GLAUC Lw aQz Sph H2O
 0159): PHNG PUMPI CHLORITE GLAUC Lw aQz Sph H2O = PHNG PUMPI CHLORITE GLAUC Di Lw aQz Sph H2O
 0160): AMPH PHNG EPI CHLORITE (2)FSP aQz Sph Zo H2O = AMPH PHNG EPI CHLORITE (2)FSP aQz Sph H2O
 0161): AMPH GRNT ILMENITE BIOTITE PHNG EPI CHLORITE FSP aQz H2O = GRNT ILMENITE BIOTITE PHNG EPI CHLORITE F
 0162): GRNT BIOTITE PHNG FSP Mt aQz Rt Si H2O = GRNT BIOTITE PHNG FSP Ky Mt aQz Rt H2O
 0163): GRNT ILMENITE BIOTITE FSP Cd Mt aQz Si H2O = GRNT ILMENITE BIOTITE FSP aCd Mt aQz Si H2O
 0164): GRNT ILMENITE BIOTITE FSP Cd Mt aQz Si H2O = GRNT ILMENITE BIOTITE FSP aCd Mt aQz Si H2O
 0165): GRNT ILMENITE BIOTITE FSP aCd Mt aQz Si H2O = GRNT ILMENITE BIOTITE FSP Cd Mt aQz Si H2O
 0166): GRNT ILMENITE BIOTITE FSP Cd Mt aQz Si H2O = GRNT ILMENITE BIOTITE FSP aCd Mt aQz Si H2O
 0167): GRNT ILMENITE BIOTITE FSP aCd Mt aQz Si H2O = GRNT ILMENITE BIOTITE FSP Cd Mt aQz Si H2O
 0168): GRNT ILMENITE BIOTITE FSP Cd Mt aQz Si H2O = GRNT ILMENITE BIOTITE FSP aCd Mt aQz Si H2O
 0169): GRNT ILMENITE BIOTITE FSP Cd Mt aQz Si H2O = GRNT ILMENITE BIOTITE FSP aCd Mt aQz Si H2O
 0170): GRNT ILMENITE BIOTITE FSP aCd Mt aQz Si H2O = GRNT ILMENITE BIOTITE FSP Cd Mt aQz Si H2O
 0171): GRNT ILMENITE BIOTITE FSP Cd Mt aQz Si H2O = GRNT ILMENITE BIOTITE FSP aCd Mt aQz Si H2O
 0172): GRNT ILMENITE BIOTITE FSP Cd Mt aQz Si H2O = GRNT ILMENITE BIOTITE FSP aCd Mt aQz Si H2O
 0173): GRNT ILMENITE BIOTITE FSP Cd Mt aQz Si H2O = GRNT ILMENITE BIOTITE FSP aCd Mt aQz Si H2O
 0174): GRNT ILMENITE BIOTITE FSP Cd Mt aQz Si H2O = GRNT ILMENITE BIOTITE FSP aCd Mt aQz Si H2O
 0175): GRNT ILMENITE BIOTITE FSP Mt aQz Si H2O = GRNT ILMENITE BIOTITE FSP aCd Mt aQz Si H2O
 0176): GRNT ILMENITE BIOTITE FSP Mt aQz Si H2O = GRNT ILMENITE BIOTITE FSP aCd Mt aQz Si H2O
 0177): GRNT ILMENITE BIOTITE FSP aCd Mt aQz Si H2O = GRNT ILMENITE BIOTITE FSP Mt aQz Si H2O
 0178): GRNT BIOTITE (2)FSP Mt aQz Rt Si H2O = GRNT ILMENITE BIOTITE (2)FSP Mt aQz Si H2O
 0179): GRNT BIOTITE (2)FSP Mt aQz Rt Si H2O = GRNT BIOTITE PHNG FSP Mt aQz Rt Si H2O
 0180): GRNT ILMENITE BIOTITE FSP Cd Mt aQz H2O = GRNT ILMENITE BIOTITE (2)FSP Cd Mt aQz H2O
 0181): GRNT ILMENITE BIOTITE (2)FSP Cd Mt aQz H2O = GRNT ILMENITE BIOTITE FSP Cd Mt aQz H2O
 0182): GRNT ILMENITE OPX (2)FSP Mt aQz H2O = GRNT ILMENITE OPX (2)FSP aCd Mt aQz H2O
 0183): GRNT ILMENITE OPX (2)FSP Mt aQz H2O = GRNT ILMENITE OPX (2)FSP aCd Mt aQz H2O
 0184): GRNT ILMENITE OPX (2)FSP Mt aQz H2O = GRNT ILMENITE OPX (2)FSP aCd Mt aQz H2O
 0185): GRNT ILMENITE OPX (2)FSP Mt aQz H2O = GRNT ILMENITE OPX (2)FSP aCd Mt aQz H2O
 0186): GRNT ILMENITE OPX (2)FSP Mt aQz H2O = GRNT ILMENITE OPX (2)FSP aCd Mt aQz H2O
 0187): GRNT ILMENITE OPX (2)FSP Mt aQz H2O = GRNT ILMENITE OPX (2)FSP aCd Mt aQz H2O
 0188): GRNT ILMENITE OPX (2)FSP Mt aQz H2O = GRNT ILMENITE OPX (2)FSP aCd Mt aQz H2O
 0189): AMPH ILMENITE PHNG EPI CHLORITE (2)FSP aQz H2O = AMPH ILMENITE BIOTITE PHNG EPI CHLORITE (2)FSP aQz
 0190): AMPH ILMENITE BIOTITE PHNG EPI CHLORITE (2)FSP aQz H2O = ILMENITE BIOTITE PHNG EPI CHLORITE (2)FSP a
 0191): ILMENITE BIOTITE PHNG EPI CHLORITE (2)FSP aQz H2O = GRNT ILMENITE BIOTITE PHNG EPI CHLORITE (2)FSP a
 0192): GRNT ILMENITE BIOTITE PHNG EPI CHLORITE (2)FSP aQz H2O = GRNT ILMENITE BIOTITE PHNG EPI CHLORITE FSP
 0193): GRNT ILMENITE BIOTITE FSP aCd Mt aQz Si H2O = GRNT ILMENITE BIOTITE FSP Mt aQz Si H2O
 0194): GRNT ILMENITE BIOTITE FSP Cd Mt aQz Si H2O = GRNT ILMENITE BIOTITE FSP Cd Mt aQz Si H2O
 0195): GRNT ILMENITE BIOTITE FSP aCd Mt aQz Si H2O = GRNT ILMENITE BIOTITE (2)FSP aCd Mt aQz H2O

Appendix 2 – DOMINO reactions for T6

0196): GRNT ILMENITE BIOTITE FSP Mt aQz Si H2O = GRNT ILMENITE BIOTITE FSP Cd Mt aQz Si H2O
0197): GRNT ILMENITE BIOTITE FSP Mt aQz Si H2O = GRNT ILMENITE BIOTITE FSP Cd Mt aQz Si H2O
0198): GRNT ILMENITE BIOTITE (2)FSP aCd Mt aQz H2O = GRNT ILMENITE BIOTITE OPX (2)FSP aCd Mt aQz H2O
0199): GRNT ILMENITE BIOTITE OPX (2)FSP Cd Mt aQz H2O = GRNT ILMENITE OPX (2)FSP Cd Mt aQz H2O
0200): GRNT ILMENITE BIOTITE OPX (2)FSP Cd Mt aQz H2O = GRNT ILMENITE BIOTITE (2)FSP Cd Mt aQz H2O
0201): GRNT ILMENITE BIOTITE (2)FSP Mt aQz H2O = GRNT ILMENITE BIOTITE (2)FSP aCd Mt aQz H2O
0202): AMPH ILMENITE PHNG EPI CHLORITE FSP aQz Sph Zo H2O = AMPH ILMENITE PHNG EPI CHLORITE FSP aQz Zo H2O
0203): AMPH GRNT ILMENITE PHNG EPI CHLORITE FSP aQz Zo H2O = AMPH GRNT ILMENITE PHNG EPI CHLORITE (2)FSP aQz
0204): GRNT BIOTITE (2)FSP Mt aQz Rt H2O = GRNT BIOTITE (2)FSP Mt aQz Rt Si H2O
0205): GRNT ILMENITE BIOTITE (2)FSP Mt aQz Rt H2O = GRNT ILMENITE BIOTITE (2)FSP Mt aQz Si H2O
0206): GRNT ILMENITE BIOTITE PHNG EPI CHLORITE FSP aQz H2O = GRNT ILMENITE BIOTITE PHNG EPI CHLORITE FSP Mt
0207): GRNT ILMENITE BIOTITE PHNG EPI CHLORITE FSP Mt aQz H2O = GRNT ILMENITE BIOTITE PHNG CHLORITE FSP Mt
0208): GRNT ILMENITE BIOTITE PHNG CHLORITE FSP Mt aQz H2O = GRNT BIOTITE PHNG CHLORITE FSP Mt aQz Rt H2O
0209): GRNT ILMENITE BIOTITE PHNG FSP Ky Mt aQz H2O = GRNT ILMENITE BIOTITE PHNG FSP Mt aQz Si H2O
0210): GRNT ILMENITE BIOTITE PHNG CHLORITE FSP Mt aQz H2O = GRNT ILMENITE BIOTITE PHNG FSP Ky Mt aQz H2O
0211): AMPH PHNG EPI CHLORITE FSP aQz Sph Zo H2O = AMPH PHNG EPI CHLORITE FSP aQz Rt Sph Zo H2O
0212): AMPH PHNG EPI CHLORITE FSP aQz Rt Sph Zo H2O = AMPH PHNG EPI CHLORITE FSP aQz Rt Zo H2O
0213): AMPH PHNG EPI CHLORITE FSP aQz Rt Zo H2O = AMPH ILMENITE PHNG EPI CHLORITE FSP aQz Rt Zo H2O
0214): AMPH ILMENITE PHNG EPI CHLORITE FSP aQz Rt Zo H2O = AMPH GRNT PHNG EPI CHLORITE FSP aQz Rt Zo H2O
0215): AMPH GRNT PHNG EPI CHLORITE FSP aQz Rt Zo H2O = AMPH GRNT PHNG EPI CHLORITE Pg aQz Rt Zo H2O
0216): AMPH GRNT ILMENITE PHNG EPI CHLORITE FSP aQz Rt H2O = AMPH GRNT ILMENITE PHNG CHLORITE FSP Mt aQz Rt
0217): AMPH GRNT ILMENITE PHNG CHLORITE FSP Mt aQz Rt H2O = AMPH GRNT BIOTITE PHNG CHLORITE FSP Mt aQz Rt H
0218): AMPH GRNT BIOTITE PHNG CHLORITE FSP Mt aQz Rt H2O = AMPH GRNT BIOTITE PHNG EPI CHLORITE FSP aQz Rt H
0219): AMPH PHNG EPI CHLORITE GLAUC Pg aQz Sph Zo H2O = AMPH PHNG EPI CHLORITE FSP Pg aQz Sph Zo H2O
0220): AMPH PHNG EPI CHLORITE Pg aQz Sph Zo H2O = AMPH PHNG EPI CHLORITE Pg aQz Rt Sph Zo H2O
0221): AMPH PHNG EPI CHLORITE Pg aQz Rt Sph Zo H2O = AMPH PHNG EPI CHLORITE Pg aQz Rt Zo H2O
0222): AMPH GRNT PHNG EPI CHLORITE Pg aQz Sph H2O = AMPH GRNT PHNG EPI CHLORITE Pg aQz Rt Zo H2O
0223): AMPH GRNT PHNG CHLORITE Mt Pg aQz Rt H2O = AMPH GRNT PHNG CHLORITE FSP Mt Pg aQz Rt H2O
0224): AMPH GRNT PHNG Mt Pg aQz Rt H2O = AMPH GRNT BIOTITE PHNG Mt Pg aQz Rt H2O
0225): AMPH GRNT BIOTITE PHNG Mt Pg aQz Rt H2O = AMPH GRNT PHNG FSP Mt Pg aQz Rt H2O
0226): PHNG PUMPI CHLORITE GLAUC Di Lw aQz Sph H2O = ACTINOLITE PHNG PUMPI CHLORITE GLAUC Lw aQz Sph H2O
0227): AMPH PHNG EPI CHLORITE FSP aQz Sph Zo H2O = AMPH PHNG EPI CHLORITE (2)FSP aQz Sph H2O
0228): GRNT ILMENITE BIOTITE PHNG EPI CHLORITE (2)FSP aQz H2O = GRNT ILMENITE BIOTITE PHNG CHLORITE FSP Mt
0229): GRNT ILMENITE BIOTITE FSP Cd Mt aQz Si H2O = GRNT ILMENITE BIOTITE (2)FSP Cd Mt aQz H2O
0230): GRNT ILMENITE BIOTITE FSP Cd Mt aQz Si H2O = GRNT ILMENITE BIOTITE (2)FSP Cd Mt aQz H2O
0231): GRNT ILMENITE BIOTITE (2)FSP aCd Mt aQz H2O = GRNT ILMENITE BIOTITE FSP aCd Mt aQz H2O
0232): GRNT ILMENITE BIOTITE FSP Cd Mt aQz Si H2O = GRNT ILMENITE BIOTITE (2)FSP aCd Mt aQz H2O
0233): GRNT ILMENITE BIOTITE OPX FSP Cd Mt aQz H2O = GRNT ILMENITE BIOTITE OPX FSP aCd Mt aQz H2O
0234): GRNT ILMENITE BIOTITE FSP Cd Mt aQz H2O = GRNT ILMENITE BIOTITE OPX FSP Cd Mt aQz H2O
0235): GRNT ILMENITE BIOTITE (2)FSP aCd Mt aQz H2O = GRNT ILMENITE BIOTITE FSP aCd Mt aQz H2O
0236): GRNT ILMENITE BIOTITE FSP aCd Mt aQz H2O = GRNT ILMENITE BIOTITE (2)FSP aCd Mt aQz H2O
0237): AMPH ILMENITE PHNG EPI CHLORITE FSP aQz Zo H2O = AMPH ILMENITE PHNG EPI CHLORITE (2)FSP aQz H2O
0238): GRNT ILMENITE BIOTITE PHNG FSP Mt aQz Si H2O = GRNT ILMENITE BIOTITE (2)FSP Mt aQz Si H2O
0239): GRNT ILMENITE BIOTITE OPX (2)FSP Mt aQz H2O = GRNT ILMENITE BIOTITE OPX (2)FSP Cd Mt aQz H2O
0240): GRNT ILMENITE OPX (2)FSP Cd Mt aQz H2O = GRNT ILMENITE BIOTITE OPX (2)FSP Cd Mt aQz H2O
0241): GRNT ILMENITE OPX (2)FSP Mt aQz H2O = GRNT ILMENITE OPX (2)FSP Cd Mt aQz H2O
0242): GRNT ILMENITE OPX (2)FSP Mt aQz H2O = GRNT ILMENITE OPX (2)FSP Cd Mt aQz H2O
0243): GRNT ILMENITE OPX (2)FSP Mt aQz H2O = GRNT ILMENITE OPX (2)FSP Cd Mt aQz H2O
0244): AMPH ILMENITE PHNG EPI CHLORITE (2)FSP aQz H2O = AMPH ILMENITE PHNG EPI CHLORITE FSP aQz H2O
0245): AMPH ILMENITE PHNG EPI CHLORITE FSP aQz H2O = AMPH ILMENITE BIOTITE PHNG EPI CHLORITE (2)FSP aQz H2O
0246): GRNT ILMENITE BIOTITE PHNG EPI CHLORITE (2)FSP aQz H2O = AMPH GRNT ILMENITE PHNG EPI CHLORITE (2)FSP
0247): AMPH GRNT ILMENITE PHNG EPI CHLORITE FSP aQz Rt H2O = AMPH GRNT PHNG EPI CHLORITE FSP Mt aQz Rt H2O
0248): AMPH GRNT ILMENITE PHNG EPI CHLORITE FSP aQz H2O = AMPH GRNT ILMENITE PHNG EPI CHLORITE FSP Mt aQz H
0249): AMPH GRNT ILMENITE PHNG EPI CHLORITE FSP Mt aQz H2O = AMPH GRNT ILMENITE PHNG CHLORITE FSP Mt aQz Rt
0250): AMPH GRNT ILMENITE BIOTITE PHNG EPI CHLORITE FSP aQz H2O = GRNT BIOTITE PHNG EPI CHLORITE FSP aQz Rt
0251): GRNT BIOTITE PHNG FSP Ky Mt aQz Rt H2O = GRNT ILMENITE BIOTITE PHNG FSP Ky Mt aQz Rt H2O
0252): GRNT ILMENITE BIOTITE PHNG FSP Ky Mt aQz Rt H2O = GRNT ILMENITE BIOTITE PHNG FSP Ky Mt aQz H2O
0253): GRNT BIOTITE PHNG (2)FSP Mt aQz Rt H2O = GRNT BIOTITE (2)FSP Mt aQz Rt Si H2O
0254): AMPH PHNG EPI CHLORITE FSP aQz Rt Zo H2O = AMPH GRNT PHNG EPI CHLORITE FSP aQz Rt Zo H2O
0255): AMPH PHNG EPI CHLORITE FSP Pg aQz Rt Zo H2O = AMPH PHNG EPI CHLORITE FSP aQz Rt Zo H2O
0256): AMPH PHNG EPI CHLORITE Pg aQz Rt Zo H2O = AMPH PHNG EPI CHLORITE FSP Pg aQz Rt Zo H2O
0257): AMPH GRNT PHNG EPI CHLORITE Pg aQz Sph H2O = AMPH GRNT PHNG EPI CHLORITE Pg aQz Rt Sph H2O
0258): AMPH GRNT PHNG EPI CHLORITE Pg aQz Rt Sph H2O = AMPH GRNT PHNG EPI CHLORITE Pg aQz Rt H2O
0259): AMPH GRNT PHNG EPI CHLORITE FSP Pg aQz Rt H2O = AMPH GRNT PHNG EPI CHLORITE Mt Pg aQz Rt H2O
0260): AMPH GRNT PHNG CHLORITE Mt Pg aQz Rt H2O = AMPH GRNT BIOTITE PHNG Mt Pg aQz Rt H2O

Appendix 2 – DOMINO reactions for T6

0261): AMPH PHNG EPI CHLORITE FSP aQz Sph Zo H2O = AMPH PHNG EPI CHLORITE (2)FSP aQz Sph H2O
 0262): AMPH PHNG EPI CHLORITE (3)FSP aQz Sph H2O = PHNG EPI CHLORITE (3)FSP aQz Sph H2O
 0263): AMPH PHNG EPI CHLORITE (2)FSP aQz Sph H2O = AMPH PHNG EPI CHLORITE (3)FSP aQz Sph H2O
 0264): AMPH PHNG EPI CHLORITE (2)FSP aQz Sph Zo H2O = AMPH PHNG EPI CHLORITE (2)FSP aQz Sph H2O
 0265): AMPH PHNG EPI CHLORITE FSP aQz Sph Zo H2O = AMPH PHNG EPI CHLORITE (2)FSP aQz Sph Zo H2O
 0266): GRNT ILMENITE BIOTITE PHNG CHLORITE FSP Mt aQz H2O = ILMENITE BIOTITE PHNG CHLORITE FSP Mt aQz St H2
 0267): GRNT ILMENITE BIOTITE (2)FSP aCd Mt aQz H2O = GRNT ILMENITE BIOTITE (2)FSP Cd Mt aQz H2O
 0268): GRNT ILMENITE BIOTITE FSP Cd Mt aQz H2O = GRNT ILMENITE BIOTITE FSP aCd Mt aQz H2O
 0269): GRNT ILMENITE BIOTITE OPX FSP Cd Mt aQz H2O = GRNT ILMENITE BIOTITE OPX (2)FSP Cd Mt aQz H2O
 0270): GRNT ILMENITE BIOTITE OPX (2)FSP Cd Mt aQz H2O = GRNT ILMENITE BIOTITE OPX (2)FSP aCd Mt aQz H2O
 0271): GRNT ILMENITE BIOTITE (2)FSP Cd Mt aQz H2O = GRNT ILMENITE BIOTITE FSP Cd Mt aQz H2O
 0272): GRNT ILMENITE BIOTITE OPX (2)FSP Cd Mt aQz H2O = GRNT ILMENITE BIOTITE OPX (2)FSP aCd Mt aQz H2O
 0273): GRNT ILMENITE BIOTITE OPX (2)FSP Mt aQz H2O = GRNT ILMENITE BIOTITE OPX (2)FSP aCd Mt aQz H2O
 0274): GRNT ILMENITE BIOTITE OPX (2)FSP aCd Mt aQz H2O = GRNT ILMENITE OPX (2)FSP Cd Mt aQz H2O
 0275): GRNT ILMENITE OPX (2)FSP aCd Mt aQz H2O = GRNT ILMENITE BIOTITE OPX (2)FSP Cd Mt aQz H2O
 0276): GRNT ILMENITE BIOTITE OPX (2)FSP Mt aQz H2O = GRNT ILMENITE BIOTITE OPX (2)FSP Cd Mt aQz H2O
 0277): GRNT ILMENITE BIOTITE (2)FSP Cd Mt aQz H2O = GRNT ILMENITE BIOTITE (2)FSP aCd Mt aQz H2O
 0278): GRNT ILMENITE BIOTITE (2)FSP Mt aQz Si H2O = GRNT ILMENITE BIOTITE (2)FSP aCd Mt aQz H2O
 0279): GRNT ILMENITE BIOTITE FSP Cd Mt aQz Si H2O = GRNT ILMENITE BIOTITE (2)FSP Cd Mt aQz H2O
 0280): GRNT ILMENITE BIOTITE FSP aCd Mt aQz Si H2O = GRNT ILMENITE BIOTITE (2)FSP Cd Mt aQz H2O
 0281): GRNT ILMENITE BIOTITE (2)FSP Cd Mt aQz H2O = GRNT ILMENITE BIOTITE (2)FSP aCd Mt aQz H2O
 0282): GRNT ILMENITE OPX (2)FSP Mt aQz H2O = GRNT ILMENITE OPX (2)FSP Cd Mt aQz H2O
 0283): GRNT ILMENITE OPX (2)FSP Cd Mt aQz H2O = GRNT ILMENITE OPX (2)FSP aCd Mt aQz H2O
 0284): GRNT ILMENITE OPX (2)FSP Mt aQz H2O = GRNT ILMENITE OPX (2)FSP Cd Mt aQz H2O
 0285): GRNT ILMENITE OPX (2)FSP Mt aQz H2O = GRNT ILMENITE OPX (2)FSP Cd Mt aQz H2O
 0286): GRNT ILMENITE OPX (2)FSP aCd Mt aQz H2O = GRNT ILMENITE OPX (2)FSP Cd Mt aQz H2O
 0287): AMPH GRNT ILMENITE PHNG EPI CHLORITE (2)FSP aQz H2O = AMPH ILMENITE BIOTITE PHNG EPI CHLORITE (2)FSP
 0288): AMPH GRNT ILMENITE PHNG EPI CHLORITE FSP aQz Zo H2O = AMPH GRNT ILMENITE PHNG EPI CHLORITE FSP aQz H
 0289): AMPH PHNG EPI CHLORITE FSP aQz Rt Sph Zo H2O = AMPH ILMENITE PHNG EPI CHLORITE FSP aQz Rt Zo H2O
 0290): AMPH GRNT BIOTITE PHNG EPI FSP Mt aQz Rt H2O = AMPH GRNT BIOTITE PHNG EPI CHLORITE FSP aQz Rt H2O
 0291): AMPH GRNT BIOTITE PHNG EPI CHLORITE FSP aQz Rt H2O = AMPH GRNT BIOTITE PHNG EPI FSP aQz Rt H2O
 0292): GRNT BIOTITE PHNG EPI CHLORITE FSP Mt aQz Rt H2O = GRNT BIOTITE PHNG EPI FSP Mt aQz Rt H2O
 0293): GRNT BIOTITE PHNG EPI CHLORITE FSP Mt aQz Rt H2O = GRNT BIOTITE PHNG FSP Mt aQz Rt H2O
 0294): AMPH GRNT BIOTITE PHNG EPI FSP aQz Rt H2O = GRNT BIOTITE PHNG EPI CHLORITE FSP aQz Rt H2O
 0295): GRNT ILMENITE BIOTITE PHNG EPI CHLORITE FSP aQz H2O = GRNT BIOTITE PHNG EPI CHLORITE FSP aQz Rt H2O
 0296): GRNT BIOTITE PHNG EPI CHLORITE FSP aQz Rt H2O = GRNT BIOTITE PHNG CHLORITE FSP Mt aQz Rt H2O
 0297): GRNT BIOTITE PHNG FSP Ky Mt aQz Rt H2O = GRNT ILMENITE BIOTITE PHNG FSP Ky Mt aQz H2O
 0298): AMPH PHNG EPI CHLORITE FSP Pg aQz Sph Zo H2O = AMPH PHNG EPI CHLORITE FSP aQz Rt Zo H2O
 0299): AMPH PHNG EPI CHLORITE GLAUC Pg aQz Sph Zo H2O = AMPH PHNG EPI CHLORITE GLAUC FSP aQz Sph Zo H2O
 0300): AMPH PHNG EPI CHLORITE Pg aQz Sph Zo H2O = AMPH PHNG EPI CHLORITE Pg aQz Rt Sph Zo H2O
 0301): AMPH PHNG EPI CHLORITE Pg aQz Rt Sph Zo H2O = AMPH PHNG EPI CHLORITE Pg aQz Rt Zo H2O
 0302): AMPH PHNG EPI CHLORITE Pg aQz Sph Zo H2O = AMPH GRNT PHNG EPI CHLORITE Pg aQz Rt Zo H2O
 0303): AMPH GRNT PHNG EPI CHLORITE FSP Pg aQz Rt H2O = AMPH GRNT PHNG CHLORITE FSP Mt Pg aQz Rt H2O
 0304): AMPH GRNT PHNG CHLORITE FSP Mt aQz Rt H2O = AMPH GRNT ILMENITE PHNG CHLORITE FSP Mt aQz Rt H2O
 0305): AMPH GRNT PHNG CHLORITE FSP Mt Pg aQz Rt H2O = AMPH GRNT BIOTITE PHNG FSP Mt Pg aQz Rt H2O
 0306): AMPH GRNT BIOTITE PHNG FSP Mt Pg aQz Rt H2O = AMPH GRNT BIOTITE PHNG FSP Mt aQz Rt H2O
 0307): AMPH GRNT BIOTITE PHNG CHLORITE Mt Pg aQz Rt H2O = AMPH GRNT PHNG CHLORITE FSP Mt Pg aQz Rt H2O
 0308): GRNT ILMENITE BIOTITE FSP Mt aQz Si H2O = GRNT ILMENITE BIOTITE FSP Cd Mt aQz Si H2O
 0309): GRNT ILMENITE BIOTITE FSP Mt aQz Si H2O = GRNT ILMENITE BIOTITE FSP aCd Mt aQz Si H2O
 0310): GRNT ILMENITE BIOTITE FSP Cd Mt aQz Si H2O = GRNT ILMENITE BIOTITE FSP aCd Mt aQz Si H2O
 0311): GRNT ILMENITE BIOTITE FSP Mt aQz Si H2O = GRNT ILMENITE BIOTITE FSP aCd Mt aQz Si H2O
 0312): AMPH PHNG EPI CHLORITE (2)FSP aQz Sph Zo H2O = AMPH PHNG EPI CHLORITE (3)FSP aQz Sph H2O
 0313): PHNG EPI CHLORITE (3)FSP aQz Sph H2O = BIOTITE PHNG EPI CHLORITE (2)FSP aQz Sph H2O
 0314): AMPH ILMENITE PHNG EPI CHLORITE (2)FSP aQz Sph H2O = AMPH ILMENITE BIOTITE PHNG EPI CHLORITE (2)FSP
 0315): ILMENITE BIOTITE PHNG CHLORITE (2)FSP Mt aQz H2O = GRNT ILMENITE BIOTITE PHNG CHLORITE FSP Mt aQz H2
 0316): GRNT ILMENITE BIOTITE FSP Cd Mt aQz Si H2O = GRNT ILMENITE BIOTITE (2)FSP Cd Mt aQz H2O
 0317): GRNT ILMENITE BIOTITE (2)FSP Cd Mt aQz H2O = GRNT ILMENITE BIOTITE (2)FSP aCd Mt aQz H2O
 0318): GRNT ILMENITE BIOTITE (2)FSP Cd Mt aQz H2O = GRNT ILMENITE BIOTITE FSP Cd Mt aQz H2O
 0319): GRNT ILMENITE BIOTITE FSP aCd Mt aQz H2O = GRNT ILMENITE BIOTITE FSP Cd Mt aQz H2O
 0320): GRNT ILMENITE BIOTITE (2)FSP Cd Mt aQz H2O = GRNT ILMENITE BIOTITE (2)FSP aCd Mt aQz H2O
 0321): GRNT ILMENITE BIOTITE FSP Cd Mt aQz H2O = GRNT ILMENITE BIOTITE FSP aCd Mt aQz H2O
 0322): GRNT ILMENITE BIOTITE OPX (2)FSP aCd Mt aQz H2O = GRNT ILMENITE BIOTITE OPX (2)FSP Cd Mt aQz H2O
 0323): GRNT ILMENITE OPX (2)FSP aCd Mt aQz H2O = GRNT ILMENITE OPX (2)FSP Cd Mt aQz H2O
 0324): GRNT ILMENITE BIOTITE OPX (2)FSP aCd Mt aQz H2O = GRNT ILMENITE BIOTITE OPX (2)FSP Cd Mt aQz H2O
 0325): AMPH ILMENITE PHNG EPI CHLORITE FSP aQz Zo H2O = AMPH ILMENITE PHNG EPI CHLORITE (2)FSP aQz H2O

Appendix 2 – DOMINO reactions for T6

0326): AMPH ILMENITE PHNG EPI CHLORITE (2)FSP aQz Zo H2O = AMPH ILMENITE PHNG EPI CHLORITE (2)FSP aQz H2O
0327): AMPH ILMENITE PHNG EPI CHLORITE FSP aQz Zo H2O = AMPH ILMENITE PHNG EPI CHLORITE (2)FSP aQz Zo H2O
0328): GRNT ILMENITE BIOTITE (2)FSP Mt aQz Si H2O = GRNT ILMENITE BIOTITE (2)FSP aCd Mt aQz H2O
0329): GRNT ILMENITE BIOTITE (2)FSP Cd Mt aQz H2O = GRNT ILMENITE BIOTITE (2)FSP aCd Mt aQz H2O
0330): GRNT ILMENITE BIOTITE FSP Mt aQz Si H2O = GRNT ILMENITE BIOTITE FSP aCd Mt aQz Si H2O
0331): GRNT ILMENITE OPX (2)FSP Mt aQz H2O = GRNT ILMENITE OPX (2)FSP Cd Mt aQz H2O
0332): GRNT ILMENITE OPX (2)FSP Mt aQz H2O = GRNT ILMENITE OPX (2)FSP aCd Mt aQz H2O
0333): GRNT ILMENITE BIOTITE OPX (2)FSP Mt aQz H2O = GRNT ILMENITE OPX (2)FSP Cd Mt aQz H2O
0334): AMPH ILMENITE PHNG EPI CHLORITE FSP aQz H2O = AMPH GRNT ILMENITE PHNG EPI CHLORITE (2)FSP aQz H2O
0335): AMPH PHNG EPI CHLORITE FSP aQz Sph Zo H2O = AMPH ILMENITE PHNG EPI CHLORITE FSP aQz Rt Zo H2O
0336): AMPH GRNT ILMENITE PHNG EPI CHLORITE FSP aQz Rt H2O = AMPH GRNT ILMENITE PHNG EPI CHLORITE FSP aQz Z
0337): AMPH GRNT ILMENITE PHNG EPI CHLORITE FSP Mt aQz H2O = AMPH GRNT ILMENITE BIOTITE PHNG EPI CHLORITE F
0338): GRNT BIOTITE PHNG CHLORITE FSP Mt aQz Rt H2O = GRNT BIOTITE PHNG FSP Mt aQz Rt H2O
0339): GRNT BIOTITE PHNG FSP Ky Mt aQz Rt H2O = GRNT ILMENITE BIOTITE PHNG FSP Ky Mt aQz H2O
0340): AMPH PHNG EPI CHLORITE FSP Pg aQz Sph Zo H2O = AMPH PHNG EPI CHLORITE FSP aQz Rt Sph Zo H2O
0341): AMPH PHNG EPI CHLORITE Pg aQz Sph Zo H2O = AMPH PHNG EPI CHLORITE Pg aQz Rt Sph Zo H2O
0342): AMPH PHNG EPI CHLORITE Pg aQz Rt Sph Zo H2O = AMPH PHNG EPI CHLORITE Pg aQz Rt Zo H2O
0343): AMPH PHNG EPI CHLORITE Pg aQz Rt Sph Zo H2O = AMPH GRNT PHNG EPI CHLORITE Pg aQz Rt Zo H2O
0344): GRNT ILMENITE BIOTITE FSP aCd Mt aQz Si H2O = GRNT ILMENITE BIOTITE FSP Cd Mt aQz Si H2O
0345): GRNT ILMENITE BIOTITE (2)FSP aCd Mt aQz H2O = GRNT ILMENITE BIOTITE FSP aCd Mt aQz Si H2O
0346): GRNT ILMENITE BIOTITE (2)FSP Cd Mt aQz H2O = GRNT ILMENITE BIOTITE (2)FSP aCd Mt aQz H2O
0347): GRNT ILMENITE BIOTITE FSP aCd Mt aQz Si H2O = GRNT ILMENITE BIOTITE (2)FSP Cd Mt aQz H2O
0348): GRNT ILMENITE BIOTITE FSP Mt aQz Si H2O = GRNT ILMENITE BIOTITE FSP Cd Mt aQz Si H2O
0349): GRNT ILMENITE BIOTITE FSP Cd Mt aQz Si H2O = GRNT ILMENITE BIOTITE FSP aCd Mt aQz Si H2O
0350): GRNT ILMENITE BIOTITE FSP aCd Mt aQz Si H2O = GRNT ILMENITE BIOTITE FSP Cd Mt aQz Si H2O
0351): GRNT ILMENITE BIOTITE FSP Mt aQz Si H2O = GRNT ILMENITE BIOTITE FSP aCd Mt aQz Si H2O
0352): GRNT ILMENITE BIOTITE FSP aCd Mt aQz H2O = GRNT ILMENITE BIOTITE FSP Cd Mt aQz H2O
0353): GRNT ILMENITE BIOTITE (2)FSP Mt aQz H2O = GRNT ILMENITE BIOTITE (2)FSP aCd Mt aQz H2O
0354): GRNT ILMENITE BIOTITE FSP Cd Mt aQz Si H2O = GRNT ILMENITE BIOTITE (2)FSP Cd Mt aQz H2O
0355): GRNT ILMENITE BIOTITE (2)FSP Cd Mt aQz H2O = GRNT ILMENITE BIOTITE (2)FSP aCd Mt aQz H2O
0356): GRNT ILMENITE BIOTITE FSP Cd Mt aQz Si H2O = GRNT ILMENITE BIOTITE (2)FSP aCd Mt aQz H2O
0357): GRNT ILMENITE OPX (2)FSP aCd Mt aQz H2O = GRNT ILMENITE OPX (2)FSP Cd Mt aQz H2O
0358): GRNT ILMENITE BIOTITE FSP Cd Mt aQz Si H2O = GRNT ILMENITE BIOTITE FSP aCd Mt aQz Si H2O

Appendix 3 - DOMINO reactions for AA02-15

Appendix 3 - DOMINO reactions for AA02-15

0 64): ILMENITE BIOTITE PHNG EPI CHLORITE FSP aQz Rt Sph H2O = ILMENITE BIOTITE PHNG EPI CHLORITE FSP aQz S
 0 65): ILMENITE BIOTITE PHNG EPI CHLORITE FSP aQz Sph H2O = ILMENITE BIOTITE PHNG EPI CHLORITE FSP aQz H2O
 0 66): GRNT ILMENITE BIOTITE PHNG CHLORITE FSP Mt aQz H2O = GRNT ILMENITE BIOTITE PHNG CHLORITE FSP Mt aQz
 0 67): GRNT ILMENITE BIOTITE PHNG CHLORITE FSP Mt aQz St H2O = GRNT ILMENITE BIOTITE PHNG FSP Mt aQz St H2O
 0 68): GRNT ILMENITE BIOTITE PHNG FSP Mt aQz St H2O = GRNT ILMENITE BIOTITE PHNG FSP Mt aQz Si St H2O
 0 69): GRNT ILMENITE BIOTITE PHNG FSP Mt aQz Si H2O = GRNT ILMENITE BIOTITE PHNG (2)FSP Mt aQz Si H2O
 0 70): GRNT ILMENITE BIOTITE PHNG (2)FSP Mt aQz Si H2O = GRNT ILMENITE BIOTITE (2)FSP Mt aQz Si H2O
 0 71): PHNG PUMPI CHLORITE FSP Lw Pg aQz Sph FStp H2O = PHNG PUMPI CHLORITE FSP Lw Pg aQz Sph H2O
 0 72): PHNG PUMPI CHLORITE FSP Lw Pg aQz Sph H2O = PHNG EPI CHLORITE FSP Lw Pg aQz Sph H2O
 0 73): PHNG EPI CHLORITE FSP Lw Pg aQz Sph H2O = PHNG EPI CHLORITE FSP Pg aQz Sph Zo H2O
 0 74): GRNT ILMENITE BIOTITE PHNG CHLORITE FSP Mt aQz H2O = GRNT ILMENITE BIOTITE PHNG FSP Ky Mt aQz H2O
 0 75): GRNT ILMENITE BIOTITE PHNG FSP Ky Mt aQz H2O = GRNT ILMENITE BIOTITE PHNG FSP Mt aQz Si H2O
 0 76): PHNG CHLORITE Hm Lw Pg aQz Sph FStp H2O = PHNG PUMPI CHLORITE Hm Lw Pg aQz Sph FStp H2O
 0 77): PHNG PUMPI CHLORITE Hm Lw Pg aQz Sph FStp H2O = PHNG PUMPI CHLORITE Lw Pg aQz Sph FStp H2O
 0 78): PHNG PUMPI CHLORITE Lw Pg aQz Sph FStp H2O = PHNG PUMPI CHLORITE FSP Lw Pg aQz Sph FStp H2O
 0 79): PHNG EPI CHLORITE FSP Pg aQz Sph H2O = PHNG EPI CHLORITE FSP Pg aQz Rt Sph H2O
 0 80): PHNG EPI CHLORITE FSP Pg aQz Rt Sph H2O = PHNG EPI CHLORITE FSP aQz Rt Sph H2O
 0 81): PHNG EPI CHLORITE FSP aQz Rt Sph H2O = ILMENITE EPI CHLORITE FSP aQz Rt Sph H2O
 0 82): ILMENITE PHNG EPI CHLORITE FSP aQz Rt Sph H2O = ILMENITE PHNG EPI CHLORITE FSP aQz Sph H2O
 0 83): ILMENITE PHNG EPI CHLORITE FSP aQz Sph H2O = ILMENITE BIOTITE PHNG EPI CHLORITE FSP aQz Sph H2O
 0 84): ILMENITE BIOTITE PHNG EPI CHLORITE FSP aQz Sph H2O = GRNT ILMENITE BIOTITE PHNG EPI CHLORITE FSP aQz
 0 85): GRNT ILMENITE BIOTITE PHNG EPI CHLORITE FSP aQz Sph H2O = GRNT ILMENITE BIOTITE PHNG EPI CHLORITE FS
 0 86): GRNT ILMENITE BIOTITE PHNG EPI CHLORITE FSP aQz H2O = GRNT ILMENITE BIOTITE PHNG EPI CHLORITE FSP Mt
 0 87): GRNT ILMENITE BIOTITE PHNG EPI CHLORITE FSP Mt aQz H2O = GRNT ILMENITE BIOTITE PHNG CHLORITE FSP Mt
 0 88): GRNT ILMENITE BIOTITE PHNG CHLORITE FSP Mt aQz H2O = GRNT ILMENITE BIOTITE PHNG CHLORITE FSP Mt aQz
 0 89): GRNT ILMENITE BIOTITE PHNG CHLORITE FSP Mt aQz Rt H2O = GRNT BIOTITE PHNG CHLORITE FSP Mt aQz Rt H2O
 0 90): GRNT BIOTITE PHNG CHLORITE FSP Mt aQz Rt H2O = GRNT BIOTITE PHNG FSP Ky Mt aQz Rt H2O
 0 91): GRNT BIOTITE PHNG FSP Ky Mt aQz Rt H2O = GRNT BIOTITE PHNG FSP Mt aQz Rt Si H2O
 0 92): GRNT BIOTITE PHNG FSP Mt aQz Rt Si H2O = GRNT ILMENITE BIOTITE PHNG FSP Mt aQz Rt Si H2O
 0 93): GRNT ILMENITE BIOTITE PHNG FSP Mt aQz Rt Si H2O = GRNT ILMENITE BIOTITE PHNG FSP Mt aQz Si H2O
 0 94): GRNT ILMENITE BIOTITE PHNG (2)FSP Mt aQz Si H2O = GRNT BIOTITE PHNG (2)FSP Mt aQz Rt Si H2O
 0 95): GRNT BIOTITE PHNG (2)FSP Mt aQz Rt Si H2O = GRNT BIOTITE (2)FSP Mt aQz Rt Si H2O
 0 96): PHNG CHLORITE GLAUC Hm Lw Pg aQz Rt FStp H2O = PHNG CHLORITE Hm Lw Pg aQz Rt Sph FStp H2O
 0 97): PHNG CHLORITE Hm Lw Pg aQz Rt Sph FStp H2O = PHNG CHLORITE Hm Lw Pg aQz Sph FStp H2O
 0 98): PHNG PUMPI CHLORITE Lw Pg aQz Sph FStp H2O = PHNG PUMPI CHLORITE Lw Pg aQz Sph H2O
 0 99): PHNG PUMPI CHLORITE Lw Pg aQz Sph H2O = PHNG PUMPI CHLORITE GLAUC Lw Pg aQz Sph H2O
 0100): PHNG PUMPI CHLORITE GLAUC Lw Pg aQz Sph H2O = PHNG PUMPI CHLORITE FSP Lw Pg aQz Sph H2O
 0101): GRNT ILMENITE PHNG EPI CHLORITE FSP aQz Sph H2O = ILMENITE PHNG EPI CHLORITE FSP aQz Sph H2O
 0102): GRNT ILMENITE PHNG EPI CHLORITE FSP aQz Sph H2O = GRNT ILMENITE BIOTITE PHNG EPI CHLORITE FSP aQz Sp
 0103): GRNT ILMENITE BIOTITE PHNG EPI CHLORITE FSP aQz Sph H2O = GRNT ILMENITE BIOTITE PHNG EPI CHLORITE FS
 0104): GRNT ILMENITE BIOTITE PHNG EPI CHLORITE FSP aQz Rt H2O = GRNT ILMENITE BIOTITE PHNG EPI CHLORITE FSP
 0105): GRNT ILMENITE BIOTITE PHNG EPI CHLORITE FSP aQz Rt H2O = GRNT ILMENITE BIOTITE PHNG CHLORITE FSP Mt
 0106): GRNT BIOTITE PHNG CHLORITE FSP Mt aQz Rt H2O = GRNT BIOTITE PHNG CHLORITE FSP Mt Pg aQz Rt H2O
 0107): GRNT BIOTITE PHNG CHLORITE FSP Mt Pg aQz Rt H2O = GRNT BIOTITE PHNG FSP Ky Mt Pg aQz Rt H2O
 0108): GRNT BIOTITE PHNG FSP Ky Mt Pg aQz Rt H2O = GRNT BIOTITE PHNG FSP Ky Mt aQz Rt H2O
 0109): GRNT BIOTITE PHNG FSP Ky Mt aQz Rt H2O = GRNT BIOTITE PHNG FSP Mt aQz Rt H2O
 0110): GRNT BIOTITE PHNG FSP Mt aQz Rt H2O = GRNT BIOTITE PHNG (2)FSP Mt aQz Rt H2O
 0111): GRNT BIOTITE PHNG (2)FSP Mt aQz Rt H2O = GRNT BIOTITE PHNG (2)FSP Mt aQz Rt Si H2O
 0112): GRNT (2)FSP Mt aQz Rt Si H2O = GRNT BIOTITE (2)FSP Mt aQz Rt Si H2O
 0113): PHNG CHLORITE Hm Lw Pg aQz Rt FStp H2O = PHNG CHLORITE GLAUC Hm Lw Pg aQz Rt FStp H2O
 0114): PHNG CHLORITE GLAUC Hm Lw Pg aQz Rt FStp H2O = PHNG CHLORITE GLAUC Hm Lw Pg aQz Rt H2O
 0115): PHNG CHLORITE GLAUC Hm Lw Pg aQz Rt H2O = PHNG CHLORITE GLAUC Hm Lw Pg aQz Sph H2O
 0116): PHNG CHLORITE GLAUC Hm Lw Pg aQz Sph H2O = PHNG PUMPI CHLORITE GLAUC Lw Pg aQz Sph H2O
 0117): PHNG PUMPI CHLORITE GLAUC Lw Pg aQz Sph H2O = PHNG EPI CHLORITE GLAUC Lw Pg aQz Sph H2O
 0118): PHNG PUMPI CHLORITE GLAUC Lw Pg aQz Sph H2O = PHNG EPI CHLORITE GLAUC Lw Pg aQz Sph H2O
 0119): PHNG EPI CHLORITE GLAUC Lw Pg aQz Sph H2O = PHNG PUMPI CHLORITE GLAUC Lw Pg aQz Sph H2O
 0120): PHNG EPI CHLORITE GLAUC Lw Pg aQz Sph H2O = PHNG PUMPI CHLORITE GLAUC Lw Pg aQz Sph H2O
 0121): PHNG EPI CHLORITE GLAUC Lw Pg aQz Sph H2O = PHNG EPI CHLORITE FSP Lw Pg aQz Sph H2O
 0122): GRNT PHNG EPI CHLORITE FSP Pg aQz Sph H2O = PHNG EPI CHLORITE FSP Pg aQz Sph H2O
 0123): GRNT PHNG EPI CHLORITE FSP Pg aQz Sph H2O = GRNT PHNG EPI CHLORITE FSP Pg aQz Rt Sph H2O
 0124): GRNT PHNG EPI CHLORITE FSP Pg aQz Rt Sph H2O = GRNT PHNG EPI CHLORITE FSP aQz Rt Sph H2O
 0125): GRNT PHNG EPI CHLORITE FSP aQz Rt Sph H2O = GRNT BIOTITE PHNG EPI CHLORITE FSP aQz Rt Sph H2O
 0126): GRNT BIOTITE PHNG EPI CHLORITE FSP aQz Rt Sph H2O = GRNT BIOTITE PHNG EPI CHLORITE FSP aQz Rt H2O

Appendix 3 - DOMINO reactions for AA02-15

0127): GRNT BIOTITE PHNG EPI CHLORITE FSP aQz Rt H2O = GRNT BIOTITE PHNG EPI CHLORITE FSP Mt aQz Rt H20
 0128): GRNT BIOTITE PHNG EPI CHLORITE FSP Mt aQz Rt H2O = GRNT BIOTITE PHNG CHLORITE FSP Mt aQz Rt H20
 0129): GRNT BIOTITE PHNG CHLORITE FSP Mt Pg aQz Rt H2O = GRNT BIOTITE PHNG EPI FSP Mt Pg aQz Rt H20
 0130): GRNT BIOTITE PHNG EPI FSP Mt Pg aQz Rt H2O = GRNT BIOTITE PHNG FSP Mt Pg aQz Rt H20
 0131): GRNT BIOTITE PHNG FSP Mt Pg aQz Rt H2O = GRNT BIOTITE PHNG FSP Mt aQz Rt H20
 0132): PHNG CHLORITE GLAUC Hm Lw Pg aQz Sph H2O = PHNG EPI CHLORITE GLAUC Lw Pg aQz Sph H20
 0133): PHNG EPI CHLORITE GLAUC Lw Pg aQz Sph H2O = PHNG EPI CHLORITE GLAUC Pg aQz Sph Zo H20
 0134): PHNG EPI CHLORITE GLAUC Pg aQz Sph Zo H2O = PHNG EPI CHLORITE FSP Pg aQz Sph Zo H20
 0135): GRNT PHNG EPI CHLORITE FSP Pg aQz Sph Zo H2O = PHNG EPI CHLORITE FSP Pg aQz Sph Zo H20
 0136): GRNT PHNG EPI CHLORITE FSP Pg aQz Sph H2O = GRNT PHNG EPI CHLORITE FSP Pg aQz Sph Zo H20
 0137): GRNT PHNG EPI CHLORITE FSP Pg aQz Rt Sph H2O = GRNT PHNG EPI CHLORITE FSP Pg aQz Rt H20
 0138): GRNT PHNG EPI CHLORITE FSP Pg aQz Rt H2O = GRNT PHNG EPI CHLORITE FSP aQz Rt H20
 0139): GRNT PHNG EPI CHLORITE FSP aQz Rt H2O = GRNT BIOTITE PHNG EPI CHLORITE FSP aQz Rt H20
 0140): GRNT BIOTITE PHNG EPI CHLORITE FSP aQz Rt H2O = GRNT BIOTITE PHNG EPI CHLORITE FSP Pg aQz Rt H20
 0141): GRNT BIOTITE PHNG EPI CHLORITE FSP Pg aQz Rt H2O = GRNT BIOTITE PHNG EPI CHLORITE Pg aQz Rt H20
 0142): GRNT BIOTITE PHNG EPI CHLORITE Pg aQz Rt H2O = GRNT BIOTITE PHNG EPI Pg aQz Rt H20
 0143): GRNT BIOTITE PHNG EPI Pg aQz Rt H2O = GRNT BIOTITE PHNG EPI FSP Pg aQz Rt H20
 0144): GRNT BIOTITE PHNG EPI FSP Pg aQz Rt H2O = GRNT BIOTITE PHNG EPI FSP Mt Pg aQz Rt H20
 0145): GRNT BIOTITE PHNG (2)FSP Mt aQz Rt H2O = GRNT PHNG (2)FSP Mt aQz Rt H20
 0146): GRNT PHNG (2)FSP Mt aQz Rt H2O = GRNT PHNG (2)FSP Ky Mt aQz Rt H20
 0147): PHNG CHLORITE GLAUC Hm Lw Pg aQz Rt H2O = PHNG EPI CHLORITE GLAUC Lw Pg aQz Rt H20
 0148): PHNG EPI CHLORITE GLAUC Lw Pg aQz Rt H2O = PHNG EPI CHLORITE GLAUC Pg aQz Sph H20
 0149): PHNG EPI CHLORITE GLAUC Pg aQz Sph Zo H2O = GRNT PHNG EPI CHLORITE GLAUC Pg aQz Sph Zo H20
 0150): GRNT PHNG EPI CHLORITE GLAUC Pg aQz Sph Zo H2O = GRNT PHNG EPI CHLORITE GLAUC Pg aQz Sph H20
 0151): GRNT PHNG EPI CHLORITE GLAUC Pg aQz Sph H2O = GRNT PHNG EPI CHLORITE GLAUC FSP Pg aQz Sph H20
 0152): GRNT PHNG EPI CHLORITE GLAUC FSP Pg aQz Sph H2O = GRNT PHNG EPI CHLORITE FSP Pg aQz Sph H20
 0153): GRNT PHNG EPI CHLORITE FSP Pg aQz Rt Sph H2O = GRNT BIOTITE PHNG EPI CHLORITE Pg aQz Rt Sph H20
 0154): GRNT BIOTITE PHNG EPI CHLORITE Pg aQz Rt Sph H2O = GRNT BIOTITE PHNG EPI CHLORITE Pg aQz Rt H20
 0155): GRNT PHNG EPI CHLORITE GLAUC Pg aQz Sph H2O = GRNT PHNG EPI CHLORITE GLAUC Pg aQz Rt Sph H20
 0156): GRNT PHNG EPI CHLORITE GLAUC Pg aQz Rt Sph H2O = GRNT PHNG EPI CHLORITE GLAUC Pg aQz Rt H20
 0157): GRNT PHNG EPI CHLORITE GLAUC Pg aQz Rt H2O = GRNT BIOTITE PHNG EPI CHLORITE GLAUC Pg aQz Rt H20
 0158): GRNT BIOTITE PHNG EPI CHLORITE GLAUC Pg aQz Rt H2O = GRNT BIOTITE PHNG EPI CHLORITE Pg aQz Rt H20
 0159): PHNG CHLORITE Hm Lw Pg aQz Rt FStp H2O = PHNG CHLORITE Hm Jd Lw Pg aQz Rt FStp H20
 0160): PHNG CHLORITE Hm Jd Lw Pg aQz Rt FStp H2O = PHNG CHLORITE GLAUC Hm Lw Pg aQz Rt FStp H20
 0161): GRNT BIOTITE PHNG EPI CHLORITE GLAUC Pg aQz Rt H2O = GRNT BIOTITE PHNG EPI GLAUC Pg aQz Rt H20
 0162): GRNT BIOTITE PHNG EPI GLAUC Mt Pg aQz Rt H2O = GRNT BIOTITE PHNG EPI GLAUC Pg aQz Rt H20
 0163): GRNT BIOTITE PHNG EPI GLAUC Mt Pg aQz Rt H2O = GRNT BIOTITE PHNG GLAUC Mt Pg aQz Rt H20
 0164): GRNT BIOTITE PHNG GLAUC Mt Pg aQz Rt H2O = GRNT BIOTITE PHNG FSP Mt Pg aQz Rt H20
 0165): PHNG PUMPI CHLORITE FSP Lw Pg aQz Sph H2O = PHNG PUMPI CHLORITE FSP Pg aQz Sph Lmt H20
 0166): ILMENITE BIOTITE PHNG FSP Mt aQz Si St H2O = ILMENITE BIOTITE PHNG FSP Mt aQz St H20
 0167): ILMENITE BIOTITE PHNG FSP Mt aQz St H2O = ILMENITE BIOTITE PHNG CHLORITE FSP Mt aQz St H20
 0168): ILMENITE BIOTITE PHNG CHLORITE FSP Mt aQz St H2O = GRNT ILMENITE BIOTITE PHNG CHLORITE FSP Mt aQz St H20
 0169): GRNT ILMENITE BIOTITE PHNG CHLORITE FSP Mt aQz Rt H2O = GRNT ILMENITE BIOTITE PHNG EPI CHLORITE FSP
 0170): GRNT BIOTITE PHNG EPI FSP Pg aQz Rt H2O = GRNT BIOTITE PHNG EPI CHLORITE FSP Pg aQz Rt H20
 0171): GRNT BIOTITE PHNG EPI GLAUC Pg aQz Rt H2O = GRNT BIOTITE PHNG EPI Pg aQz Rt H20
 0172): GRNT ILMENITE BIOTITE PHNG FSP Ky Mt aQz Rt H2O = GRNT ILMENITE BIOTITE PHNG FSP Ky Mt aQz H20
 0173): GRNT BIOTITE PHNG FSP Ky Mt aQz Rt H2O = GRNT ILMENITE BIOTITE PHNG FSP Ky Mt aQz Rt H20
 0174): GRNT ILMENITE BIOTITE (2)FSP Mt aQz Rt Si H2O = GRNT ILMENITE BIOTITE (2)FSP Mt aQz Si H20
 0175): GRNT BIOTITE (2)FSP Mt aQz Rt Si H2O = GRNT ILMENITE BIOTITE (2)FSP Mt aQz Rt Si H20
 0176): GRNT ILMENITE BIOTITE (2)FSP Mt aQz Si H2O = GRNT ILMENITE BIOTITE (2)FSP Cd Mt aQz Si H20
 0177): GRNT ILMENITE BIOTITE (2)FSP Mt aQz Si H2O = GRNT ILMENITE BIOTITE (2)FSP Cd Mt aQz Si H20
 0178): GRNT ILMENITE BIOTITE (2)FSP Mt aQz Si H2O = GRNT ILMENITE BIOTITE (2)FSP Cd Mt aQz Si H20
 0179): GRNT ILMENITE BIOTITE (2)FSP Mt aQz Si H2O = GRNT ILMENITE BIOTITE (2)FSP Cd Mt aQz Si H20
 0180): GRNT BIOTITE (2)FSP Mt aQz Rt Si H2O = GRNT ILMENITE BIOTITE (2)FSP Mt aQz Si H20
 0181): GRNT (2)FSP Mt aQz Rt Si H2O = GRNT (2)FSP Ky Mt aQz Rt H20
 0182): GRNT (2)FSP Ky Mt aQz Rt H2O = GRNT PHNG (2)FSP Ky Mt aQz Rt H20
 0183): PHNG EPI PUMPI CHLORITE FSP Pg aQz Sph H2O = PHNG EPI CHLORITE FSP Pg aQz Sph Zo H20
 0184): ILMENITE PHNG EPI CHLORITE FSP aQz Rt Sph H2O = ILMENITE BIOTITE PHNG EPI CHLORITE FSP aQz Sph H20
 0185): ILMENITE BIOTITE PHNG EPI CHLORITE FSP aQz H2O = GRNT ILMENITE BIOTITE PHNG EPI CHLORITE FSP aQz H20
 0186): ILMENITE BIOTITE PHNG CHLORITE FSP Mt aQz H2O = ILMENITE BIOTITE PHNG CHLORITE FSP Mt aQz St H20
 0187): ILMENITE BIOTITE PHNG FSP Mt aQz Si St H2O = GRNT ILMENITE BIOTITE PHNG FSP Mt aQz Si H20
 0188): ILMENITE BIOTITE PHNG FSP Mt aQz Si St H2O = GRNT ILMENITE BIOTITE PHNG FSP Mt aQz Si H20
 0189): GRNT ILMENITE BIOTITE (2)FSP Mt aQz Si H2O = GRNT ILMENITE BIOTITE (2)FSP Cd Mt aQz Si H20

Appendix 3 - DOMINO reactions for AA02-15

0190): GRNT ILMENITE BIOTITE (2)FSP aCd Mt aQz Si H2O = GRNT ILMENITE (2)FSP Cd Mt aQz Si H2O
 0191): GRNT ILMENITE BIOTITE (2)FSP Mt aQz Si H2O = GRNT ILMENITE BIOTITE (2)FSP aCd Mt aQz Si H2O
 0192): GRNT ILMENITE BIOTITE (2)FSP aCd Mt aQz Si H2O = GRNT ILMENITE (2)FSP aCd Mt aQz Si H2O
 0193): GRNT ILMENITE BIOTITE (2)FSP aCd Mt aQz Si H2O = GRNT ILMENITE (2)FSP aCd Mt aQz Si H2O
 0194): GRNT ILMENITE BIOTITE (2)FSP aCd Mt aQz Si H2O = GRNT ILMENITE (2)FSP aCd Mt aQz Si H2O
 0195): GRNT PHNG EPI CHLORITE FSP aQz Rt Sph H2O = GRNT PHNG EPI CHLORITE FSP aQz Rt H2O
 0196): GRNT BIOTITE PHNG FSP Mt aQz Rt Si H2O = GRNT BIOTITE PHNG (2)FSP Mt aQz Rt Si H2O
 0197): GRNT BIOTITE PHNG FSP Mt aQz Rt H2O = GRNT BIOTITE PHNG FSP Mt aQz Rt Si H2O
 0198): PHNG PUMPI CHLORITE Lw Pg aQz Sph FStp H2O = PHNG PUMPI CHLORITE GLAUC Lw Pg aQz Sph FStp H2O
 0199): PHNG PUMPI CHLORITE GLAUC Lw Pg aQz Sph FStp H2O = PHNG PUMPI CHLORITE GLAUC Lw Pg aQz Sph H2O
 0200): PHNG CHLORITE Hm Lw Pg aQz Sph FStp H2O = PHNG CHLORITE GLAUC Hm Lw Pg aQz Sph FStp H2O
 0201): PHNG CHLORITE GLAUC Hm Lw Pg aQz Sph FStp H2O = PHNG CHLORITE GLAUC Hm Lw Pg aQz Sph H2O
 0202): GRNT PHNG EPI CHLORITE FSP aQz Rt Sph H2O = PHNG EPI CHLORITE FSP aQz Rt Sph H2O
 0203): GRNT PHNG EPI CHLORITE FSP aQz Rt Sph H2O = GRNT ILMENITE PHNG EPI CHLORITE FSP aQz Rt Sph H2O
 0204): GRNT ILMENITE PHNG EPI CHLORITE FSP aQz Rt Sph H2O = GRNT BIOTITE PHNG EPI CHLORITE FSP aQz Rt Sph H2O
 0205): GRNT ILMENITE PHNG EPI CHLORITE FSP aQz Sph H2O = GRNT ILMENITE PHNG EPI CHLORITE FSP aQz Rt Sph H2O
 0206): GRNT PHNG (2)FSP Mt aQz Rt H2O = GRNT PHNG (2)FSP Mt aQz Rt Si H2O
 0207): GRNT PHNG (2)FSP Mt aQz Rt Si H2O = GRNT (2)FSP Mt aQz Rt Si H2O
 0208): GRNT BIOTITE PHNG CHLORITE FSP Mt Pg aQz Rt H2O = GRNT BIOTITE PHNG FSP Mt Pg aQz Rt H2O
 0209): GRNT BIOTITE PHNG FSP Mt Pg aQz Rt H2O = GRNT BIOTITE PHNG FSP Ky Mt Pg aQz Rt H2O
 0210): GRNT PHNG EPI CHLORITE GLAUC Pg aQz Rt Sph H2O = GRNT BIOTITE PHNG EPI CHLORITE GLAUC Pg aQz Rt H2O
 0211): GRNT BIOTITE PHNG EPI CHLORITE Pg aQz Rt Sph H2O = GRNT PHNG EPI CHLORITE GLAUC Pg aQz Rt Sph H2O
 0212): GRNT PHNG EPI CHLORITE FSP Pg aQz Rt H2O = GRNT BIOTITE PHNG EPI CHLORITE Pg aQz Rt H2O
 0213): GRNT PHNG EPI CHLORITE FSP Pg aQz Rt H2O = GRNT BIOTITE PHNG EPI CHLORITE Pg aQz Rt H2O
 0214): PHNG PUMPI CHLORITE FSP Pg aQz Sph H2O = PHNG EPI CHLORITE FSP Pg aQz Sph Zo H2O
 0215): ILMENITE BIOTITE PHNG FSP Mt aQz Si St H2O = ILMENITE BIOTITE PHNG FSP Mt aQz Si H2O
 0216): GRNT ILMENITE BIOTITE (2)FSP Mt aQz Si H2O = GRNT ILMENITE BIOTITE (2)FSP Cd Mt aQz Si H2O
 0217): GRNT ILMENITE BIOTITE (2)FSP Mt aQz Si H2O = GRNT ILMENITE BIOTITE (2)FSP aCd Mt aQz Si H2O
 0218): GRNT ILMENITE BIOTITE (2)FSP Mt aQz Si H2O = GRNT ILMENITE BIOTITE (2)FSP aCd Mt aQz Si H2O
 0219): GRNT ILMENITE BIOTITE (2)FSP Mt aQz Si H2O = GRNT ILMENITE BIOTITE (2)FSP Cd Mt aQz Si H2O
 0220): GRNT ILMENITE BIOTITE (2)FSP Mt aQz Si H2O = GRNT ILMENITE BIOTITE (2)FSP Cd Mt aQz Si H2O
 0221): GRNT ILMENITE BIOTITE (2)FSP Mt aQz Si H2O = GRNT ILMENITE BIOTITE (2)FSP aCd Mt aQz Si H2O
 0222): GRNT ILMENITE (2)FSP aCd Mt aQz Si H2O = GRNT ILMENITE BIOTITE (2)FSP aCd Mt aQz Si H2O
 0223): GRNT ILMENITE BIOTITE (2)FSP aCd Mt aQz Si H2O = GRNT ILMENITE (2)FSP Cd Mt aQz Si H2O
 0224): GRNT ILMENITE BIOTITE (2)FSP Cd Mt aQz Si H2O = GRNT ILMENITE BIOTITE (2)FSP aCd Mt aQz Si H2O
 0225): GRNT ILMENITE BIOTITE PHNG FSP Mt aQz St H2O = GRNT ILMENITE BIOTITE PHNG FSP Ky Mt aQz St H2O
 0226): GRNT ILMENITE BIOTITE PHNG FSP Ky Mt aQz St H2O = GRNT ILMENITE BIOTITE PHNG FSP Ky Mt aQz H2O
 0227): PHNG EPI CHLORITE FSP Pg aQz Rt Sph H2O = GRNT PHNG EPI CHLORITE FSP Pg aQz Rt Sph H2O
 0228): GRNT ILMENITE BIOTITE PHNG EPI CHLORITE FSP aQz Rt H2O = GRNT BIOTITE PHNG EPI CHLORITE FSP Mt aQz R
 0229): GRNT ILMENITE BIOTITE PHNG EPI CHLORITE FSP aQz Rt H2O = GRNT BIOTITE PHNG EPI CHLORITE FSP aQz Rt H
 0230): PHNG PUMPI CHLORITE GLAUC Lw Pg aQz Sph H2O = PHNG EPI PUMPI CHLORITE GLAUC Lw Pg aQz Sph H2O
 0231): PHNG EPI PUMPI CHLORITE GLAUC Lw Pg aQz Sph H2O = PHNG EPI CHLORITE GLAUC Lw Pg aQz Sph H2O
 0232): GRNT BIOTITE PHNG EPI Pg aQz Rt H2O = GRNT BIOTITE PHNG EPI Mt Pg aQz Rt H2O
 0233): GRNT BIOTITE PHNG EPI Mt Pg aQz Rt H2O = GRNT BIOTITE PHNG EPI FSP Mt Pg aQz Rt H2O
 0234): GRNT BIOTITE PHNG EPI GLAUC Mt Pg aQz Rt H2O = GRNT BIOTITE PHNG EPI Mt Pg aQz Rt H2O
 0235): PHNG EPI PUMPI CHLORITE FSP Pg aQz Sph H2O = PHNG EPI CHLORITE FSP Pg aQz Sph Zo H2O
 0236): PHNG PUMPI CHLORITE FSP Pg aQz Sph H2O = PHNG EPI CHLORITE FSP Pg aQz Sph Zo H2O
 0237): PHNG EPI CHLORITE FSP Pg aQz Sph H2O = PHNG EPI CHLORITE FSP aQz Rt Sph H2O
 0238): ILMENITE BIOTITE PHNG EPI CHLORITE FSP aQz Rt H2O = BIOTITE PHNG EPI CHLORITE FSP aQz Rt Sph H2O
 0239): ILMENITE BIOTITE PHNG EPI CHLORITE FSP Mt aQz H2O = GRNT ILMENITE BIOTITE PHNG EPI CHLORITE FSP Mt a
 0240): ILMENITE BIOTITE PHNG CHLORITE FSP Mt aQz H2O = ILMENITE BIOTITE PHNG FSP Mt aQz Si St H2O
 0241): ILMENITE BIOTITE PHNG (2)FSP Mt aQz Si H2O = GRNT ILMENITE BIOTITE (2)FSP Mt aQz Si H2O
 0242): GRNT ILMENITE (2)FSP aCd Mt aQz Si H2O = GRNT ILMENITE (2)FSP Cd Mt aQz Si H2O
 0243): GRNT ILMENITE BIOTITE (2)FSP aCd Mt aQz Si H2O = GRNT ILMENITE BIOTITE (2)FSP Cd Mt aQz Si H2O
 0244): GRNT ILMENITE BIOTITE (2)FSP Cd Mt aQz Si H2O = GRNT ILMENITE (2)FSP Cd Mt aQz Si H2O
 0245): GRNT ILMENITE BIOTITE (2)FSP aCd Mt aQz Si H2O = GRNT ILMENITE (2)FSP Cd Mt aQz Si H2O
 0246): GRNT ILMENITE BIOTITE (2)FSP Cd Mt aQz Si H2O = GRNT ILMENITE (2)FSP aCd Mt aQz Si H2O
 0247): GRNT ILMENITE BIOTITE (2)FSP aCd Mt aQz Si H2O = GRNT ILMENITE (2)FSP Cd Mt aQz Si H2O
 0248): PHNG PUMPI CHLORITE FSP Lw Pg aQz Sph H2O = PHNG EPI CHLORITE FSP Pg aQz Sph Zo H2O
 0249): PHNG EPI CHLORITE FSP Pg aQz Sph Zo H2O = GRNT PHNG EPI CHLORITE FSP Pg aQz Sph H2O
 0250): PHNG EPI CHLORITE FSP aQz Rt Sph H2O = ILMENITE BIOTITE PHNG EPI CHLORITE FSP aQz Rt Sph H2O
 0251): GRNT ILMENITE BIOTITE PHNG FSP Mt aQz St H2O = ILMENITE BIOTITE PHNG FSP Mt aQz St H2O
 0252): GRNT ILMENITE BIOTITE PHNG FSP Ky Mt aQz St H2O = GRNT ILMENITE BIOTITE PHNG FSP Mt aQz Si St H2O

Appendix 3 - DOMINO reactions for AA02-15

0253): GRNT ILMENITE BIOTITE PHNG FSP Ky Mt aQz Rt H2O = GRNT ILMENITE BIOTITE PHNG FSP Mt aQz Rt Si H2O
 0254): PHNG CHLORITE GLAUC Hm Lw Pg aQz Sph FStp H2O = PHNG PUMPI CHLORITE Hm Lw Pg aQz Sph H2O
 0255): PHNG PUMPI CHLORITE Hm Lw Pg aQz Sph H2O = PHNG PUMPI CHLORITE Lw Pg aQz Sph H2O
 0256): ILMENITE PHNG EPI CHLORITE FSP aQz Rt Sph H2O = GRNT ILMENITE PHNG EPI CHLORITE FSP aQz Rt Sph H2O
 0257): GRNT PHNG (2)FSP Mt aQz Rt Si H2O = GRNT BIOTITE PHNG (2)FSP Mt aQz Rt Si H2O
 0258): PHNG CHLORITE GLAUC Hm Lw Pg aQz Rt FStp H2O = PHNG CHLORITE GLAUC Hm Lw Pg aQz Sph H2O
 0259): PHNG PUMPI CHLORITE Lw Pg aQz Sph FStp H2O = PHNG PUMPI CHLORITE GLAUC Lw Pg aQz Sph H2O
 0260): GRNT BIOTITE PHNG EPI CHLORITE FSP Pg aQz Rt H2O = GRNT BIOTITE PHNG CHLORITE FSP Mt Pg aQz Rt H2O
 0261): GRNT BIOTITE PHNG FSP Mt Pg aQz Rt H2O = GRNT BIOTITE PHNG Ky Mt aQz Rt H2O
 0262): GRNT BIOTITE PHNG FSP Mt aQz Rt H2O = GRNT BIOTITE PHNG (2)FSP Mt aQz Rt Si H2O
 0263): PHNG EPI PUMPI CHLORITE GLAUC Lw Pg aQz Sph H2O = PHNG PUMPI CHLORITE GLAUC Lw Pg aQz Sph H2O
 0264): PHNG EPI CHLORITE GLAUC Lw Pg aQz Sph H2O = PHNG EPI PUMPI CHLORITE GLAUC Lw Pg aQz Sph H2O
 0265): GRNT PHNG EPI CHLORITE GLAUC Pg aQz Sph H2O = GRNT BIOTITE PHNG EPI CHLORITE GLAUC Pg aQz Sph H2O
 0266): GRNT BIOTITE PHNG EPI CHLORITE GLAUC Pg aQz Sph H2O = GRNT BIOTITE PHNG EPI CHLORITE Pg aQz Rt Sph H2O
 0267): GRNT PHNG EPI CHLORITE FSP Pg aQz Rt H2O = GRNT BIOTITE PHNG EPI CHLORITE FSP Pg aQz Rt H2O
 0268): GRNT PHNG (2)FSP Ky Mt aQz Rt H2O = GRNT PHNG (2)FSP Mt aQz Rt Si H2O
 0269): GRNT BIOTITE PHNG EPI CHLORITE FSP Pg aQz Rt H2O = GRNT PHNG EPI CHLORITE FSP Pg aQz Rt H2O
 0270): GRNT BIOTITE PHNG EPI CHLORITE Pg aQz Rt H2O = GRNT BIOTITE PHNG EPI CHLORITE FSP Pg aQz Rt H2O
 0271): PHNG EPI CHLORITE FSP Pg aQz Rt Sph H2O = PHNG EPI CHLORITE FSP aQz Rt Sph H2O
 0272): PHNG EPI CHLORITE FSP Pg aQz Sph H2O = PHNG EPI CHLORITE FSP Pg aQz Rt Sph H2O
 0273): ILMENITE BIOTITE PHNG (2)FSP Mt aQz Si H2O = GRNT ILMENITE BIOTITE PHNG (2)FSP Mt aQz Si H2O
 0274): GRNT ILMENITE BIOTITE (2)FSP Mt aQz Si H2O = GRNT ILMENITE BIOTITE (2)FSP Cd Mt aQz Si H2O
 0275): GRNT ILMENITE BIOTITE (2)FSP Mt aQz Si H2O = GRNT ILMENITE BIOTITE (2)FSP Cd Mt aQz Si H2O
 0276): GRNT ILMENITE BIOTITE (2)FSP aCd Mt aQz Si H2O = GRNT ILMENITE BIOTITE (2)FSP Cd Mt aQz Si H2O
 0277): GRNT ILMENITE BIOTITE (2)FSP Mt aQz Si H2O = GRNT ILMENITE BIOTITE (2)FSP aCd Mt aQz Si H2O
 0278): GRNT ILMENITE BIOTITE (2)FSP Cd Mt aQz Si H2O = GRNT ILMENITE (2)FSP aCd Mt aQz Si H2O
 0279): GRNT ILMENITE BIOTITE (2)FSP aCd Mt aQz Si H2O = GRNT ILMENITE BIOTITE (2)FSP Cd Mt aQz Si H2O
 0280): GRNT ILMENITE (2)FSP aCd Mt aQz Si H2O = GRNT ILMENITE BIOTITE (2)FSP aCd Mt aQz Si H2O
 0281): GRNT ILMENITE BIOTITE (2)FSP Cd Mt aQz Si H2O = GRNT ILMENITE (2)FSP Cd Mt aQz Si H2O
 0282): GRNT ILMENITE BIOTITE (2)FSP aCd Mt aQz Si H2O = GRNT ILMENITE BIOTITE (2)FSP Cd Mt aQz Si H2O
 0283): GRNT ILMENITE (2)FSP Cd Mt aQz Si H2O = GRNT ILMENITE (2)FSP aCd Mt aQz Si H2O
 0284): GRNT ILMENITE BIOTITE (2)FSP Mt aQz Si H2O = GRNT ILMENITE BIOTITE (2)FSP aCd Mt aQz Si H2O
 0285): GRNT ILMENITE BIOTITE (2)FSP aCd Mt aQz Si H2O = GRNT ILMENITE (2)FSP aCd Mt aQz Si H2O
 0286): GRNT ILMENITE BIOTITE PHNG CHLORITE FSP Mt aQz St H2O = ILMENITE BIOTITE PHNG CHLORITE FSP Mt aQz St H2O
 0287): GRNT ILMENITE BIOTITE PHNG CHLORITE FSP Mt aQz H2O = GRNT ILMENITE BIOTITE PHNG CHLORITE FSP Mt aQz H2O
 0288): GRNT ILMENITE BIOTITE (2)FSP aCd Mt aQz Si H2O = GRNT ILMENITE (2)FSP Cd Mt aQz Si H2O
 0289): GRNT ILMENITE BIOTITE (2)FSP aCd Mt aQz Si H2O = GRNT ILMENITE (2)FSP aCd Mt aQz Si H2O
 0290): ILMENITE PHNG EPI CHLORITE FSP aQz Rt Sph H2O = ILMENITE BIOTITE PHNG EPI CHLORITE FSP aQz Rt Sph H2O
 0291): ILMENITE BIOTITE PHNG EPI CHLORITE FSP aQz Sph H2O = GRNT ILMENITE BIOTITE PHNG EPI CHLORITE FSP aQz Sph H2O
 0292): GRNT ILMENITE BIOTITE PHNG CHLORITE FSP Mt aQz H2O = GRNT ILMENITE BIOTITE PHNG FSP Ky Mt aQz St H2O
 0293): PHNG PUMPI CHLORITE GLAUC Lw Pg aQz Sph FStp H2O = PHNG PUMPI CHLORITE FSP Lw Pg aQz Sph FStp H2O
 0294): GRNT BIOTITE PHNG CHLORITE FSP Mt aQz Rt H2O = GRNT ILMENITE BIOTITE PHNG FSP Ky Mt aQz Rt H2O
 0295): GRNT ILMENITE BIOTITE PHNG FSP Ky Mt aQz Rt H2O = GRNT ILMENITE BIOTITE PHNG FSP Mt aQz Si H2O
 0296): PHNG EPI CHLORITE FSP aQz Rt Sph H2O = GRNT ILMENITE PHNG EPI CHLORITE FSP aQz Rt Sph H2O
 0297): GRNT ILMENITE BIOTITE PHNG EPI CHLORITE FSP aQz H2O = GRNT ILMENITE BIOTITE PHNG CHLORITE FSP Mt aQz H2O
 0298): PHNG CHLORITE GLAUC Hm Lw Pg aQz Sph H2O = PHNG PUMPI CHLORITE Hm Lw Pg aQz Sph H2O
 0299): GRNT ILMENITE BIOTITE PHNG EPI CHLORITE FSP aQz Sph H2O = GRNT BIOTITE PHNG EPI CHLORITE FSP aQz Sph H2O
 0300): GRNT BIOTITE PHNG FSP Mt Pg aQz Rt H2O = GRNT BIOTITE PHNG FSP Ky Mt aQz Rt H2O
 0301): GRNT BIOTITE PHNG FSP Ky Mt Pg aQz Rt H2O = GRNT BIOTITE PHNG FSP Ky Mt aQz Rt H2O
 0302): GRNT BIOTITE PHNG FSP Mt Pg aQz Rt H2O = GRNT BIOTITE PHNG FSP Ky Mt Pg aQz Rt H2O
 0303): PHNG PUMPI CHLORITE GLAUC Lw Pg aQz Sph H2O = PHNG EPI PUMPI CHLORITE GLAUC Lw Pg aQz Sph H2O
 0304): PHNG EPI PUMPI CHLORITE GLAUC Lw Pg aQz Sph H2O = PHNG EPI CHLORITE GLAUC Lw Pg aQz Sph H2O
 0305): GRNT PHNG EPI CHLORITE GLAUC FSP Pg aQz Sph H2O = GRNT PHNG EPI CHLORITE FSP Pg aQz Rt Sph H2O
 0306): GRNT PHNG EPI CHLORITE FSP aQz Rt Sph H2O = GRNT BIOTITE PHNG EPI CHLORITE FSP aQz Rt H2O
 0307): GRNT BIOTITE PHNG EPI GLAUC Mt Pg aQz Rt H2O = GRNT BIOTITE PHNG EPI FSP Mt Pg aQz Rt H2O
 0308): PHNG EPI CHLORITE GLAUC FSP Pg aQz Sph Zo H2O = PHNG EPI CHLORITE FSP Pg aQz Sph Zo H2O
 0309): GRNT ILMENITE BIOTITE PHNG FSP Mt aQz Si St H2O = GRNT ILMENITE BIOTITE PHNG FSP Mt aQz Si H2O
 0310): ILMENITE BIOTITE PHNG FSP Mt aQz Si St H2O = GRNT ILMENITE BIOTITE PHNG FSP Mt aQz Si St H2O
 0311): GRNT ILMENITE BIOTITE (2)FSP Cd Mt aQz Si H2O = GRNT ILMENITE (2)FSP Cd Mt aQz Si H2O
 0312): GRNT ILMENITE BIOTITE (2)FSP aCd Mt aQz Si H2O = GRNT ILMENITE (2)FSP Cd Mt aQz Si H2O
 0313): GRNT ILMENITE BIOTITE (2)FSP Mt aQz Si H2O = GRNT ILMENITE BIOTITE (2)FSP aCd Mt aQz Si H2O
 0314): GRNT ILMENITE (2)FSP aCd Mt aQz Si H2O = GRNT ILMENITE BIOTITE (2)FSP aCd Mt aQz Si H2O
 0315): GRNT ILMENITE BIOTITE (2)FSP Mt aQz Si H2O = GRNT ILMENITE BIOTITE (2)FSP aCd Mt aQz Si H2O

Appendix 3 - DOMINO reactions for AA02-15

Appendix 4 – DOMINO reactions for AA02-23

Appendix 4 – DOMINO reactions for AA02-23

0 64): PHNG CHLORITE FSP Pg aQz Rt Sph FStp H2O = PHNG CHLORITE FSP Pg aQz Rt Sph H2O
 0 65): GRNT ILMENITE PHNG CHLORITE FSP aQz St H2O = GRNT ILMENITE BIOTITE PHNG FSP aQz St H2O
 0 66): GRNT ILMENITE BIOTITE (2)FSP aQz Si H2O = GRNT ILMENITE (2)FSP aQz Si H2O
 0 67): PHNG CHLORITE Pg aQz Rt Sph FStp H2O = PHNG CHLORITE FSP Pg aQz Rt Sph FStp H2O
 0 68): ILMENITE PHNG CHLORITE FSP Pg aQz H2O = GRNT ILMENITE PHNG CHLORITE FSP Pg aQz H2O
 0 69): GRNT ILMENITE PHNG CHLORITE FSP Pg aQz H2O = GRNT ILMENITE PHNG CHLORITE FSP Pg aQz St H2O
 0 70): GRNT ILMENITE PHNG CHLORITE FSP Pg aQz St H2O = GRNT ILMENITE PHNG CHLORITE FSP aQz St H2O
 0 71): GRNT ILMENITE BIOTITE PHNG FSP Ky aQz St H2O = GRNT ILMENITE BIOTITE PHNG FSP aQz St H2O
 0 72): GRNT ILMENITE BIOTITE PHNG FSP Ky aQz St H2O = GRNT ILMENITE BIOTITE PHNG FSP Ky aQz H2O
 0 73): GRNT ILMENITE BIOTITE PHNG FSP Ky aQz H2O = GRNT ILMENITE BIOTITE PHNG FSP aQz Si H2O
 0 74): PHNG CHLORITE Lw Pg aQz Rt FStp H2O = PHNG CHLORITE Lw Pg aQz Rt Sph FStp H2O
 0 75): PHNG CHLORITE Lw Pg aQz Rt Sph FStp H2O = PHNG CHLORITE Pg aQz Rt Sph FStp H2O
 0 76): PHNG CHLORITE Pg aQz Rt Sph FStp H2O = PHNG CHLORITE Pg aQz Rt Sph H2O
 0 77): PHNG CHLORITE Pg aQz Rt Sph H2O = PHNG CHLORITE FSP Pg aQz Rt Sph H2O
 0 78): GRNT ILMENITE PHNG CHLORITE FSP Pg aQz H2O = GRNT ILMENITE BIOTITE PHNG CHLORITE FSP Pg aQz H2O
 0 79): GRNT ILMENITE BIOTITE PHNG CHLORITE FSP Pg aQz H2O = GRNT ILMENITE BIOTITE PHNG FSP Pg aQz H2O
 0 80): GRNT ILMENITE BIOTITE PHNG FSP Pg aQz H2O = GRNT ILMENITE BIOTITE PHNG FSP Ky Pg aQz H2O
 0 81): GRNT ILMENITE BIOTITE PHNG FSP Ky Pg aQz H2O = GRNT ILMENITE BIOTITE PHNG FSP Ky aQz H2O
 0 82): PHNG CHLORITE Lw Pg aQz Rt Sph FStp H2O = PHNG CHLORITE Lw Pg aQz Rt Sph H2O
 0 83): PHNG CHLORITE Lw Pg aQz Rt Sph H2O = PHNG CHLORITE Pg aQz Rt Sph H2O
 0 84): PHNG CHLORITE Pg aQz Rt Sph H2O = PHNG CHLORITE GLAUC Pg aQz Rt Sph H2O
 0 85): PHNG CHLORITE GLAUC Pg aQz Rt Sph H2O = PHNG CHLORITE FSP Pg aQz Rt Sph H2O
 0 86): PHNG CHLORITE FSP Pg aQz Rt Sph H2O = ILMENITE PHNG CHLORITE FSP Pg aQz Rt Sph H2O
 0 87): ILMENITE PHNG CHLORITE FSP Pg aQz Rt Sph H2O = ILMENITE PHNG CHLORITE FSP Pg aQz Rt H2O
 0 88): GRNT ILMENITE BIOTITE PHNG FSP Pg aQz H2O = GRNT ILMENITE BIOTITE PHNG FSP Pg aQz Rt H2O
 0 89): GRNT ILMENITE BIOTITE PHNG FSP Pg aQz Rt H2O = GRNT BIOTITE PHNG FSP Pg aQz Rt H2O
 0 90): GRNT BIOTITE PHNG FSP Pg aQz Rt H2O = GRNT BIOTITE PHNG FSP Ky Pg aQz Rt H2O
 0 91): GRNT BIOTITE PHNG FSP Ky Pg aQz Rt H2O = GRNT BIOTITE PHNG FSP Ky aQz Rt H2O
 0 92): GRNT PHNG FSP Ky aQz Rt H2O = GRNT BIOTITE PHNG FSP Ky aQz Rt H2O
 0 93): GRNT PHNG FSP Ky aQz Rt H2O = GRNT PHNG FSP aQz Rt Si H2O
 0 94): GRNT PHNG FSP aQz Rt Si H2O = GRNT PHNG (2)FSP aQz Rt Si H2O
 0 95): GRNT PHNG (2)FSP aQz Rt Si H2O = GRNT (2)FSP aQz Rt Si H2O
 0 96): ILMENITE PHNG CHLORITE FSP Pg aQz Rt Sph H2O = ILMENITE PHNG CHLORITE FSP Pg aQz Sph H2O
 0 97): ILMENITE PHNG CHLORITE FSP Pg aQz Sph H2O = GRNT ILMENITE PHNG CHLORITE FSP Pg aQz Sph H2O
 0 98): GRNT ILMENITE PHNG CHLORITE FSP Pg aQz Sph H2O = GRNT ILMENITE PHNG CHLORITE FSP Pg aQz H2O
 0 99): GRNT BIOTITE PHNG FSP Pg aQz Rt H2O = GRNT PHNG FSP Pg aQz Rt H2O
 0100): GRNT PHNG FSP Pg aQz Rt H2O = GRNT PHNG FSP Ky Pg aQz Rt H2O
 0101): GRNT PHNG FSP Ky Pg aQz Rt H2O = GRNT PHNG FSP Ky aQz Rt H2O
 0102): GRNT PHNG FSP Ky aQz Rt H2O = GRNT PHNG (2)FSP Ky aQz Rt H2O
 0103): GRNT PHNG (2)FSP Ky aQz Rt H2O = GRNT PHNG (2)FSP aQz Rt Si H2O
 0104): PHNG CHLORITE Lw Pg aQz Rt FStp H2O = PHNG CHLORITE Lw Pg aQz Rt H2O
 0105): PHNG CHLORITE Lw Pg aQz Rt H2O = PHNG CHLORITE GLAUC Lw Pg aQz Rt H2O
 0106): PHNG CHLORITE GLAUC Lw Pg aQz Rt H2O = PHNG CHLORITE Lw Pg aQz Rt Sph H2O
 0107): GRNT ILMENITE PHNG CHLORITE FSP Pg aQz Sph H2O = GRNT ILMENITE PHNG CHLORITE FSP Pg aQz Rt H2O
 0108): GRNT ILMENITE PHNG CHLORITE FSP Pg aQz Rt H2O = GRNT ILMENITE PHNG CHLORITE FSP Pg aQz H2O
 0109): GRNT ILMENITE PHNG CHLORITE FSP Pg aQz H2O = GRNT ILMENITE BIOTITE PHNG CHLORITE Pg aQz H2O
 0110): GRNT ILMENITE PHNG CHLORITE FSP Pg aQz H2O = GRNT ILMENITE BIOTITE PHNG CHLORITE Pg aQz H2O
 0111): GRNT ILMENITE BIOTITE PHNG CHLORITE Pg aQz H2O = GRNT ILMENITE BIOTITE PHNG Pg aQz H2O
 0112): GRNT ILMENITE BIOTITE PHNG Pg aQz H2O = GRNT ILMENITE BIOTITE PHNG FSP Pg aQz H2O
 0113): GRNT PHNG (2)FSP Ky aQz Rt H2O = GRNT (2)FSP Ky aQz Rt H2O
 0114): PHNG CHLORITE GLAUC Pg aQz Rt Sph H2O = ILMENITE PHNG CHLORITE GLAUC Pg aQz Rt Sph H2O
 0115): ILMENITE PHNG CHLORITE GLAUC Pg aQz Rt Sph H2O = GRNT PHNG CHLORITE GLAUC Pg aQz Rt Sph H2O
 0116): GRNT PHNG CHLORITE GLAUC Pg aQz Rt Sph H2O = GRNT PHNG CHLORITE GLAUC Pg aQz Rt H2O
 0117): GRNT PHNG CHLORITE GLAUC Pg aQz Rt H2O = GRNT ILMENITE PHNG CHLORITE GLAUC Pg aQz Rt H2O
 0118): GRNT ILMENITE PHNG CHLORITE GLAUC Pg aQz Rt H2O = GRNT ILMENITE PHNG CHLORITE FSP Pg aQz H2O
 0119): PHNG CHLORITE GLAUC Lw Pg aQz Rt H2O = PHNG CHLORITE GLAUC Pg aQz Rt Sph H2O
 0120): PHNG CHLORITE GLAUC Pg aQz Rt Sph H2O = GRNT PHNG CHLORITE GLAUC Pg aQz Rt Sph H2O
 0121): GRNT PHNG CHLORITE GLAUC Pg aQz Rt H2O = GRNT BIOTITE PHNG CHLORITE GLAUC Pg aQz Rt H2O
 0122): GRNT BIOTITE PHNG CHLORITE GLAUC Pg aQz Rt H2O = GRNT BIOTITE PHNG GLAUC Pg aQz Rt H2O
 0123): GRNT BIOTITE PHNG GLAUC Pg aQz Rt H2O = GRNT ILMENITE BIOTITE PHNG GLAUC Pg aQz Rt H2O
 0124): GRNT ILMENITE BIOTITE PHNG GLAUC Pg aQz Rt H2O = GRNT ILMENITE BIOTITE PHNG FSP Pg aQz Rt H2O
 0125): GRNT PHNG CHLORITE GLAUC Pg aQz Rt H2O = GRNT PHNG GLAUC Pg aQz Rt H2O
 0126): GRNT PHNG GLAUC Pg aQz Rt H2O = GRNT PHNG GLAUC FSP Pg aQz Rt H2O

Appendix 4 – DOMINO reactions for AA02-23

0127): GRNT PHNG GLAUC FSP Pg aQz Rt H2O = GRNT BIOTITE PHNG GLAUC FSP Pg aQz Rt H2O
 0128): GRNT BIOTITE PHNG GLAUC FSP Pg aQz Rt H2O = GRNT BIOTITE PHNG FSP Pg aQz Rt H2O
 0129): GRNT ILMENITE BIOTITE PHNG FSP aQz Si St H2O = GRNT ILMENITE BIOTITE PHNG FSP aQz Si H2O
 0130): GRNT ILMENITE BIOTITE PHNG FSP aQz Si St H2O = ILMENITE BIOTITE PHNG FSP aQz Si St H2O
 0131): ILMENITE BIOTITE PHNG FSP aQz St H2O = ILMENITE BIOTITE PHNG FSP aQz Si St H2O
 0132): GRNT PHNG GLAUC Pg aQz Rt H2O = GRNT BIOTITE PHNG GLAUC Pg aQz Rt H2O
 0133): GRNT ILMENITE BIOTITE PHNG FSP Ky aQz Rt H2O = GRNT ILMENITE BIOTITE PHNG FSP Ky aQz H2O
 0134): GRNT BIOTITE PHNG FSP Ky aQz Rt H2O = GRNT ILMENITE BIOTITE PHNG FSP Ky aQz Rt H2O
 0135): GRNT ILMENITE BIOTITE PHNG FSP aQz Rt Si H2O = GRNT ILMENITE BIOTITE PHNG FSP aQz Si H2O
 0136): GRNT BIOTITE PHNG FSP aQz Rt Si H2O = GRNT ILMENITE BIOTITE PHNG FSP aQz Rt Si H2O
 0137): GRNT PHNG FSP aQz Rt Si H2O = GRNT BIOTITE PHNG FSP aQz Rt Si H2O
 0138): GRNT ILMENITE BIOTITE (2)FSP Cd aQz Si H2O = GRNT ILMENITE BIOTITE (2)FSP aQz Si H2O
 0139): GRNT ILMENITE BIOTITE (2)FSP aQz Si H2O = GRNT ILMENITE BIOTITE (2)FSP Cd aQz Si H2O
 0140): GRNT ILMENITE (2)FSP aQz Rt Si H2O = GRNT ILMENITE BIOTITE (2)FSP aQz Si H2O
 0141): GRNT (2)FSP aQz Rt Si H2O = GRNT ILMENITE (2)FSP aQz Rt Si H2O
 0142): GRNT ILMENITE (2)FSP aQz Si H2O = GRNT ILMENITE (2)FSP Cd aQz Si H2O
 0143): GRNT ILMENITE (2)FSP Cd aQz Si H2O = GRNT ILMENITE (2)FSP aQz Si H2O
 0144): GRNT ILMENITE (2)FSP aQz Si H2O = GRNT ILMENITE (2)FSP Cd aQz Si H2O
 0145): GRNT ILMENITE (2)FSP aQz Si H2O = GRNT ILMENITE (2)FSP Cd aQz Si H2O
 0146): GRNT ILMENITE (2)FSP Cd aQz Si H2O = GRNT ILMENITE (2)FSP aQz Si H2O
 0147): GRNT ILMENITE (2)FSP aQz Si H2O = GRNT ILMENITE (2)FSP Cd aQz Si H2O
 0148): GRNT ILMENITE (2)FSP aQz Rt Si H2O = GRNT ILMENITE (2)FSP aQz Si H2O
 0149): GRNT (2)FSP Ky aQz Rt H2O = GRNT (2)FSP aQz Rt Si H2O
 0150): ILMENITE BIOTITE PHNG FSP aQz Si St H2O = GRNT ILMENITE BIOTITE PHNG FSP aQz Si H2O
 0151): GRNT PHNG (2)FSP aQz Rt Si H2O = GRNT BIOTITE PHNG (2)FSP aQz Rt Si H2O
 0152): GRNT BIOTITE PHNG (2)FSP aQz Rt Si H2O = GRNT BIOTITE (2)FSP aQz Rt Si H2O
 0153): GRNT BIOTITE (2)FSP aQz Rt Si H2O = GRNT (2)FSP aQz Rt Si H2O
 0154): GRNT ILMENITE BIOTITE (2)FSP aQz Si H2O = GRNT ILMENITE BIOTITE (2)FSP aCd aQz Si H2O
 0155): GRNT ILMENITE BIOTITE (2)FSP aQz Si H2O = GRNT ILMENITE BIOTITE (2)FSP aCd aQz Si H2O
 0156): GRNT ILMENITE BIOTITE (2)FSP aQz Si H2O = GRNT ILMENITE BIOTITE (2)FSP aCd aQz Si H2O
 0157): GRNT ILMENITE BIOTITE (2)FSP aQz Si H2O = GRNT ILMENITE BIOTITE (2)FSP aCd aQz Si H2O
 0158): GRNT ILMENITE BIOTITE (2)FSP aCd aQz Si H2O = GRNT ILMENITE BIOTITE (2)FSP Cd aQz Si H2O
 0159): GRNT ILMENITE BIOTITE (2)FSP Cd aQz Si H2O = GRNT ILMENITE BIOTITE (2)FSP aCd aQz Si H2O
 0160): GRNT ILMENITE BIOTITE (2)FSP Cd aQz Si H2O = GRNT ILMENITE (2)FSP aCd aQz Si H2O
 0161): GRNT ILMENITE BIOTITE (2)FSP Cd aQz Si H2O = GRNT ILMENITE (2)FSP aCd aQz Si H2O
 0162): GRNT ILMENITE (2)FSP aCd aQz Si H2O = GRNT ILMENITE BIOTITE (2)FSP Cd aQz Si H2O
 0163): GRNT ILMENITE BIOTITE (2)FSP Cd aQz Si H2O = GRNT ILMENITE (2)FSP aCd aQz Si H2O
 0164): GRNT ILMENITE (2)FSP aCd aQz Si H2O = GRNT ILMENITE BIOTITE (2)FSP Cd aQz Si H2O
 0165): GRNT ILMENITE (2)FSP aCd aQz Si H2O = GRNT ILMENITE BIOTITE (2)FSP Cd aQz Si H2O
 0166): GRNT ILMENITE BIOTITE (2)FSP aQz Si H2O = GRNT ILMENITE BIOTITE (2)FSP Cd aQz Si H2O
 0167): GRNT ILMENITE BIOTITE (2)FSP aQz Si H2O = GRNT ILMENITE BIOTITE (2)FSP Cd aQz Si H2O
 0168): GRNT ILMENITE BIOTITE PHNG FSP aQz St H2O = GRNT ILMENITE BIOTITE PHNG FSP aQz Si St H2O
 0169): GRNT ILMENITE BIOTITE PHNG FSP aQz Si H2O = GRNT ILMENITE BIOTITE PHNG FSP aQz Si St H2O
 0170): GRNT ILMENITE BIOTITE PHNG FSP aQz St H2O = GRNT ILMENITE BIOTITE PHNG FSP aQz Si St H2O
 0171): GRNT ILMENITE BIOTITE PHNG FSP aQz Si H2O = GRNT ILMENITE BIOTITE PHNG FSP aQz Si St H2O
 0172): GRNT ILMENITE BIOTITE PHNG CHLORITE FSP Pg aQz H2O = GRNT ILMENITE PHNG CHLORITE FSP Pg aQz H2O
 0173): GRNT ILMENITE PHNG CHLORITE GLAUC Pg aQz Rt H2O = GRNT ILMENITE BIOTITE PHNG CHLORITE GLAUC Pg aQz H2O
 0174): GRNT ILMENITE BIOTITE PHNG CHLORITE GLAUC Pg aQz H2O = GRNT ILMENITE BIOTITE PHNG CHLORITE Pg aQz H2O
 0175): GRNT ILMENITE BIOTITE PHNG CHLORITE FSP Pg aQz H2O = GRNT ILMENITE BIOTITE PHNG CHLORITE Pg aQz H2O
 0176): GRNT BIOTITE PHNG GLAUC Pg aQz Rt H2O = GRNT BIOTITE PHNG GLAUC FSP Pg aQz Rt H2O
 0177): GRNT PHNG CHLORITE GLAUC Pg aQz Rt H2O = GRNT BIOTITE PHNG GLAUC Pg aQz Rt H2O
 0178): ILMENITE PHNG CHLORITE FSP Pg aQz Sph H2O = ILMENITE PHNG CHLORITE FSP Pg aQz H2O
 0179): GRNT ILMENITE PHNG CHLORITE FSP Pg aQz St H2O = ILMENITE PHNG CHLORITE FSP Pg aQz St H2O
 0180): GRNT ILMENITE BIOTITE (2)FSP aQz Rt Si H2O = GRNT ILMENITE BIOTITE (2)FSP aQz Si H2O
 0181): GRNT BIOTITE (2)FSP aQz Rt Si H2O = GRNT ILMENITE BIOTITE (2)FSP aQz Rt Si H2O
 0182): GRNT ILMENITE BIOTITE (2)FSP aQz Si H2O = GRNT ILMENITE BIOTITE (2)FSP aCd aQz Si H2O
 0183): GRNT ILMENITE BIOTITE (2)FSP aQz Si H2O = GRNT ILMENITE BIOTITE (2)FSP aCd aQz Si H2O
 0184): GRNT ILMENITE BIOTITE (2)FSP aQz Si H2O = GRNT ILMENITE BIOTITE (2)FSP aCd aQz Si H2O
 0185): GRNT ILMENITE BIOTITE (2)FSP aQz Si H2O = GRNT ILMENITE BIOTITE (2)FSP aCd aQz Si H2O
 0186): GRNT ILMENITE BIOTITE (2)FSP aQz Si H2O = GRNT ILMENITE BIOTITE (2)FSP aCd aQz Si H2O
 0187): GRNT ILMENITE BIOTITE (2)FSP aQz Si H2O = GRNT ILMENITE BIOTITE (2)FSP aCd aQz Si H2O
 0188): GRNT ILMENITE BIOTITE (2)FSP aCd aQz Si H2O = GRNT ILMENITE BIOTITE (2)FSP Cd aQz Si H2O
 0189): GRNT ILMENITE BIOTITE (2)FSP aCd aQz Si H2O = GRNT ILMENITE BIOTITE (2)FSP Cd aQz Si H2O

Appendix 4 – DOMINO reactions for AA02-23

0190): GRNT ILMENITE BIOTITE (2)FSP Cd aQz Si H₂O = GRNT ILMENITE BIOTITE (2)FSP aQz Si H₂O
 0191): GRNT ILMENITE BIOTITE (2)FSP aQz Si H₂O = GRNT ILMENITE BIOTITE (2)FSP Cd aQz Si H₂O
 0192): GRNT ILMENITE BIOTITE (2)FSP aCd aQz Si H₂O = GRNT ILMENITE (2)FSP aCd aQz Si H₂O
 0193): GRNT ILMENITE BIOTITE (2)FSP aQz Si H₂O = GRNT ILMENITE (2)FSP aCd aQz Si H₂O
 0194): GRNT ILMENITE PHNG CHLORITE FSP Pg aQz St H₂O = GRNT ILMENITE BIOTITE PHNG FSP Pg aQz St H₂O
 0195): GRNT ILMENITE BIOTITE PHNG FSP Pg aQz St H₂O = GRNT ILMENITE BIOTITE PHNG FSP aQz St H₂O
 0196): GRNT ILMENITE BIOTITE PHNG FSP aQz St H₂O = GRNT ILMENITE BIOTITE PHNG FSP aQz Si H₂O
 0197): GRNT BIOTITE PHNG FSP Ky aQz Rt H₂O = GRNT BIOTITE PHNG FSP aQz Rt Si H₂O
 0198): PHNG CHLORITE Lw Pg aQz Rt FStp H₂O = PHNG CHLORITE Lw Pg aQz Rt Sph H₂O
 0199): ILMENITE PHNG CHLORITE GLAUC Pg aQz Rt Sph H₂O = ILMENITE PHNG CHLORITE FSP Pg aQz Sph H₂O
 0200): GRNT ILMENITE PHNG CHLORITE GLAUC Pg aQz Rt H₂O = GRNT ILMENITE PHNG CHLORITE FSP Pg aQz Rt H₂O
 0201): GRNT ILMENITE PHNG CHLORITE GLAUC Pg aQz Rt H₂O = GRNT ILMENITE BIOTITE PHNG GLAUC Pg aQz Rt H₂O
 0202): GRNT ILMENITE BIOTITE PHNG GLAUC Pg aQz Rt H₂O = GRNT ILMENITE BIOTITE PHNG Pg aQz Rt H₂O
 0203): GRNT ILMENITE BIOTITE PHNG Pg aQz Rt H₂O = GRNT ILMENITE BIOTITE PHNG FSP Pg aQz Rt H₂O
 0204): GRNT ILMENITE BIOTITE PHNG Pg aQz Rt H₂O = GRNT ILMENITE BIOTITE PHNG Pg aQz H₂O
 0205): GRNT BIOTITE PHNG FSP aQz Rt Si H₂O = GRNT BIOTITE PHNG (2)FSP aQz Rt Si H₂O
 0206): GRNT ILMENITE BIOTITE (2)FSP aQz Si H₂O = GRNT ILMENITE BIOTITE (2)FSP aCd aQz Si H₂O
 0207): GRNT ILMENITE BIOTITE (2)FSP aQz Si H₂O = GRNT ILMENITE BIOTITE (2)FSP aCd aQz Si H₂O
 0208): GRNT ILMENITE BIOTITE (2)FSP aQz Si H₂O = GRNT ILMENITE BIOTITE (2)FSP aCd aQz Si H₂O
 0209): GRNT ILMENITE BIOTITE (2)FSP aQz Si H₂O = GRNT ILMENITE BIOTITE (2)FSP aCd aQz Si H₂O
 0210): GRNT ILMENITE BIOTITE (2)FSP aQz Si H₂O = GRNT ILMENITE BIOTITE (2)FSP aCd aQz Si H₂O
 0211): GRNT ILMENITE BIOTITE (2)FSP aQz Si H₂O = GRNT ILMENITE BIOTITE (2)FSP aCd aQz Si H₂O
 0212): GRNT ILMENITE BIOTITE (2)FSP aCd aQz Si H₂O = GRNT ILMENITE (2)FSP aCd aQz Si H₂O
 0213): GRNT ILMENITE BIOTITE (2)FSP aCd aQz Si H₂O = GRNT ILMENITE (2)FSP aCd aQz Si H₂O
 0214): GRNT ILMENITE (2)FSP Cd aQz Si H₂O = GRNT ILMENITE BIOTITE (2)FSP aCd aQz Si H₂O
 0215): GRNT ILMENITE (2)FSP aQz Si H₂O = GRNT ILMENITE (2)FSP aCd aQz Si H₂O
 0216): GRNT ILMENITE PHNG CHLORITE FSP aQz St H₂O = ILMENITE BIOTITE PHNG FSP aQz St H₂O
 0217): ILMENITE BIOTITE PHNG FSP aQz Si St H₂O = GRNT ILMENITE BIOTITE PHNG FSP aQz Si St H₂O
 0218): GRNT ILMENITE BIOTITE PHNG FSP aQz Si St H₂O = ILMENITE BIOTITE PHNG FSP aQz Si St H₂O
 0219): GRNT ILMENITE BIOTITE PHNG FSP aQz Si St H₂O = GRNT ILMENITE BIOTITE PHNG FSP aQz Si H₂O
 0220): GRNT ILMENITE BIOTITE PHNG FSP aQz Si H₂O = GRNT ILMENITE BIOTITE PHNG FSP aQz Si St H₂O
 0221): ILMENITE PHNG CHLORITE FSP Pg aQz Sph H₂O = GRNT ILMENITE PHNG CHLORITE FSP Pg aQz H₂O
 0222): GRNT ILMENITE BIOTITE PHNG CHLORITE FSP Pg aQz H₂O = GRNT ILMENITE BIOTITE PHNG FSP Pg aQz St H₂O
 0223): GRNT ILMENITE BIOTITE PHNG FSP aQz St H₂O = GRNT ILMENITE BIOTITE PHNG FSP aQz Si H₂O
 0224): GRNT ILMENITE BIOTITE PHNG FSP aQz Si H₂O = GRNT ILMENITE BIOTITE PHNG FSP aQz Si St H₂O
 0225): GRNT ILMENITE BIOTITE PHNG FSP aQz St H₂O = GRNT ILMENITE BIOTITE PHNG FSP aQz Si St H₂O
 0226): GRNT ILMENITE BIOTITE PHNG FSP Ky Pg aQz H₂O = GRNT ILMENITE BIOTITE PHNG FSP Pg aQz Rt H₂O
 0227): ILMENITE PHNG CHLORITE GLAUC Pg aQz Rt Sph H₂O = ILMENITE PHNG CHLORITE FSP Pg aQz Rt Sph H₂O
 0228): ILMENITE PHNG CHLORITE GLAUC Pg aQz Rt Sph H₂O = ILMENITE PHNG CHLORITE GLAUC Pg aQz Sph H₂O
 0229): ILMENITE PHNG CHLORITE GLAUC Pg aQz Sph H₂O = GRNT ILMENITE PHNG CHLORITE GLAUC Pg aQz Sph H₂O
 0230): GRNT ILMENITE PHNG CHLORITE GLAUC Pg aQz Sph H₂O = GRNT PHNG CHLORITE GLAUC Pg aQz Rt Sph H₂O
 0231): PHNG CHLORITE Lw Pg aQz Rt H₂O = PHNG CHLORITE Lw Pg aQz Rt Sph H₂O
 0232): GRNT ILMENITE PHNG CHLORITE GLAUC Pg aQz Rt H₂O = GRNT ILMENITE BIOTITE PHNG CHLORITE Pg aQz Rt H₂O
 0233): GRNT ILMENITE BIOTITE PHNG CHLORITE Pg aQz Rt H₂O = GRNT ILMENITE BIOTITE PHNG Pg aQz Rt H₂O
 0234): GRNT BIOTITE PHNG CHLORITE GLAUC Pg aQz Rt H₂O = GRNT ILMENITE BIOTITE PHNG GLAUC Pg aQz Rt H₂O
 0235): GRNT ILMENITE BIOTITE (2)FSP aQz Rt Si H₂O = GRNT ILMENITE (2)FSP aQz Rt Si H₂O
 0236): GRNT ILMENITE BIOTITE (2)FSP aCd aQz Si H₂O = GRNT ILMENITE (2)FSP aCd aQz Si H₂O
 0237): GRNT ILMENITE (2)FSP aCd aQz Si H₂O = GRNT ILMENITE (2)FSP aQz Si H₂O
 0238): GRNT ILMENITE (2)FSP aQz Si H₂O = GRNT ILMENITE (2)FSP aCd aQz Si H₂O
 0239): GRNT ILMENITE (2)FSP aCd aQz Si H₂O = GRNT ILMENITE (2)FSP aQz Si H₂O
 0240): GRNT ILMENITE (2)FSP aQz Si H₂O = GRNT ILMENITE (2)FSP aCd aQz Si H₂O
 0241): GRNT ILMENITE BIOTITE PHNG (2)FSP aQz Si H₂O = GRNT BIOTITE PHNG (2)FSP aQz Rt Si H₂O
 0242): GRNT ILMENITE BIOTITE (2)FSP aCd aQz Si H₂O = GRNT ILMENITE (2)FSP Cd aQz Si H₂O
 0243): GRNT ILMENITE (2)FSP Cd aQz Si H₂O = GRNT ILMENITE BIOTITE (2)FSP aCd aQz Si H₂O
 0244): GRNT ILMENITE BIOTITE (2)FSP aQz Si H₂O = GRNT ILMENITE BIOTITE (2)FSP aCd aQz Si H₂O
 0245): GRNT ILMENITE BIOTITE (2)FSP aCd aQz Si H₂O = GRNT ILMENITE (2)FSP aCd aQz Si H₂O
 0246): GRNT ILMENITE BIOTITE (2)FSP Cd aQz Si H₂O = GRNT ILMENITE BIOTITE (2)FSP aQz Si H₂O
 0247): GRNT ILMENITE BIOTITE (2)FSP aCd aQz Si H₂O = GRNT ILMENITE (2)FSP aCd aQz Si H₂O
 0248): GRNT ILMENITE BIOTITE (2)FSP aCd aQz Si H₂O = GRNT ILMENITE (2)FSP Cd aQz Si H₂O
 0249): GRNT ILMENITE BIOTITE (2)FSP aQz Si H₂O = GRNT ILMENITE (2)FSP aCd aQz Si H₂O
 0250): GRNT ILMENITE (2)FSP Cd aQz Si H₂O = GRNT ILMENITE (2)FSP aCd aQz Si H₂O
 0251): GRNT ILMENITE (2)FSP Cd aQz Si H₂O = GRNT ILMENITE (2)FSP aCd aQz Si H₂O
 0252): GRNT ILMENITE (2)FSP aCd aQz Si H₂O = GRNT ILMENITE (2)FSP Cd aQz Si H₂O

Appendix 4 – DOMINO reactions for AA02-23

0253): ILMENITE BIOTITE PHNG FSP aQz Si St H2O = GRNT ILMENITE BIOTITE PHNG FSP aQz Si H2O
 0254): GRNT ILMENITE BIOTITE PHNG FSP aQz Si H2O = GRNT ILMENITE BIOTITE PHNG FSP aQz Si St H2O
 0255): GRNT ILMENITE BIOTITE PHNG FSP aQz St H2O = GRNT ILMENITE BIOTITE PHNG FSP aQz Si St H2O
 0256): GRNT ILMENITE PHNG CHLORITE FSP Pg aQz St H2O = GRNT ILMENITE BIOTITE PHNG FSP aQz St H2O
 0257): GRNT ILMENITE BIOTITE PHNG CHLORITE FSP Pg aQz H2O = GRNT ILMENITE BIOTITE PHNG FSP Ky Pg aQz H2O
 0258): GRNT ILMENITE PHNG CHLORITE FSP Pg aQz H2O = GRNT ILMENITE BIOTITE PHNG FSP Pg aQz H2O
 0259): GRNT BIOTITE PHNG FSP Ky Pg aQz Rt H2O = GRNT ILMENITE BIOTITE PHNG FSP Ky Pg aQz H2O
 0260): GRNT BIOTITE PHNG GLAUC FSP Pg aQz Rt H2O = GRNT ILMENITE BIOTITE PHNG FSP Pg aQz Rt H2O
 0261): GRNT PHNG FSP Ky aQz Rt H2O = GRNT PHNG (2)FSP aQz Rt Si H2O
 0262): GRNT ILMENITE PHNG CHLORITE GLAUC Pg aQz Sph H2O = GRNT ILMENITE PHNG CHLORITE FSP Pg aQz Sph H2O
 0263): GRNT ILMENITE BIOTITE PHNG CHLORITE Pg aQz H2O = GRNT ILMENITE BIOTITE PHNG CHLORITE Pg aQz Rt H2O
 0264): GRNT PHNG CHLORITE GLAUC Pg aQz Rt H2O = GRNT ILMENITE BIOTITE PHNG GLAUC Pg aQz Rt H2O
 0265): GRNT ILMENITE PHNG CHLORITE GLAUC Pg aQz Rt H2O = GRNT ILMENITE PHNG CHLORITE GLAUC FSP Pg aQz H2O
 0266): GRNT ILMENITE BIOTITE PHNG CHLORITE GLAUC Pg aQz H2O = GRNT ILMENITE PHNG CHLORITE GLAUC FSP Pg aQz H2O
 0267): GRNT ILMENITE PHNG CHLORITE GLAUC FSP Pg aQz H2O = GRNT ILMENITE PHNG CHLORITE FSP Pg aQz H2O
 0268): GRNT ILMENITE (2)FSP Cd aQz Si H2O = GRNT ILMENITE (2)FSP aCd aQz Si H2O
 0269): GRNT ILMENITE BIOTITE (2)FSP aCd aQz Si H2O = GRNT ILMENITE BIOTITE (2)FSP Cd aQz Si H2O
 0270): GRNT ILMENITE BIOTITE (2)FSP aCd aQz Si H2O = GRNT ILMENITE BIOTITE (2)FSP Cd aQz Si H2O
 0271): GRNT ILMENITE BIOTITE PHNG CHLORITE FSP Pg aQz H2O = GRNT ILMENITE BIOTITE PHNG CHLORITE Pg aQz H2O
 0272): GRNT ILMENITE (2)FSP aCd aQz Si H2O = GRNT ILMENITE BIOTITE (2)FSP Cd aQz Si H2O
 0273): GRNT ILMENITE (2)FSP aCd aQz Si H2O = GRNT ILMENITE (2)FSP Cd aQz Si H2O
 0274): GRNT ILMENITE BIOTITE (2)FSP aCd aQz Si H2O = GRNT ILMENITE (2)FSP aCd aQz Si H2O
 0275): GRNT ILMENITE BIOTITE (2)FSP aCd aQz Si H2O = GRNT ILMENITE BIOTITE (2)FSP Cd aQz Si H2O
 0276): GRNT ILMENITE (2)FSP aCd aQz Si H2O = GRNT ILMENITE BIOTITE (2)FSP Cd aQz Si H2O
 0277): GRNT ILMENITE (2)FSP Cd aQz Si H2O = GRNT ILMENITE BIOTITE (2)FSP aCd aQz Si H2O
 0278): GRNT ILMENITE BIOTITE (2)FSP aCd aQz Si H2O = GRNT ILMENITE (2)FSP aCd aQz Si H2O
 0279): GRNT ILMENITE BIOTITE (2)FSP aQz Si H2O = GRNT ILMENITE BIOTITE (2)FSP Cd aQz Si H2O
 0280): GRNT ILMENITE BIOTITE (2)FSP aCd aQz Si H2O = GRNT ILMENITE (2)FSP Cd aQz Si H2O
 0281): GRNT ILMENITE BIOTITE (2)FSP aQz Si H2O = GRNT ILMENITE BIOTITE (2)FSP aCd aQz Si H2O
 0282): GRNT ILMENITE BIOTITE (2)FSP aCd aQz Si H2O = GRNT ILMENITE (2)FSP aCd aQz Si H2O
 0283): GRNT ILMENITE (2)FSP Cd aQz Si H2O = GRNT ILMENITE (2)FSP aCd aQz Si H2O
 0284): GRNT ILMENITE BIOTITE (2)FSP Cd aQz Si H2O = GRNT ILMENITE (2)FSP Cd aQz Si H2O
 0285): GRNT ILMENITE BIOTITE (2)FSP aQz Si H2O = GRNT ILMENITE BIOTITE (2)FSP Cd aQz Si H2O
 0286): GRNT ILMENITE (2)FSP Cd aQz Si H2O = GRNT ILMENITE (2)FSP aCd aQz Si H2O
 0287): GRNT ILMENITE (2)FSP aCd aQz Si H2O = GRNT ILMENITE (2)FSP Cd aQz Si H2O
 0288): GRNT ILMENITE BIOTITE (2)FSP Cd aQz Si H2O = GRNT ILMENITE (2)FSP Cd aQz Si H2O
 0289): GRNT ILMENITE BIOTITE (2)FSP aQz Si H2O = GRNT ILMENITE (2)FSP Cd aQz Si H2O
 0290): GRNT ILMENITE (2)FSP Cd aQz Si H2O = GRNT ILMENITE (2)FSP aCd aQz Si H2O
 0291): GRNT ILMENITE (2)FSP Cd aQz Si H2O = GRNT ILMENITE (2)FSP aCd aQz Si H2O
 0292): GRNT ILMENITE (2)FSP Cd aQz Si H2O = GRNT ILMENITE (2)FSP aCd aQz Si H2O
 0293): GRNT ILMENITE (2)FSP aCd aQz Si H2O = GRNT ILMENITE (2)FSP Cd aQz Si H2O
 0294): GRNT ILMENITE (2)FSP aQz Si H2O = GRNT ILMENITE (2)FSP Cd aQz Si H2O
 0295): GRNT ILMENITE BIOTITE PHNG FSP aQz St H2O = GRNT ILMENITE BIOTITE PHNG FSP aQz Si St H2O
 0296): GRNT ILMENITE BIOTITE PHNG FSP aQz Si St H2O = GRNT ILMENITE BIOTITE PHNG FSP aQz Si H2O
 0297): GRNT ILMENITE BIOTITE PHNG FSP aQz Si H2O = GRNT ILMENITE BIOTITE PHNG FSP aQz Si St H2O
 0298): ILMENITE BIOTITE PHNG FSP aQz Si St H2O = GRNT ILMENITE BIOTITE PHNG FSP aQz Si St H2O
 0299): GRNT ILMENITE PHNG CHLORITE FSP aQz St H2O = ILMENITE BIOTITE PHNG FSP aQz St H2O
 0300): ILMENITE BIOTITE PHNG CHLORITE FSP aQz St H2O = ILMENITE BIOTITE PHNG FSP aQz St H2O
 0301): GRNT ILMENITE PHNG CHLORITE FSP aQz St H2O = ILMENITE BIOTITE PHNG CHLORITE FSP aQz St H2O
 0302): GRNT ILMENITE BIOTITE PHNG FSP aQz St H2O = GRNT ILMENITE BIOTITE PHNG FSP aQz Si St H2O
 0303): GRNT ILMENITE BIOTITE PHNG FSP aQz Si H2O = GRNT ILMENITE BIOTITE PHNG FSP aQz Si St H2O
 0304): GRNT ILMENITE BIOTITE (2)FSP Cd aQz Si H2O = GRNT ILMENITE BIOTITE (2)FSP aQz Si H2O
 0305): GRNT ILMENITE (2)FSP aCd aQz Si H2O = GRNT ILMENITE BIOTITE (2)FSP Cd aQz Si H2O
 0306): PHNG CHLORITE Pg aQz Rt Sph FStp H2O = PHNG CHLORITE FSP Pg aQz Rt Sph H2O
 0307): GRNT ILMENITE BIOTITE PHNG FSP Ky Pg aQz H2O = GRNT ILMENITE BIOTITE PHNG FSP Pg aQz St H2O
 0308): PHNG CHLORITE Lw Pg aQz Rt Sph FStp H2O = PHNG CHLORITE Pg aQz Rt Sph H2O
 0309): GRNT BIOTITE PHNG FSP Ky Pg aQz Rt H2O = GRNT ILMENITE BIOTITE PHNG FSP Ky aQz Rt H2O
 0310): PHNG CHLORITE GLAUC Lw Pg aQz Rt H2O = PHNG CHLORITE Pg aQz Rt Sph H2O
 0311): PHNG CHLORITE Lw Pg aQz Rt Sph H2O = PHNG CHLORITE Pg aQz Rt Sph H2O
 0312): PHNG CHLORITE GLAUC Lw Pg aQz Rt H2O = PHNG CHLORITE Lw Pg aQz Rt Sph H2O
 0313): PHNG CHLORITE GLAUC Pg aQz Rt Sph H2O = ILMENITE PHNG CHLORITE FSP Pg aQz Rt Sph H2O
 0314): GRNT PHNG FSP aQz Rt Si H2O = GRNT BIOTITE PHNG (2)FSP aQz Rt Si H2O
 0315): ILMENITE PHNG CHLORITE GLAUC Pg aQz Sph H2O = ILMENITE PHNG CHLORITE FSP Pg aQz Sph H2O

Appendix 4 – DOMINO reactions for AA02-23

Appendix 4 – DOMINO reactions for AA02-23

0379): GRNT ILMENITE (2)FSP Cd aQz Si H2O = GRNT ILMENITE (2)FSP aCd aQz Si H2O
 0380): GRNT ILMENITE (2)FSP Cd aQz Si H2O = GRNT ILMENITE BIOTITE (2)FSP aCd aQz Si H2O
 0381): GRNT ILMENITE BIOTITE (2)FSP Cd aQz Si H2O = GRNT ILMENITE (2)FSP Cd aQz Si H2O
 0382): GRNT ILMENITE BIOTITE (2)FSP aQz Si H2O = GRNT ILMENITE BIOTITE (2)FSP Cd aQz Si H2O
 0383): ILMENITE BIOTITE PHNG FSP aQz Si St H2O = GRNT ILMENITE BIOTITE PHNG FSP aQz Si H2O
 0384): GRNT ILMENITE BIOTITE PHNG FSP aQz St H2O = GRNT ILMENITE BIOTITE PHNG FSP aQz Si St H2O
 0385): GRNT ILMENITE BIOTITE (2)FSP Cd aQz Si H2O = GRNT ILMENITE BIOTITE (2)FSP aQz Si H2O
 0386): GRNT ILMENITE (2)FSP Cd aQz Si H2O = GRNT ILMENITE (2)FSP aCd aQz Si H2O
 0387): GRNT ILMENITE BIOTITE (2)FSP aQz Si H2O = GRNT ILMENITE (2)FSP Cd aQz Si H2O
 0388): GRNT ILMENITE PHNG CHLORITE FSP Pg aQz H2O = GRNT ILMENITE BIOTITE PHNG FSP Pg aQz St H2O
 0389): GRNT ILMENITE BIOTITE PHNG FSP Ky aQz Rt H2O = GRNT ILMENITE BIOTITE PHNG FSP aQz Si H2O
 0390): PHNG CHLORITE GLAUC FSP Pg aQz Rt Sph H2O = ILMENITE PHNG CHLORITE FSP Pg aQz Rt Sph H2O
 0391): GRNT BIOTITE PHNG FSP Pg aQz Rt H2O = GRNT PHNG FSP Ky Pg aQz Rt H2O
 0392): GRNT PHNG FSP Ky Pg aQz Rt H2O = GRNT BIOTITE PHNG FSP Ky Pg aQz Rt H2O
 0393): GRNT BIOTITE PHNG FSP Ky aQz Rt H2O = GRNT PHNG FSP aQz Rt Si H2O
 0394): GRNT PHNG (2)FSP Ky aQz Rt H2O = GRNT PHNG (2)FSP aQz Rt Si H2O
 0395): GRNT PHNG (2)FSP Ky aQz Rt H2O = GRNT (2)FSP aQz Rt Si H2O
 0396): GRNT PHNG CHLORITE GLAUC Pg aQz Rt Sph H2O = GRNT ILMENITE PHNG CHLORITE FSP Pg aQz Rt H2O
 0397): GRNT ILMENITE PHNG CHLORITE FSP Pg aQz H2O = GRNT ILMENITE BIOTITE PHNG FSP Pg aQz H2O
 0398): GRNT ILMENITE BIOTITE PHNG FSP Pg aQz H2O = GRNT ILMENITE BIOTITE PHNG CHLORITE FSP Pg aQz H2O
 0399): ILMENITE PHNG CHLORITE GLAUC Pg aQz Rt Sph H2O = GRNT ILMENITE PHNG CHLORITE GLAUC Pg aQz Sph H2O
 0400): GRNT PHNG CHLORITE GLAUC Pg aQz Rt H2O = GRNT ILMENITE BIOTITE PHNG GLAUC Pg aQz Rt H2O
 0401): GRNT BIOTITE PHNG CHLORITE GLAUC Pg aQz Rt H2O = GRNT ILMENITE BIOTITE PHNG GLAUC Pg aQz Rt H2O
 0402): GRNT PHNG (2)FSP aQz Rt Si H2O = GRNT BIOTITE PHNG (2)FSP aQz Rt Si H2O
 0403): GRNT ILMENITE (2)FSP aQz Si H2O = GRNT ILMENITE (2)FSP aCd aQz Si H2O
 0404): GRNT ILMENITE BIOTITE (2)FSP Cd aQz Si H2O = GRNT ILMENITE BIOTITE (2)FSP aQz Si H2O
 0405): GRNT ILMENITE (2)FSP Cd aQz Si H2O = GRNT ILMENITE BIOTITE (2)FSP aCd aQz Si H2O
 0406): GRNT ILMENITE BIOTITE (2)FSP aCd aQz Si H2O = GRNT ILMENITE (2)FSP aCd aQz Si H2O
 0407): GRNT ILMENITE BIOTITE (2)FSP Cd aQz Si H2O = GRNT ILMENITE BIOTITE (2)FSP aCd aQz Si H2O
 0408): GRNT ILMENITE (2)FSP aCd aQz Si H2O = GRNT ILMENITE (2)FSP Cd aQz Si H2O
 0409): GRNT ILMENITE BIOTITE (2)FSP Cd aQz Si H2O = GRNT ILMENITE (2)FSP Cd aQz Si H2O
 0410): GRNT ILMENITE BIOTITE (2)FSP aCd aQz Si H2O = GRNT ILMENITE BIOTITE (2)FSP Cd aQz Si H2O
 0411): GRNT ILMENITE (2)FSP Cd aQz Si H2O = GRNT ILMENITE (2)FSP aCd aQz Si H2O
 0412): GRNT ILMENITE BIOTITE (2)FSP aCd aQz Si H2O = GRNT ILMENITE (2)FSP Cd aQz Si H2O
 0413): GRNT ILMENITE BIOTITE PHNG FSP aQz St H2O = GRNT ILMENITE BIOTITE PHNG FSP aQz Si St H2O
 0414): GRNT ILMENITE BIOTITE (2)FSP Cd aQz Si H2O = GRNT ILMENITE BIOTITE (2)FSP aQz Si H2O
 0415): GRNT ILMENITE BIOTITE (2)FSP aCd aQz Si H2O = GRNT ILMENITE BIOTITE (2)FSP Cd aQz Si H2O
 0416): GRNT ILMENITE BIOTITE (2)FSP aQz Si H2O = GRNT ILMENITE BIOTITE (2)FSP aCd aQz Si H2O
 0417): GRNT ILMENITE (2)FSP Cd aQz Si H2O = GRNT ILMENITE BIOTITE (2)FSP aCd aQz Si H2O
 0418): GRNT ILMENITE (2)FSP Cd aQz Si H2O = GRNT ILMENITE (2)FSP aCd aQz Si H2O
 0419): GRNT ILMENITE BIOTITE (2)FSP aQz Si H2O = GRNT ILMENITE (2)FSP aCd aQz Si H2O
 0420): GRNT ILMENITE BIOTITE (2)FSP Cd aQz Si H2O = GRNT ILMENITE (2)FSP aCd aQz Si H2O
 0421): GRNT ILMENITE BIOTITE (2)FSP aQz Si H2O = GRNT ILMENITE BIOTITE (2)FSP Cd aQz Si H2O
 0422): GRNT ILMENITE PHNG CHLORITE GLAUC Pg aQz Rt H2O = GRNT ILMENITE BIOTITE PHNG Pg aQz Rt H2O
 0423): GRNT ILMENITE (2)FSP Cd aQz Si H2O = GRNT ILMENITE (2)FSP aCd aQz Si H2O
 0424): GRNT ILMENITE (2)FSP aCd aQz Si H2O = GRNT ILMENITE BIOTITE (2)FSP Cd aQz Si H2O
 0425): GRNT ILMENITE BIOTITE (2)FSP Cd aQz Si H2O = GRNT ILMENITE BIOTITE (2)FSP aQz Si H2O
 0426): ILMENITE BIOTITE PHNG FSP aQz Si St H2O = GRNT ILMENITE BIOTITE PHNG FSP aQz Si St H2O
 0427): GRNT ILMENITE PHNG CHLORITE GLAUC Pg aQz Rt H2O = GRNT ILMENITE BIOTITE PHNG CHLORITE Pg aQz H2O
 0428): GRNT ILMENITE BIOTITE (2)FSP Cd aQz Si H2O = GRNT ILMENITE BIOTITE (2)FSP aQz Si H2O
 0429): GRNT ILMENITE BIOTITE (2)FSP aCd aQz Si H2O = GRNT ILMENITE BIOTITE (2)FSP Cd aQz Si H2O
 0430): GRNT ILMENITE (2)FSP Cd aQz Si H2O = GRNT ILMENITE BIOTITE (2)FSP aCd aQz Si H2O
 0431): GRNT ILMENITE (2)FSP Cd aQz Si H2O = GRNT ILMENITE (2)FSP aCd aQz Si H2O
 0432): GRNT ILMENITE BIOTITE (2)FSP Cd aQz Si H2O = GRNT ILMENITE (2)FSP Cd aQz Si H2O
 0433): GRNT ILMENITE BIOTITE (2)FSP Cd aQz Si H2O = GRNT ILMENITE (2)FSP aCd aQz Si H2O
 0434): GRNT ILMENITE (2)FSP Cd aQz Si H2O = GRNT ILMENITE (2)FSP aCd aQz Si H2O
 0435): GRNT ILMENITE (2)FSP Cd aQz Si H2O = GRNT ILMENITE (2)FSP aCd aQz Si H2O
 0436): GRNT ILMENITE (2)FSP aCd aQz Si H2O = GRNT ILMENITE (2)FSP Cd aQz Si H2O
 0437): GRNT ILMENITE (2)FSP aCd aQz Si H2O = GRNT ILMENITE (2)FSP Cd aQz Si H2O
 0438): GRNT ILMENITE (2)FSP aCd aQz Si H2O = GRNT ILMENITE (2)FSP Cd aQz Si H2O
 0439): GRNT ILMENITE (2)FSP Cd aQz Si H2O = GRNT ILMENITE (2)FSP aCd aQz Si H2O
 0440): GRNT ILMENITE (2)FSP Cd aQz Si H2O = GRNT ILMENITE (2)FSP aCd aQz Si H2O